AeroShield: Fire Suppression and Oil Spill Mitigation by UAV Swarms

Final Draft

AE3200 Design Synthesis

Group 26

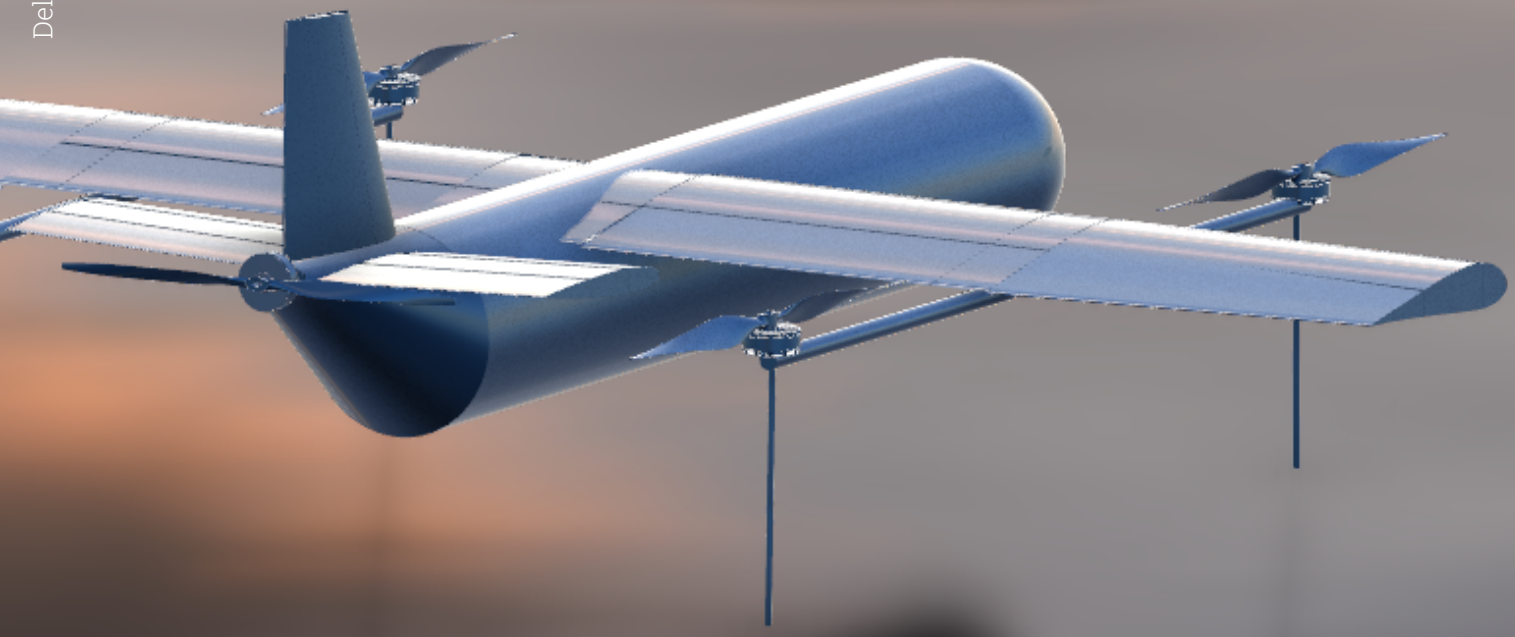

Delft University of Technology

TU Delft

This page was intentionally left blank.

AeroShield: Fire Suppression and Oil Spill Mitigation by UAV Swarms

Final Draft

by

Group 26

Student Name	Student Number	Student Name	Student Number
Luc Sijgers	5738008	Sanne van Hal	5562090
Igor Ruland	5497272	Juan Pablo Avila Paez	5467608
Maria Kars	5383773	Theodor Stefan Radomirescu	5517818
Freya van Apeldoorn	5524539	Kaj Casias	5458870
Pragya Agrawal	5679362	Wietske Overdijkink	5409691

Tutor:	B. Kumru
Coaches:	J.P. Ramirez & R. Meireles
Teaching Assistant:	A. de Rato Pueyo
Project Duration:	22 April, 2025 - 27 June, 2025
Faculty:	Faculty of Aerospace Engineering, Delft

Cover: AeroShield concept image by OpenAI's ChatGPT

Style: TU Delft Report Style, with modifications by Daan Zwaneveld

TU Delft

Executive Overview

- B. Kumru (Tutor)
- J.P. Ramirez (Coach)
- R. Meireles (Coach)
- F. van Apeldoorn
- J.P. Avila Paez
- T.S. Radomirescu
- P. Agrawal
- M. Kars
- K. Casias
- W. Overdijkink
- I. Ruland
- L. Sijgers
- S. van Hal

Natural disasters such as wildfires and oil spills cause severe environmental and economic damage, demanding a rapid and precise initial response to limit damage. Existing mitigation methods tend to be costly, slow, and labour-intensive. AeroShield, UAV swarm system, was developed to address this need. With the use of aerogel, a heat-resistant and lipophilic material, the UAVs are capable of mitigating both wildfires and oil spill disasters. The UAVs are deployed from transportable “nest” containers near the disaster site and autonomously deploy the aerogel to mitigate the disaster.

Based on the market gap the team established the Mission Need Statement: ”To provide a sustainable method to mitigate wildfires and oil spills in oceans by containing and minimising them.” The Mission Need Statement led to the Project Objective Statement: ”To develop a sustainable and autonomous swarm of at least 20 UAVs capable of deploying aerogel for mitigating wildfires and oil spills with a range of at least 20 km, by 10 students in 10 weeks.”

Requirements

The initial requirements for this project were provided by the client. Based on these requirements and a more in depth analysis of the project as a whole a complete list of requirements were identified. This list is split into stakeholder requirements and system requirements, which were then broken down into subsystem requirements. The key requirements derived during this process are listed in Table 1.

Table 1: Key System Requirements

Identification	Description
REQ-SYS-06	The system shall comprise at least 50% recyclable components by mass.
REQ-SYS-11	The UAV shall be able to operate in conditions with wind speeds of up to 30 km/h.
REQ-SYS-12	The UAV shall have a range of at least 20 km.
REQ-SYS-16	The UAV shall be able operate in a temperature range from -20°C to 140°C.
REQ-SYS-21	The UAV swarm shall be able to create a wildfire containment perimeter of 500 m.
REQ-SYS-22	The UAV swarm shall be able to create an oil spill containment perimeter of 7000 kg of oil.
REQ-SYS-23	The UAV shall have a production cost less than €50,000 (excluding raw materials).
REQ-SYS-24	Total system cost must not exceed €3,000,000 (excluding aerogels and ground ops).
REQ-SYS-25	The UAV shall have a weight less than 25 kg.
REQ-SYS-26	The UAV shall be able to pick up a payload of up to 5 kg.
REQ-SYS-30	The internal electronics shall be protected by heat resistant casings.

Market Gap

The global aerogel market is experiencing significant growth, with a predicted annual growth rate (CAGR) of 17% from 2025 to 2030 [1]. This growth is attributed to aerogel's excellent thermal conductivity of $0.02[W/mK]$ and its low density of $200[kg/m]$ [1]. Currently, aerogel is primarily utilized in the oil and gas sector or used as insulation material.

In the wildfire market, the occurrence of wildfires has been decreasing over the past few decades [2]. However, the total burned area in recent years (2022-2024) remains higher than the long-term average. Additionally, climate change contributes to the increased severity of individual wildfires, longer wildfire seasons, and sustained high-risk levels for protected areas and humans[2]. For instance, in 2022, 43% of the total burned area was within protected Natura 2000 areas [3], and the wildfire season in 2023 resulted in 41 deaths, including both civilians and firefighters [4].

Similar trends can be observed in the oil spill market, which also shows a decrease in the number of oil spills from 1970 to 2024 [5] . Data on tanker oil spills indicates that the largest portion of incidents is caused by collisions. However, crude oil from tankers and oil rigs is toxic and adversely affects marine life through ingestion, inhalation, and external exposure, resulting in skin and eye irritation [6].

It is identified that there is a clear market gap in both markets, considering the accessibility to remote locations and human risk in the wildfire market and in terms of accessibility and fast deployment in the oil spill market. AeroShield shows a strong potential market position in these areas, due to its autonomous flight, its accessibility to remote locations and reducing the human risks. Especially, for oil spill missions where the nest is located on oil tankers and oil rigs, resulting in a fast response method.

Mission Overview

For wildfire missions, the nest will be transported to a specific area, from which the UAVs are deployed one by one. Once the spread rate and direction are known, a perimeter will be established, and UAVs can start deploying the aerogel. The most limiting mission profile is displayed in Figure 1. At 20 km distance the round trip of one UAV to lay a sheet of aerogel takes about 44 minutes. For oil spill missions, the nest will already be stored on oil tankers or oil rigs to minimize response times.

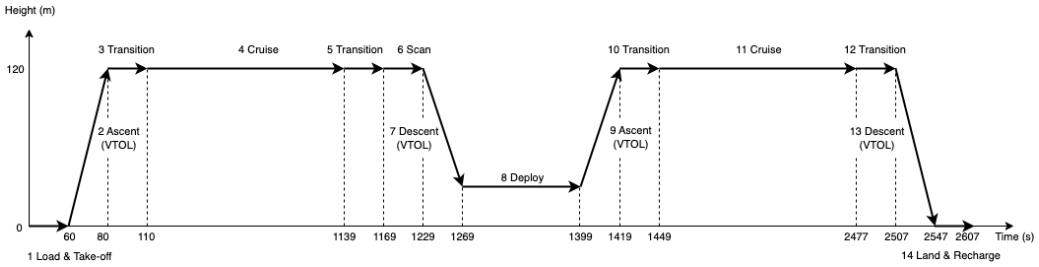

Figure 1: AeroShield Mission Profile

Preliminary Design Overview

The preliminary design phase consisted of conducting trade-offs for the aerogel configuration, the deployment mechanism, the autonomy of the system, power of the nest and the configuration of the UAV. The trade-off was performed based on criteria which reflected the requirements of the mission and stakeholders. The weights of each criteria are dependent on their importance in meeting the set requirements. The final trade-off results are summarised in Table 2.

[1] https://www.mqindustry.com/heat-resistant-aerogel-insulation-blankets

[2] https://civil-protection-humanitarian-aid.ec.europa.eu/news-stories/news/2023-among-5-worst-years-wildfires-europe-commission-report-shows-2024-11-19_en[accessed: 17/06/2025]

Table 2: Final Trade-Off Design

Trade-Off Component	Choice
Aerogel	Blanket
Deployment Mechanism	Winch + Magnet
Frame	Fixed Wing VTOL
Tail	Conventional Tail
Nest Autonomy	Manual
Nest Power	Bio-Fuel Generator

Detailed Design UAV

The detailed design phase of the UAV is divided into the different subsystems of the UAV, which include the deployment mechanism, power and propulsion, aerodynamics, stability and control, thermal and structures and materials. Additionally, all the hardware in the UAV had to be selected and correctly placed. The final UAV design is presented in Figure 2. The total mass of the UAV excluding the aerogel payload is $26.8 \pm 0.5[kg]$ for the oil spill mission and $26.6 \pm 0.5[kg]$ for the wildfire mission. The difference in mass arises from the modular design of the UAV.

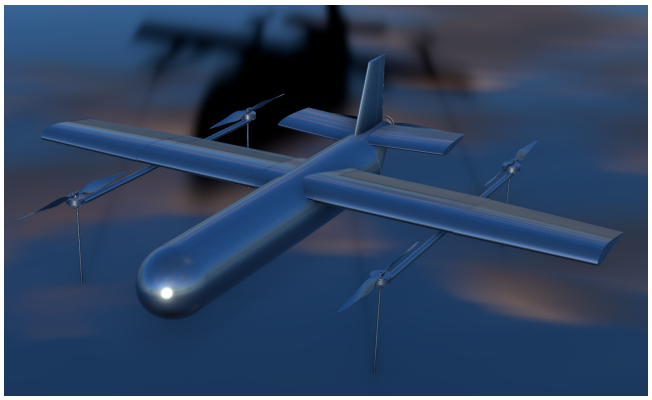

Figure 2: AeroShield UAV CAD Model

Hardware The UAV features a modular design, allowing it to be utilized for both wildfire and oil spill missions. For wildfire operations, the UAV is equipped with a DJI Zenmuse H20T thermal camera, while for oil spill missions, it uses a DJI Zenmuse L2 LiDAR sensor and an additional buoy system will be used to ensure retrieval in case of failure. The detection sensors are located within the nose cone. Additionally, all essential hardware, including the Onboard Computer (OBC), flight controller, GPS, and communication systems, is also housed in the nose cone. The winch motor is located at the front of the UAV. Due to the large aerogel blanket occupying most of the UAV's body, space is limited in the fuselage. As a result, the batteries are positioned within the wings alongside a heat sink to help regulate the UAV's internal temperature. Electrical cabling runs through the fuselage, wings, and propeller booms to connect to the actuators for the control surfaces and the propeller motors. For safety compliance, lights are installed on the tips of the wings and on the tail. Four VTOL propellers are located at the ends of the propeller booms including the electrical speed controller, A cruise propeller is mounted at the end of the tail.

Deployment Mechanism The deployment system is responsible for accurately deploying and positioning the aerogel blankets which weigh $3[kg]$. Each UAV carries the rolled-up adapted aerogel blanket inside the fuselage. The aerogel blanket has a length of $3.33[m]$, a width of $1.5[m]$ and a thickness of $3[mm]$ Two ferromagnets per top corner control the configuration and connection to the UAV, while a bottom weight ensures gravitational unfurling (having a total weight of $2.0[kg]$). The deployment system uses a dual-spool winch, pulleys, and electropermanent magnets to control the deployment and release of the aerogel, this allows for deployment from up to $15[m]$. The sheet positioning has an accuracy of $0.5[m]$ and correct overlapping is checked using the RGB camera. The deployment strategy is optimized separately for each mission scenario (oil spill and wildfire).

Power and Propulsion The propulsion subsystem was split into two sections the power required for VTOL and the power required for cruise. The power for VTOL applied during the ascent and descent to cruise altitude, as

well as during deployment. The cruise power applies during the cruise phase. It was assumed that the hovering power is the same as the VTOL power, as this is the worst-case and provides a conservative estimate. After performing the calculations, it was found that the total power required for VTOL is $3.48[kW]$ and for cruise it is $0.849[kW]$. In the transition between VTOL and cruise, it is estimated that both systems are active at once.

Based on the power required calculated the motor and propeller sizing was carried out. The motor that was selected was the U8 Lite L Efficiency Multirotor, it is used both for cruise and for the VTOL mode. This motor was chosen due to its high thrust to weight ratio of 1.5. Following the motor choice, a compatible propeller was also chosen. The propeller that was chosen was the G30*10.5 propeller. These propellers have a diameter of $762[mm]$ and a pitch of $268[mm]$. However, these propellers have an operating range of up to $65[C]$. Therefore, the propellers will have to be custom made with a different carbon fibre composite. Based on this combination of motor and propeller about 75% throttle will be needed during operation. Therefore the motors will use around $1.0[kW]$ at around $22[A]$. This matches the battery specifications which will be explained in a moment.

With the selection of the motors the power budget for the mission was calculated. This is shown in Table 3.

Table 3: Estimated power consumption per mission phase

Mission Phase	Power (kW)
Power Ascent	4.48
Power Transition	5.58
Power Scanning	4.37
Power Cruise	1.14
Power Descent	4.48
Power Deployment	4.49

With this power budget, the required energy was calculated which amounted to $1.08[kWh]$ for one cycle. With an efficiency of 90% the required energy of the battery was calculated to be $1.19[kWh]$. The actual battery capacity was calculated by multiplying the capacity by the Depth of Discharge (DoD), which results into a capacity of $1.43[kWh]$. Based on this the Tattu 17000 mAh 14S LiPo battery was chosen. It has a high energy density of $260[Wh/kg]$ and weighs $3.62[kg]$.

Aerodynamics The lifting surfaces were designed for a lift coefficient of 0.455 at a cruise speed of $100[km/h]$. The main wing consists of the E1233 aerofoil and is located at 53% of the fuselage length aft of the nose. The aerofoil is relatively thick to allow the battery to fit inside the wing, with a thickness to chord ratio of $\frac{t}{c} = 0.189$. The vertical and horizontal stabiliser both have a NACA0012 airfoil. Key aerodynamic values are highlighted in Table 5.

Table 4: Lift Curve Properties

Variable	Description	Value	Unit
CL_{max}	Maximum Lift Coefficient	1.31	$[-]$
α_s	Stall Angle of Attack	15.5	$[°]$
CL_α	Lift Curve Slope	0.071	$[1/°]$

Table 5: Cruise Drag Properties

Variable	Description	Value	Unit
CD_0	Total Zero Lift Drag	0.051	$[-]$
$\frac{CL}{CD}_{cruise}$	Lift over Drag Cruise	7.3	$[-]$
D	Drag Cruise	36.6	$[N]$

Stability & Control The UAVs must be stable and controllable in both cruise and VTOL mode, which requires separate considerations for each. For stability in cruise mode, the hardware placement and positioning of the wing and horizontal tail gives a position of the CG at 53% of the fuselage length and a neutral point at 55.7% of the fuselage, giving a static margin of 13.8%. For control, the UAVs are designed with conventional control surfaces: a rudder on the vertical tail, an elevator on the horizontal tail, and ailerons on the main wing. Considering gust controllability and manoeuvrability requirements, sizing of the control surfaces resulted in:

- A 0.9 vertical tail span rudder, with a chord-to-vertical-tail-chord ratio of 0.5 and a maximum symmetrical deflection of $25[°]$.

- A full horizontal tail span elevator, with a chord-to-horizontal-tail-chord ratio of 0.2, and a maximum symmetrical deflection of $15[^\circ]$.
- Ailerons placed between 58% and 97% of the half-wing span for both sides of the wing, a chord-to-wing-chord ratio of 0.3, and a maximum upwards deflection of $25[^\circ]$ with an aileron differential of 0.75.

For VTOL mode, the UAVs are controlled through the use of differential thrust or rotation across the 4 VTOL motors, as required. In this mode, controllability under gusts was determined to be the most critical case, given the need for precision deployment of the aerogel payloads. As the motors and propellers had already been chosen, however, it was only necessary to evaluate if the current configuration allowed for it. The critical disturbance moments from gusts hitting the UAVs were calculated for the yaw, pitch, and roll axes. It was determined that the designed configuration with the chosen VTOL motors was enough to counteract the disturbance moments for all axes, while still allowing for margin in thrust settings for additional manoeuvring or climbing.

Thermal The thermal regulation system allows the UAVs to perform in extreme environments with temperatures ranging from $-20°C$ to $140°C$. The design is driven by wildfire mission scenarios, with some adaptions for oil spill missions. Internally, insulation, phase-changing material, and heat sinks regulate the temperature to remain within a safe range of $-10°C$ to $45°C$ for all components. The thermal system is designed for minimum power and mass. Externally, reflective and insulating coatings are used to prevent components and the motors from the environmental heat in wildfire missions. While superhydrophobic coatings are used to limit ice accretion for oil spill missions.

Structures and Materials The main requirements driving the material selection for the UAV were operational temperature limits, weight, and sustainability. The materials considered included titanium, aluminium foam sandwich, carbon fibre, and glass fibre. Among these, glass fibre (Evopreg PFC502 with 43% fibre content) was found to be the most suitable option. Glass fibre possesses excellent strength properties, is recyclable, non-flammable, corrosion-resistant, can operate within a temperature range of $-40C$ to $-200C$, and has a density of $1840[kg/m^3]$. The glass fibre composite has a ply thickness of $0.26[mm]$. To achieve in-plane stiffness in all directions, three plies are necessary, resulting in a minimum manufacturable thickness of $0.78[mm]$.

The wing's internal structure was designed based on a wing box and Finite Element Method (FEM) analysis. This led to a spar placement of 17% and 60% of the chord, with three ribs positioned at the root, tip, and the location of the propeller booms on the wing. The thickness of the spars, ribs, and skin is uniformly $0.78[mm]$. Due to the relatively low loads on the wing compared to the strength of the material, the thickness is determined by the minimum manufacturable thickness for the composite. The wings are detachable to allow for compact storage within the nest. The detachment occurs slightly behind the propeller booms to ensure that in the event of a failure, the UAV can still fly using its VTOL propellers. The detachable part of the wing features a spar that extends outward and slides into designated locks in the inner wing structure, while click-in latches secure the connection. Additionally, a push-to-open access panel on the top of the wing enhances the modularity of the UAV, providing access to the batteries.

The fuselage measures $2.15[m]$ in length and has an inner diameter of $0.32[m]$, designed to accommodate the necessary hardware and payload. At the bottom of the fuselage is a deployment bay door that slides laterally inward, facilitating the deployment of the aerogel. The thickness of the fuselage is set at $0.78[mm]$, due to the same reasoning as the wing. A wing box, with a thickness of $4.68[mm]$, is located between the spars and serves to transfer and distribute loads from the wing to the fuselage.

The propeller booms are positioned on the wing to ensure adequate clearance between the tips of the propellers. Each boom measures $1.52[m]$ length, with an inner diameter of $3.0[mm]$ to allow space for the wires running through them, and a thickness of $7.5[mm]$. The UAV's landing gear consists of four rods placed beneath the motors on the propeller booms, each measuring $48.0[cm]$ in length and $9.0[mm]$ in diameter.

Detailed Design Nest

The nest of the UAV swarm consists of three 20ft ISO containers. One container is the command container, holding five UAVs, which includes the main power source, a $48[kW]$ bio-fuel generator with capacity of charging up to 67 battery charging stations, and a commanding cabinet that includes telecommunication modules, environmental controls, and powerful computing capabilities. The other two containers are purely storage containers, and can hold up to ten UAVs. The UAVs are stored using a drawer system, allowing for easy access for the operators, as well as a stable attachment during transport. The command container and storage container are visible in Figure 3 and Figure 4 respectively.

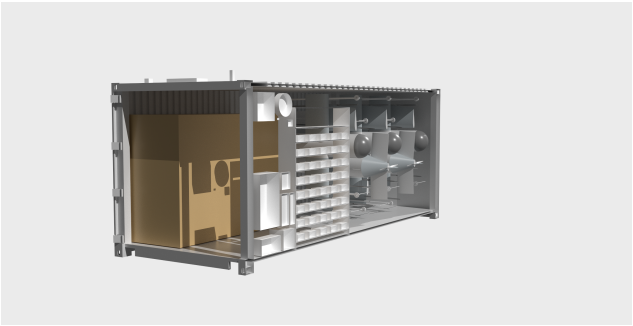

Figure 3: Configuration of command container of nest.

Figure 4: Configuration of storage container of nest.

RAMS

The RAMS analysis (Reliability, Availability, Maintainability, Safety) shows that AeroShield shows a reliability of 98.14% for a single mission, considering a mission time of 20 h, which is the mission time for wildfires. For oil spills the mission time is around 7 h, which thus results in a higher reliability. In order to achieve a reliability of 85% AeroShield can perform approximately eight missions. However, this is a conservative approach assuming that if one UAV fails the whole mission fails. Depending on the area of the wildfire or oil spill, there is a possibility that the mission can still be completed with a reduced number of UAVs, which increases the reliability of the system. Furthermore, due to the modular design of AeroShield, a high availability can be achieved. The nest also contributes to this high availability, since small maintenance such as cleaning sensors and control surfaces can be on site at the nest location. Scheduled maintenance, after eight missions, to check the critical components of the UAV. Potential hazards such as collision with environment and loss of control are identified and incorporated in the design. For example, critical systems such as the communication module are made redundant by including two different systems, and a buoy system is added to allow recovery of the UAV in case of a crash in water.

Sustainability

A life cycle assessment was performed to establish the carbon costs in the materials and big components used in AeroShield. The glass fibre, battery, and aerogel were taken into account, because they account for the most mass in the UAV, and the sustainability requirement set by the client dictated a 50% recyclable system. The carbon costs for the production of the UAV are then summed to be $405[kgCO_2]$, which is a very compatible number compared to other UAVs, as they generally range between 432 and $545[kgCO_2]$. The product development and manufacturing utilizes existing infrastructures to avoid environmental and economic costs for building new facilities. In end-of-life planning, the modularity of AeroShield plays a big role, because a handful of components can be easily taken out of the UAV and be recycled.

Performance

To evaluate the final performance, the relevant metrics are the total response time and the deployment rate. The total response time is defined as the time from the arrival on site to the time the last UAV lands, and the deployment rate is defined as either the mass of the oil absorbed at the end of the mission or the length of perimeter built. Both these metrics vary based on the specifics of the mission. To evaluate, a standard case is considered with 20 UAVs and six workers, which create a $500[m]$ perimeter or absorb $7000[kg]$ of oil. For the standard case, it is assumed that the UAVs will have to fly the maximum range of $20[km]$ in order to get to the deployment location.

For the total response time this results in seven hours for the oil spill case, and 20 hours for the wildfire case, assuming a firebreak width of $3[m]$ is required. The deployment rate is $944[kg/h]$ for oil spills and $24[m/h]$ for wildfires.

Verification and Validation

Verification and validation ensure that the tools for analysis and design developed by the team work as intended and apply to the real-world AeroShield mission. First, the followed verification procedures, consisting of unit, module, and system-wide tests for the design tools, are outlined. These tools include UAV sizing, nest sizing, and performance analysis. Additionally, future design goals for the expansion of the operational performance analysis tool are set, including, for example, the addition of oil-spill and wildfire spreading dynamics to optimize the deployment strategy around them. These expansions are then paired with planned verification procedures.

Finally, mission-wide verification and validation procedures are outlined to evaluate the performance of the entire AeroShield system in a real-world mission scenario. To this end, verification is focused on end-to-end

mission simulations with all components of the system. Validation is based on an incremental approach, starting with small-scale test fires or oil spills in controlled environments, and ending with concurrent testing in emergency-response scenarios for non-critical applications. For instance, this latter type of tests includes the testing of wildfire barrier creation in non-critical sites threatened by a wildfire, while fire departments focus on the main response with ground crews and manned aircraft. This approach to verification and validation allows for the proper assessment of the functioning of the designed AeroShield system.

Business Case Evaluation

AeroShield's business model combines one-time hardware sales with recurring services to give customers a clear cost-per-mission advantage and investors a predictable cash-flow. AeroShield (20 UAVs with the three container nest) is priced at €$850,000$ for wildfire missions and €$920,000$ for oil spill missions (the cost difference comes from the oil spill UAVs requiring more expensive hardware). A 25% margin is built into the price which includes manufacturing cost. Clients then pay €$10,000$ for initial three-person operator training (renewed annually at €$5,000$) to earn a certificate that is required to keep the system under warranty and authorises operators to perform first-line repairs, such as swapping propellers or sensors. This training teaches how AeroShield is operated, emergency-response drills, field-level hardware repair, and practical changes for software updates for that year. Clients also buy proprietary aerogel blankets at €12.24 each (20% profit margin) that are made to be compatible with AeroShield's deployment mechanism. For wildfires, this delivers partially reusable firebreaks at €$4,633[1/km]$, which is twice the wage-only cost of firefighting ground crews, yet non-stop deployable. AeroShield also lands far below the price of the €30 million firefighting water-scoopers[3]. For oil spills, the same blankets remove oil for €$0.30[1/L]$ (equivalent to €312.59 per ton of oil), which comes out more than 90% cheaper than sorbents, beating the cost of oil skimmers by over 47 times, while remaining reusable at 85% capacity for at least six cycles.

With a €2 million investment to cover the final €0.5 million of R&D and 12-18 months of fixed overhead, AeroShield reaches cash-flow break-even in 36–62 months, depending on demand. In the conservative case, after 5 years, the yearly profit is just over €1.78 million. The optimal case has the profits climb to €3.10 million by year 5, a 155% yearly return on the original investment. Pursuing EU grants could offset a large part of the costs and accelerate growth, pulling the break-even point forward, but is not included in the projections as it is not guaranteed.

Post Design Process

After the design process, steps like contacting potential customers, manufacturing and validating prototypes and eventually selling the product will be undertaken. The finalisation of the cost breakdown is also done in the post design process. This stage also includes refining the cost breakdown and conducting R&D to establish a profitable revenue stream.

[3] https://www.euronews.com/my-europe/2023/09/17/will-the-eus-720-million-gamble-on-firefighting-planes-pay-off [accessed: 13/06/2025]

Acknowledgements

Group 26 is extremely grateful to Dr. Baris Kumru, for giving us the opportunity to work on this project, and guiding us through all the steps of the process. His expertise on structures and materials were to great value for our project. We would also like to give special thanks to Jane Ramirez and Ruben Meireles for coaching us through the system engineering process, and keeping us accountable to our tasks, as well as sitting through our meetings and answering (obvious) questions. We would also like to give a special shout out to Dimitris Apostolidis for the very tasteful beers on the Friday afternoons! We'd also like to recognise Ir. Calvin Rans for the help with the structural calculations. Finally, we would love to thank our family, friends, roommates, and other loved ones for pushing us through these ten weeks.

Group 26 Delft, June 2025

Contents

Nomenclature

Abbreviations

Abbreviation	Definition
CG	Center of Gravity
DSE	Design Synthesis Exercise
EOL	End-of-Life
ESC	Electronic Speed Control
EPM	Electro-Permanent Magnet
FC	Flight Controller
FEM	Finite Element Method
FFD	Functional Flow Diagram
FM	Figure of Merit
GFRP	Glass Fibre Reinforced Polymer
GPS	Global Positioning System
IPS	Ice Protection System
ISO	International Organisation for Standardisation
LCA	Life Cycle Assessment
LiDAR	Light Detection and Ranging
MAC	Mean Aerodynamic Chord
MTOW	Maximum Take-Off Weight
OBC	Onboard Computer
PCM	Phase-Changing Material
PSO	Particle Swarm Optimisation
PDB	Power Distribution Board
PEEK	Polyetheretherketone
PSO	Particle Swarm Optimisation
PTFE	Polytetrafluoroethylene
RAMS	Reliability, Availability, Maintainability, Safety
R&D	Research & Development
RGB	Red, Green, Blue
ROC	Rate of Climb
RPM	Rotation per Minute
SHP	Super-Hydrophobic
T/W	Thrust over Weight
UAV	Unmanned Aerial Vehicle
VTOL	Vertical Take-Off and Landing

Abbreviation	Definition
DoD	Depth of Discharge

Symbols

Symbol	Definition	Unit
A_{eff}	Effective area	$[m^2]$
A_m	Cross sectional area	$[m^2]$
AR	Aspect ratio	$[-]$
b	Span	$[m]$
C	Costs	[]
C	Discharge rate	$[\frac{m^3}{s}]$
C_D	Drag coefficient	$[-]$
c_{d_0}	Zero-lift drag	$[-]$
C_L	Lift coefficient	$[-]$
C_{L_α}	Lift-curve slope	$[\frac{1}{rad}]$
$C_{l_{\delta_\alpha}}$	Aileron roll moment control derivative	$[-]$
C_{l_p}	Roll stability derivative	$[-]$
C_Q	Non-dimensional propeller torque coefficient	$[-]$
C_P	Non-dimensional power coefficient	$[-]$
c_w	Chord wing	$[m]$
d_a	Aileron differential	$[-]$
DoD	Depth of discharge	$[\%]$
E	Energy	$[J]$
E	Young's Modulus	$[Pa]$
e	Oswald efficiency factor	$[-]$
F	Force	$[N]$
FF	Form factor	$[-]$
h	Altitude	$[m]$
h_{air}	Thermal convection coefficient	$[\frac{W}{m^2 \cdot K}]$
I	Current	$[A]$
I	Moment of inertia	$[m^4]$
k	Thermal conductivity	$[\frac{W}{mK}]$
L	Length	$[m]$
L	Lift	$[N]$
M	Moment	$[Nm]$
M_D	Pitch disturbance moment	$[Nm]$

Symbol	Definition	Unit
m	Mass	$[kg]$
N	Reaction moment	$[Nm]$
n	Load factor	$[-]$
n_{batt}	Number of batteries	$[-]$
Nu	Nusselt number	$[-]$
P	Power	$[W]$
Pr	Prandtl number	$[m^2/s]$
Q	First moment of area	$[m^3]$
$\dot{Q}$	Heat dissipation	$[W]$
q	Dynamic pressure	$[\frac{kg}{ms^2}]$
R	Radius	$[m]$
R	Range	$[m]$
R	Reliability	$[-]$
R	Thermal resistance	$[\frac{K}{W}]$
Re	Reynolds number	$[-]$
ROC	Rate of Climb	$[\frac{m}{s}]$
S	Surface area	$[m^2]$
T	Temperature	$[K]$
T	Thrust	$[N]$
t	Thickness	$[m]$
t	Time	$[s]$
u	Horizontal velocity	$[m/s]$
V	Battery potential	$[V]$
V	Shear force	$[N]$
V	Velocity	$[m/s]$
V	Volume	$[m^3]$
W	Weight	$[N]$
w	Width	$[m]$
h	Height	$[m]$
α	Angle of attack	$[rad]$
β	Sideslip angle	$[rad]$
δ	Deflection	$[^\circ]$
η	Efficiency	$[-]$
θ	Angle of cutout	$[rad]$
$\Lambda_{0.5c}$	Sweep angle at half cord	$[rad]$
λ	Failure rate	$[\frac{1}{h}]$

Symbol	Definition	Unit
ρ	Density	$[kg/m^3]$
σ	Stress	$[Pa]$
τ	Shear strength	$[Pa]$
ω	Angular velocity	$[\frac{rad}{s}]$

1

Introduction

Due to rising global temperatures from climate change, wildfires have now become ever more frequent and devastating in Europe. Therefore, there is a growing need for effective technologies to both prevent or mitigate their consequences. A particular strategy for wildfire mitigation is containment, where a barrier is created to prevent the spread of a wildfire without necessarily actively suppressing it. To this end, aerogel emerges as a novel and high-performance material for such barriers given its lightweight and extremely insulating properties. This lead to the project objective statement of this report: ”To develop a sustainable and autonomous swarm of at least 20 UAVs capable of deploying aerogel for mitigating wildfires and oil spills with a range of at least 20 km, by 10 students in 10 weeks.” AeroShield, a system consisting of a swarm of autonomous UAVs to contain wildfires by deploying aerogel blanket barriers, is the team’s solution to leverage aerogels’ properties for a rapid response to spreading wildfires. Additionally, given the extremely hydrophobic and equally lipophilic characteristics of aerogel, the same system can be used in an entirely different market: oil spill absorption and containment.

This report presents the complete design cycle of AeroShield, including the design of the UAVs, the nest, the mission, and the business plan. First, in chapter 2, the financially viability of AeroShield will be investigated. Then the requirements and mission definition will be covered in chapter 3 and chapter 4. Next, the preliminary design will be quickly summarised in chapter 5, after which the system overview of AeroShield will be presented in chapter 6. Chapter 7 goes into the details of the deployment mechanism, and then the subsystems of the UAV will be discussed: power and propulsion in chapter 8, lifting surface design in chapter 9, stability and control in chapter 10, structures and materials in chapter 11, and the thermal regulation in chapter 12. Following this, the system integration of the UAV is explained in chapter 13. Then, the nest will be designed in chapter 14, the mission logistics will be set up in chapter 4, and the mission performance will be explained in chapter 16. Thereafter, the RAMS and technical risk assessment will be performed in chapter 17 and chapter 18, respectively. Chapter 19 will comprise of the verification and validation methods, and chapter 20 includes the production plan of AeroShield. Finalising the design, the last chapters will contain the business case evaluation (chapter 21), the sustainability analysis (chapter 22), and the post-design steps (chapter 23).

Altogether, this report brings together the technical, operational, and commercial aspects of AeroShield. It demonstrates how innovative materials and autonomous UAVs can be combined into a practical solution for real-world problems like wildfires and oil spills. The goal is not only to demonstrate the system’s feasibility but also to highlight its potential impact across multiple industries.

2

Market Analysis

In order to ensure that AeroShield is financially viable, it is crucial to conduct a market analysis. At first, an overview of the current market trends for aerogel (section 2.1), wildfires (section 2.2), and oil spills (section 2.3) are given. Next, an analysis of the potential market position of AeroShield is described in section 2.4. Lastly, section 2.5 presents a SWOT analysis to determine AeroShield's strategic position in the market, and section 2.6 describes its potential customers.

2.1. Aerogel Market Analysis

Aerogels are synthetic, porous, ultralight materials characterized by extremely high porosity, low density, and ultra-low thermal conductivity. They are produced by removing pore fluid, commonly methanol or ethanol, from a gel, resulting in a nanoporous structure with air compromising 80 to 99% of the material. Common aerogel types include silica, polymers, and carbon. Among these, silica aerogels dominate the market, accounting for 64.9% of the global revenue share in 2024. This dominance is attributed to their beneficial chemical properties, including a high specific surface area, enhanced porosity, low density, reduced dielectric constant, and excellent heat insulation capabilities [1]. AeroShield will use aerogel blankets which have a density of 0.2 g/cm^3 and a thermal conductivity of $0.02[W/mK]$ [1].

The global aerogel market was valued at USD 1.38 billion in 2024 and is projected to grow at a robust compound annual growth rate (CAGR) of 17% from 2025 to 2030 [1]. The market is partially consolidated, with a limited number of suppliers. Aspen Aerogels is the market leader as of 2025 [1, 7].

North America led the market with a 44.4% revenue share in 2024. Europe accounted for 29.9% of the market in 2024 [1]. The aerospace, automotive and housing sectors play a significant role in this demand, as they seek lightweight, high-performance insulating materials.

Aerogels are widely used across various industries, such as the oil and gas, construction, automotive, aerospace and marine industry. The oil & gas sector represented the largest market share at 61% in 2024 [1]. Aerogels are highly valued for their exceptional thermal insulation properties, making them ideal for building insulation and industrial thermal protection. Their low density and high efficiency also align with global efforts to reduce environmental impact, offering a sustainable solution for various industries aiming to lower their carbon footprint.

The main drawback of aerogel is that it is expensive to manufacture. Granulated or powdered aerogels are generally cheaper. Online marketplaces have powder price ranges of $10-$100 per kilogram, and $5-$35 per square meter of blankets or sheets, depending on thickness and quality [8].

2.2. Wildfire Market

Europe has experienced a troubling rise in the frequency, intensity, and unpredictability of wildfires. Recent years have seen catastrophic events, with 2023 marking the largest single wildfire ever recorded in the EU, near Alexandroupolis, Greece [9].

Climate change is a key driver behind these shifts, contributing to longer fire seasons, more intense fires, and the emergence of wildfires in areas previously unaffected. The traditional June–September season now extends into early spring and late autumn, creating sustained pressure on emergency services [2].

Burned area statistics reflect this challenge: in 2022, over 837,212 hectares were affected, with 43% in protected Natura 2000 areas [3]. Although this decreased to 504,002 hectares in 2023 and 419,298 hectares in 2024, both years remained above the long-term average [4] [10]. Portugal alone saw 100,000 hectares burned

[1] https://www.mqindustry.com/heat-resistant-aerogel-insulation-blankets

[2] https://civil-protection-humanitarian-aid.ec.europa.eu/news-stories/news/2023-among-5-worst-years-wildfires-europe-commission-report-shows-2024-11-19_en[accessed:17/06/2025]

in just one week in September 2024. Natura 2000 sites continued to account for a large share of damage. Furthermore, 2023 also recorded 41 wildfire-related deaths, including both civilians and fire-fighters.

Therefore, while recent statistics may suggest a reduction in total wildfire area burned, climate change is contributing to longer wildfire seasons and sustained high levels of risk for both protected plants and animal species, as well as humans.

The challenge of mitigating wildfires is the rapid spread of the wildfire and the hard-to-reach locations on which wildfires occur. Wildfires spread on average around $22[km/h]$ [11], this number can be even further increased depending on weather conditions and locations. Therefore, a quick containment or mitigation method is needed for the fire before emergency services can arrive, especially in cases where it is difficult for them to reach.

Wildfire Mitigation Competitors

The market of UAVs used for wildfire mitigation is less occupied. Main competitors in this field are ALTA X and the Sap UAV. The ALTA X UAV is used by the US fire department. It deploys small balls, which are ignited, intentionally creating a fire [12]. The purpose of this fire is to burn a small patch of vegetation to create a buffer zone for the fire, to prevent the spread of the wildfire. Another mitigation strategy is directly combating the fire with a fire retardant. The Sap UAV is an example of this. It sprays water, pumped from a fire truck, on the fire, thereby extinguishing it. This UAV is in the final development stage, but yet to be implemented in real wildfires [13]. Other solutions being developed involve dropping balls with fire retardant [14].

It is also important to mention that for wildfire mitigation competition, AeroShield also faces competition from many other wildfire management products (not necessarily only technologically advanced products). This is due to the way wildfire mitigation is funded. Funding is provided per year from one central budget. The organisations responsible for wildfire management then spend this budget on what is necessary to manage wildfires. This means that AeroShield is in direct competition with all other firefighting technologies.

2.3. Oil spill Market

Oil spills are the result of several different causes. The most common cause is simply due to natural seeps. These natural seeps account for approximately 50% of all spills[15]. However, their impact on the environment is minimal because lifeforms in these areas have adapted to the oil in the water [16]. Next to natural leaks, the largest percentage comes from tanker spills (8%). Other sources, such as pipeline leaks, accidents during extraction, and vessel operations account for smaller amounts. Historically, the largest spills have occurred during oil extraction operations, but due to improved regulations and technology, it only accounts for 3% of the total petroleum spills [15].

Looking more specifically at the data regarding oil tanker spills, it can be seen that the number of oil spills has reduced significantly over the last 50 years. When considering large spills (over 7 tonnes), the number has actually reduced by 90% as shown in Figure 2.1a. Similar trends can also be seen in the actual volume of the oil spills. It should be noted that the available data for oil spills considers larger spill incidents because smaller spills are more difficult to track and document. Tanker oil spill data shows that the largest portion of accidents are caused by allision or collision (Figure 2.1b) [5].

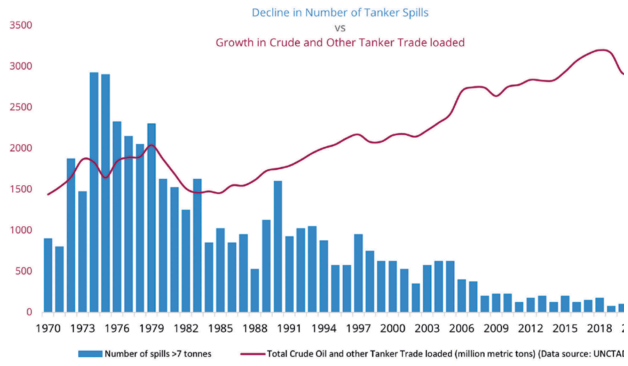

(a) Oil spills from tankers from 1970-2024.

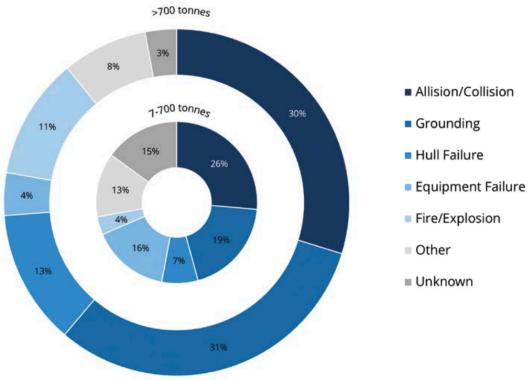

(b) Tankers oil spill causes for different size spills.

Figure 2.1: Trends for tanker oil spills between 1970 and 2024 based on ITOPF data [5]

Although the oil spill market is decreasing, effective containment and removal of oil spills are essential for preventing damage to marine ecosystems. Oil contains chemical and toxic components, and can thus affect

marine life internally through ingestion or inhalation, and externally through skin and eye irritation. Additionally, oil can also smother small fish or invertebrates, as well as coat feathers and fur of birds and mammals, reducing their ability to maintain body temperature [6].

The challenge of containing oil spills is the rapid spread of the oil when it hits the water. The effectiveness of oil spill containment is influenced by the time it takes from the initial spill until it is contained. This also includes the time it takes for equipment and personnel to transport them to the site [17]. Additionally, the ability to be able to deploy mitigation technologies in various terrain conditions is vital. Oil spills can happen in hard-to-reach marine conditions, such as deep-sea environments or isolated coastlines (shallow waters) [18]. This makes cleaning logistically challenging, and hinders mitigation efforts. A fast response method to operate in various terrain conditions is thus required.

Oil Spill Mitigation Competitors

Similarly to wildfire control, UAVs are currently used for mainly detection rather than mitigation. They are used to monitor certain areas to detect oil spills and to map larger spills after a major leak [19]. For these types of purposes, many different commercial UAVs exist, such as the Parrot ANAFI USA, DJI Matrice 300 RTK, or eBeeX. These types of UAVs are built to fly long distances and carry high-resolution camera's and sensors to provide high coverage [20, 21, 22]. For the mitigation of oil spills there are currently no solutions based on the use of UAV's. Therefore, using UAVs to mitigate or contain oil spills is a relatively new concept, therefore demonstrating a market gap.

Another competitor that should be considered is Unmanned Surface Vehicles (USV). These vehicles are more commonly used for oil spill mitigation. Generally, the USVs are used to deploy traditional oil spill mitigation methods such as containment booms or skimmers. One of the leading companies in this sector is L3Harris [23]. An example is the C-TUG 3, which was deployed by a major oil company to tow an oil containment boom. It has onboard detectors that can be used to monitor the spill and can even operate in the harshest conditions. It can be deployed in minutes, enabling rapid response to spills. Furthermore, it does not require any additional manned intervention for recovering the vehicle [24]. These vehicles would fulfil the same purpose as the AeroShield UAVs, creating direct competition with a proven concept.

Besides the autonomous competition, the UAVs would also compete with the more traditional methods (the manned boats), which use skimming and booming, chemical and sorbent dispersions, in situ burning, and bioremediation [25]. Skimming and booming requires the oil to be contained by booms, from which it is then picked up by a skimmer. The skimmer surface attracts the oil and then transfers it into a tank [25]. Chemical dispersions usually use vehicles like planes that release chemicals onto the oil spill, breaking down the oil into smaller droplets, and thereby allowing it to mix more easily into the water. It is usually done so that less oil stays at the surface of the water, where it could affect birds, fish, or drift into vulnerable coastal areas. However, it might adversely affect marine life [25]. During in situ burning, the spilled oil is burned. The success of the mission is highly dependent on collecting a thick enough layer of oil to maintain a sustained burn. However, overall, burning the oil releases a lot of smoke and therefore might not be an equal competitor, especially in terms of sustainability [25]. Sorbents are inert, insoluble materials that absorb the oil. One organic example is peat moss, which can absorb up to 15 times its weight in oil, although synthetic sorbents can absorb up to 70 times their weight. Sorbents have to be retrieved and disposed of properly unless they can biodegrade, such as peat moss; however, this process takes years. Lastly, there is bioremediation, where bacteria that are capable of degrading oil-related pollutants are released.

2.4. AeroShield Market Position

Based on the market analysis, five market needs can be identified, which include mitigation effectiveness, accessibility, response time, and human risk. Based on these needs, it can be assessed where AeroShield fills a gap in the market. Additionally, the cost is evaluated, since this influences whether potential customers perceive the product as a reasonable and viable investment.

The primary objective of a disaster response is the thorough removal or neutralisation of the hazard. For wildfires, this does not only include extinguishing fires, but can also mean preventing their spread in order to protect ecosystems and human settlements [26]. For oil spills, effective containment and removal of the oil is essential, preventing damage to marine ecosystems. All of these factors fall under the criteria of mitigation effectiveness. Note that at this stage of the design a rough estimate will be made, a detailed evaluation is performed in chapter 16.

Accessibility refers to the ability to deploy mitigation technologies in various terrain conditions. As wildfires often occur in remote locations, it can be challenging for ground crews to effectively reach the affected areas with the right equipment [26]. Similarly, oil spills can happen in hard-to-reach marine conditions, such as deep-sea

environments or isolated coastlines (shallow waters) [18]. This makes cleaning logistically challenging, and hinders mitigation efforts.

Due to the rapid spreading of both wildfires and oil spills, a key need for a wildfire or oil spill mitigation solution is for a fast response time. The response time consists of detection, transport, deployment, and the operation itself, which all need to be done as quickly as possible.

The safety of the team involved in the disaster mitigation is another key criteria for a successful solution to the market need. Wildfires invoke several human risks, including intense heat, smoke inhalation and the risk of entrapment. Oil spills on the other hand may expose workers to toxic substances, posing a risk of chronic health effects [27].

AeroShield for Wildfire Mitigation

Based on the wildfire market and mitigation competitor analysis, it can be observed that there is a gap in the market for a low-response time, high-accessibility and low-human-risk solution for wildfire mitigation. AeroShield, being a UAV-based system could offer several advantages to the market.

Mitigation Effectiveness

The aerogel blanket has a thermal conductivities as low as $0.02[W/mK]$, better than mineral wool or fibreglass [8]. Aerogel is thus very resistant to fire and can form a fire resistant barrier. The blanket is also exceptionally light with a density of 0.2 g/cm^3 [3]. This makes it easy to transport with UAVs. Each UAV carries an aerogel blanket of size $3.33[m] \times 1.5[m]$. Assuming a UAV swarm of 20 UAVs, this results in a conservative $100[m^2]$ coverage area per swarm deployment.

Accessibility

Theoretically, AeroShield can reach any type of terrain, as long as there is a suitable point to locate the nest. This includes steep terrain such as mountains and ravines (which traditionally would be highly inaccessible for ground crews), along with dense forests, isolated rural structures, and night-time operations, which are not always safe for crewed aircraft. AeroShield significantly extends the operational range far beyond that of the ground crews, while allowing for precise fire protection.

Response time

Similar to traditional methods, it will still take time to transport the swarm to a location that is within range of the disaster. The benefits in response time can be observed in the actual operation when the UAV swarm has been deployed. The swarm will be able to fly to the target, analyse the situation and carry out the required response. Unlike traditional methods, the UAVs will be able to approach the fire more closely in a short time. Furthermore, the UAVs allow for quick redeployment if the batteries are exchanged and are not limited by human recovery times. Finally, if nests are placed in high risk areas pre-emptively, the response time would be reduced even further.

Human Risk

AeroShield removes human exposure from the frontline entirely. The ability for autonomous operation eliminates the need for human involvement, thereby greatly reducing the risk for injury or deaths. It can also be used to protect ground crews if they get caught somewhere in a fire. The UAVs can be deployed to create a barrier around the crew and their equipment giving them time to find an escape route or call for help.

Cost

The cost of AeroShield can be evaluated based on buying the single product. The cost of AeroShield, which includes the nest and the 20 UAVs, is approximated at €$850,000$ (chapter 21), which is significantly lower compared to for example a fire fighting aircraft such as the Canadair CL-415 which start at around $\$30$ million[4]. As another price reference, the cost of buying a new firefighting truck can vary between $\$200,000 - 1$ million[5]. A more detailed cost analysis will be given in chapter 21.

AeroShield for Oil Spill Mitigation

Based on the oil spill market and competitor analysis, it can be observed that there is a gap in the market for a low-response time, high-accessibility and low-human-risk solution for oil spill mitigation. AeroShield, with its transportable nest could offer several advantages to the market.

[3] https://www.mqindustry.com/heat-resistant-aerogel-insulation-blankets[accessed:17/06/2025]
[4] https://en.wikipedia.org/wiki/Canadair_CL-415[accessed:17/06/2025]
[5] https://www.fentonfire.com/blog/fire-truck-cost/[accessed:17/06/2025]

Mitigation Effectiveness

Silica aerogels are able to absorb large amounts of oil compared to its weight. High absorption can be achieved by modifying aerogels, with for example, fluorocarbon functional groups, to achieve a ratio of 1:237, meaning 1 gram of aerogel can absorb up to 237 g of oil [28]. However, aerogels absorption capacities range anywhere from $2[g/g]$ to +$200[g/g]$ so knowing and picking the Aerogel with a high capacity is important.

Oil spills are typically categorised in small (<7 tons), medium (7-700 tons) and large sizes (>700 tons). Considering a 700 ton oil spill, and using silica aerogels, around 70 tons of aerogel is needed at an absorption capacity of $10[g/g]$. The UAV can carry at most $3[kg]$ of aerogel. This means that with a swarm of 20 UAVs, the total swarm has to go back and forth around 1167 times in order to fully contain the oil spill. Looking at a small sized oil spill of 7 tons, 12 swarm deployment cycles are enough to fully contain the oil spill.

Note that the oil containment effectiveness can be decreased significantly when winds and water currents spread the oil. In fact, oil can travel more than $30[km]$ in a single day and thus cover a large area [29]. However, the effectiveness is also highly dependent on when the UAV response takes place after the oil spill. If the response is immediate, the oil spill doesn't have enough time to spread and less UAVs are needed.

Response Time

The response time for oil spills can vary significantly depending on the cause, conditions, and severity. For large spills, the response is generally quite slow, such as in the Deepwater Horizon oil spill. Due to the severity of these incidents, coordination between many different organisations are required, therefore taking up time to plan and implement the strategy. The actual clean-up can then also take multiple years due to the amount of oil that is released into the environment [30].

The placement of AeroShield on oil tankers and oil rigs would provide a quick response to contain or mitigate the oil spill, before it has a chance to spread. AeroShield can slow down the spread of the spill until other clean-up methods can reach the scene and start mitigating.

Accessibility

Since AeroShield is a UAV-based system, it offers a significant advantage in accessing and operating in shallow water environments: areas where conventional mitigation methods using boats are often ineffective or not able to operate. Furthermore, when AeroShield is located on oil rigs and oil tankers, it can contain oil spills in hard-to-reach and deep-sea environments.

Cost

AeroShield itself costs around €$920,000$ with each aerogel blanket costing the client €12.24 (chapter 21). AeroShield costs €312.59 to remove a ton of aerogel, which is equivalent to €0.30 per litre of oil removed. Looking at the traditional oil spill mitigation methods, sorbents shows the lowest cost with €3520 per ton, and skimming/booming has the highest cost with €14.34 per litre[31]. It should be noted that depending on the reusability of the aerogels, the mission costs could be decreased significantly.

Human Risk

AeroShield poses minimal to no risk to human operators in comparison to competitors. AeroShield is able to contain the oil spills autonomously, human interaction is only needed for taking the UAVs out of the nest and loading them with aerogel. This does not pose a great human risk as human risks consist of exposure to hazardous substances from oil by-products, dispersants, detergents and degreasers, and the risk of slipping, tripping, or falling [32].

2.5. Market Analysis Conclusion

To investigate AeroShield strategic market position a SWOT analysis was performed. The first row of Table 2.1 discusses the internal strengths and weaknesses of the AeroShield product. The effect of the market trends and competitors is considered in the second row, which describes the external opportunities and threats.

Table 2.1: AeroShield SWOT Analysis

	Helpful	**Harmful**
Internal	Strengths • The team has a direct connection with TU Delft, therefore increasing access to knowledge, expertise and funding. • Swarm UAV technology provides larger scale mitigation methods through coordination than already existing single UAVs. • UAV technology allows for access in more remote and high risk areas. • The UAV will be made out of 50% recyclable materials and causes minimal damage to wildlife. This makes the product a more sustainable solution for wildfire and oil spill mitigation.	Weaknesses • The resources (time and money) available for this project are limited compared to the companies in the industry. • The product is designed for two very different environments, making it less optimal for each individual use case. • In case of large oil spills or wildfires, containing and mitigation them fully takes a considerable amount of aerogel and time. • UAVs operational conditions are limited when compared to large aircraft or non-air solutions. • There is no proof of concept aerogel solution, making it harder to raise additional funds to finance the development.
External	Opportunities • The project is the first swarm UAV natural disaster mitigation technology to market. This gives it the first mover advantage, helping the project get ahead of competition. • Wildfire mitigation is a growing market. Profitability will therefore be easier due to a growing market for solutions. • There is a market gap for autonomous wildfire mitigation. • The current methods for oil spill mitigation have a relatively slow response time, this means that a fast deploying solution would lead the market.	Threats • The wildfire market is hard to penetrate because of the small amount of designated governmental organisations, that must use a central budget for all aspects of wildfire mitigation. • There are already existing UAV competitors for wildfire mitigation, making it more difficult to achieve a greater market share. • There is already a wide range of mitigation methods available on the market for oil spill mitigation with which Aeroshield will have to compete.

The SWOT analysis shows that both the wildfire and oil spill mitigation markets are not easy to penetrate for a new product. Existing solutions are well tested and optimised for use in disaster response. In order to be successful the product will have to be designed to solve the problems that existing solutions do not address.

For wildfires, the main market gap that AeroShield could fill is the need for methods with high accessibility and low human risk. An UAV swarm can be the ideal solution to fill this gap, however, the costs will likely be a defining factor for success.

For oil spills, the main market gap that AeroShield could fill is the need for a fast deploying method that is able to reach various terrains such as deep-sea environments and shallow waters. This is achieved through the strategic location of the aerogel nest on oil tankers and oil rigs, which allows for a fast deployment and high accessibility. Furthermore, AeroShield shows strong promise in terms of cost, making it well-positioned to enter the market.

2.6. Potential Customers

In terms of wildfires, the government is typically the main authority responsible for overseeing wildfire control and mitigation efforts. As a result, they represent a significant potential customer. AeroShield could attract their interest because it has the potential to reach areas that are currently inaccessible. For instance, in the European Union, wildfire management is largely coordinated at the national level but receives significant support through the EU Civil Protection Mechanism and the rescEU reserve, which allocates centralized funding and equipment across member states for disaster response, including wildfires [33]. Considering, that the largest wildfires occur in southern Europe, potential local customers are the National Fire and Protection Services,

such as the Hellenic Fire Service in Greece.

For oil spills the most logical customers are integrated oil companies that perform drilling and transport of crude oils. This includes companies such as Shell, Chevron, British Petroleum (BP) and Total Energies. These companies are responsible for any spills from their rigs or tanker transportation. Placing AeroShield nests on their assets could therefore by an interesting mitigation method to limit the potential environmental damage of any spills.

Next to the primary customers described above another group of potential customers could be private emergency response companies. Companies such as O'Briens Response Management or the National Response Corporation focus on different types environmental disasters, including oil spills [34][35] and wildfires. This makes the duel application of AeroShield more interesting for these companies.

3 Requirements

The aim of this chapter is to list all requirements. The requirements are conditions which must be complied with. They are split into user, stakeholder and system requirements, which can be broken down further into subsystem requirements. The user requirements are presented in section 3.1. The stakeholders together with their requirements are discussed in section 3.2, and system and subsystem requirements are presented in section 3.3 and section 3.4, respectively.

3.1. User Requirements

The user requirements are summarised in Table 3.1. These requirements are defined by the client and are stated in the project guide [36]. Every requirement has a unique identifier. The first letter indicates that it is a user requirement 'U-XXX-XX'. The three-letter code in the middle, 'X-GEN-XX', indicates the category, and finally the 'X-XXX-01' provides the numbering within a category.

Table 3.1: User Requirements.

Category	ID	Requirement
General System	U-GEN-01	The UAV swarm shall consist of at least 20 drones capable of autonomous operation and communication.
	U-GEN-02	The UAV swarm shall coordinate deployment patterns for optimised coverage.
	U-GEN-03	A 'UAV nest' shall be designed for operational purposes.
Performance	U-PER-01	The UAV swarm shall withstand temperatures up to 140°C.
	U-PER-02	The UAV swarm shall have an operational range of at least 20 km from the deployment vessel.
	U-PER-03	The UAV swarm shall be able to operate under wind conditions up to 30 km/h.
	U-PER-04	The UAV swarm shall be able to operate under temperatures as low as -20°C.
	U-PER-05	The UAV swarm shall be able to operate within the operational range: 5–150 m.
Safety & Reliability	U-SAF-01	The aerogel shall be able to be retrieved without breakage after deployment.
	U-SAF-02	The UAVs shall be equipped with heat-resistant casings.
	U-SAF-03	The UAVs shall be water-resistant.
	U-SAF-04	The UAVs shall be able to operate in marine conditions.
Sustainability	U-SUS-01	The aerogel shall not increase the toxicity levels in marine ecosystems.
	U-SUS-02	The aerogel shall not leave behind any residue in the environment.
	U-SUS-03	The UAV swarm shall be powered by renewable electricity.
	U-SUS-04	The UAV shall consist of at least 50% recyclable components.
Engineering Budgets	U-BUD-01	The UAV shall have a production cost less than €50,000 (excluding raw materials).
	U-BUD-02	The UAV shall have a weight less than 25 kg.

Category	ID	Requirement
	U-BUD-03	The UAV shall have a maximum payload capacity of 5 kg.
Cost	U-COS-01	Total system cost must not exceed €3,000,000 (excluding aerogels and ground ops).

3.2. Stakeholder Requirements

In this section, stakeholders and stakeholder requirements are identified. These are essential to the project as they ensure that the results are relevant and usable. By identifying the stakeholders, it is ensured that all aspects of the project are considered carefully and no major oversights will be made regarding functionality. First, the stakeholders themselves will be discussed and in Table 3.2 these findings are formulated into requirements. Each requirement has an identifier, formatted as 'REQ-STH-XX' where 'STH' stands for Stakeholder and 'XX' indicates the number. The table also indicates the type of requirement. Three different types of requirements are identified [37]:

- Driving requirements: These requirements dominate the overall design of the mission and have a significant impact on the performance of the mission, cost, risk, and schedule.
- Killer requirements: These requirements drive the design to an unacceptable level. It these requirements are not met, they should be negotiated with the customer to reduce mission capability.
- Key requirements: Requirements that are of primary importance for the customer or that are expected to be a risk.

Coast Guard and Firefighters

These will be the main users of AeroShield. It is imperative for them that the swarm is effective, so that it can aid in their goal of putting out fire or removing oil. They will also probably be the owners and operators of the swarm, so they have a large stake in that the controls are not convoluted and that the storage and maintenance are reasonable. The coastguard also often hire external companies to aid in oil spill clean-up [38], so these also benefit. These also have a higher stake in the clean-up being low-cost, as they are commercial parties.

Wildlife & Marine Life

These stakeholders represent the need to limit damage to the environment. In case of wildlife, the park rangers can also be considered as stakeholders since the effective mitigation of the disasters is also part of the park rangers job.

The primary disturbance that UAVs (unmanned aerial vehicles) cause to wildlife and marine life is due to the noise they produce. Marine animals, such as dolphins, rely on sound waves for orientation, communication, echolocation, and threat detection. Noise generated by UAVs can interfere with these vital functions. Additionally, wildlife is also affected. For instance, black bears exhibit elevated heart rates in response to UAV sounds [39].

Oil Companies

Not only are oil companies usually responsible for oil spills, they are also the ones paying for clean-up [40]. Therefore, they have a high stake in this clean-up being both fast and cheap. They can be considered as one of the customers for AeroShield.

UAV and Aerogel production companies

The UAVs will have to be produced. This production should be manageable. If the design of the UAVs is overly complicated it will hinder or even prevent construction, especially in large quantities.

Government and Air Traffic Control

It is important that the AeroShield is in compliance with all laws and regulations surrounding UAV flight. If this is not the case, the UAV swarm will not be able to be deployed. For example, UAVs are not allowed in no-fly zones [41].

Because of the user requirement U-BUD-02 and U-BUD-03, the UAV will have a maximum take-off weight of 25kg. This means that the UAV will not enter in the "Open" EASA category, but the "Specific" EASA category [42]. Therefore, the UAV will need to show conformity with foundational requirements, and the UAV operator will need to obtain operational authorisation from the national aviation authority. For wildfire mitigation this will be easier, as the state itself will be the user of the UAV, and civil aviation rules may be waived under state flight exemptions. For oil spill clean ups this is slightly more difficult, as private companies will likely be operating the

UAVs, but is helped by the fact that in most oil spills the coast guard is aiding the mission. Furthermore, the UAVs will be used in emergency situations, and in both disaster situations they are located far from populations, meaning few to no people are possibly endangered by the UAVs. Thus, obtaining permission and compliance certificates for the UAVs will be made easier. For missions crossing borders, AeroShield must notify—and receive acceptance from—each Member State's aviation authority in advance, while maintaining remote-ID broadcasts and adhering to noise, altitude, and safety-zone restrictions.

Requirement Identification	Stakeholder	Requirement Description	Type
REQ-STH-01	Firefighters	AeroShield shall be able to help contain wildfires	Key
REQ-STH-02	Coast Guards	AeroShield shall be able to help clean up oil spills	Key
REQ-STH-03	Coast Guards and Firefighters	AeroShield shall be easy to operate, even in difficult weather	Key
REQ-STH-04	Coast Guards and Firefighters	AeroShield shall be easy to transport	Driving
REQ-STH-05	Coast Guards and Firefighters	AeroShield shall be easy to store	-
REQ-STH-06	Coast Guards and Firefighters	AeroShield shall decrease the time for disaster relief	-
REQ-STH-07	Wildlife and Marine Life	AeroShield shall minimize acoustic disturbance to wildlife and marine life	-
REQ-STH-08	Wildlife and Marine Life	AeroShield shall not cause lasting damage to the environment	-
REQ-STH-09	Oil Companies	AeroShield usage shall decrease oil spill clean-up costs	-
REQ-STH-10	Production Companies	The UAVs shall be commercially manufacturable at a reasonable cost	Driving
REQ-STH-11	Government and ATC	AeroShield shall follow laws and regulations.	Key
REQ-STH-12	Government and ATC	The UAVs shall not fly in restricted areas except with explicit permission	-

Table 3.2: Stakeholder Requirements

3.3. System Requirements

In this section the system requirements will be outlined. The system requirements are categorised into sustainability requirements, performance requirements, budget requirements, and safety and reliability requirements. Each requirement has an identifier in the following structure: 'REQ-SYS-XX', where 'SYS' indicates system and 'XX' indicates the number of the requirement. All requirements are formulated according to the VALID criteria (Verifiable, Achievable, Logical, Integral, Definite).

Table 3.3 lists the requirements and describes where the requirements are derived from, such as the stakeholder requirements and the user requirements. It also indicates if the requirement is considered a driving, key or killer requirement as explained in section 3.2.

Table 3.3: System Requirements

Identification	Description	Derived from	Type
Sustainability			
REQ-SYS-01	Aerogel shall release no more than 0.01 % by weight of particles between 100 nm and 10 nm.	U-SUS-02	–
REQ-SYS-02	Aerogel shall demonstrate no increase in marine toxicity (LC_{50}).	U-SUS-01	–
REQ-SYS-05	The nest shall source 100 % of its electricity from renewable energy.	U-SUS-03	Driving

Continued on next page

Table 3.3 — Continued from previous page

Identification	Description	Derived from	Type
REQ-SYS-06	The system shall comprise at least 50 % recyclable components by mass.	U-SUS-04	Key
REQ-SYS-07	The system shall be modular.	U-SUS-04	Driving
Performance			
REQ-SYS-08	The UAV shall be able to take-off within 3 × 3 m.	–	Driving
REQ-SYS-09	The UAV shall be able to take-off within a maximum of 60 s.	–	Driving
REQ-SYS-10	The UAV shall have a minimum lift of 130 % of MTOW [N].	–	Driving
REQ-SYS-11	The UAV shall be able to operate in conditions with wind speeds of up to 30 km/h.	U-PER-03	Key
REQ-SYS-12	The UAV shall have a range of at least 20 km.	U-PER-02	Key
REQ-SYS-13	The UAV shall be able to operate at altitudes up to 3000 m.	[43]	Driving
REQ-SYS-15	The UAV shall be able to deploy the aerogel with an accuracy of 0.5 m^2.	U-GEN-02	Driving
REQ-SYS-16	The UAV shall be able operate in a temperature range from –20 °C to 140 °C.	U-PER-04	Key
REQ-SYS-17	The UAV swarm shall be able to deploy 100 kg aerogel in 180 min.	–	Driving
REQ-SYS-18	The UAV shall be able to land within 3 × 3 m^2.	–	Driving
REQ-SYS-19	The UAV shall be able to operate in conditions with a humidity up to 100 %.	–	–
REQ-SYS-20	The UAV shall be able to reach 150 m in vertical distance from the ground.	U-PER-05	Driving
REQ-SYS-21	The UAV swarm shall be able to create a wildfire containment perimeter of 500 m within one day.	REQ-STH-01	Key
REQ-SYS-22	The UAV swarm shall be able to absorb 7000 kg of oil within one day.	REQ-STH-02	Key
Budget			
REQ-SYS-23	The UAV shall have a production cost less than €50 000 (excluding raw materials).	U-BUD-01	Key
REQ-SYS-24	Total system cost must not exceed €3 000 000 (excluding aerogels and ground ops).	U-BUD-02	Key
REQ-SYS-25	The UAV shall have a weight less than 25 kg.	U-BUD-02	Key
REQ-SYS-26	The UAV shall be able to pick up a payload of up to 5 kg.	U-BUD-03	Key
REQ-SYS-27	The UAV shall have a maximum total power usage of 4000 W.	–	Driving
Safety and Reliability			
REQ-SYS-28	The aerogel shall be 99 % recoverable after deployment.	U-SAF-01	Killer
REQ-SYS-29	The UAV shall be retrievable in case of a crash.	–	Killer
REQ-SYS-30	The internal electronics shall be protected by heat-resistant casings.	U-SAF-02	Key

Continued on next page

Table 3.3 — Continued from previous page

Identification	Description	Derived from	Type
REQ-SYS-31	The UAV shall conform to the standards of IP66 rating for electronic casings.	U-SAF-04	Driving
REQ-SYS-32	The UAV shall maintain full functionality in heavy rain conditions (7 mm/h – 50 mm/h) for <TBD> minutes at all angles.	U-SAF-04	Key
REQ-SYS-33	The UAV shall be corrosion-resistant up to <TBD> in salt-water environments.	U-SAF-04	Key
REQ-SYS-34	The UAV shall be able to operate under light sea spray (ISO 9227) for at least the duration of the UAV's lifetime.	U-SAF-04	Driving
REQ-SYS-35	The UAV shall be able to operate for 30 full-range cycles.	–	Driving

3.4. Subsystem Requirements

The subsystem requirements are categorised into the following subsystems: Power & Propulsion ('PRP'), Deployment ('DEP'), Nest ('NST'), Thermal ('THM'), Structure ('STR'), Communication ('COM'), Control ('CON') and Autonomy & Coordination ('AUC'). The subsystem requirements are listed in Table 3.4. Each requirement is assigned an identifier, and when applicable, the type of requirement is specified as either driving key or killer requirement. The identification follows the naming convention: 'REQ-SYS-XXX-XX', where the first 'XXX' represents the subsystem and the last 'XX' indicates the sequential numbering.

Table 3.4: Subsystem Requirements

Identification	Description	Type
Power & Propulsion		
REQ-SYS-PRP-01	The power subsystem shall indicate its battery charge level.	-
REQ-SYS-PRP-02	The VTOL propulsion subsystem shall provide a thrust of at least 1.2 times the MTOW.	-
REQ-SYS-PRP-03	The propulsion subsystem shall provide a minimum pitching moment of 20.4 Nm	-
REQ-SYS-PRP-04	The propulsion subsystem shall provide a minimum rolling moment of 52 Nm.	-
REQ-SYS-PRP-05	The propulsion subsystem shall provide a minimum yawing moment 12.23 Nm in VTOL.	-
REQ-SYS-PRP-06	The propulsion subsystem shall have a throttle resolution higher than 1 N.	-
REQ-SYS-PRP-07	UAV batteries shall be rechargeable from 20% to 100% in 2500 seconds.	-
REQ-SYS-PRP-08	The power subsystem shall be able to power all of the UAV electrical components for the duration of the mission.	-
REQ-SYS-PRP-10	The UAVs power source shall be replaceable.	Driving
REQ-SYS-PRP-11	The UAVs power source shall be able to connect to the nest power source.	Driving
Deployment		
REQ-SYS-DEP-01	The deployment mechanism shall ensure a secure connection to the aerogel during flight.	Driving
REQ-SYS-DEP-02	The deployment subsystem shall be able to pick up aerogel with dimensions 1.5 x 0.003 x 3.33 m³.	Driving

Table 3.4: Subsystem Requirements

Identification	Description	Type
REQ-SYS-DEP-03	The deployment subsystem shall provide an aerogel positioning accuracy of 0.5m.	Driving
REQ-SYS-DEP-04	The deployment mechanism shall not compromise the structural integrity of the aerogel payload	-
REQ-SYS-DEP-06	The deployment mechanism shall be capable of emergency release of the aerogel in case of critical failure	-
Structure		
REQ-SYS-STR-01	The structure's subsystem shall provide a secure connection to all other subsystems.	-
REQ-SYS-STR-02	The structure's subsystem shall use materials that maintain 95% of their stiffness in the operational temperature range.	Key
REQ-SYS-STR-03	The structure shall not degrade past its operational limit over a minimum of 50000 full-range load cycles.	Driving
REQ-SYS-STR-04	The critical structural elements shall be inspectable through non-destructive methods.	-
REQ-SYS-STR-05	The structure shall not yield under a UAV weight of 25 kg at a load factor of 3.5.	-
REQ-SYS-STR-06	The structure shall not yield, while supporting the payload at a load factor of 3.5.	-
REQ-SYS-STR-07	The structure shall not yield to dynamic loads during flight with a safety factor of 3.5.	-
REQ-SYS-STR-08	The natural frequencies of the UAV structure shall be outside of the frequency range created through all operational loads.	-
REQ-SYS-STR-09	The exposed UAV surfaces shall not be flammable	Key
Control		
REQ-SYS-CON-01	The UAV shall be controllable in flight on all three axes without payload.	-
REQ-SYS-CON-02	The UAV shall be controllable in flight on all three axes when carrying 0.015 m^3 of aerogel.	-
REQ-SYS-CON-04	The UAV shall remain stable while deploying the aerogel.	Driving
REQ-SYS-CON-05	The UAV shall be controllable during take-off.	-
REQ-SYS-CON-06	The UAV shall be controllable during landing.	-
REQ-SYS-CON-07	The UAV shall remain stable under gusts up to 30 km/h.	Key
REQ-SYS-CON-08	The UAV shall remain stable under disturbances from water sprays up to <TBD>.	Driving
Thermal		
REQ-SYS-THM-01	The thermal subsystem shall prevent ice from forming on the UAV.	-
REQ-SYS-THM-02	The thermal subsystem shall regulate the temperature of the motors such that it remains within the temperature range from -20°C to 60°C.	-

Table 3.4: Subsystem Requirements

Identification	Description	Type
REQ-SYS-THM-07	The thermal subsystem shall regulate the internal temperature of the wing and fuselage compartments such that they remain within the temperature range from -10°C to 45°C.	-
Communication		
REQ-SYS-COM-01	The UAV shall be able to transmit communication signals within a range of at least 7.5 km.	-
REQ-SYS-COM-02	The UAV shall be able to receive communication signals within a range of at least 7.5 km.	-
REQ-SYS-COM-03	The transmission loss will be a maximum of 2 bits/km.	-
REQ-SYS-COM-04	The UAV shall be able to communicate with other UAVs from the swarm at a range of at least 7.5 km.	Driving
REQ-SYS-COM-05	The nest shall be able to maintain a connection with the ground station with 0.1% information loss for the duration of the mission.	-
Nest		
REQ-SYS-NST-01	The nest shall be able to charge the UAVs in 42 minutes.	-
REQ-SYS-NST-02	The nest shall have enough capacity to charge the batteries of all UAVs at least one time.	Driving
REQ-SYS-NST-03	The nest shall be able to dock all UAVs at the same time.	Driving
REQ-SYS-NST-04	The nest shall provide sufficient attachment points for transportation.	Driving
REQ-SYS-NST-05	The nest shall be able to operate within a temperature range of -20 and 35°C.	-
REQ-SYS-NST-06	The nest shall be able to sustain 1.5g lateral accelerations	-
REQ-SYS-NST-07	The nest shall maintain structural stability during UAV deployment.	-
Autonomy & Coordination		
REQ-SYS-AUC-01	The UAV swarm shall be able to autonomously pick up the correct shape of aerogel.	-
REQ-SYS-AUC-02	The UAVs shall be able to navigate around obstacles autonomously.	Driving
REQ-SYS-AUC-03	The UAVs shall be able to detect fire.	Driving
REQ-SYS-AUC-04	The UAVs shall be able to detect oil in water.	Driving
REQ-SYS-AUC-05	The UAVs shall be able to autonomously adapt the deployment strategy to deploy the aerogel.	Driving
REQ-SYS-AUC-06	The UAV swarm shall be able to autonomously perform a takeoff sequence.	-
REQ-SYS-AUC-07	The UAV swarm shall be able to autonomously perform a landing sequence.	-
REQ-SYS-AUC-08	The UAV swarm shall be able to autonomously navigate to a specified GPS location.	-

4

Mission Definition

In this chapter the mission operations and logistics will be discussed. First, the functional diagrams are presented in section 4.1. Then, the mission strategy will be defined, this contains the deployment strategies for the wildfires, oil spills and any failure that might occur. Next, external operations are discussed that happen before, during and after deployment. After this the swarm logistics will be discussed. In this section different algorithms are defined which the swarm will incorporate. Lastly, the mission definition will be displayed. This consists of the mission timeline.

4.1. Functional Diagrams

The Functional Flow diagram (FFD) is visible in Figure 4.4. The FFD displays the three phases of AeroShield: the manufacturing phase, operable phase, and end-of-life phase, which form the top-level of the FDD. Two additional levels describe them in more detail. Aborted operations are visible in red. There is still a possibility to continue after aborting, providing that the system is inspected and able to safely continue. The Functional Breakdown Structure, visible in Figure 4.5, adds an additional level compared to the FFD, showing the subsystem-level. These fourth level functions are shown in white.

4.2. Mission Strategy

In this section the Mission Strategy will be further explained. First explaining the different deployment strategies for wildfires and oil spills. Then, outlining the failure strategies that the swarm will implement should a potential failure occur.

Deployment Strategy Wildfires

The UAVs are deployed one by one with a margin of time Δt in between them. The first UAV to reach the specified location will scan the area. The number of UAVs will be determined by the area that needs to be covered, and is a design parameter that the firefighting stakeholder can decide. This will be done by planning the route to scan the area using thermal scanners. Once the mapping is complete, this will be fed into a fire predictive algorithm which predicts the behaviour of the fire.

Once the spread rate and direction of the fire is determined by the algorithm, a perimeter will be established according to the spread and deployment rate of the entire swarm. The aerogel will be placed at a distance equivalent to the spread over one hour, plus a safety margin of $1[km]$. A target perimeter equal to the maximum perimeter achievable in one hour is used as input for the algorithm. For example, if the deployment perimeter rate is $30[m/h]$, the algorithm input is $30[m]$.

Once this perimeter is established all UAVs, including the two that were previously scanning, start deploying the aerogel by starting at the centre of the established perimeter. Once the perimeter is covered, all UAVs return and reload the aerogel. Then, the same number of UAVs scan the area again and establish a new perimeter to be covered. This cycle is repeated until the threat is neutralised or resources run out.

Deployment Strategy Oil Spills

For oil spills, instead of transporting the nest to the location of disaster, the nest stored on-site on oil tankers and oil rigs to minimise the response time. Similar to wild fires scenarios, a set number UAVs will scan the area, depending on the size of this area, to establish the spread distance of the oil spill from the initial spill location. This is done by oil detection scanners. Once the oil-covered area is established, the UAVs start deploying aerogel. Several UAVs will deploy along the perimeter of the oil spill to contain it. The remaining UAVs will deploy aerogel near the leak site to prevent further spread of the oil spill. The number of UAVs used for containment will be determined by the initial scan of the UAVs, taking two factors into account: the area covered by oil, and the distance from the nest. Once all the aerogel is deployed a third party will come and

retrieve the aerogel, aeroshield is not involved in this process. In most cases it will be a boat.

Failure Strategies

Failure strategies are built into the system architecture of the UAVs through distributed information sharing and collaborative decision-making, which is later elaborated upon in section 4.4. The use of UAVs in a swarm configuration introduces redundancy, ensuring that the failure of a single UAV does not compromise the mission. Other UAVs within the swarm can adapt and continue the operation, thereby maintaining the likelihood of successful mitigation. Each UAV operates semi-independently using local information as well as neighbour communication to avoid single points of failure, by using a consensus algorithm [44]. In the event a UAV fails during a wildfire mission, the UAV will be recovered by emergency services once the fire is extinguished. In the event a UAV fails during an oil spill mission, its onboard buoy system will activate to ensure that the UAV stays afloat. Both strategies are designed to prevent environmental contamination and ensure recoverability, as per REQ-STH-08.

4.3. External Operations

This section addresses the operational framework of the AeroShield mission. This consists of three phases: before, during, and after deployment.

Before deployment

Once a disaster is identified, the relevant authorities will be alerted to assess whether AeroShield should be deployed for mitigation. For the oil spill missions, the nest is either pre-positioned on an oil rig or tanker, or transported to a nearby coastal area. For the wildfire missions, the optimal nest deployment site will be determined by the authorities. Air traffic control is notified to check and grant permission to deploy from the determined position. The deployment site must be assessed for viability, and the environmental factors need to comply with the operational limits of the swarm, i.e. wind speed, precipitation, visibility, and wave height. Simultaneously, the nest readiness is verified. The main things to be checked are the battery and fuel levels, the aerogel storage, and whether the nest is correctly sealed and ready for transport. Then, if needed, the nest can be transported. Once on site, the UAVs are deployed by the personnel by clipping on the wings of the UAV. Note that the aerogel is already loaded in the fuselage for the initial deployment.

During deployment

When the UAVs are in flight, they fly autonomously while maintaining a constant connection with the emergency responders and the ground personnel. Their location and battery levels can be monitored continuously to aid decision-making on rerunning or charging for the continuation of the mission. Ground personnel at the nest will be in charge of reloading the aerogel and replacing batteries of the UAVs.

After deployment

After the mitigation mission of AeroShield is completed, the UAVs are disassembled and stored back into the nest. The containers can then be transported back to the original storing position, and checked for maintenance. These checks will be performed by employees of the AeroShield company. The personnel operating the nest during the mission are trained by the company.

4.4. Swarm Logistics

Swarm logistic is divided into the mission planning, detection and allocation, communication, and collision avoidance. The mission planning consists of planning the route to the defined coordinates. Detection and allocation develops a strategy for disaster mitigation. Communication entails inter-UAV communication. Lastly, collision avoidance consists of avoiding obstacles and other UAVs. All these algorithms will need to be outsourced from a third party.

Mission Planning

The mission planning consists of intelligent route planning for the UAVs. A search engine is used to search a digitised map of the terrain, and to generate an optimal route in terms of distance, safety and manoeuvring. It is then further optimised and smoothed by a route filter [45]. Next, a high-level intelligent supervisory module is used to configure the search engine and assign weights to the 3 criteria to satisfy the mission objective. Furthermore, it takes previous route plans and an intelligent learning support system is used to collect that data and build a knowledge base that is used to provide better heuristics to the search engine[45].

The algorithm used by the route planner is an A* search algorithm. The digitised map is in the form of a mesh, where each cell is occupied or free from an obstacle. The A* algorithm is then used to search the map's free

cells and construct a cell-based route from the start-point to the destination coordinates [45]. A flow diagram of the route planner is shown in Figure 4.1. This computation is done within the nest computer.

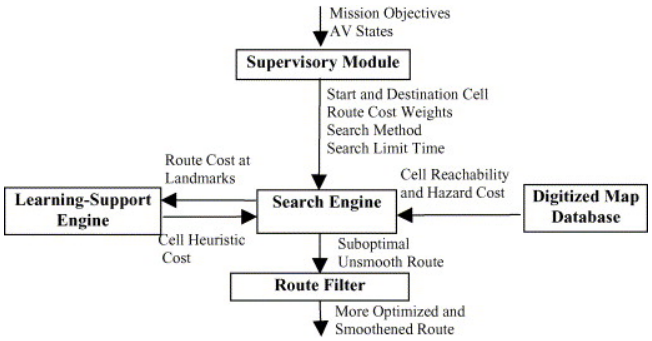

Figure 4.1: Route Planner Flow Diagram[45]

Detection and Allocation

Detection and allocation consist of mapping the disaster area and identifying the location where the aerogel needs to be deployed. For the mapping, the strategy proposed by Patrinopoulou et al. [46] will be used. In this method, an initial digitised map will be provided by the emergency services/ground station. The algorithm splits this map into cells, where a set amount of cells will covered by one UAV. The optimal number of cells per UAV will be calculated based on the time one UAV can cover a certain area. The UAV will loiter around in the cells allocated to it and collect sensor input which will then be sent to the nest computer which will update the map.

For oil spills, a part of the UAV swarm will map the oil spill in detail using oil spill detection sensors as mentioned before, and then the rest of the swarm will be provided the coordinates of the perimeter of the oil spill, in order to deploy the aerogel. Furthermore, each UAV as it deploys the aerogel will also scan the local area for oil, for a more effective deployment.

For wildfires, a digitized map of the area to be scanned will be preloaded into the UAV, and as mentioned it will only scan the area allocated to it. The model to be used for wildfire prediction is the Rothermel forward propagation model [47]. It will be used to determine the main propagation direction and the steady-state rate of spread (RoS), the propagation speed along the main propagation direction. The model uses the fuel, wind and terrain slope. The fuel factor depends on the set of vegetation types. When the wildfire propagation is predicted, the perimeter where the aerogel should be placed will be calculated and the coordinates will be communicated towards the UAVs, as explained in section 4.2.

Communication

Most drone swarm communication is a wireless mesh network [48]. A mesh network is a topology in which each node in the network transmits data. If all nodes are connected to each other, it is a fully connected network. A mesh network can be designed using two techniques: a routing technique and a flooding technique. In the case of AeroShield, the flooding technique will be used. In flooding, instead of using a specific route for sending a message from one node to another, the message is sent simultaneously to all nodes [48]. This technique is simplistic and highly reliable, as any blockages in the path are usually of no consequence, and there is no routing, meaning the controller is extremely simple, requiring minimal computing power and memory and thus low cost. The system will be fully connected at all time.

One of the main challenges for flooding the network are avoiding ”broadcast storms”. That is, how to propagate the message efficiently without any energy wastage. One way to solve this is to use a synchronised flooding approach. In this approach the retransmissions occur simultaneously so that the message propagates one hop in all directions at the same time to avoid any collisions. During each hop, the nodes only retransmit relevant information, and the number of retransmissions corresponds to the number of hops in the network. One example of a network is shown in Figure 4.2.

REQ-SYS-COM-01 and *REQ-SYS-COM-02* require the UAVs to be able to transmit and receive communication signals within a range of $7[km]$, which is supported by the connected network [49].

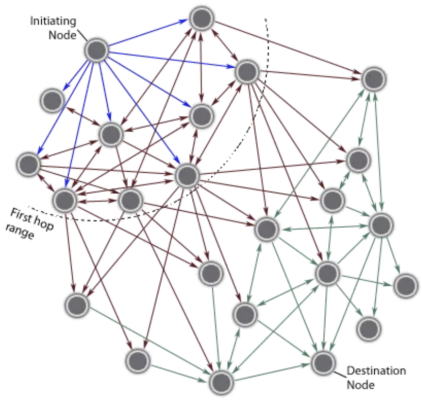

Figure 4.2: A synchronised flooding diagram representing a 24, three-hop network. The first hop signal propagation is blue, the second is purple, and the third is green [48].

Collision Avoidance

Collision avoidance is critical in a UAV swarm, as collisions are highly mission-critical. This includes collisions with external objects such as trees or boats, and also inter-UAV collisions. The article ”Drone swarm strategy for the detection and tracking of occluded targets in complex environments” ([50]) presents a signal processing technique using the PSO (particle swarm optimisation) algorithm, which presents a technique to exploit collision avoidance. The PSO accuracy, and thereby the ability to avoid objects, is dependent on the field of view (fov) of the camera that is used by the UAV. This specific camera will be modular, with the configuration depending on mission specifics such as whether it is light or dark outside. This PSO algorithm plays a critical role during the AeroShield mission by maintaining UAV separation, particularly during aerogel deployment.

4.5. Mission Profile and Timeline

Defining the mission profile in detail is important, as this is required for the design of subsystems such as the battery. The overview of the mission for wildfire mitigation in shown in Figure 4.3. The aerogel loading phase (Phase 1) is estimated to take $60[s]$ per UAV once the mission has started. This includes magnetically attaching the rolled-up aerogel into the deployment system ($\approx 30[s]$), and implementing any pre-flight checks up the UAV ($\approx 30[s]$). Similarly, the land & recharge phase (Phase 14) is estimated to take another minute, and includes the landing time and battery swap, assuming two on-site workers. The scanning phase (Phase 6) is based on $40[s]$ for data acquisition and LiDAR [51] and $20[s]$ for planning & communication. The transition time was assumed to be $30[s]$ based on a moderate acceleration to $100[km/h]$ of about $1[m/s^2]$. For a $30[kg]$ UAV, thus results in an extra thrust of about $30[N]$, which is just 3% of the hover thrust budget. Although this is quite a conservative estimate, transition is quite an unpredictable phase. Deployment time is determined based on deployment mechanism design (chapter 7) to be $2.5[min]$. The landing phase includes the time needed for the UAV to land and either be reloaded with aerogel or, in case of a depleted battery, be turned off for a battery swap.

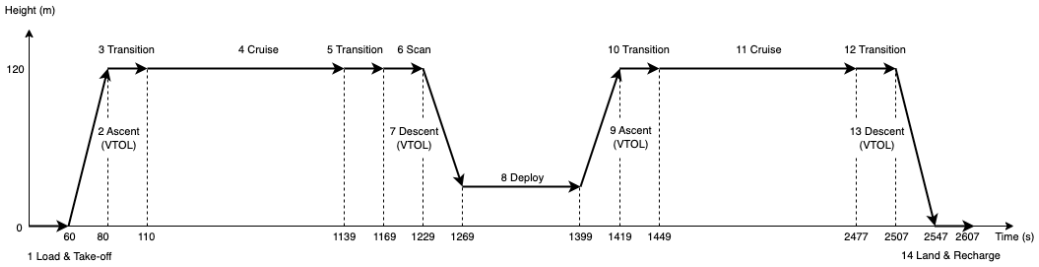

Figure 4.3: Mission Profile

Additionally, cruise height is assumed to be $120[m]$ to provide sufficient clearance above the forest canopy in the wildfire missions, as even the tallest tree in the world, a Coast redwood, is $116[m]$ in height [52]. The climb and descent speeds are selected to be $6[m/s]$ and $3[m/s]$ respectively, based on the characteristics of similar UAVs [53]. The UAV is designed to cruise at a V_{cruise} of $100[km/h]$. The maximum operational range R_{max}, is given by requirements, and is $20[km]$. In oil spill missions it is likely that the UAVs is close to the mitigation zone, so a minimum operational range of $1[km]$ is set. While the descent speed is the same for Phase 7

and 13 of Figure 4.3, it is important to note that in Phase 7 the UAV descends to a height of $15[m]$, which is necessary for deployment. In wildfire missions, the $15[m]$ altitude gives the UAV the possibility to not have to descend between the trees. In the oil spill missions, the height prevents the UAV from being exposed to large waves. Based on these values, the preliminary climb, descend time, and cruise time can be calculated using Equation 4.1 and Equation 4.2. The sum of the times for all the phases then results in a total mission time of 2607 seconds.

$$t_{\text{climb}} = \frac{h_{\text{cruise}} - h_{\text{ground}}}{ROC} \tag{4.1}$$

$$t_{\text{cruise}} = \frac{R_{\text{max}}}{V_{\text{cruise}}} \tag{4.2}$$

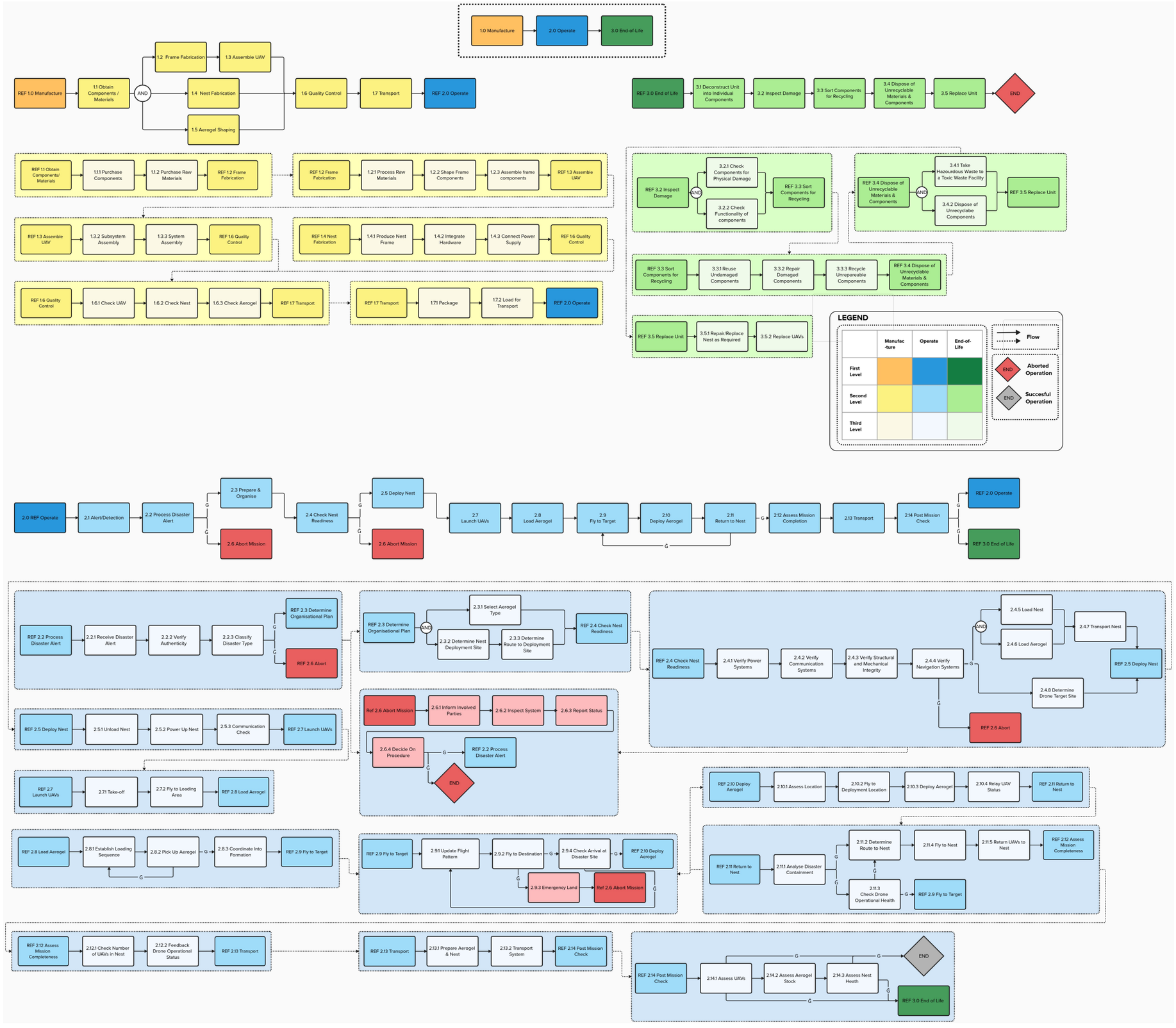

Figure 4.4: Functional Flow Diagram

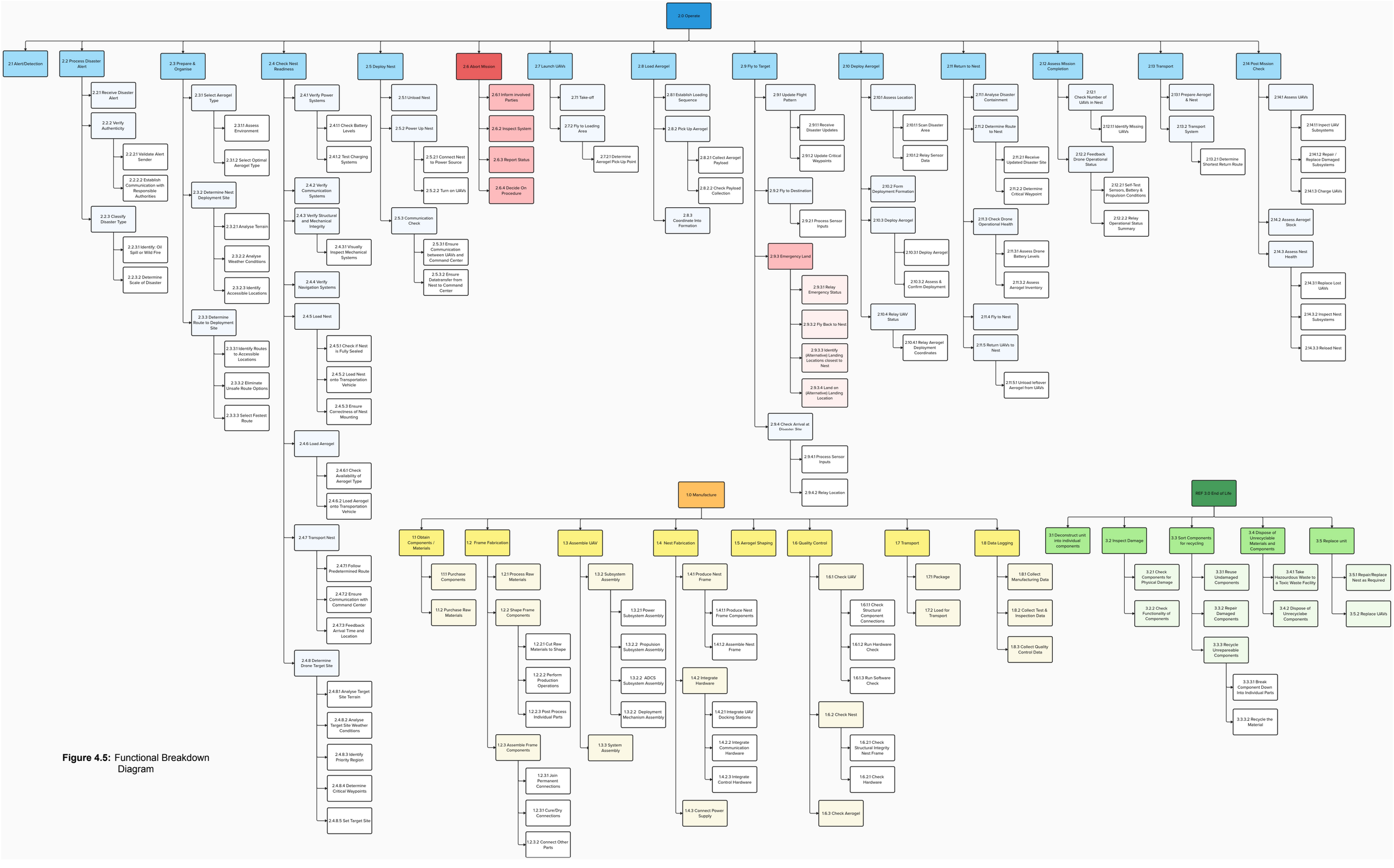

Figure 4.5: Functional Breakdown Diagram

5

Preliminary Design Summary

In this chapter, the preliminary design phase is summarized. In the preliminary design, a trade-off was conducted for the aerogel configuration, the deployment mechanism, the UAV frame, the tail configuration, the autonomy of the system, and the power of the nest. To identify the best option in each trade-off, a scoring system was used. For each option, the final score was calculated using a weighted sum of its criterion values. Finally, the robustness of each choice was verified through a sensitivity analysis.

5.1. Deployment Trade-Off

The deployment trade-off was divided into two parts: an aerogel shape trade-off, and a deployment mechanism trade-off. The aerogel was traded off first, as it immediately relates to the mission. To allow for versatility, the deployment mechanism should be compatible with different aerogel shapes; therefore the trade-off was made taking the preferred aerogel shape into account.

Aerogel Trade-off

For the aerogel trade-off, three design options were considered: blocks, carpets, and panels. Blocks refer to rigid aerogel cubes or thick rectangles, carpets are flexible sheets of aerogel that can be rolled up, and panels refer to rigid and thin rectangles. The density across these options was assumed constant.

Trade-off Criteria

Six criteria have been determined for the aerogel trade-off: aerodynamics (UAV), aerodynamics (deployment), mitigation effectiveness, containment effectiveness, manufacturability, and price.

- **UAV aerodynamics** refers to the aerodynamic influence of the carried aerogel on the UAV flight. This criterion significantly influences the UAV performance for a substantial amount of the mission duration. Therefore, it was given a 5/5 weight. The UAV performance mostly considered drag and controllability.
- **Deployment aerodynamics** considers the resilience of the deployed aerogel to unwanted movement. It takes the movements due to turbulence, gusts and wake effects into account. The mission success depends heavily on the successful deployment of the aerogel, and therefore, this criterion is also given a $5/5$.
- **Mitigation effectiveness** is defined as the ability to suppress wildfires and clean up oil-spills. The mitigation effectiveness considers the amount of aerogel needed and placement procedure complexity. Both wildfire and oil-spill mitigation are considered in this criterion. While the mitigation effectiveness is important for mission success, it marginally influences UAV performance and was thus weighted a $4/5$.
- **Containment effectiveness** is defined as the ability to create a perimeter around the disaster, resulting in prevention or slowing of the spread of a wildfire or oil spill. Similar to mitigation effectiveness, this also includes both scenarios and accounts for both aerogel usage and deployment complexity. Following similar reasoning as for mitigation effectiveness, it is assigned a weight of $4/5$.
- **Commercial availability** of the aerogel was taken into consideration, because the aerogel will be needed in large quantities. The production of aerogel is outside the scope of AeroShield, therefore it must be commercially available. Apart from initial availability, the criterion does not influence the mission dynamics, therefore it was weighted $2/5$.
- **Density** of the aerogel is considered, because of its impact on mass carried per unit volume. Where other criteria are concerned with the plausibility of the mission, density is concerned with mission optimization. After establishing a feasible aerogel shape, density becomes most important for optimising mission performance. Therefore it was weighted $3/5$.
- **Price** of the aerogel is the last criterion considered. It was weighted $1/5$. Firstly, because the market is quite large, as long as the price stays within reasonable bounds, acquisition will play no significant role

in the mission. Secondly, the aerogel will likely be reusable, reducing the cost per use-case. Price was compared in €$/m^2$, rather than €$/m^3$, as surface area primarily influences mitigation effectiveness. This does not mean that thickness does not play a role, but that the influence on size is less relevant.

This trade-off was performed, and the carpets were deemed to fit the criteria the best.

Deployment Mechanism

Five design options were considered for the deployment mechanism trade-off. The first option is a winch-based system, which envisions an extendable and retractable tether connected to the aerogel. The second option is a mechanical clamp, which uses mechanical force to clamp the aerogel in place. The third option uses magnetic clamping to keep the aerogel in place. The fourth option is a hybrid mechanical clamp and winch system. The fifth option is a hybrid magnetic clamp and winch system. These hybrid designs add redundancy and rigidity to the winch by providing additional clamping.

Trade-off Criteria

Six criteria have been determined for the deployment trade-off: technical reliability, environmental robustness, adaptability, deployment distance, carriage integration, and weight. Required power was considered but excluded from the trade-off, as it did not differ significantly across the options. All mechanisms can be designed to only require power to change the state (holding vs. releasing), so the required power would be negligible compared to the UAV's power.

- **Technical reliability** concerns failure by internal design. It connects to the chance of the mechanism failing and the redundancy that is available. The criterion was given a weighting of 5/5 as successful deployment is critical for mission success.
- **Environmental robustness** is concerned with an increase in failure due to external circumstances (e.g. extreme outside temperatures). A 5/5 weighting was given, as successful deployment must be guaranteed, even under harsh conditions.
- **Adaptability** refers to how flexible the mechanism is for loading different sizes and shapes of aerogel. This criterion's importance is due to the double application for both oil-spills and wildfires, which can benefit from different aerogel shapes. Additionally, it ensures adaptability in case of supply issues. Therefore, this was weighted a 4/5.
- **Deployment distance** is related to the ease of aerogel delivery to a certain location and the accuracy of the deployment. Depending on the mechanism, the UAV might have to closely approach the deployment location. If the UAV cannot approach the deployment location, the aerogel might have to be dropped, reducing accuracy. A weight of 3/5 is given since deployment distance improves mission performance, but is not critical for success.
- **Carriage integration** takes into account the size of the mechanism and the complexity of integrating it within the UAV. The size and placement of the mechanism also has an effect on the aerodynamics of the entire UAV, which is taken into account as well. Although this is an important criteria, there are different design possibilities to overcome integration challenges. Therefore, it was weighted 1/5.
- **Weight** was considered as this will affect the efficiency of the UAV. Nevertheless the criteria was only weighed 1/5, since the mechanism is only a small portion of the UAV mass.

Based on this trade-off, a hybrid magnet winch system was deemed the most suitable design.

5.2. UAV Trade-Off

The UAV trade-off regards the frame and tail of the UAV design. The frame was considered first, as the choice for frame has influence on the tail design.

Frame Trade-off

For the frame trade-off two design options were considered; fixed-wing VTOL and rotorcraft. Fixed-wing VTOL refers to a hybrid between a rotorcraft and fixed-wing. Rotorcraft refers to a traditional quad-propeller UAV design.

Trade-off Criteria

Six criteria have been determined for the frame of the UAV: cruise efficiency, manoeuvrability, aerogel compatibility, size, speed, and manufacturability.

- **Cruise efficiency** includes the UAVs ability to be as power-efficient as possible to extend the duration and range of mission. It is weighted a 4/5 because the mission range of $30[km]$ is a key requirement.

Furthermore, the operation duration is important due to the nature of the mission, as coordination between the UAV swarm might require UAVs to wait for other UAVs to perform certain manoeuvres.

- **Manoeuvrability** includes the ability of attaining specified orientation and location, while avoiding obstacles. Although the mission would be jeopardised if the UAV is not able to avoid obstacles and attain a specified location, this can be designed around by obstacle detection and autonomous pathing. Therefore, this criterion is given a weight of 3/5.
- **Aerogel compatibility** refers to the ability of the UAV frame to carry aerogel. Mainly, the ability to mitigate aerodynamic disturbances on the UAV by the aerogel is considered, since carrying and deploying the aerogel is the main task of the UAV. This criterion is given a weight of 5/5.
- **Size** refers to the physical size of each UAV frame. This translates into how easily UAVs can be handled, transported, and deployed, as well as how much the nest design is impacted by increasing the number of UAVs. While this does influence the design, it barely influences mission performance compared to other criteria mentioned. Therefore, the criterion is given a weight of 1/5. It should be noted that size influences manoeuvrability. This is only accounted for in the manoeuvrability criterion, ensuring no doubled weightings.
- **Speed** refers directly to how fast the UAVs can move during the whole mission. This not only impacts the response time, but also the response effectiveness. Faster UAVs reduce the mission turnaround time and allow for more aerogel deployment, potentially increasing the benefit of the mission. Therefore, this criteria is given a weight of 4/5.
- **Manufacturability** of the UAV is important to consider for the cost of production and the ease of design. This is an important criterion to keep track of, as the UAV solution must fit within the cost requirement (U-BUD-01), but it is not crucial to the mission and can be designed around. Therefore, this criterion is given a weight of 2/5.

Based on the trade-off, a hybrid VTOL UAV was deemed the most suitable solution.

Tail configuration Trade-Off

Given the choice of a fixed-wing configuration, a trade-off for the type of tail will be conducted. The options analysed include: no tail (flying wing), conventional tail, V-tail, boom-tail, and T-tail.

Trade-off Criteria

Four criteria have been established for evaluating the tails: drag, weight, stability & controllability, and Manufacturability.

- **Drag** is a critical aerodynamic force that opposes the UAV's motion through the air. It is considered the most important evaluation criterion in this context, as it directly influences flight performance and endurance. Therefore, a weight of 5/5 was assigned. The drag is quantified as cl/cd in level cruise flight of 100km/h. Preliminary sizing of each tail type was conducted, keeping main wing surface area constant across designs. The corresponding C_L/C_D were then obtained using XFLR5 simulations.
- **Weight** refers to the mass of the tail, measured as a percentage of MTOW. The criteria was given a weight of 3/5. Although the total weight of the UAV must stay within the weight limit, it is not as important to mission performance as other criteria. Therefore, it has a slightly lower weight.
- **Stability & Controllability** refers to the ability of the UAV to withstand disturbances. It has a weight of 4/5 because of requirement that the UAVs should be operable in 30 km/h wind conditions (U-PER-03).
- **Manufacturability** refers to the cost of production and ease of design. It is an important criterion to keep track of, considering the cost requirement (U-BUD-01) , but since it can be designed around and is not crucial to the mission, this criteria is given a weight of 2/5.

Based on this trade-off, a conventional tail was chosen.

Autonomy Trade-off

For the autonomy trade-off, three design options were created. A fully autonomous nest supports a completely autonomous UAV operation, allowing the UAVs to take-off, land, and recharge autonomously. The semi-autonomous option allows several operations, such as deployment, to be performed autonomously, but human interaction is still needed for tasks such as UAV battery swaps. The manual option refers to a high degree of involvement from an on-site operation crew. This would include the unloading, deployment, and aerogel loading of the UAVs.

Trade-off Criteria

To choose an optimal design, six criteria were selected for the trade-off: deployment speed, space efficiency, cost, safety, complexity, and reliability.

- **Cost** of the system has been given a weight of 2/5. While it needs to be considered, it is not mission defining. Manufacturing, as well as operating costs, are included here.
- **Deployment speed** corresponds to the speed with which the UAVs are unloaded. The unloading phase starts the moment that the nest arrives at its target location, until all UAVs are deployed and loaded with aerogel. As this is a driving requirement (REQ-SYS-09), a weight of 5/5 was given.
- **Space efficiency** is the next criterion. It refers to the size of the nest and the compactness of its UAV storage. This criterion was given a weight of 4/5, because nest size is the main influence on the transportability, which in turn influences the accessibility of disaster zones.
- **Safety** refers to safety for nest and humans. Nest safety is the risk of the nest failing due to the environment. Human safety is concerned with the risk humans face during operation. The criterion has been given a weight of 3/5. It is a key selling point of the system. However, as the nest will be located far from the disaster, the likelihood of harm occurring is relatively low.
- **Design complexity** refers to the level of interdependence of components in the nest, as well as integrability with the external systems. It does not consider the reliability of the system itself. The criterion was given a weight of 2/5. While complexity does influence development and production price, it should not be a driving factor and does not heavily affect mission success.
- **Reliability** refers to the chance of failure of the system and ease of repairing said failure. After mission performance, mission reliability was considered most important. Therefore, this criterion was weighted 3/5.

Based on the trade-off, a manual nest was chosen.

Power

For the nest's power subsystem, three options were considered. Firstly, a solar panel + battery configuration. Here, the solar panels would be deployed around the nest for charging UAV batteries. The second option is a generator, which would be stored inside the nest along with sufficient bio-fuel for the full mission duration. The last option is fully battery-based storage, where all required energy for the UAVs is stored in batteries, and power can be drawn directly from them.

Trade-off Criteria

The nest's power system has been traded off based on 5 criteria: charging time, total energy availability, sustainability, size & weight, and reliability.

- **Charging time** refers to the charging speed of the UAVs by the nest. This criterion has been given a weight of 5/5, as fast turnaround time is crucial for effective containment in spreading conditions.
- **Total energy availability** refers to the amount of energy available for the mission. It is key to mission success that the nest can provide power for the entire mission duration. Thus, this criterion has been given a weight of 4/5. As the mission duration is dependent on charging time, this criterion is rated slightly lower.
- **Sustainability** refers to the sustainability of the power source. Once the sustainability requirement is met, the influence on the mission is negligible. Therefore, a rating of 2/5 was given.
- **Size & Weight** refers to both size and weight of the power source. It was given a weight of 3/5. Although the nest must remain transportable, the power and energy are the mission defining criteria for the power source. Thus, this criterion was rated slightly lower.
- **Reliability** was lastly included. Its weight is 2/5. Reliability is important to ensure that the nest remains operable. However, a lower rating was given as it is possible to design for redundancy.

Based on the trade-off, a bio-fuel generator power source was chosen.

5.3. Final Trade-Off Design

The final design based on weighted sum in the trade-off and sensitivity analysis is summarised in Table 5.1:

Table 5.1: Final Trade-Off Design

Trade-Off Component	**Choice**
Aerogel	Carpet (section 5.1)
Deployment Mechanism	Winch + Magnet (section 5.1)
Frame	Fixed Wing VTOL (section 5.2)
Tail	Conventional tail (section 5.2)
Nest Autonomy	Semi-Autonomous (section 5.2)
Nest Power	Generator (section 5.2)

6

System Overview

Based on the trade-off from the preliminary design, the nest and UAV can be further developed. In this chapter, a system overview will be given. This includes the design methodology that will be followed to further design the UAV systems, the hardware that will be used, and lastly the communications structure between different elements of the UAV and nest.

6.1. Design Methodology

In this section the design methodology will be explained. An N2 chart will be used to present this design methodology, which is shown in Figure 6.1. As can be seen in the chart, the grey blocks represent the individual subsystems, and the white blocks represent the inputs and outputs.

Mission Definition	• Payload parameters	• Deployment speed requirements	• Performance requirements	• Mission power requirements		• Performance requirements	• Operational limits	• Mission information		• Mission information	
	Payload	• Payload sizing	• Payload weight		• Payload sizing				• Payload loads		• Aerogel dimensions
		Deployment		• Deployment power requirement	• Deployment stability derivatives • Wing sizing	• Deployment C.G. shifts			• Deployment system loads • Required attachment points		
			Propulsion	• Propulsion power requirements		• Available thrust • Available torque			• Wing Loading (W/S) • Required moment arms		
			• Battery weight	**Power**			• Power requirement	• Available power	• Structural loads • Wing loading (W/S) • Battery mass		
			• Aerodynamics refinement		**Aerodynamics**	• Aerodynamic forces & moments • Aerodynamic coefficients • Stability derivatives • Gust loads			• Aerodynamic loads		
			• Control propulsion requirements			**Control and Stability**			• Disturbance loads	• Control limits	
				• Power provision			**Thermal Management**		• Material properties		
				• Power provision				**Communication**	• Communication system loads • Required attachment points	• Mission information	• Communication range
			• Structural weight distribution • Thrust & Moments	• Power provision	• Structure shape		• Material changes	• Updated attachment points	**Structure**		• Attachment points • UAV dimensions
		• Deployment characteristics		• Power provision		• Controllability & stability requirements		• Mission information		**Autonomy & Coordination**	• Autonomy requirements
	• Aerogel dimensions			• Total power requirement		• Nest disturbances			• UAV dimension refinement	• Landing, take-off and charging procedures	**Nest**

Figure 6.1: N2 Chart

The N2 chart provides an insight into all the subsystem relations, inputs and outputs. This helps have an overview of the design process that will take place as what needs to be calculated is present, and what is needed to calculate that value is also present. It also demonstrates if any iterations might be needed if outputs change, and which subsystems they affect.

6.2. Hardware Block Diagram

In this section, the hardware block diagram is presented in Figure 6.2. The block diagram shows the energy flow (blue lines), and the data flow (red lines) between the different components. The mechanical transmission of the motors is shown with a dotted blue line. Human involvement is indicated with dotted black lines. The

hardware block diagram is split into three sections, the UAV hardware (section 6.2), nest hardware (Table 6.2) and external hardware.

The external hardware consist of antennas used by the GPS system to receive the current location of the UAVs. The nest includes a cleaning system operated by the human operator in order to clean the UAVs and nest in case of contaminants, fire residue or dust. A human operator is responsible for swapping the batteries and loading the UAVs with aerogel before, during and after the mission. The rest of this chapter will discuss the functions of all the hardware of the UAV and Nest and why these components were chosen.

UAV Hardware

The UAV is powered by two batteries, which supply electricity to the motors for cruise and for VTOL, as well as the power distribution board (PDB). This board distributes power to the lower voltage systems such as the servo motors that control the flight surfaces, the flight controller, the detection sensors, lights, the onboard computer, the winch motor, winch magnets, and the telemetry module. The motor and battery choices will be explained in the power and propulsion chapter 8. More details about the rest of the hardware is given in this section. A complete overview of the hardware is provided in Table 6.1. The placement of all the hardware inside the UAV will be discussed in chapter 13.

Component	Commercial Product	Mass [g]	Power [W]	Unit Cost [€]
Wildfire Detection Sensor	DJI Zenmuse H30T	920	58	13,500
Oil Detection Sensor	Zenmuse L2	905	58	14,280
Gymbal Connection	SDK Skyport 2.0	70	-	39
Flight Controller	Pixhawk 6X	32	7.5	310
Onboard Computer	Developer Kit Jetson AGX Orin 64 GB	700	60	2625
GPS System	CUAV NEO 3 Pro	33	1	107
Communication Module	CUAV Air Link 4G	52	5	176
Communication Module	mini-OEM Dual-Band Mesh Rider Radio	36.5	8	1613
Communication Module	RockBLOCK 9603	36	2.25	300
Motor	U8LiteL KV110	230	Variable	265
Electronic Speed Controller	V80A	110	Variable	150
Propellers	G30*10.5	97	-	-
Winch Motor	XD-10	1170	100	3,200
Deployment Magnets	Hyab EPM	39	20	0.90
Servo motor	MKS HV6130	22.5	13.5	84
Power Distribution Panel	Flightcore MK2	156	-	200
Lights	Whelen Orion 660	117	1.8	600
Batteries	Tattu 17,000 mAh 14S	3619	-	390

Table 6.1: Mass and Cost Breakdown Hardware Components

Power Distribution Board

The power distribution board (PDB) regulates the output from the batteries and distributes electricity at the correct voltage to all the different subsystems. The chosen one is the Flightcore MK2 [1], and it allows for 6 connections at the output voltage of the battery. These will be used for the five motors and the detection sensors. The rest of the connections are used for supplying to correct voltages at 24V, 12V and 5V to the other subsystems of the UAV. The lower voltage ports also include over current and short circuit protection. The PDB also allows for current and voltage measurements across all the different ports. This information will be relayed to the OBC for the monitoring of all the electrical systems.

On-Board Computer

The onboard computer (OBC) is responsible for the central control of the UAV as a whole. It will be processing all the data from the detection sensors and managing the data flow for the rest of the hardware. All of the hardware is connected to this OBC as this will be the system that turns on/off different systems and monitors the health of the components.

[1] https://vectortechnics.com/products/pdb-flightcore-mk2?srsltid=AfmBOornofMLABIJQ1QFhXyTarmVm9dq0J8ZbaEQO3neWYBFoIjI9QOX, [accessed: 18/06/2025]

The Jetson AGX Orin 64GB [2] was chosen for its compact form, low mass, and its cutting-edge AI computing platforms. This OBC allows for the UAV to operate autonomously and process information from the sensors directly. Next to processing the data from the detection sensors, the OBC handles the data flow between the telemetry module, navigation system and flight controller.

Flight Controller

The Pixhawk 6X [3] will be utilized as flight controller. This FC developed by Holybro is used widely within the UAV industry for high-performance UAV applications. The system is based on the open-source PX4 autopilot software, which allows for easier integration with the OBC. It has an integrated inertial measurement unit (IMU) with triple redundancy. A barometer is also included to allow for altitude determination. A dual microcontroller configuration provides a fail-safe processer for increased reliability.

Navigation System

For navigation, the Pixhawk is connected to the CUAV NEO 3 Pro [4]. This GPSS module has simultaneous reception with the 4 major satellite systems (BeiDou, Galileo, GLONASS, GPS) ensuring a position accuracy of up to 0.7m. The GPSS includes a RM3100 magnetometer. It is also specifically designed to be compatible with the PX4 Autopilot.

Detection Sensors

For the oil spill mission, the UAV will be equipped with the DJI Zenmuse L2 sensor[5]. It integrates a high-precision LiDAR (Light Detection and Ranging) sensor with an RGB mapping camera. LiDAR sensors can detect oil on water by measuring changes in the reflected or refracted light when a laser beam interacts with the oil slick.

For the wildfire mission, the UAV will be equipped with the DJI Zenmuse H30T sensor[6]. It has an infrared thermal camera, visible light camera, NIR auxiliary light and laser range finder. An infrared density filter will be added on the camera, this increases the temperature measurement range to -20°- 150° for high gain. The infrared camera has a diagonal field of view of 45.2 °.

Telemetry System

For the telemetry system different types of communication methods were combined to meet all the requirements for this module. The UAV will include a CUAV Air Link 4G, RockBLOCK 9603 and mini-OEM Dual-Band Mesh Rider Radio. The CUAV Air Link [7] provides low latency beyond line of sight communication through a 4G LTE connection. The range is not limited as long as there is a 4G connection available. This module allows for up to 140 Mbps of downlink and 50 Mbps uplink, which is sufficient for HD transmission of sensor video (36 Mbps) and other UAV data. This allows for the ground station to monitor the UAVs as well as gather information about how the environmental disaster is developing.

Although the 4G connection is ideal for low latency transmission and provides extensive range the coverage might be limited by in marine applications. Furthermore, in wildfire can cause grid failures resulting in problems with cell towers. Due to these risks it is necessary to have a second means of communication. That is why the mini-OEM Dual-Band Mesh Rider Radio [8] is included in the telemetry system. This compact radio module can be used at 915 Mhz and 2.4 GHz frequency bands.

Finally, a satellite communication module (RockBLOCK 9603 [9]) was added to the UAV. This provides another level of redundancy and a last resort for communicating critical information to the ground station. The module allows for small transmission of 340 bytes every 40 seconds. Using the Global Iridium Constellation the SATCOM module provides global coverage.

Buoy System

The buoy system is designed for use in the event of an oil spill. It will resemble the Flyfire Buoy [10], but will be larger in size to accommodate the AeroShield-designed UAVs. This buoy system is equipped with an integrated liquid sensor that detects when the buoy is in the water. Upon contact with the water, an airbag is automatically inflated which can hold the UAV for 24 hours. This ensures the UAV can be safely retrieved from the ocean, preventing any damage to the environment.

[2] https://www.nvidia.com/en-us/autonomous-machines/embedded-systems/jetson-orin/, [accessed: 18/06/2025]
[3] https://docs.holybro.com/autopilot/pixhawk-6x, [accessed: 18/06/2025]
[4] https://www.cuav.net/en/neo-3-pro-en/, [accessed: 18/06/2025]
[5] https://enterprise.dji.com/zenmuse-l2, [accessed: 18/6/2025]
[6] https://enterprise.dji.com/zenmuse-h30-series/specs, [accessed: 18/06/2025]
[7] https://www.cuav.net/en/air-link-en/, [accessed: 18/06/2025]
[8] https://techlibrary.doodlelabs.com/doodle-labs-rm-1700-22m-mesh-rider-radio, [accessed: 18/06/2025]
[9] https://www.groundcontrol.com/product/rockblock-9603-compact-plug-and-play-satellite-transmitter/, [accessed: 16/06/2025]
[10] https://flyfiretech.com/products/drone-buoy-system-device-for-dji-various-series-models, [accessed: 16/06/2025]

Nest Hardware

The nest is a fully self-contained storage and command centre for the UAV swarm. A single 50kVA John Deere Tier 4 generator is used to power the whole nest, feeding into a rack-mounted power-distribution unit (PDU), uninterruptible power supply (UPS), which combined, deliver a constant, clean uninterrupted power supply to all nest electronics. Inside the nest, environmental controls such as the Dyna-Glo heater and VEVOR Exhaust fan keep the temperature and air-quality within safe operational limits. A high-performance workstation (Lambda Scalar) is utilised to run mission-planning software and telemetry aggregation. Additionally, there are three parallel communication links: a local 2.4 GHz mesh, a mid-range cellulat LTE/5G system, and a global GEO satellite connection. Together, they provide a reliable connection to the ground-station and UAVs. Other subsystems such as the switch and VPN firewall ensure reliable and secured data transfer, and enable sub-10 ms swarm coordination, high-bandwidth video, and last-resort connectivity anywhere on Earth. The inter-workings of the hardware is outlined in Figure 6.2, showing the power and dataflow between components

Component	**Commercial Product**	**Mass [g]**	**Power [W]**	**Unit Cost [€]**
Container	20ft ISO Container	2250	-	5200
Ventilation System	VEVOR Exhaust Fan	3.66	40	100
Heater	Dyna-Glo 4800W Heater	5.90	4800	230
Battery Chargers	Tattu TA1000	1.7	500 (charging)	260
Generator	GPR-J50-60T4iF Portable Generator	1514	-	53500
PDU	Tripp Lite PDUMH15ATNET	4.99	-	183
UPS	APC Smart-UPS C 1500VA	24.09	900	820
Nest Computer	Lambda Scalar MGX AMD	30.6	8000	104000
Switch	UniFi Switch 8 150W	1.7	150	200
Firewall	MikroTik CCR1009-7G-1C-1S+	4.54	39	495
RF Antenna	OmniLOG® PRO H	0.6	100	398
Mesh Base	Doodle Labs EK-2450-11N3	0.026	8	208
4G Antenna	Panorama B4BE	0.39	30	46
Router	TELTONIKA RUTX11	0.456	16	350
Satellite Antenna	Selfsat H30D	1.1	2.85	94
Satellite Modem	Cobham EXPLORER 323	3.5	35	3800
Rails	VEVOR SBR20-2200mm	14.9	-	160

Table 6.2: Mass and Cost Breakdown Hardware Components

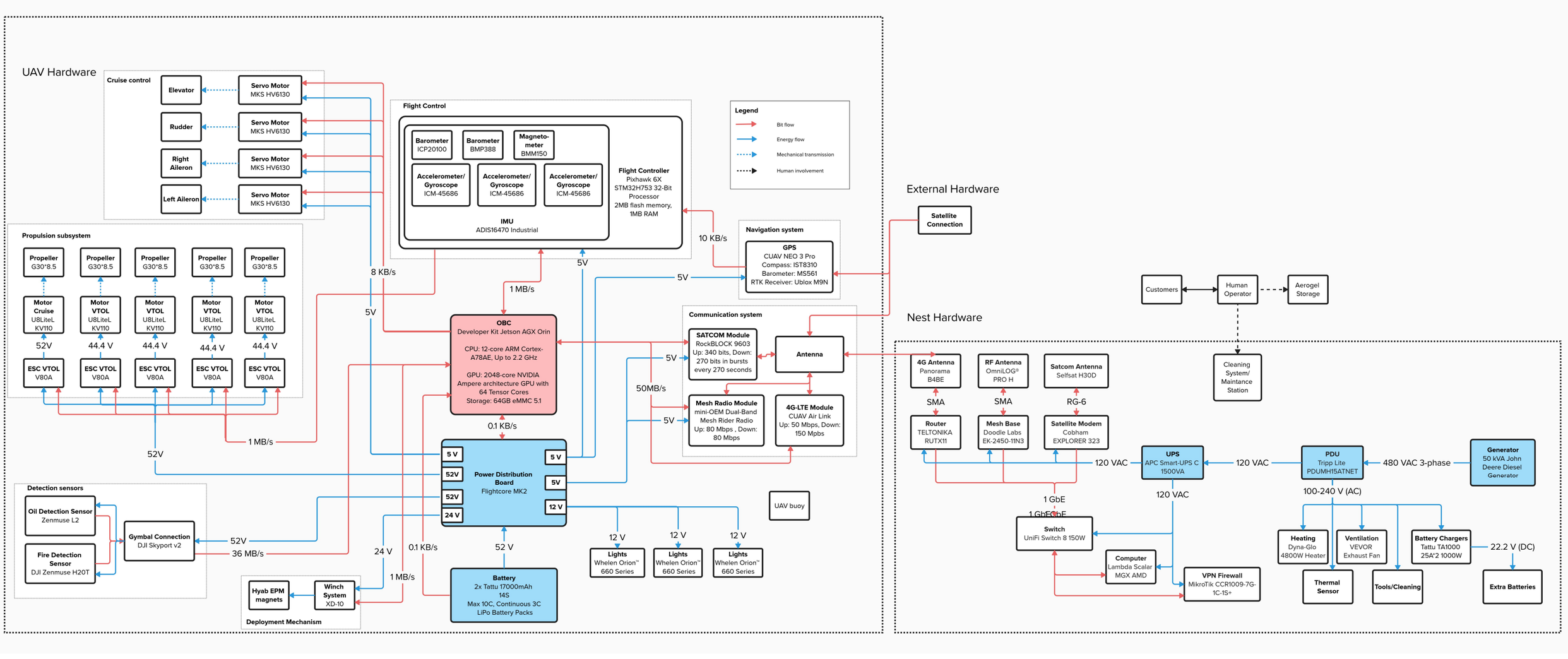

Figure 6.2: Hardware Diagram

6.3. Communication Flow Diagram

The communication flow diagram is visible in Figure 6.3. It contains all the communications that will occur within the UAV and the Nest, and also the communications between them and to external communication sources. The component of the UAV are presented in pink, the nest components are presented in blue and the external communication is light green.

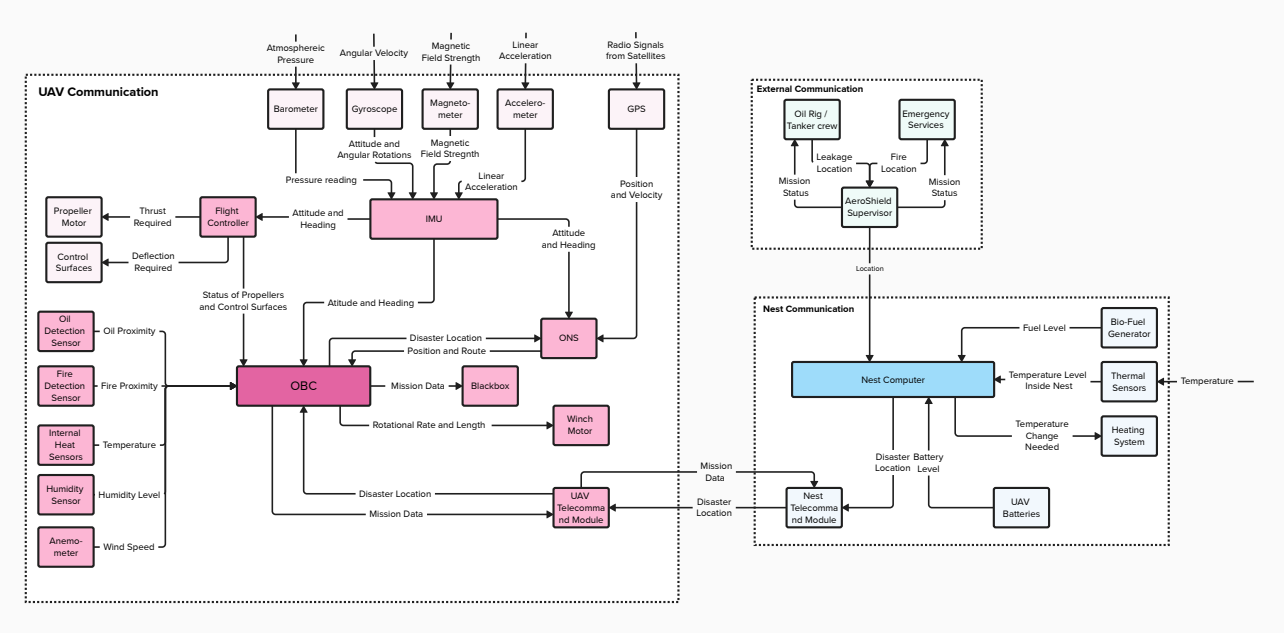

Figure 6.3: Communication Flow Diagram

Furthermore, the UAV swarm is also able to perform inter-swarm communication. This will be done via the telecommand modules and consist of communicating their current location, deployment status and transmitting/receiving coordinates.

7

Deployment Mechanism

This chapter outlines the design of the deployment mechanism. Firstly, section 7.1 discusses the optimised size of the aerogel blanket and the design adaptations made to use it effectively for AeroShield missions. Secondly, the deployment system and effectiveness are described in section 7.2. Lastly, the requirement compliance matrix is discussed in section 7.3.

7.1. Aerogel Sizing

Each UAV carries a rolled-up aerogel sheet. The chosen aerogel blankets are the heat resistant aerogel insulation blankets from MQ Industry [1] with a $3[mm]$ thickness. While the width is set by the manufacturer to $1.5[m]$, the length is maximised within the available payload to be $3.33[m]$. The layered structure of the aerogel blanket allows them to be partly split along the edges so that additions can be added in and secured by a simple running stitch around the additions perimeter. Each aerogel sheet is adapted to contain 4 ferromagnets along the top edge, 2 in each corners. They primarily form the attachment points for the deployment mechanism, but also function as corners weights after deployment. Additionally, a weight is integrated along the bottom edge to primarily assist gravitational unfurling, and to function as edge weight after deployment.

Given the dimensions of the sheet, the dimensions of the rolled up cylinder can be approximated as a Archimedean spiral, with an initial diameter equal to the fixed bottom weight width.

7.2. Deployment System Sizing

The deployment system consists of a dual-spool winch that controls two parallel conducting wires synchronously. The wires are each guide through two pulleys before attaching to the aerogel. At the aerogel, the wires split into a shorter and longer branch, each with an electro-permanent magnet (EPM) at its end. The short branches secure the top corners of the aerogel by connecting to the inner ferromagnets embedded in the aerogel blanket. The long branches loop around the roll to attach to the outer ferromagnets to keep the roll closed. Once the UAV is in the correct position, an electrical pulse is sent through the wires to deactivate the outer EPMs. Springs located around the long sides of the wire ensure smooth retraction of these to allow unfurling and ensure a retracted wire length of $12[cm]$ to ensure that the wires can fully fit within the fuselage [54]. The unfurling is assisted by the weight located along the bottom of the aerogel sheet. A sketch of the system is displayed in Figure 7.1.

[1] https://www.mqindustry.com/heat-resistant-aerogel-insulation-blankets

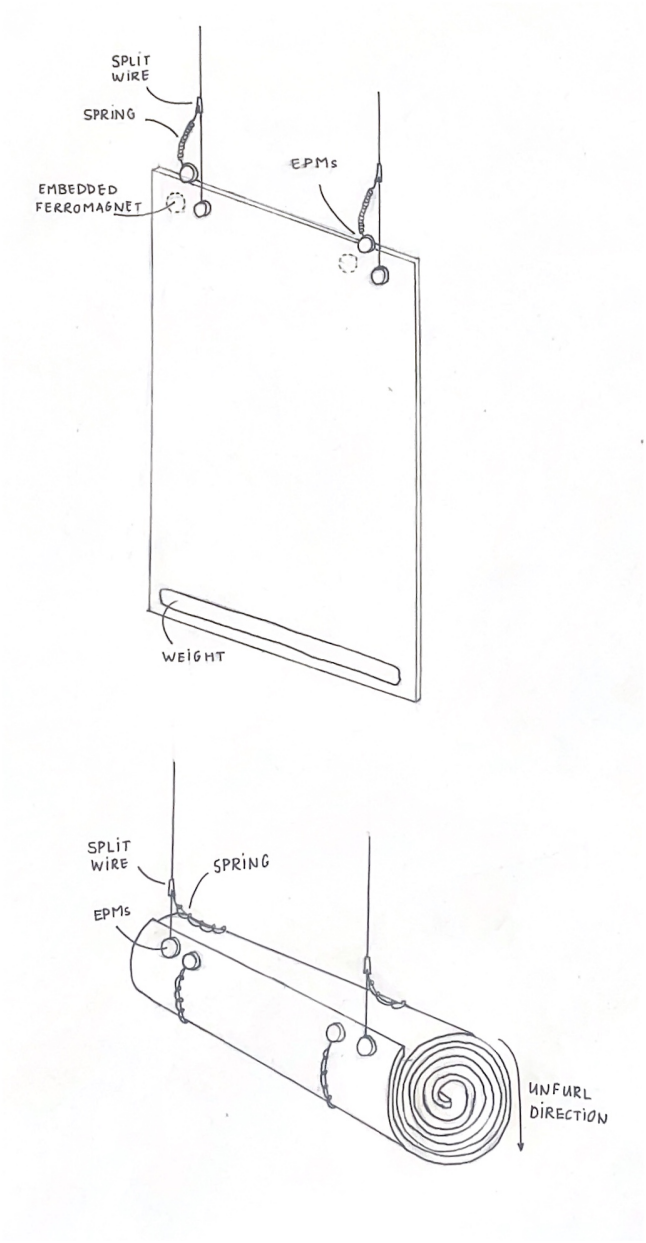

Figure 7.1: Aerogel Sketch

The full system is comprised of:

- 1 $\times$ XD-10 winch from WingFly (adjusted to contain dual-spool winch, $10[kg]$ capacity, $0.3[m/s]$, tension and swing monitoring, emergency cut-off) [55].
- 2 $\times$ wires (split-capable, temperature resistant) [56].
- 4 $\times$ the RP113 pulley from CMI (anodized aluminum) [57].
- 4 $\times$ the 71-2515 EPM from Hyab Magneter (60N force, saltwater resistant) [58].
- 2 $\times$ the LE 037E 13 S stainless steel spring from Lee Springs (max. load of $15[N]$, free length of $12.7[cm]$, max. extended length of $63[cm]$, temperature resistant) [54].

The 2 inner EPMs are responsible for keeping the aerogel attached until the right moment for deployment. Each magnet has a holding force of $60[N]$, ensuring a minimum safety factor of 2 for holding the payload (max. $5[kg]$). For the spring sizing it was important to consider elongation and retraction limits. The spring should allow the wire to retract sufficiently so that it would completely fit into the fuselage, while also allowing sufficient elongation to wrap around the aerogel, all without plastic deformation occurring. Additionally, the pull force had to be below $30[N]$ to prevent excessive spring-back and to avoid the springs having sufficient power to detach the magnets (again using a safety factor of 2).

Deployment Effectiveness

For the deployment effectiveness, the first thing to consider is the mass of aerogel deployed per unit of time. This is a valid metric for oil spill mitigation as it directly correlates to the amount of oil removed, but for wildfires, the effectiveness is more related to the length of the deployed firebreak. For this, there are two strategies: laying the aerogel lengthwise, where the longer side of the aerogel is aligned with the perimeter, or laying the aerogel widthwise, where the shorter side is aligned with the perimeter. Depending on the width of the firebreak and the length of the aerogel sheet, either method might be the more effective one. Additionally, due to the deployment not being 100% accurate, a certain amount of overlap occurs, which also varies between lengthwise and widthwise deployment.

First, it is derived how many sheets of aerogel need to lay next to each other to span the firebreak in both lengthwise and widthwise configuration, taking into account a $0.5[m]$ overlap between each sheet. The effective length is then defined as the dimension of the sheet parallel to the deployment direction minus the deployment accuracy. By dividing the effective length by the amount of layers, it is evident which of the two methods is more effective for maximising the length of the barrier. Deployment is considered ”effective” if two adjacent sheets overlap. As the UAVs aim to deploy the sheets with $0.5[m]$ overlap, the deployment should be effective for a deviation of maximum deployment accuracy of $0.5[m]$ in either direction. After deployment, the overlap is checked using the RGB camera. If no overlap is achieved, the closest UAV from the swarm is redirected to close the gap.

When calculating the perimeter length, two more things must be taken into account: the first is that the aerogel at the ends of the perimeter only have one end that overlaps with another sheet instead of two, the second it is not possible to deploy half a sheet of aerogel, and that a perimeter is not effective when only part of the layers is deployed in that area, so it is not possible to simply linearise the deployment based on the effective length.

Since the sheet is deployed in a rolled-up configuration, which is being lowered down from the winch, and only deployed when it is close to the ground, the influence of the aerodynamic loads and controllability can now be considered. The diameter of the roll reduces as the deployment process continues, and the height between the roll and the ground decreases. The UAV will need to keep stability during this whole process, and it is important to consider this. The stability and control specifics will be addressed in chapter 10. During the final placement of the aerogel blanket, aerodynamic loads can be assumed consistent with those during the winch-lowering phase. The UAV fly in counter to the unfurling direction to ensure complete deployment and proper alignment of the magnets and weighted section of the blanket.

7.3. Compliance Matrix

Table 7.1 shows the compliance matrix of the deployment system requirements considering the previously presented design. Requirements that require further analysis are discussed further.

Identification	Description	Compliance	Method of Verification
REQ-SYS-DEP-01	The deployment mechanism shall ensure a secure connection to the aerogel during flight.	✓	Analysed in section 7.1 and section 7.2.
REQ-SYS-DEP-02	The deployment subsystem shall be able to pick up aerogel with dimensions 1.5 x 0.003 x 3.33 m³.	✓	UAV is designed to carry these dimensions at outlined in section 7.2.
REQ-SYS-DEP-03	The deployment subsystem shall provide an aerogel positioning accuracy of 0.5m.	×	Analytically analysed in Figure 7.2, however further simulation required.
REQ-SYS-DEP-04	The deployment mechanism shall not compromise the structural integrity of the aerogel payload	✓	Analysed in section 7.1.
REQ-SYS-DEP-06	The deployment mechanism shall be capable of emergency release of the aerogel in case of critical failure	✓	Integrated function of the XD-10 winch as mentioned in section 7.2.

Table 7.1: Compliance Matrix Deployment Requirements

As mentioned in the Table 7.1, REQ-SYS-DEP-03 requires further simulation. While the deployment accuracy has been analysed by considering the swing-monitoring properties of the winch and the size of the aerogel,

additional aerodynamic simulation of the deployment would lead to a more refined estimate.

8

Power and Propulsion

In this chapter the design of the power and propulsion subsystem will be explained. To design this system the first step was to determine an initial estimate of the required power of the motors for VTOL and cruise. The method for calculating this is explained in section 8.1. Based on the results of this analysis, the motors and propellers could be sized and selected in section 8.2. Taking into account the motor selection, the power budget can be constructed. This is explained in section 8.3. The final step of the design for this subsystem is the battery sizing. This is explained in section 8.4, the last section of the chapter.

8.1. Propulsion Requirement Analysis

The propulsion subsystem was split into 2 sections, the power required for VTOL, and the power required for cruise (i.e. the fixed wing). The power for hovering was assumed to be the same as the power required for VTOL. In theory it's less than VTOL requirement, but since the same motors and propellers will be used, it is considered as a worst case scenario. Once the required power is calculated, the motors and rotors can be chosen, which gives the power available, the masses and the sizing. A summary of the power required that is calculated is given in Table 8.1.

Table 8.1: Propulsion System Specifications

Variable	Description	Value	Unit
$P_{r_{\text{VTOL}}}$	Total Power Required VTOL	3475	$[W]$
$P_{r_{\text{Cruise}}}$	Total Power Required Cruise	849	$[W]$
$(d \text{ x } p)_{\text{prop,VTOL}}$	Propeller Dimensions	0.762 x 0.267	$[m]$

First the VTOL power required will be calculated and then the Cruise Power required. The inputs that are used to calculate them are shown in Table 8.2.

Table 8.2: Inputs for Propulsion System Sizing

Variable	Description	Value	Unit
ROC_{VTOL}	VTOL Rate of Climb	6	$[m/s]$
rho	Density at 3000 m	0.9093	$[kg/m^3]$
W_{TO}	Maximum Take-off Weight	294.3	$[N]$
η_{prop}	Efficiency of the propeller	0.83	-
M_{TO}	Maximum Take-off Mass	30	$[kg]$
V_{cruise}	Velocity at Cruise	27.78	$[m/s]$
C_{D_0}	Zero Lift Drag	0.040	-
AR	Aspect Ratio	7	-
e	Oswald Efficiency Factor	0.7	-
$ROC_{service}$	Rate of Climb at Service Ceiling	0.5	$[m/s]$
V_{stall}	Stall Velocity	19	$[m/s]$
$C_{L_{max}}$	Maximum Lift Coefficient	1.34	-

VTOL Power Required

To calculate the required VTOL power Equation 8.1 must be used . Where T is the total thrust, v_i is the induced axial climb velocity and FM is the figure of merit [59].

$$P_{\text{req}}^{\text{VTOL}} = \frac{Tv_i}{\text{FM}} \tag{8.1}$$

The v_i and FM can be calculated via Equation 8.2 and Equation 8.3, where the FM is based on a regression model.

$$\frac{v_i}{v_h} = -\frac{(ROC)_{VTOL}}{2v_h} + \sqrt{(\frac{(ROC)_{\text{VTOL}}}{2v_h})^2 + 1} \tag{8.2}$$

$$\text{FM} = 0.4742 \cdot T^{0.0793} \tag{8.3}$$

To calculate the v_i, the hover velocity is also needed, which can be calculated with Equation 8.4. Where T is the total thrust and S_{prop} is the propeller surface area [59].

$$v_h = \sqrt{\frac{T}{2\rho S_{\text{prop}}}} \tag{8.4}$$

To calculate T Equation 8.5 can be used, it only needs to be multiplied with the maximum takeoff weight to get the total thrust. To calculate S_{prop} Equation 8.6 and Equation 8.7 can be used, where DL is the propeller disk loading [59].

$$(T/W)_{\text{climb}^{\text{VTOL}}} = 1.2(1 + \frac{1}{W/S}\rho(ROC)^2_{\text{VTOL}}(S_{\text{tot}}/S_{\text{w}})) \tag{8.5}$$

$$S_{prop} = \frac{W_{\text{TO}}}{DL \cdot n_{\text{prop}}} \tag{8.6}$$

$$DL = 3.2261M_{\text{to}} + 74.991 \tag{8.7}$$

Now, since all the values in Equation 8.1 are known, they can be substituted in, yielding the result in Table 8.1.

Cruise Power Required

After the VTOL sizing the cruise propulsion sizing can be done. Or in other words the fixed wing propulsion sizing. The first step in cruise sizing is to perform a constraints analysis, which is a graph consisting of the power loading (P/W) against the wing loading (W/S). From this graph a (P/W) will be determined for cruise which will be used to size the cruise propulsion system[59].

The cruise power can be calculated with Equation 8.8. Where T/W is the thrust to weight ratio. The T/W for the fixed wing has to be calculated during cruise, during climb and at the service ceiling. The V is the velocity, for cruise the cruise velocity will be used, for climb the ROC will be used, and for the service ceiling the service ceiling ROC will be used [59].

$$P/W = \frac{(T/W)V}{\eta_{\text{prop}}} \tag{8.8}$$

To calculate the different T/W Equation 8.9, Equation 8.10 and Equation 8.11 will be used [59]. Equation 8.10 will also be used for the service ceiling but with the ROC at the service ceiling. Furthermore the T/W ratio will be calculated for different wing loadings so that a graph can be produced .

$$(T/W)_{\text{cruise}} = qC_{D_0}\frac{1}{W/S} + k\frac{1}{q}W/S \tag{8.9}$$

$$(T/W)_{\text{climb}} = \frac{ROC}{V_{\text{ROC}}} + \frac{q}{W/S}C_{D_0} + \frac{k}{q}(W/S) \tag{8.10}$$

$$V_{\text{ROC}} = \sqrt{\frac{2}{\rho}W/S\sqrt{k}3C_{D_0}} \tag{8.11}$$

In addition to the power loading the for the different T/W ratios the wing loading at stall will also need to be calculated for the constraints diagram. This is calculated with Equation 8.12 [59].

$$(W/S)_{\text{stall}} = 0.5 V_{\text{stall}}^2 \rho C_{L_{\max}} \tag{8.12}$$

Once all the equation are obtained they can be plotted on a graph. This is shown in Figure 8.1.

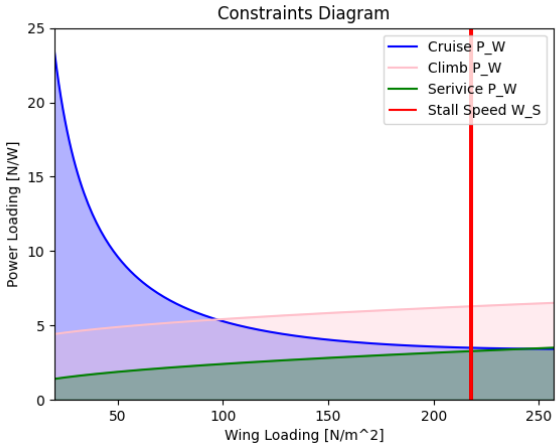

Figure 8.1: Constraints Diagram

As can be seen from the graph the most constraining equation is the climb power for the fixed wing. Therefore, the point that will be taken as the required power loading for cruise (for the fixed wing) will be the intersection between the climb equation and the wing loading at stall. Multiplying this power loading by the maximum takeoff weight gives the optimal cruise power which is shown in Table 8.1.

8.2. Motor and Propeller Sizing

Based on the requirements provided in Table 8.1 motors can be selected for the UAV. The motor that was selected is the U8 Lite L Efficiency Multirotor UAV Motor (KV110) produced by T-motor. This motor will be utilized for both VTOL and cruise. The driving choice for this motor was the high thrust that it can provide for the low mass. With a mass of $280[g.]$ for a maximum thrust of $11.2[kg]$ (or a ratio of 40 T/m) this motor significantly outperformed other options such as the VL8018 (26.8 T/m) from T-motor. The U8 Lite L motor provides the UAV with a VTOL T/W of 1.5. Generally for VTOL a T/W between 1.2 and 1.5 is suggested for stability during take-off and other disturbances [60]. The motor operates between $48 - 52[V]$ and will each be controlled by a separate T-motor V80A electronic speed controller (ESC). This ESC allows or $40[A]$ continuous current and is rated for up to $59[V]$ (14S battery configuration). Both the ESC and FC (Pixhawk 6X) support communication protocols like DShot [1] [2]. This allows for high resolution 16-bit commands (65,536 levels). Based on the thrust curve of the motor the throttle resolution can be calculated to be $0.003[N]$.

The choice for the propeller can then be made based on the compatibility with the motor. T-motor advises twin blade propellers with varying diameters and pitch. The propeller diameter is limited by the space available next to the tail surfaces of the UAV. Additionally, the propellers have to be spaced with at least one diameter distance between them to avoid any interference between them [61]. Choosing larger propellers would thus increase boom spacing and increase the structural mass of the wing, which has to support the booms. Taking these constraints and the thrust requirement into account the G30*10.5 propeller was selected. These propellers have a diameter of $762[mm]$ and pitch of $268[mm]$. Based on this combined choice of propeller and motor about 75% throttle will be required during the VTOL operation. At this point the motors are using a bit more than $1000[W]$ at around $22[A]$. This matches the specifications of the battery which will be explained in section 8.4.

However, the propellers produced by T-motor only have an ambient operating temperature range up to 65 degrees. Therefore, custom propellers of the same size will have to be produced with a material which is able to operate in these conditions. The CYCOM® 5250-4 Carbon Fibre prepreg matches the necessary requirements for these propellers. This material can operate up to temperature of 204 degree Celcius. Producing custom propellers also allows for the integration of an anti-icing system. This will be discussed further in section 12.2. The propeller surface shape will stay the same as the T-motor G30*10.5 propellers.

[1] `https://store.tmotor.com/product/v80a-bldc-foc-drone-esc.html`, [accessed: 18/06/2025]
[2] `https://docs.holybro.com/autopilot/pixhawk-6x`, [accessed: 18/06/2025]

8.3. Power Budget

With the selection of the motors it is possible to create a power budget for the entire mission. This can then be used to size the battery. The main requirements for the power budget come from the motor power that is used, but all the other subsystems on board also need to be taken into account. A list of the power requirements for all the hardware are given in Table 6.1.

To calculate the total capacity requirement an analysis of the equipment necessary during all the phases was done based on the worst case mission profile (section 4.5). The systems that are assumed to always be turned on are the OBC, FC, GPS, all communication modules and the lights. The winch motor has an idle power consumption of $10[W]$, which also requires power throughout the mission. During deployment the power increases to $100[W]$. The EPM magnets will also require a short burst of power during this phase. Furthermore, the sensors vary in power consumption. During all phases the RGB camera is turned on to provide visuals for the UAV, which requires about $30[W]$. During the scanning phase the other sensors integrated in the module are also utilized increasing the power consumption to a maximum of $58[W]$. Lastly, the servo motor required to actuate the control surfaces are only turned on when the UAV start to transition from VTOL to cruise.

For the different phases the motors being used also vary. During ascent, descent, scanning and deployment only the VTOL motors will be used. As mentioned in section 8.2 the power consumption will be at $1057[W]$ per motor and $4228[W]$ total. Due to the slow climb rate it was assumed that that this would not require a significant increase in power. For the transition phase the VTOL and cruise propeller will be delivering varied thrust as the UAV accelerates. This phase is quite complex to model therefore a conservative estimate was made instead. It was assumed that the VTOL and cruise motors both operate at the nominal 75 % throttle throughout the entire phase. For cruise only the cruise motor is turned on. A throttle setting of 70% was selected for during cruise based on the estimated total drag of the UAV. The calculation for the total drag will be elaborated on in subsection 9.3.2. The power consumption based on the combination of propulsion and other hardware for the different phases are shown in Table 8.3.

Table 8.3: Estimated power consumption per mission phase

Mission Phase	Power (kW)
Power Ascent	4.48
Power Transition	5.58
Power Scanning	4.37
Power Cruise	1.14
Power Descent	4.48
Power Deployment	4.49

Based on Equation 8.13 the required energy in [Wh] for the total mission can be calculated. P_{phase_i} is the sum of the maximum power required for all the systems during that phase, n indicates the amount of times this phase is repeated during the mission and t_{phase_i} is the maximum amount of time that the phase will last.

$$E_{mission} = \frac{\sum(P_{phase_i} \cdot n \cdot t_{phase_i})}{3600} \tag{8.13}$$

The total energy required for the UAV to complete one cycle then amounts to $1.08[kWh]$. As mentioned in section 6.2 the UAV will have a PDB which regulates the voltage for different pieces of hardware. Transforming to lower voltages does introduce some losses. The PDB makes use of Voltrox converters which have an efficiency around 90 %. The voltage does not have to be transformed for the motors and sensor thus the efficiency is higher. However, for simplicity and in order to make a conservative estimate the 90 % efficiency is applied over the total required energy. The required energy from the battery is thus $1.19[kWh]$.

8.4. Battery Sizing

Based on the power budget the battery for the UAV can be sized. To calculate the actual capacity required for the battery the capacity should be multiplied by the depth of discharge (DoD) of the battery. The depth of discharge is designed for 80 % to increase the life time of the battery. Limiting the DoD to 80 % can increase the amount of discharge cycles by more than 20 % [62]. This also provides a safety margin to prevent over discharge, which could damage the cells. Taking into account the DoD the required battery capacity is $1.43[kWh]$.

Next to the capacity it is important to consider the continuous amperage required during the mission. For each phase this was calculated by simply adding the amperage required for each system to determine the total value.

The limiting phase turned out to be the deployment phase where the continuous current amounts to $102[A]$.

For peak currents the maximum power of the motors should be considered on top of the other subsystems. The limiting case is then again during deployment assuming that all VTOL motors have to supply full thrust. The current required per motor at this point is $45.8[A]$, thus the total current required in peak loading conditions is $196.2[A]$.

Based on these requirements the battery that was selected for the mission is the Tattu 17000 mAh 14S LiPo battery. The high energy density of $260Wh/kg$ ensure a light weight solution with a singular battery weighing $3619[g]$. To meet the requirement for the UAV two of these batteries will be used in parallel to obtain a capacity of $1768[Wh]$. This provides a bit more than 20% additional capacity. This provides a buffer in case of unforeseen circumstances during a mission.

This battery allows for a continuous discharge rate of 3C. The amperage can then be calculated based on Equation 8.14.

$$A = E_{capacity} \cdot C_{rate} \tag{8.14}$$

Where $E_{capacity}$ is the battery capacity in $[Ah]$. The continuous current that can be supplied by batteries is thus $102[A]$, which meets the requirement stated above. The peak discharge rate is 10C or $340[A]$ for less than 15 seconds, which is well above the peak requirement for the UAV. The fast charging rate for this battery is at 1C so charging it would require 1 hour. However, according to the power budget the batteries are only being discharged to about 40 % in normal mission operation. This would reduce the charging time to about 36 minutes, which is within the mission time. In collaboration with the manufacturer it could be possible to configure custom batteries which have a higher charge rate. However, due to the time constraints of this project this has been left for the next phase of development.

8.5. Compliance Matrix

In this section the requirement compliance matrix will be presented. It will show whether the propulsion and power requirements have been met and how they have been met. The compliance matrix can be seen in Table 8.4. One Requirement was removed from the initial formulation of the requirements which is REQ-SYS-PRP-09 which states that ”The power system shall have an efficiency of at least <TBD>”. This requirement was not relevant any more as the design is more power-constrained rather than efficiency-constrained.

Table 8.4: Propulsion and Power Compliance Matrix

Identification	Description	Compliance	Method of Verification
REQ-SYS-PRP-01	The power subsystem shall indicate its battery charge level.	✓	The UAV gets updated about the battery charge level
REQ-SYS-PRP-02	The VTOL propulsion subsystem shall provide a thrust of at least 1.2 times the MTOW.	✓	This thrust level was incorporated in the analysis stage
REQ-SYS-PRP-03	The propulsion subsystem shall provide a minimum pitching moment of 20.4 Nm in VTOL.	✓	Analysis: see section 10.4
REQ-SYS-PRP-04	The propulsion subsystem shall provide a minimum rolling moment of 17 Nm in VTOL.	✓	Analysis: see section 10.4
REQ-SYS-PRP-05	The propulsion subsystem shall provide a minimum yawing moment 12.23 Nm in VTOL.	✓	Analysis: see section 10.4
REQ-SYS-PRP-06	The propulsion subsystem shall have a throttle resolution higher than 1 N.	✓	Analysis: see section 8.2
REQ-SYS-PRP-07	UAV batteries shall be rechargeable from 20% to 80% in 2500 seconds.	✓	Analysis, see section 8.4
REQ-SYS-PRP-08	The power subsystem shall be able to power all of the UAV electrical components for the duration of the mission.	✓	Analysis: see section 8.4
REQ-SYS-PRP-10	The UAVs power source shall be replaceable	✓	The Batteries are removable
REQ-SYS-PRP-11	The UAVs shall be able to connect to the nest power source.	✓	The batteries are removable and are compatible with the nest generator.

8.6. Sensitivity Analysis

To further investigate the feasibility of the design and establish the performance boundaries of the power and propulsion subsystem a sensitivity analysis was performed. The battery is a critical component of the UAV, therefore it is important to analyse how the degradation of this component will effect the performance of the

UAV. To analyse this the UAV range was calculated depending on the amount of load cycles that the battery has endured.

The results of this analysis are presented in Figure 8.2 and show that for 900 cycles of 80% discharge the battery degrades to 70% of initial capacity. As a reference the degradation for 100% discharge is also shown. For full discharge cycles the batteries reduce to 70 % capacity after only 600 cycles. As mentioned in the previous section 8.4, a DoD of only 80% is required for the most constraining mission trip. Due to the margin in battery capacity the UAV range only decreases after more than 750 cycles. Once the batteries do not allow for the full range requirements to be met, they are no longer suitable for wildfire mitigation. However, they could still be used in the oil spill application. For oil spill mitigation a smaller range is required since the nests are located on freighters and oil rigs.

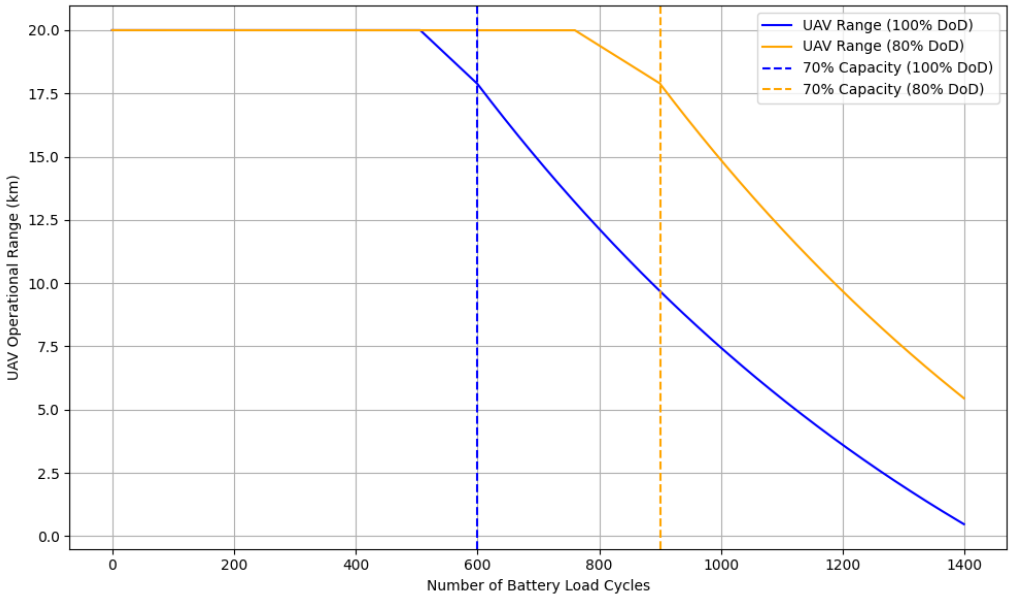

Figure 8.2: UAV Range Depending on the Number of Battery Load Cycles.

To model the battery degradation a linear model was assumed up to 70% of the initial capacity according to research done with LiPo cells for different DoD fractions [3]. After this 70% threshold the battery degrades at a quicker rate and was modelled according to an exponential relationship [63]. It should be noted that the battery discharges at varying rates throughout the mission and operates in higher ambient temperature. This also has an effect on the degradation, however, this was not taken into account in this initial analysis. During the testing of the UAV, the battery degradation should be monitored to obtain a more accurate estimation of the lifetime.

To ensure that the VTOL motors provide enough thrust margin a sensitivity analysis was performed which varies the gust loading conditions. Based on the gust loading the margin for stability in VTOL is determined. This analysis is discussed in detail in section 10.6.

[3] `https://batteryuniversity.com/article/bu-808-how-to-prolong-lithium-based-batteries?`, [accessed 22/06/2025]

9

Lifting Surface Design

In this chapter the sizing and placement of main wing and empennage will be explained. Firstly main wing design is described in section 9.1. Afterward the empennage design is described in section 9.2. Following the sizing and placement, aerodynamic analysis of whole configuration is described in section 9.3. At the end, in section 9.4, a sensitivity analysis on the lifting surface design will be laid out.

During the design the tool XFLR5 has been used for estimations of performance. It should be mentioned that XFLR5 has its limitations. It is a potential flow solver, which tends to lose accuracy beyond the linear region or at low Reynolds numbers. Since XFLR5 is used for estimates in cruise conditions, which falls within the linear, high Reynolds region, the model should be reliable. However results should still be critically evaluated.

9.1. Main Wing Design

In this section the main wing design will be explained. The design consists of two parts. Firstly in subsection 9.1.1 the wing planform will be detailed. Secondly in subsection 9.1.2 the aerofoil selection will be explained.

9.1.1. Main Wing Sizing

From a preliminary estimate on the wing loading of the wing, the wing planform was constructed. The aspect ratio and wing area were kept constant across planform iterations. According to Equation 9.1, the wing was sized for $C_{l_{des}}$ of 0.455.

$$C_{l_{des}} = \frac{1}{q} \cdot [(\frac{W}{S})_{MTOW} + (\frac{W}{S})_{OEW}] \tag{9.1}$$

The taper ratio was initially set to 0.7 in order to reach a more elliptical lift distribution compared to the rectangular wing. However constrained by the battery size and wing area this ratio had to be increased to 0.85. No leading edge sweep was implemented for two reasons: less complex manufacturability and no need for increased critical Mach number as cruise velocity is sufficiently low. The wing incidence angle was set to 2° to fly in cruise conditions around zero angle of attack. The final wing modification considered was wing twist. In order to have stall occur first at the root, a wing twist of -1° was implemented at the tip. The twist varies linearly from -1 to 0 in the modular part of the wing. The placement of the wing will be discussed in section 9.2. Final wing parameters can be seen in Table 9.1.

Table 9.1: Wing Geometry

Variable	Description	Value	Unit
Cl_{des}	Design Lift Coefficient	0.455	$[-]$
S	Wing Surface Area	1.27	$[m^2]$
AR	Aspect Ratio	7.08	$[-]$
b	Wing Span	3.00	$[m]$
C_r	Root Chord	0.458	$[m]$
MAC	Mean Aerodynamic Chord	0.42	$[m]$
λ	Taper Ratio	0.85	$[-]$
Λ_{LE}	Leading Edge Sweep	0	$[°]$
θ_{root}	Root twist	0	$[°]$
θ_{tip}	Tip twist	-1.00	$[°]$
α_i	Wing Incidence angle	2	$[°]$

9.1.2. Main Wing Aerofoil Selection

From the battery sizing, it was clear that the E1210 aerofoil could not house the battery. To create space, either the chord length of the wing had to be increased, or the aerofoil could be reconsidered. The latter was chosen as this lead to minimum design snowballing.

Requiring the battery to fit at 15 [cm] spanwise (fuselage radius), the new thickness to chord ratio for the aerofoil had to be determined. In order to attain an estimate of the thickness to chord ratio, the span-wise chord length was needed. This was calculated with Equation 9.2:

$$c(y) = c_r \cdot (1 - \frac{(1-\lambda)}{b/2} \cdot y) \tag{9.2}$$

Assuming a thickness of at least 8 cm at the wing fuselage intersection. A thickness to chord ratio of 0.185 or higher was needed.

In order to retain the aerodynamic characteristics of the E1210, aerofoils within the Eppler group with the required thickness to chord ratio were selected for reconsideration. Because of the curvature of the aerofoil, the thickness to chord is not a tight criteria to check whether the battery fits. Therefore visual confirmation was done in CATIA. The aerofoil maintaining comparable aerodynamic properties, while fitting the battery, was the E1233.

The difference in performance is displayed in Figure 9.1 and Figure 9.2. Since the camber is lower, the CL-alpha curve shifted down. This is acceptable, since design lift coefficient can still be achieved at approximately three degrees angle of attack and stall speed is not limiting due to the VTOL mode. The drag bucket got less wide, however around the design lift coefficient the drag performance stayed the same. Thus the choice for E1233 degraded the performance near stall conditions, but stayed the same around cruise performance. Final aerofoil values can be found in Table 9.2.

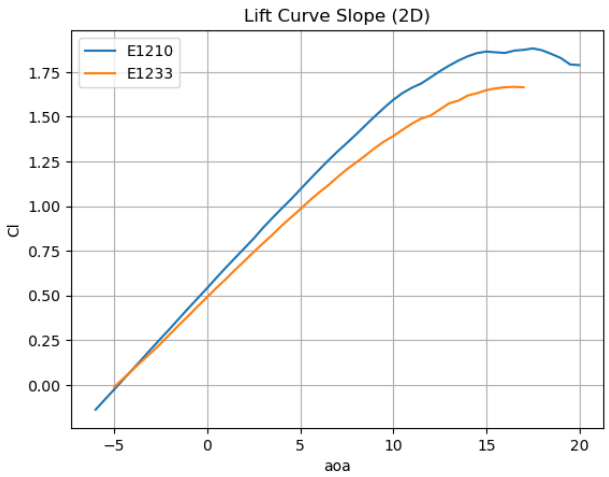

Figure 9.1: Cl vs alpha for E1210 and E1233 at Re = 780000

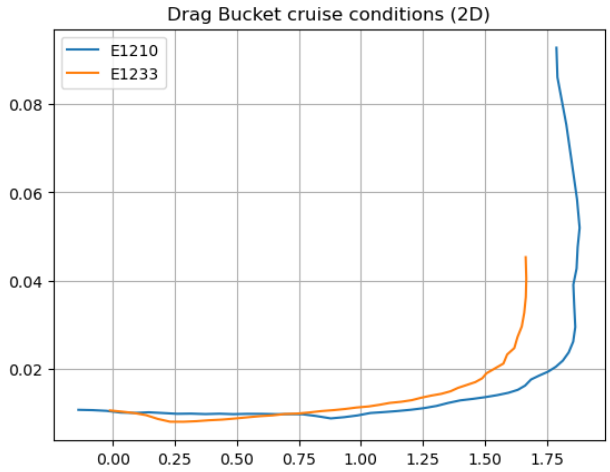

Figure 9.2: Cl vs CD for E1210 and E1233 at Re = 780000

Table 9.2: E1233 Parameters

Variable	Description	Value	Unit
$\frac{t}{c}$	Thickness to Chord Ratio	0.189	$[-]$
$\frac{x}{c}$	Location of Max Thickness	0.298	$[-]$
m	Maximum Camber	0.04	$[-]$
$\frac{x_m}{c}$	Location Maximum Camber	0.298	$[m]$
CL_{max}	Maximum Lift Coefficient	1.65	$[-]$
CL_α	Lift Slope	0.1	$[\frac{1}{\circ}]$
α_s	Stall Angle of Attack	17	$[^\circ]$
α_{L0}	Zero Lift Angle of Attack	-5	$[^\circ]$

9.2. Empennage Design

Firstly the horizontal stabiliser sizing will be described. In order to size the horizontal stabiliser a CG track and scissor plot were made, Figure 9.3 and Figure 9.4 respectively. Based on these plots the wing position was set to 48% of the fuselage length, in order to minimise tail area. This places the UAV CG on top of the payload CG, ensuring minimal CG variation. The tail was placed at the rear end of the fuselage in order to create the largest moment arm.

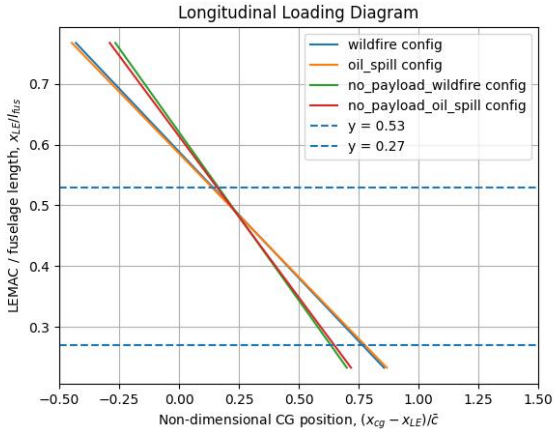

Figure 9.3: CG track of UAV, varying wing placement for payload and no payload configuration

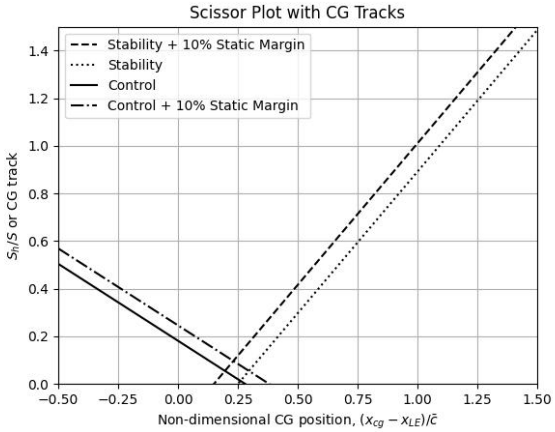

Figure 9.4: Scissor Plot UAV

However, the corresponding surface ratio did not allow for trimming at reasonable angles of attack. Therefore the horizontal stabiliser was increased in XFLR5, keeping aspect ratio constant. Iteration was done until the following criteria were met:

- $\frac{dCm}{d\alpha} < 0$
- $cm = 0$ @ $\alpha = 0$
- Static Margin $\geq$ 0.1

In the case of the static margin condition not being met, the centre of gravity of the design was revised.

A same process of iteration in XFLR5 was implemented for the vertical stabiliser. Based on the rudder sizing, which will be discussed in section 10.2, a balance between controllability and stability was sought. The starting point of the iteration were estimates from the midterm report [64]. These values were polished in XFLR5 based on yaw performance. It was required to have $\frac{dCn}{d\beta} > 0$.

The final stability curves can be seen in. All mentioned conditions are satisfied. Because the CG is placed almost directly on top of aerogel CG, only a slight shift is noted in Cm_α.

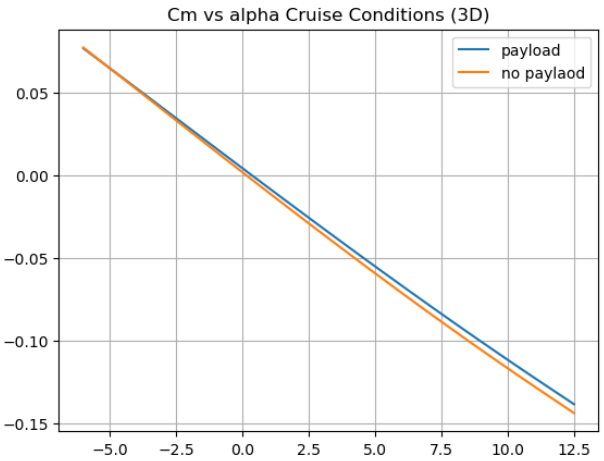

Figure 9.5: Cm vs alpha curves for payload and no payload configurations in cruise conditions (XFLR5)

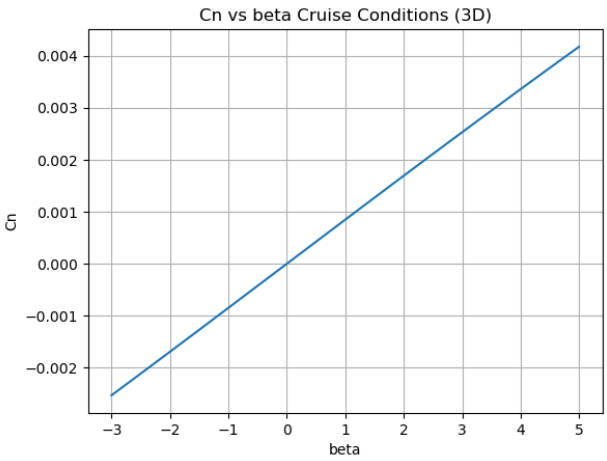

Figure 9.6: Cn vs beta in cruise conditions (XFLR5)

For both horizontal and vertical stabiliser the NACA0012 aerofoil was chosen due to its symmetric shape and moderate thickness. Final Values for tail parameters can be found in Table 9.3 and Table 9.4. Placement of lifting surfaces and stability parameters can be found in Table 9.5.

Table 9.3: Horizontal Tail Geometry

Variable	Description	Value	Unit
$\frac{S_h}{S}$	Surface Area Ratio	0.173	$[-]$
l_h	Tail Moment Arm	0.818	$[m]$
V_h	Tail Volume Coefficient	0.337	$[-]$
AR_h	Aspect Ratio	3.5	$[-]$
b_h	Span	0.88	$[m]$
C_{r_h}	Root Chord	0.25	$[m]$
MAC_h	Mean Aerodynamic Chord	0.25	$[m]$
λ_h	Taper Ratio	0	$[-]$
Λ_{LE_h}	Leading Edge Sweep Angle	0	$[^\circ]$
α_{i_h}	Incidence Angle	-3.9	$[^\circ]$

Table 9.4: Vertical Tail Geometry

Variable	Description	Value	Unit
$\frac{S_v}{S}$	Surface Area Ratio	0.071	$[-]$
l_v	Tail Moment Arm	0.768	$[m]$
V_v	Tail Volume Coefficient	0.0182	$[-]$
AR_v	Aspect Ratio	1.6	$[-]$
b_v	Span	0.38	$[m]$
C_{r_v}	Root Chord	0.3	$[m]$
MAC_v	Mean Aerodynamic Chord	0.25	$[m]$
λ_v	Taper Ratio	0.6	$[-]$
Λ_{LE_v}	Leading Edge Sweep Angle	13.5	$[^\circ]$
α_{i_v}	Incidence Angle	0	$[^\circ]$

Table 9.5: Stability and Placement Parameters

Variable	Description	Value	Unit
$\frac{x_c g}{l_f}$	Centre of Gravity	0.530	$[-]$
$\frac{x_n p}{l_f}$	Neutral Point Position	0.557	$[-]$
S.M.	Static Margin	0.138	$[-]$
$\frac{x_w}{l_f}$	Wing Position	0.484	$[-]$
$\frac{x_h}{l_f}$	Horizontal Stabiliser Position	0.884	$[-]$
$\frac{x_v}{l_f}$	Vertical Stabiliser Position	0.860	$[-]$
$\alpha_{cm=0}$	Zero Moment AOA	0.2 - 0.3	$[^\circ]$
$\frac{dCm}{d\alpha}$	Moment Coefficient Slope	-0.012	$[\frac{}{^\circ}]$
$\frac{dCn}{d\beta}$	Yaw Coefficient Slope	0.0085	$[\frac{}{^\circ}]$

9.3. Aerodynamic Performance

Two methods were used to estimate aerodynamic performance; XFLR5 and DATCOM empirical estimations. Where possible the results were cross-validated. In subsection 9.3.1 the lift estimation methods will be explained and lift performance analysed. In subsection 9.3.2 the drag estimations will be explained and drag performance analysed. In subsection 9.3.3 loading diagrams for manoeuvring and gust are created.

9.3.1. Lift Estimates

With the lift estimates used, only main wing contributions are accounted for, as it is assumed that the tail will provide a negligible contribution. Tail contributions are taken into account in XFLR5 simulations.

Firstly CL_α for the 3D wing was determined based on Equation 9.3.

$$C_{L_\alpha}[1/\text{rad}] = \frac{C_{l_\alpha} \cdot AR}{2+\sqrt{4+\left(\frac{AR\cdot\beta}{\eta}\right)^2\left(1+\frac{\tan^2\Lambda_{0.5c}}{\beta^2}\right)}} \qquad (9.3)$$

$$\beta = \sqrt{1-M^2} \qquad (9.4)$$

Where Cl_α is the aerofoil lift slope, β the Prandtl-Glauert correction term and η a correction factor set to 0.95 [65].

Then CL_{max} was estimated with Equation 9.5, where $[\frac{C_{L_{max}}}{C_{l_{max}}}]$ was determined to be 0.9 for no leading edge sweep aircraft. From here an estimate on the stall angle was made with Equation 9.6. Where $\Delta\alpha$ was determined to be two for wings with an aspect ratio of seven.[65]

$$C_{L_{max}} = \left[\frac{C_{L_{max}}}{C_{l_{max}}}\right] C_{l_{max}} \quad (9.5) \qquad \alpha_{stall} = \frac{C_{L_{max}}}{C_{L_\alpha}} + \alpha_{0L} + \Delta\alpha_{C_{L_{max}}} \quad (9.6)$$

The results of the DATCOM method and XFLR5 simulation are displayed in Figure 9.5. It can be seen that the DATCOM method and XFLR5 differ only slightly near angles of attack close to zero, showing more divergence when moving towards stall angle of attack. The wing + tail configuration has a correction factor of 0.9 included to account for propeller and fuselage interference effects. It should be noted that the methods overestimate CL near stall angle of attack. Lift curve parameters are displayed in Figure 9.6.

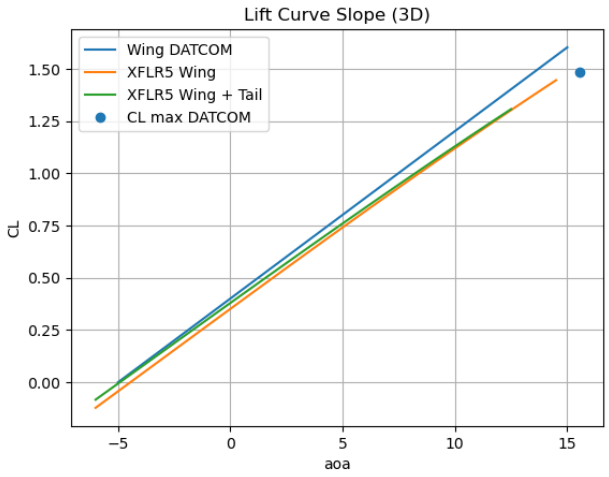

Figure 9.7: CL vs alpha curve at cruise conditions

Table 9.6: Lift Curve Parameters

Variable	Description	Value	Unit
CL_{max}	Maximum Lift Coefficient	1.31	$[-]$
α_s	Stall Angle of Attack	15.5	$[°]$
CL_α	Lift Curve Slope	0.071	$[1/°]$

9.3.2. Drag Estimates

Drag estimates were also done with both an analytical method and XFLR5. The analytical method used was Component Drag Build-Up. This method estimates a flat plate skin friction coefficient and applies correction factors in order to get zero lift drag estimates, according to Equation 9.7.

$$C_{d_0} = \frac{1}{S_{ref}} \sum_c C_{f_c} \cdot FF_c \cdot IF_c \cdot S_{wet_c} + C_{D_{misc}} \quad (9.7)$$

Where C_{f_c} is the flat plate skin friction coefficient, FF_c form factor of component, IF_c interference factor related to component, S_{wet_c} wetted area of component and C_{d_m} miscellaneous drag e.g. propellers or landing gear.

The flat plate skin friction coefficient had to be calculated for laminar and turbulent flow regimes. Equation 9.8 was used for laminar flow and Equation 9.9 for turbulent flow. The total C_f was calculated as a weighted sum of laminar and turbulent region contributions. For the main wing a laminar region of 0.1 was assumed, for the empennage 0.05 and for the fuselage 0. The Reynolds number was calculated for cruise conditions[65].

$$C_f = \frac{1.328}{\sqrt{Re}} \quad (9.8) \qquad C_f = \frac{0.455}{log_{10}(Re)^{2.58}(1+0.144M^2)^{0.65}} \quad (9.9)$$

The form factor of the wing, horizontal stabiliser and vertical stabiliser were calculated with Equation 9.10.

$$FF = [1 + \frac{0.6}{(x/c)}(\frac{t}{c}) + 100(\frac{t}{c})^4] \cdot [1.34M^{0.18}cos(\Lambda)^{0.28}] \quad (9.10)$$

Where $\frac{t}{c}$ is the thickness to chord ratio of the aerofoil and $\frac{x}{c}$ the location of max thickness on the aerofoil.

For the fuselage Equation 9.11 was used to calculate the form factor.

$$FF = 1 + \frac{60}{f^3} + \frac{f}{400} \quad (9.11) \qquad f = \frac{l_f}{\sqrt{(4/\pi)A_{max}}}$$

Where A_{max} is the maximum frontal area of the fuselage and l_f the total length of the fuselage.

The Wing, fuselage and empennage drag were estimated trough this form factor, combined with an interference factor. These values typically range from 1 to 1.5 [65]. For the wing a factor of 1.2 was assumed, due to interference with the fuselage and front two VTOL propellers. For the empennage a factor of 1.3 was assumed, due to interference with the fuselage and main wing. Finally for the fuselage a factor of 1.1 was assumed, due to interference with the wing.

The zero lift drag of the VTOL Propellers, cruise propeller and landing gear was approached differently, as the statistic relations did not hold up.

A CD_0 per component was assumed, slightly lower than the one for a flat plate in order to give a conservative estimate. These where then converted to CD_0 components of the UAV with Equation 9.12. For the propellers a CD_0 of 1.1 was assumed. The landing gear CD_0 was assumed to be 0.7, due to its cylindrical shape. The component reference areas were estimated to be rectangles.

$$D = qC_{D_c}S_c = q\frac{S_c C_{D_c}}{S_{ref}}S_{ref} = qC_{D_{ref}}S_{ref} \tag{9.12}$$

Combining all the drag components, the total drag coefficient could be calculated with Equation 9.13. Where the Oswald efficiency factor was estimated with Equation 9.14.

$$CD = CD_0 + \frac{CL^2}{\pi \cdot AR \cdot e} \tag{9.13}$$

$$e = 1.78(1 - 0.045AR^{0.68}) - 0.64 \tag{9.14}$$

The final results are displayed in Figure 9.8 and Figure 9.9. As expected XFLR5 underestimates the drag compared, however around cruise conditions both estimates do show the same trend, again indicating validity in linear regions. It can also be seen that the addition of propeller, fuselage and landing gear do increase the drag significantly. Final drag parameters are displayed in Table 9.7. It should be noted that effects of air ducts in the wing is not taken into account in this analysis. These air ducts are not likely to influence aerodynamic performance significantly [66]. However the behaviour will have to be analysed in further design.

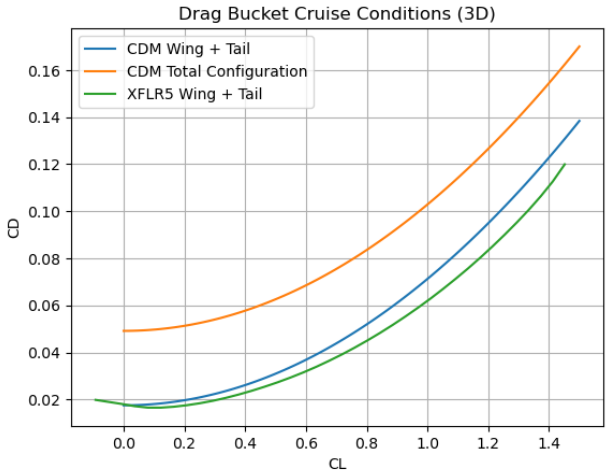

Figure 9.8: CL vs CD in cruise conditions

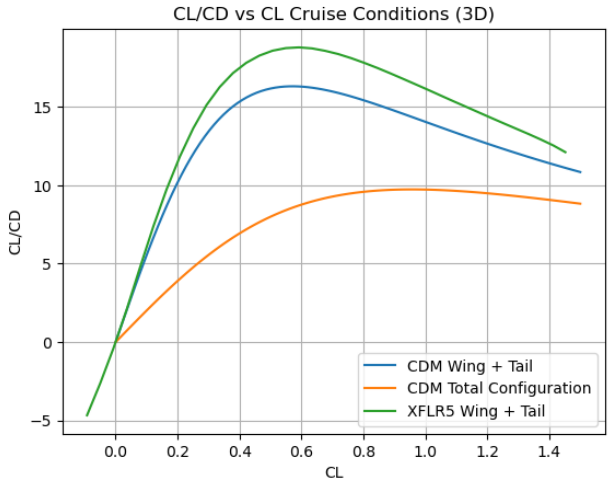

Figure 9.9: CL/CD vs CL in cruise conditions

Table 9.7: Drag Parameters

Variables	Description	Value	Unit
CD_{0_w}	Zero Lift Drag Wing	0.0152	$[-]$
CD_{0_h}	Zero Lift Drag Horizontal Stabiliser	0.0025	$[-]$
CD_{0_v}	Zero Lift Drag Vertical Stabiliser	0.0010	$[-]$
$CD_{0_{fus}}$	Zero Lift Drag Fuselage	0.0072	$[-]$
$CD_{0_{land}}$	Zero Lift Drag Landing Gear	0.0015	$[-]$
$CD_{0_{VTOL}}$	Zero Lift Drag VTOL Propellers	0.0031	$[-]$
$CD_{0_{push}}$	Zero Lift Drag Pusher Propeller	0.02	$[-]$
CD_0	Total Zero Lift Drag	0.051	$[-]$
e	Oswald Efficiency Factor	0.84	$[-]$
$\frac{CL}{CD}_{cruise}$	Lift over Drag Cruise	7.3	$[-]$
D	Drag Cruise	36.6	$[N]$

9.3.3. Loading Diagrams

Two cases where considered for the aerodynamic loading diagrams. Manoeuvring loads and gust loads.

Manoeuvring loads where calculated with Equation 9.15. Where a maximum load factor of 3.5 and minimum of -1 were implemented. The dive velocity was assumed to be 1.4 times the cruise velocity. [65]

$$n = \frac{L}{W} = \frac{q \cdot C_{L_{max}}}{W/S} \tag{9.15}$$

The gust load diagram was constructed via Equation 9.16. A gust of 30 [km/h] was assumed to hit the UAV perpendicular to the cruise velocity.

$$\Delta L = \frac{1}{2}\rho V^2 S C_{L_\alpha} \Delta\alpha \tag{9.16}$$

$$\Delta\alpha = tan^{-1}(\frac{u}{V})$$

The final loading diagram can be seen in Figure 9.10. From the figure it was concluded that the critical loading case was [n = 3.5], due to gust in cruise.

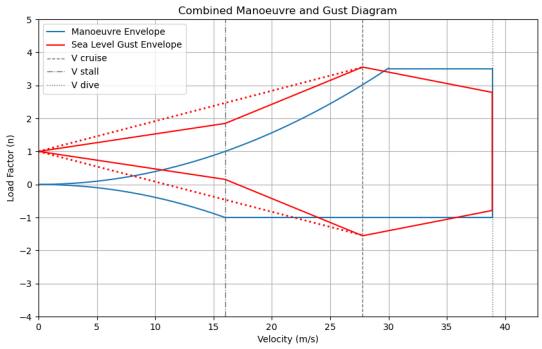

Figure 9.10: Manoeuvre and Gust loading diagram

9.4. Sensitivity Analysis

In this section the sensitivity of the aerodynamic performance will be analysed. The sensitivity of lift coefficient with corresponding angle of attack and the sensitivity of the lift drag curve to angle of attack will be laid out. The effect of changing aspect ratio on performance will also be investigated.

The sensitivity of the required lift coefficient to density and cruise speed can be seen in Figure 9.11. Its corresponding angle of attack is displayed in Figure 9.12.

It can be seen that at low densities the velocity must stay sufficiently high to avoid stall. The cruise speed of 100 [km/h] is sufficient to avoid stall at all densities. On the other side if it is found that cruise speed has to be increased, angle of attack decreases. In that case the incidence angle of the wing must be adjusted accordingly.

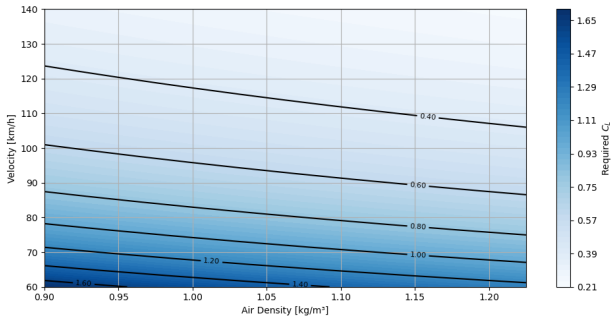

Figure 9.11: CL for varied densities and cruise velocities

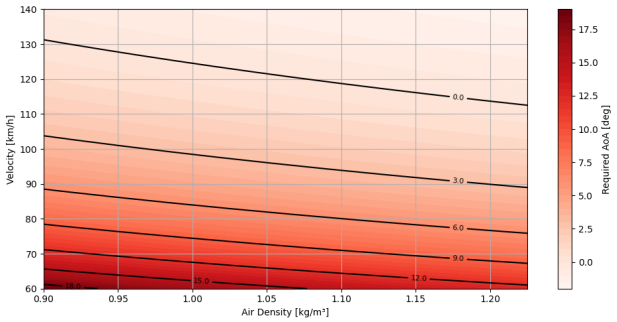

Figure 9.12: AOA corresponding to CL for varied densities and cruise velocities

In Figure 9.13 the sensitivity of the drag bucket to different aspect ratios of the main wing can be seen. It is a clear trend that for higher aspect ratio the lift over drag decreases. Ideally the aspect ratio would therefore be increased. This would however lead to the battery not being able to fit inside the wing. If the battery is decreased in size, the aspect ratio of the main wing should be reconsidered. Another consideration is the addition of winglets. In the current design these were excluded for simplicity of manufacturability, but they do tend to increase the effective aspect ratio by roughly 20% [65]. Thus if higher lift over drag is required, winglets could prove beneficial.

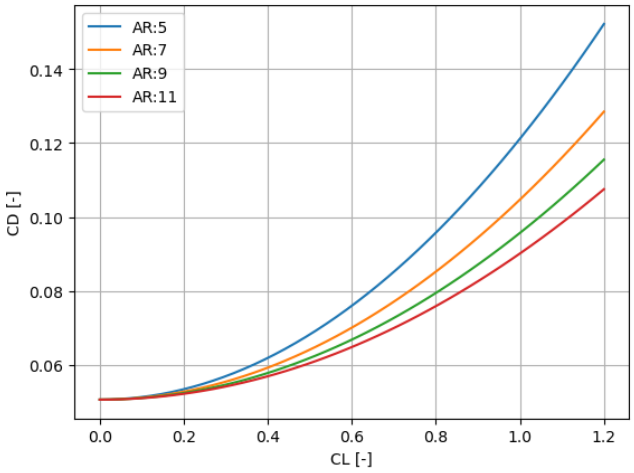

Figure 9.13: Drag Bucket Sensitivity to aspect ratio of main wing

10

Stability and Control

AeroShield UAVs must remain both stable and highly manoeuvrable during operation, which includes take-off and landing, cruising to the disaster area, hovering, and deployment of the aerogel payload. During operation, the UAVs also face up to $30[\frac{km}{h}]$ gusts, which would destabilize them if not properly accounted for.

This chapter focuses on the sizing of the control surfaces of the UAVs for cruise mode, as well as the evaluation of VTOL control during take-off, landing, and hover phases, to ensure that the UAVs can both handle the gusts and have good manoeuvrability. Finally, a compliance matrix is included for subsystem requirements related to Stability and Control.

10.1. Aileron Sizing

Ailerons are the control surfaces on the wing that allow the UAVs to have roll control during cruise. Ailerons are mainly sized from a required roll rate, which must be achievable at, at least, V_{stall}. For good roll manoeuvrability, this required roll rate is set to $35[\frac{^\circ}{s}]$ [67]. To add some margin, the roll rate requirement is evaluated at $0.8V_{stall}$.

In that sense, the UAV's roll-rate, roll stability derivative (C_{l_p}) must be calculated according to Equation 10.1. In this equation, c_{l_α} the airfoil's lift coefficient, c_{d_o} the airfoil's zero-lift drag coefficient, S the wing's surface area, b the wing span, and $c(y)$ the wing chord as a function of the spanwise position.

$$C_{l_p} = -\frac{4(c_{l_\alpha} + c_{d_0})}{S_{ref} b} \int_0^{b/2} y^2 c(y) dy \tag{10.1}$$

Then, some new parameters must be defined. First, the aileron chord to wing chord ratio ($\frac{c_a}{c}$) is assumed to be 0.3 for an initial sizing of the ailerons, based on statistical aircraft aileron data. Then, the innermost spanwise position of the aileron (b_i) is set to $0.875[m]$. This value is calculated based on the spanwise positioning of the cut in the wing, which is $0.762[m]$, plus some margin. Comparing with the statistical aircraft aileron data, b_i ranges between 40-65% [65] of the aircraft half-span. With $b_i = 0.875[m]$, it falls at 58.3% of the half-span ($1.5[m]$), which is well within the reasonable range.

Additionally, values for b_o, the outermost spanwise position of the aileron, and $\delta_{a_{max}}$, the maximum upwards aileron deflection, need to be set. $\delta_{a_{max}}$ is set to a mid-range value of $25[^\circ]$, from an aircraft data range of $12.5 - 30[^\circ]$ [65]. As an initial estimate, b_o is set to $0.9[m]$, which is an intentionally low number. This is because of how the aileron sizing code is structured, which, for an initial value of b_o, calculates if the roll-rate requirement is met and, if not, continually increases b_o and reevaluates the roll-rate requirement until it is met. For this, the UAV's aileron, roll control derivative ($C_{l_{\delta_a}}$) is calculated with Equation 10.2 [65]:

$$C_{l_{\delta_a}} = \frac{2c_{l_\alpha}\tau}{Sb} \int_{b_0}^{b_1} c(y) y dy \tag{10.2}$$

τ is the aileron effectiveness coefficient, and is obtained from a graph that relates it to $\frac{c_a}{c}$ [65]. Finally, before the achieved roll rate is calculated, the effective aileron deflection δ_a must be calculated following Equation 10.3. For this, an aileron differential d_a, the downwards-to-upwards aileron deflection ratio, is set to 0.75 based on statistical aircraft data [65].

$$\delta_a = \frac{\delta_{max}}{2} (1 + d_a) \tag{10.3}$$

Finally, the achieved roll rate can be calculated based on Equation 10.4.

$$P = -\frac{C_{l_{\delta_a}}}{C_{l_p}}\delta_a \left(\frac{2 \cdot 0.8V_{stall}}{b}\right) \tag{10.4}$$

With these calculated values, the iteration loop runs as previously specified. This results in a final value for b_o of $1.452[m]$. This value corresponds to 96.8% of the half-span, which is slightly outside of the consulted statistical range (76 - 95%) [65]. Nonetheless, it is outside of the range by only 1.8%, to the point that it is still considered reasonable at this stage of the design. Nonetheless, the proximity of b_o to the wing tip could have some additional aerodynamic implications, such as the effect of wing tip vortices on nearby section of the aileron, that should be considered more in detail in future stages. In any case, the final aileron dimensions and characteristics are summarized in Table 10.1.

Table 10.1: Aileron Dimensions and Characteristics

Variable	Description	Value	Unit
b_i	Innermost spanwise aileron position	0.875	[m]
b_o	Outermost spanwise aileron position	1.45	[m]
$\frac{c_a}{c}$	Aileron-to-wing-chord ratio	0.3	[-]
δ_{max}	Maximum upwards aileron deflection	25	[°]
d_a	Aileron differential	0.75	[-]

10.2. Rudder sizing

The rudder is the control surface on the vertical tail that allows the UAVs to have yaw control during cruise. Given the UAVs must sustain significant crosswinds and gusts of up to $30[\frac{km}{h}]$, while maintaining their intended flight headings, the rudder is sized based on this requirement. Similarly to the ailerons, this yaw control must be achievable at V_{cruise} and, to add some margin, it is evaluated at $0.8V_{cruise}$.

First, it is necessary to calculate the sideslip that such a crosswind would create, as the UAVs' stability would naturally try to eliminate this sideslip. Given a V_{cruise} of $100[\frac{km}{h}]$, a $30[\frac{km}{h}]$ crosswind would create a sideslip β_{max} of $20.51[°]$ according to Equation 10.5.

$$\beta_{max} = \arctan\left(\frac{V_{crosswind}}{0.8V_{cruise}}\right) \tag{10.5}$$

The yaw control of the UAVs is then determined by Equation 10.6, where $C_{n_{\delta_r}}$ is the UAV's rudder, yaw moment control derivative and C_{n_β} the UAV's sideslip, yaw moment stability derivative. $\delta_{r_{max}}$ is the maximum deflection of the rudder and is set to $25[°]$ according to statistical aircraft rudder data [67].

$$\left|C_{n_{\delta_r}}\right| > \left|\frac{C_{n_\beta}\beta_{max}}{\delta_{r_{max}}}\right| \tag{10.6}$$

In other words, the UAVs' rudder, yaw control derivative must be enough to counteract the natural stabilising moment of the UAVs with the maximum rudder deflection. C_{n_β} is a coefficient that is not easily obtainable analytically. Although the primary contribution for this coefficient comes from the vertical tail, the fuselage sidewash reduces its effectiveness, an effect that is hard to calculate. Because of that, this derivative is evaluated with XFLR5 with a representative model of the UAV. Given a certain rudder geometry, XFLR5 also outputs $C_{n_{\delta_r}}$, therefore the inequality can easily be checked. This allows for a manual optimization process on XFLR5, where the rudder geometry is tweaked from an initial statistically-derived geometry. This initial geometry corresponds to a rudder-to-vertical-tail-span ratio ($\frac{b_r}{b_{vt}}$) of 0.9 [67], with the rudder starting at the root chord of the vertical tail. Additionally, the rudder-to-vertical-tail-chord ratio ($\frac{c_r}{c_{vt}}$) is set to 0.3 [67]. After the optimisation process, the final rudder geometry and characteristics are summarized in Table 10.2.

Table 10.2: Rudder Dimensions and Characteristics

Variable	Description	Value	Unit
$\frac{b_r}{b_{vt}}$	Rudder-to-vertical-tail-span ratio	0.9	[-]
$\frac{c_r}{c_{vt}}$	Rudder-to-vertical-tail-chord ratio	0.5	[-]
δ_{max}	Maximum rudder deflection	25	[°]

10.3. Elevator Sizing

The elevator is the control surface on the horizontal tail that allows the UAVs to have pitch control during cruise. The elevator must also ensure that the UAVs are trimmable for the whole range of allowable CGs. However, based on the design of the AeroShield UAVs, this functionality is not critical. The only mass component in the UAVs that varies during a single mission is the aerogel payload, as it is carried to the disaster site and then deployed there. However, the placement of the aerogel payload inside the UAVs was designed in such a way that its CG coincides with the empty payload configuration. Therefore, the CG of the UAVs does not change between pre- and post-deployment of the aerogel, which makes the elevator not necessary for this trimming purpose. In practice, though, there will be a small change in CG between these two configurations, but the critical case for the sizing of the elevator will be the pitch manoeuvrability. For good pitch manoeuvrability, a pitch rate of $35[\frac{^\circ}{s}]$ is set [67], similarly to the specified roll rate in section 10.1. In that sense, to meet the pitch rate requirement, Equation 10.7 must hold true.

$$\left|C_{m_{\delta_e}}\right| > \left|\frac{C_{m_q}}{\delta_{e_{max}}} \cdot \frac{q\bar{c}}{0.8V_{stall}}\right| \tag{10.7}$$

In other words, the UAV's elevator, pitch control derivative must be enough to counteract the pitch rate damping at the desired pitch rate q with the maximum elevator deflection $\delta_{e_{max}}$. Similarly to section 10.2, these stability and control derivatives can be obtained with XFLR5, and the inequality can be checked and optimised for any given initial elevator geometry. An initial elevator-chord-to-horizontal-tail-chord ($\frac{c_e}{c_{ht}}$) of 0.3 and a $\delta_{e_{max}}$ of $25[^\circ]$ were assumed according to statistical elevator aircraft data [67]. After the optimisation process, the final elevator geometry and characteristics are outlined in Table 10.3.

Table 10.3: Elevator Dimensions and Characteristics

Variable	Description	Value	Unit
$\frac{c_e}{c_{ht}}$	Elevator-to-horizontal-tail-chord ratio	0.2	[-]
δ_{max_e}	Maximum elevator deflection	15	[°]

It was found that, even in this configuration, the UAVs would easily meet the pitch rate requirement. Therefore, in theory, the elevator could still be downsized and its maximum deflection reduced. Nonetheless, to remain within statistically reasonable limits, the design in Table 10.3 was chosen, with values at the lower end of these limits.

10.4. VTOL Control

Additionally, the UAVs must also remain controllable in VTOL mode, especially during deployment of the aerogel blankets. This section will analyse yaw, pitch, and roll control with the VTOL motors against $30[\frac{km}{h}]$ gusts. As a common approach for all three analyses, the relevant surfaces upon which gusts are acting (vertical/horizontal tail or main wing) will be approximated as flat plates with $C_D = 1.28$ [68]. In all cases, gusts will be considered to be acting perpendicularly to these surfaces, making them essentially flat rectangular plates in terms of their (area) projection. Interactions with the fuselage are not considered, but a safety factor of 2 is used in all analyses to compensate for the high uncertainty. Therefore, the force on these surfaces will be calculated with Equation 10.8 for all cases, only varying the surface area S, and evaluating with $\rho = 1.225[\frac{kg}{m^3}]$ and $V_{gust} = 30[\frac{km}{h}]$.

$$F = 2 \cdot \frac{1}{2}\rho S V_{gust}^2 C_D \tag{10.8}$$

The analyses themselves centre around the use of differential thrust or rotation, as required, between the relevant VTOL motors, which enables control around all three axes of the UAVs. The calculations for the VTOL motor thrust or RPM variations for control are first-order accurate and linearized about a nominal condition of hovering. In this nominal condition, the front two VTOL motors are operating at a higher RPM and thrust than the back two VTOL motors. This occurs because these sets of VTOL motors are not symmetrically placed about the about the CG of the UAVs. The front VTOL motors are placed $0.551[m]$ in front of the CG, while the back ones are placed $0.974[m]$ behind it. To maintain level flight, the pitching moments from both sets of VTOL motors must be equal, which results in the front VTOL motors producing $83.88[N]$ of thrust each, a mass-force equivalent of $8.45[kg]$, while the back ones produce $64.27[N]$ each, a mass-force equivalent of $6.45[kg]$.

Finally, the coupling between the control of the three axes is not considered; each axis is treated in isolation. In further stages of design, this would need to be further analysed.

Yaw Control

For analysing yaw control, the critical scenario is determined to be a full $30[\frac{km}{h}]$ gust acting perpendicularly on the vertical tail. This is because this surface has the largest moment arm to the centre of gravity and, as a result, would create the largest disturbance yaw moment. The vertical tail is approximated as a flat plate with surface area $0.09[m^2]$, with a moment arm to the CG of the UAVs of $0.71[m]$. The force on the vertical tail can then be calculated with Equation 10.8 and results in $9.8[N]$. Multiplying the force on the vertical tail by the moment arm results in a yaw disturbance moment N_D of $9.8Nm$.

To achieve yaw control with only the VTOL motors, the UAVs must make use of the reaction moments created by the propellers. For hovering, the VTOL motors, in the specified configuration, generate counteracting yawing moments that cancel each other out (two are spinning clockwise, and the other two are spinning counter-clockwise). To yaw the UAVs, these must make use of differential rotation of the propellers, creating a net yawing moment on the airframe. In other words, the RPM of motors spinning in one direction is increased by $\Delta\omega$, while the RPM of the motors spinning in the opposite direction is decreased by the same amount, creating this net yawing moment. The reaction moment on the airframe created by a single propeller is given by Equation 10.9, and its derivative with respect to ω is given by Equation 10.10. In these equations, k_q is the dimensional torque coefficient, ω the angular velocity of the propellers, n_{cw} the number of clockwise-rotating propellers (2), n_{ccw} the number of counter-clockwise-rotating propellers (2), $\bar{\omega}$ the mean angular velocity of the propellers, and $\Delta\bar{\omega}$ the change in mean angular velocity of the propellers to produce a yawing moment ΔN.

$$N = k_q\omega^2 \tag{10.9}$$

$$\Delta N = 2k_q\bar{\omega}_o(n_{cw} + n_{ccw})\Delta\bar{\omega} \tag{10.10}$$

To calculate the induced yawing moment, k_q is first needed. k_q is given by Equation 10.11 [69], where C_Q is the non-dimensional torque coefficient, D the diameter of the propellers ($0.762[m]$), and ρ the air density ($0.901[\frac{kg}{m^3}]$, the most critical value for the mission).

$$k_q = \frac{C_Q\rho D^5}{(2\pi)^2} \tag{10.11}$$

C_Q then relates to C_P, the power coefficient, by Equation 10.12 [70].

$$C_Q = \frac{C_P}{2\pi} \tag{10.12}$$

C_P is then approximated to be 0.4 from the analysed propeller closest in geometry to the one used for the AeroShield UAVs [70]. k_q results in a value of $3.81 \cdot 10^{-4}[Nms^2]$. For hover, the front two VTOL motors operate at an RPM of 3237, while the back two VTOL motors operate at an RPM of 2812 [71]. This results in a mean RPM $\bar{\omega}$ of 3025. Following Equation 10.10, a yawing moment ΔN of $12.23[Nm]$ can be achieved with a 4% variation in mean RPM of the motors. This moment can comfortably counteract N_D. For hover, this would result in the critical case of one of the front motors increasing its RPM to 3358, which is well within the operational limit of the motors ($RPM_{max} = 3666$). Therefore, the UAVs remain yaw-controllable even against the required gusts.

Pitch Control

For analysing pitch control, the critical scenario is determined to be a full $30[\frac{km}{h}]$ updraught gust acting perpendicularly only the horizontal tailplane. This is because this surface has the largest moment arm to the centre of gravity and, as a result, would create the largest disturbance pitch moment. In this sense, the horizontal stabilizer is approximated as a flat plate with surface area $0.22[m^2]$, with a moment arm to the CG of the UAVs of $0.85[m]$. The force on the horizontal tail due to the gust results in $24[N]$ and follows from Equation 10.8.

Multiplying this force by the moment arm, it results in a pitch disturbance moment M_D of $20.4[Nm]$. To counteract this moment, the front VTOL motors must increase their thrust by an amount ΔT, while the back propellers must decrease it by the same amount. This maintains vertical force equilibrium while creating a counteracting moment against the gust disturbance moment, which is pitch down. ΔT is given by Equation 10.13 and results

in $6.69[N]$, or the mass-force equivalent of $0.69[kg]$. In this equation, l_{VTOL_f} is the moment arm from the front VTOL motors to the CG of the UAVs, and l_{VTOL_b} is the same moment arm but from the back motors.

$$\Delta T = \frac{M_D}{2(l_{VTOL_f} + l_{VTOL_b})} \tag{10.13}$$

During hover, the front propellers must run at a mass-equivalent thrust of $8.55[kg]$, while the back ones must run at $6.45[kg]$. This results from the front VTOL motors being placed at a distance of $0.656[m]$ in front of the CG of the UAVs, while the back VTOL motors are placed at a distance of $0.869[m]$ behind the CG of the UAVs. The motors can have a maximum mass-equivalent thrust of $11.2[kg]$, and therefore a mass-force equivalent ΔT of $0.69[kg]$ fits well within limits with a sizeable margin to spare. As the required power during climb was assumed to be equal to the hover power, as explained in section 8.1, the UAVs remain pitch-controllable even against the required gusts.

Roll Control

For analysing roll control, the critical scenario is determined to be a full $30[\frac{km}{h}]$ gust on a single half-wing, creating a roll disturbance moment. This half-wing is approximated as a flat plate with surface $0.635[m^2]$, and the resulting drag force is assumed to act at quarter-span ($0.75[m]$) from the fuselage centreline (so half of the half-span). The force on the half-wing from a $30[\frac{km}{h}]$ gust results in a force of $69.2[N]$, following Equation 10.8. Multiplying by the quarter-span moment arm, the roll disturbance moment L_D is calculated to be $51.9[Nm]$.

To counteract this roll disturbance moment, the VTOL motors on one side (right/left) of the UAVs must increase their thrust by an amount ΔT, while the VTOL motors on the opposing side of the UAV must decrease it by the same amount. Therefore, ΔT is given by Equation 10.14 and results in $17.02[N]$, or a mass-force equivalent of $1.74[kg]$.

$$\Delta T = \frac{L_D}{4l_p} \tag{10.14}$$

This ΔT also fits within the thrust limits of the motors, and therefore the UAVs remain roll-controllable even against the required gusts.

10.5. Compliance Matrix

Table 10.4 presents the subsystem requirements for stability and control of the AeroShield UAVs, whether they have been verified and, if they have, the method of verification. Note that REQ-SYS-CON-03 has been removed, as the UAVs are no longer loaded with aerogel while in flight, in contrast to the original idea in the Baseline Report [72].

Table 10.4: Compliance Matrix Control Requirements

Identification	Description	Compliance	Method of Verification
REQ-SYS-CON-01	The UAV shall be controllable in flight on all three axes without payload.	✓	Analysis: see section 10.3
REQ-SYS-CON-02	The UAV shall be controllable in flight on all three axes when carrying $5[kg]$ of aerogel.	✓	Analysis: see section 10.1, section 10.2, section 10.3 and section 10.4
REQ-SYS-CON-04	The UAV shall remain stable while deploying the aerogel.	×	Requires further modelling of aerodynamic interaction of gusts with the flexible aerogel blanket, and how that translates into force or moment disturbances for the UAVs.
REQ-SYS-CON-05	The UAV shall be controllable during take-off.	✓	Analysis: see section 10.4
REQ-SYS-CON-06	The UAV shall be controllable during landing.	✓	Analysis: see section 10.4
REQ-SYS-CON-07	The UAV shall remain stable under gusts up to $30\frac{km}{h}$	✓	Analysis: see section 10.1, section 10.2, section 10.3 and section 10.4
REQ-SYS-CON-08	The UAV shall remain stable under disturbances from water sprays up to <TBD>.	×	Requires further modelling on the effect of water sprays on wing and propeller aerodynamics

10.6. Sensitivity Analysis

10.6.1. Cruise Mode

For cruise, where sizing is done based on crosswinds, in the case of the rudder, and manoeuvrability requirements, in the case of the elevator and ailerons, the dimensions of these surfaces can be varied within a range to check if the requirements are still met within some range of the design points. Figure 10.1 shows the sensitivity of these requirements to the varied geometrical inputs for the control surfaces (b_o for ailerons, and $\frac{c_e}{c}/\frac{c_r}{c}$ for elevator and rudder, respectively).

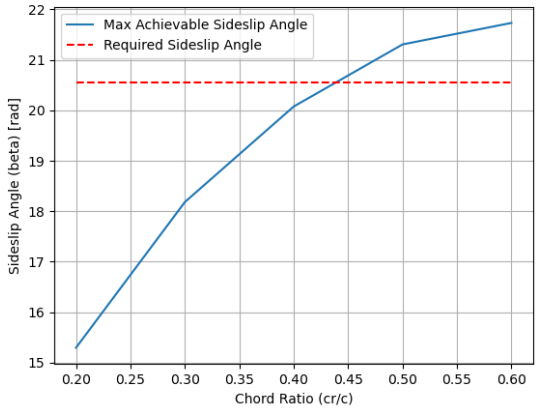

(a) Rudder sensitivity analysis

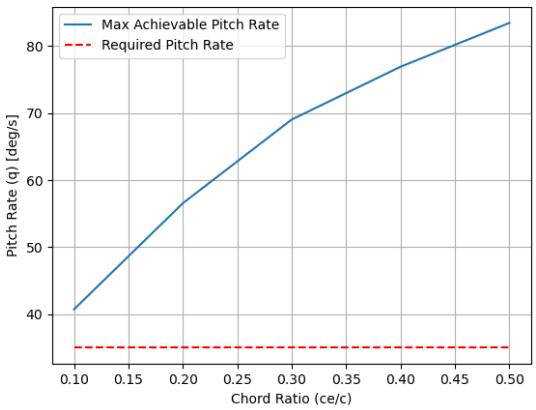

(b) Elevator sensitivity analysis

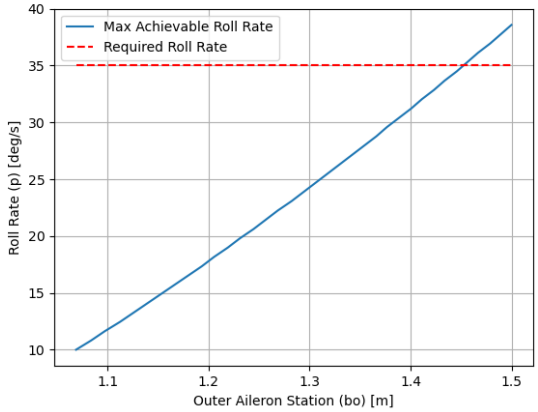

(c) Aileron sensitivity analysis

Figure 10.1: VTOL motor thrust and RPM sensitivity to disturbance moments from gusts

In general, the larger the control surface, the higher the sideslip or manoeuvrability requirements it can meet. First, from Figure 10.1a, it can be seen that the rudder could accommodate an increase in size up to 0.6 $\frac{c_r}{c}$, if in further design stages the rudder is demonstrated to be less effective than currently calculated. This would effectively require the rudder to be larger to allow the UAVs to maintain the required sideslip angle during cruise. However, this represents the highest value of the consulted statistical range for this parameter [65], and anything over that would likely require a redesign of the vertical tail.

The elevator design point, on the other hand, comfortably exceeds the required pitch rate of $35\frac{^\circ}{s}$, and could accommodate design changes of both increased or decreased size as evidenced in Figure 10.1b. However, the elevator is sized at the lowest value of the consulted statistical range [67]. Therefore, there is a large margin for the pitch rate requirement to be revised upwards in future design stages, even if the elevator is less effective than currently calculated.

For ailerons, it can be seen that, theoretically, the maximum roll rate of the UAVs could be further increased from $35\frac{^\circ}{s}$ to around $38\frac{^\circ}{s}$ in Figure 10.1c. Nonetheless, at that point the aileron would extend all the way to the tip of the wing, which would introduce additional aerodynamic issues. Therefore, there is not much room for increasing aileron size past the design point, which could present an issue at a future design stage if the ailerons are less effective than estimated, therefore requiring larger ailerons to meet the roll rate requirement.

All in all, the sizing of the control surfaces does not allow for much uncertainty in the estimated values for their effectiveness, except for the elevator, to still meet the controllability requirements. As a result, their geometry must be closely monitored in future design stages to ensure their performance is still adequate, or redesign them accordingly if necessary.

10.6.2. VTOL Mode

For VTOL, there is a high degree of uncertainty in the modelling of disturbance moments and forces from gust loads. As previously explained, this is accounted for with a safety margin of 2, but the margin, in terms of control robustness, of the selected VTOL motors and configurations must be evaluated. This is done by varying the respective disturbance moments, and evaluating up to which point stability and control can still be maintained with the VTOL motors. Figure 10.2 shows the sensitivity for VTOL stability and control for all three axes. The maximum ΔT ($2.75[kg]$ mass-force equivalent) and $\Delta\omega$ (429 RPM) are calculated based on the difference between nominal operating conditions for the front VTOL motors, as they operate at higher thrust and RPM settings than the back ones, and the maximum RPM and thrust for the motors.

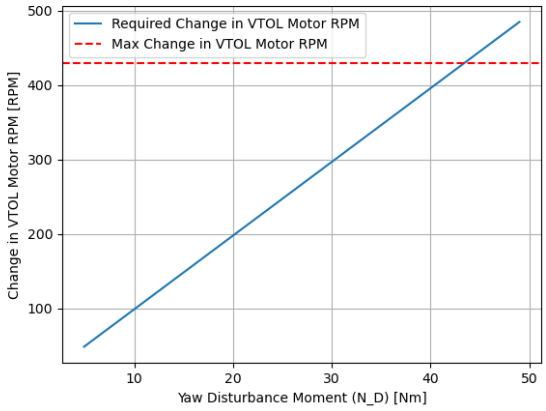

(a) Yaw VTOL sensitivity analysis

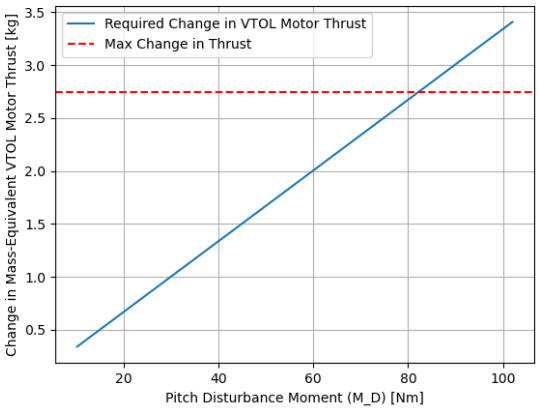

(b) Pitch VTOL sensitivity analysis

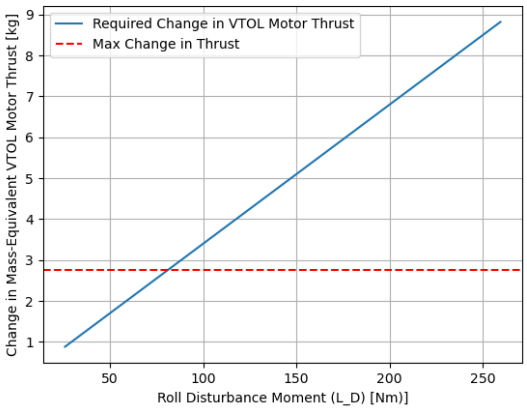

(c) Roll VTOL sensitivity analysis

Figure 10.2: VTOL motor thrust and RPM sensitivity to disturbance moments from gusts

As expected, it can be seen that, as the disturbance moments increase, so does the necessary ΔT or $\Delta\omega$ with a linear behavior. For yaw, in Figure 10.2a, a maximum disturbance moment of $43.38[Nm]$ can be counteracted, which is 4.43 times greater than estimated in Equation 10.4. For pitch, in Figure 10.2b, a maximum disturbance moment of $82.28[Nm]$ can be counteracted, which is 4.03 times greater than estimated in Equation 10.4. Finally, for roll, in Figure 10.2c, maximum disturbance moment of $80.93[Nm]$ can be counteracted, which is 1.56 times greater than estimated in Equation 10.4. Therefore, there is, in the worst case, an additional factor of 1.56 on disturbance moments under which the UAVs would remain stable. Nonetheless, if any of the real disturbance moments get close to the described limits, the UAVs would not have any extra margin in thrust or RPM to maneuver and, in that case, would need to be redesigned to manage the $30[\frac{km}{h}]$ gusts and still be operable.

11

Structures and Materials

This chapter aims to describe the structural design of the UAVs together with the selection of the material for each structural component. At first, in section 11.1, the chosen materials will be presented for each part of the structure. section 11.2 presents the design of the wing, section 11.3 describes the design of the propeller booms and placement on the wing. section 11.4 outlines the fuselage thickness and the design of the deployment bay. section 11.5 describes the landing gear design and, at last, section 11.6 shows the compliance matrix of the subsystem requirements related to structures and section 11.7 conducts a sensitivity analysis on the structure.

11.1. Material Selection

To determine the most appropriate material for the structural components of the UAVs, several materials were evaluated based on mechanical performance, density, thermal stability, corrosion resistance, manufacturability, sustainability, and cost. The UAV structure must withstand operational loads while remaining within the maximum take-off weight of $25[kg]$. Additionally, the material must operate reliably within a temperature range of -20° C to +140° C, be non-flammable, water-resistant, and sustainable according to the requirements presented in chapter 3. The materials considered in this evaluation are: Grade 5 Ti-6Al-4V titanium alloy, an aluminium foam sandwich composite (Aluminium 5052-H32 + Rohacell PMI foam), carbon fibre composite (Evopreg PC502 50%) and a glass fibre composite (Evopreg PFC502 43% fibre content).

Ti-6AI-4V (Grade 5)

Titanium Grade 5 is widely used in both aerospace and marine environments for high-stress components. It is chosen based on its good specific strength $(198.9[MPacm^3/g])$, corrosion resistance, its broad service-temperature capabilities (-210 to +400 deg), and its fatigue resistance [73]. However, its high density of $4.43[g/cm^3]$ resulted in an unacceptably high structural weight [73]. This is because the thickness would be constrained by the minimum manufacturable thickness, which would far exceed the performance needs. Based on the preliminary sizing of the UAVS, the mass estimates showed that using titanium would significantly exceed the UAV's allowable structural mass budget, leaving insufficient margin for hardware components. Therefore, titanium was rejected as a feasible option for the primary structure.

Aluminium Foam Sandwich

The aluminium foam sandwich considered consists of 5052-H32 aluminium face sheets bonded to a polymethacrylimide (PMI) foam core (Rohacell). This composite was selected because of its strengthening properties and its thermal resistance, since the foam core acts as an insulation layer. The specific aluminium alloy is chosen for its high corrosion resistance, which would be beneficial especially in marine environments [74] . Additionally, this type of aluminium alloy only loses approx. 10% of it's strength at $140^\circ C$ [75].

However, once more, the material is constrained by the manufacturability. The thinnest commercially available sheet of 5052-H32 aluminium is $0.8[mm]$ [1]. For the core, the minimum available thickness is $3[mm]$ [2]. This means that the minimum combined thickness of the sandwich would be $4.6[mm]$. While the density of the separate materials is reasonable, the thickness would again cause the structure to exceed the weight requirement, so this option was also rejected.

Carbon Fibre

Carbon Fibre (Evopreg PCF502 50% fibre content) was considered because of its high strength to weight ratio, thermal properties and corrosion resistance [76]. However, carbon fibre composites are not easily recyclable. End-of-life disposal poses environmental challenges due to energy-intensive production and limited material recovery options. For this reason, carbon fibre did not satisfy the sustainability requirements and is thus rejected.

[1] www.aluminumalloyplate.com/sale-36714917-5052-h32-aluminum-thin-sheets-0-8mm-8mm-for-rail-transportation-van-container.html [accessed: 19/06/2025]

[2] https://www.easycomposites.eu/Rohacell71-IG-F-PMI-Foam-Core [accessed: 19/06/2025]

Glass Fibre

Evopreg PFC502 with 43% glass fibre content was selected due to its thermal resistance and superior sustainability. It is non-flammable, capable of self-extinguishing within 1 second, and exhibits excellent corrosion and water resistance [76].

Compared to titanium, glass fibre offers significantly lower density, improving the structural mass budget. Compared to the aluminium foam sandwich, PFC502 provides greater strength at reduced thickness. While its strength is lower than that of carbon fibre, its enhanced manufacturability, lower environmental impact and lower cost made it the most appropriate choice for the UAVs' structure which includes the fuselage, propeller booms, wings and landing gear.

Furthermore, refering to REQ-SYS-STR-02, which states that the material shall maintain 95% of its stiffness in the operating temperature range, Evopreg PFC502 can be cured up to a temperature of $160°C$. The glass transition temperature is higher than the curing temperature and thus, if the glass fibre is cured at a temperature higher than $140°C$, the glass transition temperature will be higher. Thus, the material retains its stiffness, since only after the glass transition temperature does the stiffness of the material decreases[3].

The material properties of PFC502 are presented in Table 11.1 and Table 11.2. In order for the material to achieve in-plane stiffness in all directions, three plies are necessary. So the minimum manufacturable thickness is set at $0.78[mm]$.

Table 11.1: Mechanical properties by direction

	Fibre direction (0°)	Transverse direction (90°)
Young's Modulus	$21.9[GPa]$	$21.1[GPa]$
Compressive Yield Strength	$343[MPa]$	-
Tensile Yield Strength	$304[MPa]$	$253[MPa]$
Shear Strength	$85[MPa]$	-

Table 11.2: General material properties

Density	$1.84[g/cm^3]$
Operating Temperature	–40 ° C to +200 ° C
Min. Laminate Thickness	$0.26[mm/ply]$
Min. Manufacturable Thickness	$0.78[mm]$
Price	$7.39/m^2$

The nose cone of the fuselage will be made from infrared (IR) fused silica for the oil spill mission, and from Zinc Selenide (ZnSe) for the wildfire mission. This modular nose cone design allows each mission to benefit from a material specifically selected to match the spectral requirements of the onboard sensors, ensuring optimal optical performance, environmental protection, and structural integrity.

For the oil spill mission, the drone is equipped with the DJI Zenmuse L2 LiDAR sensor, which integrates a LiDAR sensor operating at $905[nm]$ and an RGB camera. The chosen material, IR fused silica, has excellent transmission characteristics from approximately 300 nm to 2800 nm, with over 90% transmission across this range [4]. This makes it ideal for both the visible RGB and near-infrared wavelengths used by the LiDAR system. Additionally, IR fused silica is lightweight, with a density of $2.2[g/cm^3]$ and is known for its high durability and resistance to environmental degradation, making it well-suited for maritime operations.

For the wildfire mission, the drone uses the DJI Zenmuse H30T, featuring an RGB camera and a thermal infrared sensor in the $814[m]$ range. The nose cone utilizes Zinc Selenide (ZnSe) with a dual-band AR coating, providing about 95% transmission in the longwave infrared. While its visible range transmission is lower at around 40%, this is deemed sufficient as the thermal camera is the primary tool for wildfire detection [5]. The higher density of ZnSe ($5.27[g/cm^3]$) is a trade-off justified by its superior infrared optical properties and robustness in high-temperature or smoky environments.

[3] https://www.kohesibond.com/does-cure-temperature-influence-glass-transition-temperature/[accessed: 19/06/2025]
[4] https://escooptics.com/blogs/news/ir-grade-fused-silica-window-and-lenses [accessed: 23/06/2025]
[5] https://www.thorlabs.com/newgrouppage9.cfm?objectgroup_id=9049[accessed: 23/06/2025]

11.2. Wing Internal Structure

This section describes the design process of determining the internal structure of the wing, which consists of spars and ribs. First, section 11.2 presents the distributed load on the wing and the internal shear force and moment along the wing span. section 11.2 and section 11.2 describe a wing box analysis and FEM (Finite Element Method) analysis in order to determine the spar placement, rib placement and the thickness of the skin, spars and ribs. At last, section 11.2 describe the integration and accessibility of the wing.

Loading Diagrams

To determine the internal wing structure of the UAV, first the forces acting on the wing must be clearly defined. This overview was made in the form of loading diagrams, which show the distribution of the loads, the shear forces and bending moments along half of the wing span. A right-handed coordinate system is used, where the x-axis is located on the longitudinal axis of the UAV, the y-axis along the span of the wing and the z-axis being directed downwards. Both the loading diagrams for cruise and VTOL conditions are made. Cruise condition relates to using the fixed wing as main lifting surface and VTOL condition means that the lift is generated by the propellers. The latter happens in the case of take-off, landing and hovering.

In cruise condition, the loads acting on the wing include its own weight, the weight of the batteries, and the structure of the propeller boom, which all exert a downward force, along with a lift force acting upward. The battery weight is assumed to be distributed uniformly along its length, and the wing weight decreases relative to the taper ratio. Additionally, the weight of the boom carrying the propellers is applied, which consists of the weight of the boom itself, two VTOL propellers, ESCs, and motors. The lift distribution is assumed to follow an elliptical pattern, which is sufficiently accurate for this stage of the design. This assumption is based on the understanding that the maximum and minimum loads are the key constraints, and these will not vary significantly between the elliptical distribution and the actual distribution. A load factor of 3.5 is applied, as explained in section chapter 9, to account for the additional loads imposed by gusts. The potential lift generated by the stationary propeller blades is deemed negligible and is therefore not considered in the analysis of forces and moments during cruise condition.

In VTOL conditions, the lift produced by the propellers is modelled as a point force acting upwards at the location on the wing, where the propeller booms are connected. It is assumed that the main wing does not generate a considerable amount of lift in this flight condition. A load factor of 1.5 is used, to account for ascent. The force generated by the gusts is evaluated differently, as the load factor is only applicable for cruise. Therefore, the gust force is derived from the generated dynamic pressure (Equation 11.1), considering the worst case scenario where a wing of $30[km/h]$ hits the wing orthogonally from below.

$$F_{gust} = \frac{1}{2} \cdot \rho \cdot V_{gust}^2 \cdot \frac{A_{wing}}{2} \tag{11.1}$$

Where ρ is the density at sea level (limiting case), V_{gust} is the gust velocity, and A_{wing} is the wing area, which is divided by two as the wing is plotted from the fuselage outward. This force is then distributed along the wing, the taper is neglected in this case.

The shear force is calculated with Equation 11.2 for distributed loads, for point loads the shear force is the same in magnitude but opposite in direction (sign). The bending moment is calculated with Equation 11.3.

$$V(x) = \int w(x)dx \tag{11.2}$$

$$M(x) = \int V(x)dx \tag{11.3}$$

Where, P is the point load, $w(x)$ is the distributed load along the span of the wing, $V(x)$ is the shear force along the wing span and $M(x)$ is the bending moment along the wing span.

In Figure 11.1 the internal loading diagrams of the wing in cruise condition are shown and Figure 11.2 show the internal loading diagrams in VTOL condition. The horizontal axis starts at the root of the wing and ends at the tip, meaning that the forces are in the z direction, and the bending moment is around the x-axis.

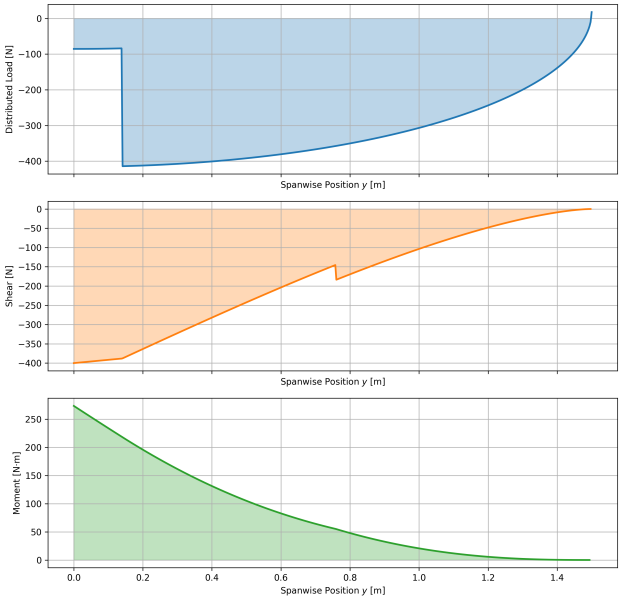

Figure 11.1: Loading diagrams for the wing in cruise condition

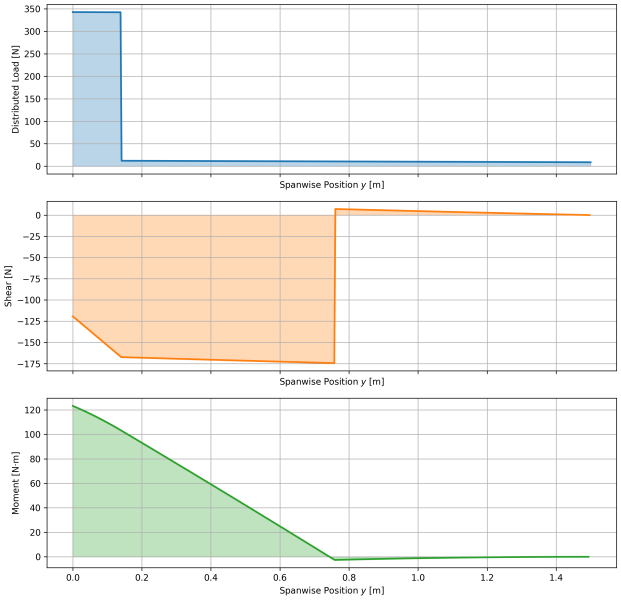

Figure 11.2: Loading diagrams for the wing in VTOL condition

As can be seen from the plots, the largest shear force and bending moments occur in cruise condition at the root of the wing. In VTOL conditions, the largest bending moment occurs also at the root of the wing, but the shear force is the largest just before the location of the propeller boom structure.

Wing Box Analysis

To determine the thickness of the wing skin and spars a wing box analysis is performed. The wingbox is modelled as the central section of the airfoil. Its length corresponds to the distance between the front and aft spars, while its height follows the contour of the E1233 airfoil. It is the area between the forward and aft spar, as can be seen in Figure 11.3. The wingbox is taken at the root, since generally there the largest moments will be generated. The spars are positioned at 17% and 50% of the chord length in order to accommodate the batteries inside the wing. The following assumptions are made for the wingbox analysis:

- The upper and lower skin panels are assumed to resist bending and torsional loads, while the spars primarily handle shear and torsional stresses.
- The thickness of the skin and spars is assumed to be the same and constant along the span of the wing.
- The spars are modelled as rectangular shapes for calculating the moment of inertia I, and the upper and lower skin panels are treated as curves with a constant thickness. This assumption may lead to an underestimation of the moment of inertia and an overestimation of the stress.
- The bending moment M and shear force V are taken from the loading diagrams, considering the highest values. The highest values will cause an overestimation of the thickness, since the loads are smaller at different places along the wing span where thus a smaller thickness is already enough to take up all the loads. This results in a conservative thickness, though it may be worse considering the weight.
- The torsional moment T is taken as the torsion that is created when only one propeller produces lift and thus creates a torsional moment on the wing.
- The shear centre is assumed to be located at the centre of the wingbox. This assumption can lead to an underestimation to the shear stress, because when the shear load does not pass through the true shear centre a torsional moment is created which is not taken into account.
- The neutral axis of the wingbox is assumed to be the centre line of the wingbox, and the point of maximum bending stress is assumed to be located at the top of the wingbox. Since the actual neutral axis will be placed slightly higher than the assumed one, the compressive stress will be slightly underestimated.
- A safety factor of two is applied between the yield stress of the material and the calculated stress, ensuring a conservative design that accounts for uncertainties in loading, material properties, and model simplifications.

The bending stress (Equation 11.4), transverse shear (Equation 11.5), and torsion (Equation 11.6) are considered on the wing box together with the assumptions stated above.

$$\sigma = -\frac{My}{I} \tag{11.4}$$

$$\tau_s = \frac{VQ}{It} \tag{11.5}$$

$$\tau_t = \frac{T}{2tA_m} \tag{11.6}$$

In these formulas, σ is the bending stress, M is the bending moment, y is the distance from the neutral axis to the point where the bending stress is calculated, I is the moment of inertia. τ_s is the shear stress, V is the shear force, Q is the first moment of inertia, t is the thickness of the skin/spar, τ_t is the torsional stress, T is the torsion, and A_m is the cross sectional area of the wingbox.

The thickness of the spar and the wing skin must be large enough such that the bending stress, shear stress and torsional stress on the structure is lower than the yield stress of the material. Taking into account the safety factor, a minimum required skin thickness lower than the minimum manufacturable thickness of the material was found, so an initial thickness of $0.78[mm]$ is set for the wing and spar.

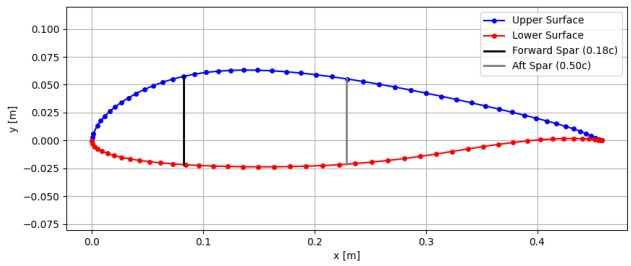

Figure 11.3: Cross-section of the wing root, illustrating the forward spar at 17% and the aft spar at 50% of the chord.

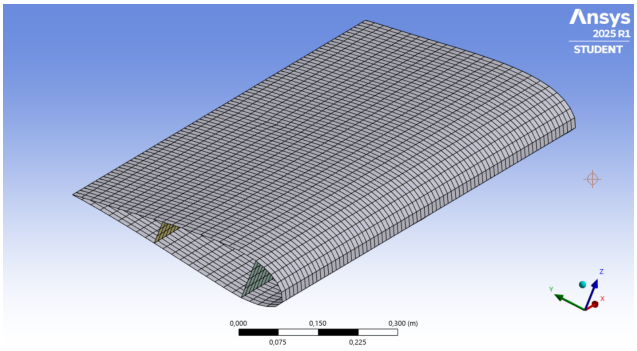

Figure 11.4: Mesh for finite element analysis.

FEM analysis

To get a more precise thickness calculation, a FEM analysis is conducted on the wing. Initially, the ribs are positioned at both the root and tip of the wing, with an additional rib located above the propeller booms to reinforce these structures. The ribs are assumed to have the same thickness as the skin and spars.

For the Finite Element Analysis, several simplifying assumptions were made. The first is that the effect of the taper ratio on the stresses is negligible. The second is that the load case is heavily simplified. Based on the loading diagrams from section 11.2, the most constricting case is during the cruise phase with a load factor of 3.5. For the FEM analysis, a distributed force is applied to the bottom of the wing of 3.5 times the MTOW, divided by half since only one side of the wing is modelled. The other forces on the wing, such as the battery weight and the entire weight of the propeller boom structure with propeller motors, are neglected since they are less than 10% of the lift force and will only decrease the stresses. Finally, a rigid connection was applied at the root to approximate the connection to the fuselage. The mesh used is shown in Figure 11.4. A square mesh was used as it resulted in an even distribution along the wing, and no non-linear effects were modelled.

With an initial spar placement at 17% and 50% of the chord and a skin and spar thickness of 0.78 mm, considerable deformation was seen in part from the aft spar to the trailing edge of the wing. A relocation of the aft spar to 60% of the chord showed optimal results considering this deformation. The deformation for the old and new spar placement can be seen in Figure 11.5 and Figure 11.6 respectively, seen from the bottom of the wing.

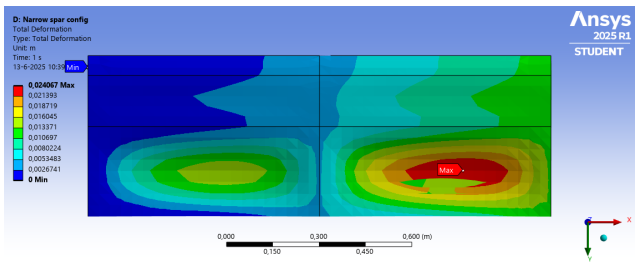

Figure 11.5: Deformation old spar placement - bottom view

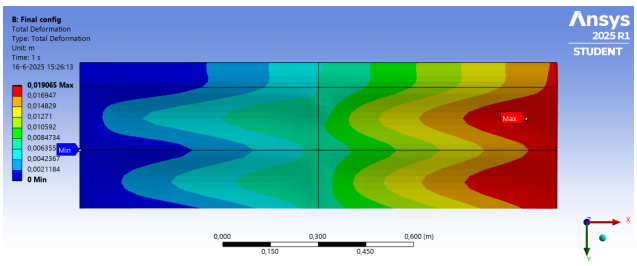

Figure 11.6: Deformation new spar placement - bottom view

Looking at the normal (bending) and shear stresses, thickness of 0.78 mm was deemed sufficient to absorb the loads with a spar placement at 17% and 60% of the chord. The stresses are visible in Figure 11.7. Since the displacement of the wing is below the maximum set deflection of $2[cm]$ and the stresses are low enough, no additional ribs are necessary.

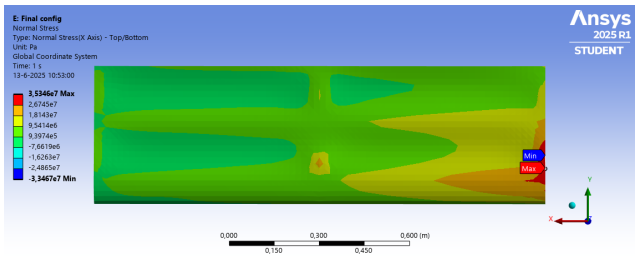

(a) Normal stresses - bottom view

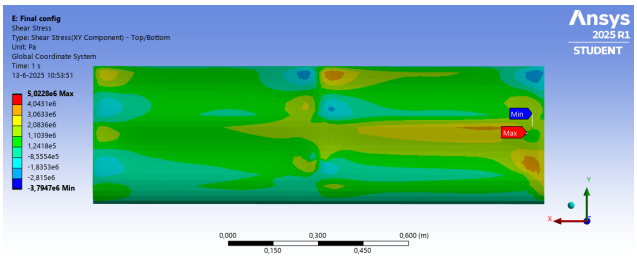

(b) Shear stresses - bottom view

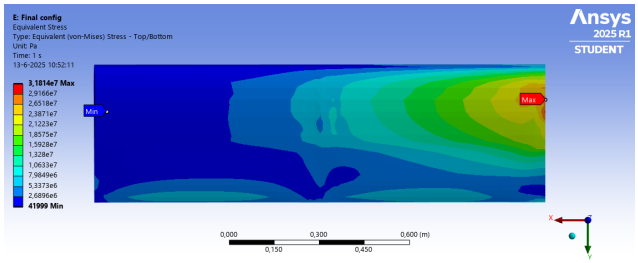

(c) Von Mises stress - top view

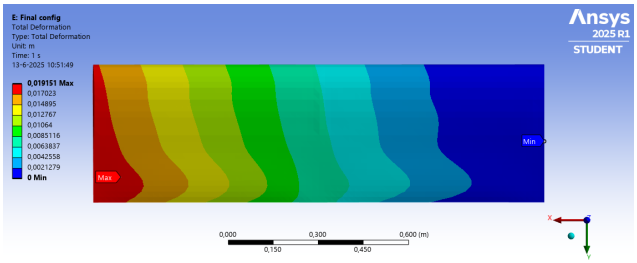

(d) Deformation - top view

Figure 11.7: Stress and deformation of the final wing configuration. (a) Normal stresses, (b) Shear stresses, (c) Von Mises stress, (d) Deformation

In VTOL conditions, the most critical case is when one propeller fails. This is simulated in the FEM analysis, with no lift force generated by the wing since it is assumed that the wing will not generate any lift in VTOL. A remote point force at the location of the propeller motors is also added, which is the lift force needed to take-off at MTOW, using a safety factor of 2, divided over three propellers, considering one propeller is not operational. The resulting shear stress and deformation in VTOL is visible in Figure 11.8 and Figure 11.9 respectively. It can be seen that the shear stress and deformation are still within the limits and, thus, a thickness of $0.78[mm]$ is sufficient.

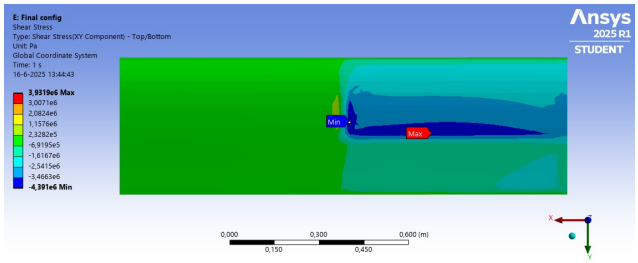

Figure 11.8: Shear stresses in VTOL condition - top view

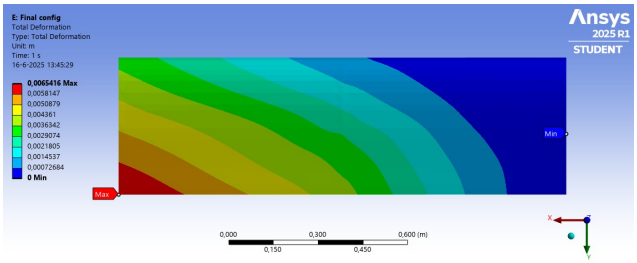

Figure 11.9: Deformation in VTOL condition - top view

Wing Integration and Accessibility

The wing is rigidly connected to the fuselage to ensure structural integrity and efficient load transfer during flight. The spars run continuously through the fuselage, enabling uniform distribution of aerodynamic and propulsion loads across the airframe and enhancing torsional rigidity. To accommodate compact storage within the UAV nest and to facilitate transport and maintenance, the wings are designed to be detachable. Additionally, an access panel is integrated near the wing root to allow for quick and easy battery replacement.

Detachable Wings

The wing is divided into an inner and outer section, with the separation located just outboard of the propeller booms at a distance of $762[mm]$ measured from the centre of the fuselage. In case of failure of the locking mechanism of the two wing parts, therefore, the UAV can still continue to fly due to the propellers.

The spar is cut at half the length of the internal part of the wing (wing part connected to fuselage), resulting in the outer part of the wing having spars that extend outward. This outer part can slide into the inner section of the wing, in the designated lock for the spars, which resist the degrees of freedom of the spars and two latches secure the wing skins together. The latches are located between the spars on the top and bottom part of the wing.

The wires running through the wing to the actuators located on the detachable section are equipped with connectors, allowing for easy disconnection and reconnection when removing or reattaching the outer wing segment.

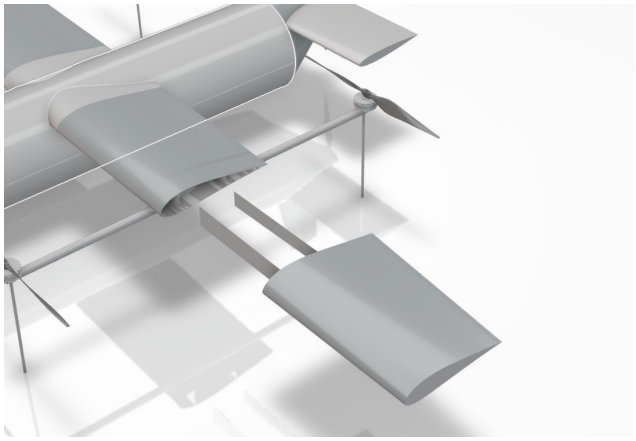

Figure 11.10: Detachable wing

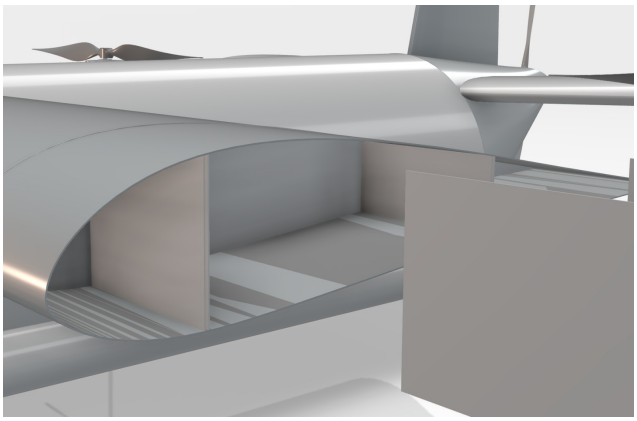

Figure 11.11: Slots for the wing spar

Access Panel

To allow for battery replacement, a rectangular access panel is integrated into the upper surface of the wing near the wing root. The batteries have a size of $118.7 \times 192[mm]$ as can be seen from the top. To provide sufficient clearance for a human operator to safely and easily remove the batteries, the access panel is sized at $180[mm]$ wide (along the wing's chord) and $240[mm]$ long (along the span). The panel is designed with a push-to-open mechanism: pressing on the panel activates a touch latch mounted on the aft wing spars, allowing the panel to spring open for convenient access. This can be seen in Figure 11.12 and Figure 11.13.

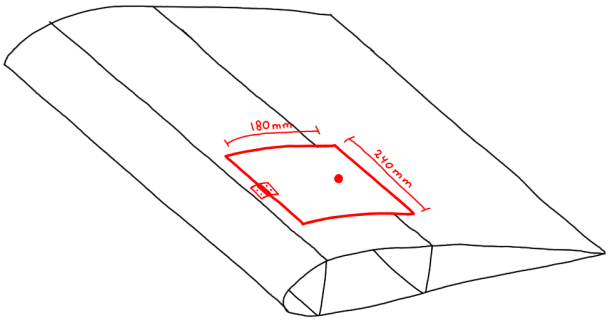

Figure 11.12: Access panel closed

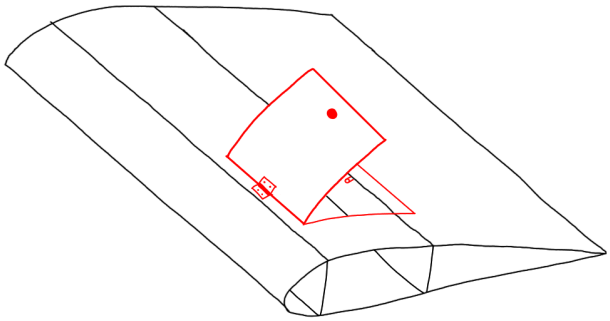

Figure 11.13: Access panel open

Air Ducts

Air ducts are needed in the wing skin to allow for airflow over the fins of the heat sink which will be placed inside the wing. In chapter 12 the operation of the heat sink will be explained in detail. On the bottom of the airfoil of the wing, near the front of the heat sink a small opening will be created. This opening allows for airflow over the fins of the heat sink during cruise. This opening can only be open when the UAV is flying in colder air as the heat sink would otherwise just act as an heating element. To close of the opening on the inside of the wing a closing mechanism will be present. This closing mechanism will be a silicone flap. A silicone flap was chosen since it has a high operating temperature and can be made flexible. This flexibility ensures that when the UAV is in cruise mode the airflow will push open the flap, creating an opening for the air to enter the wing and flow over the fins. When the UAV is operating near the wildfire it will be flying in VTOL mode so there will be no airflow pushing open the flap ensuring the heat sink is closed of from warm air. A diagram of this process is shown in Figure 11.14.

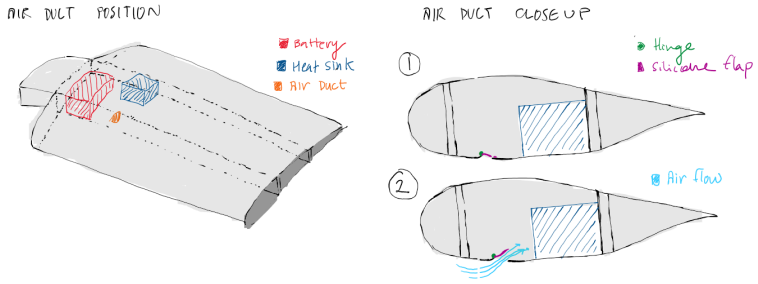

Figure 11.14: Airduct Mechanism

One problem which arises with this method is that the airflow needs to leave the wing as well. Therefore holes in the spar and another hole in the wing skin will need to be added which raises some structural concerns. This has not been analysed yet but will need to be taken into consideration when further designing the wing structure.

11.3. Propeller Boom Design

The propeller booms are placed on the wing at a distance of $762[mm]$ from the centre of the fuselage, such that there is a clearance of one diameter of the propeller blades between the tip of the propeller blades on each side of the wing. Considering the same clearance between the tip of the propellers of the propellers that are mounted on the same boom, the length of the boom is two times the diameter of the propellers which is $1.52[m]$. The propeller boom is rigid connected to the bottom of the wing.

To determine the forces that are acting on the propeller booms, loading diagrams are constructed in the same way as described in section 11.2. This plot is of the situation when the VTOL propellers are active and carrying the full weight with a load factor of 1.5, as that is the limiting case. The distributed loads consist of the weight of the boom itself, the gust loads calculated with Equation 11.1 and the lift and weight forces at the propellers. The loading diagrams are visible in Figure 11.15. Again, a right-handed coordinate system is used, where the x-axis is along the longitudinal axis of the propeller booms, the forces are directed in the z-axis. A positive internal shear force is considered downward, and a positive internal moment is considered upwards.

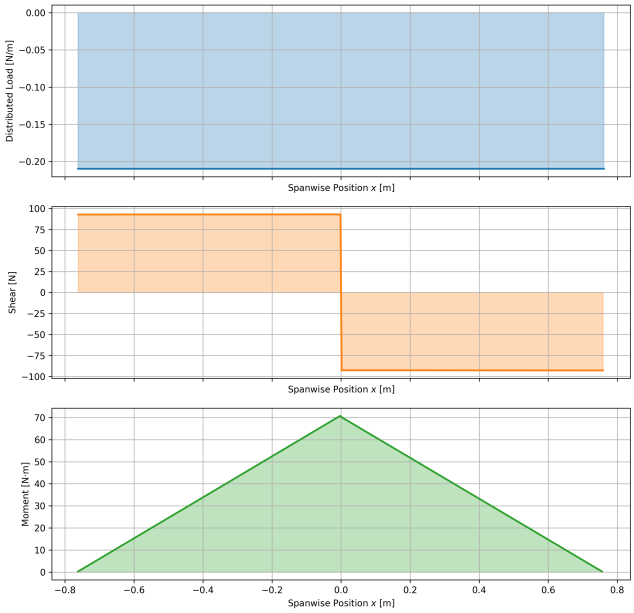

Figure 11.15: Loading diagrams for the booms in VTOL condition

The propeller boom diameter and thickness is sized based on the bending stress (Equation 11.4), shear stress (Equation 11.5), buckling load (Equation 11.11) and on setting a maximum deflection of $2[cm]$, which would be a 1.5% deflection relative to the length. The bending stress and shear stress are based on the maximum moment and shear force as visible in the NVMs. The torsional stress is assumed to be negligible. The deflection of the boom along its span is calculated with Equation 11.7 and the

$$v = -\frac{1}{EI}\iint M dy \tag{11.7}$$

$$I_{boom} = \frac{\pi}{4}(R_{outer}^4 - R_{inner}^4) \tag{11.8}$$

Where E is the young's modulus of the material, M is the moment along the span of the boom and I is the moment of inertia which is determined with Equation 11.8. In the latter, R_{outer} is the outer radius of the boom and R_{inner} is the inner radius of the boom. The moment of inertia of a hollow cylinder is considered since, inside the boom, wires need to be located in order to provide power to the propeller motors.

This concerns three wires, which together have approximately a diameter of $2[cm]$. To have some margin between the wires and the inside diameter, a minimum inside diameter of $3[cm]$ is required. A thickness of $7.5[mm]$ was deemed to be reasonable to take up the bending and shear stresses, taking into account a safety factor of 2 and a maximum deflection of $2[cm]$.

Additionally, since the landing gears are mounted on the propeller booms, it is important for the booms to withstand the loads during UAV landings. Assuming that the UAV lands evenly on its landing gear without causing any torsion in the propeller booms, the stresses can be calculated in the same manner as described earlier. A thickness of $7.5[mm]$ has been determined to be sufficient. This conclusion is based on the fact that the internal forces and moments acting on the propeller boom during dynamic loads (such as in VTOL flight conditions) are greater than those under static loading.

11.4. Fuselage Design

The fuselage has a total length of $2.15[m]$ and an inner diameter of $32[cm]$, this was required in order to accommodate the necessary space for the payload. To deploy the aerogel blanket, an opening is required on the bottom of the fuselage. The blanket, when rolled up, has a diameter of $11[cm]$ and a length of $1.5[m]$. To accommodate both the size of the aerogel and the necessary clearance for deployment, the fuselage opening is designed with dimensions of $20[cm]$ in width and $1.55[m]$ in length.

The deployment bay door consist of two symmetrical panels, each $10[cm]$ wide, which retract inwards and slide laterally along the inner surface of the fuselage. This preserves the aerodynamic shape of the fuselage

and prevents external protrusions. A rail is integrated along the internal circumference of the fuselage, and is electrically powered using a small servo motor, enabling fully autonomous operation. Figure 11.16 shows how one side of the deployment bay (green) door opens, noting that the door slides inwards of the fuselage.

It is assumed that the most critical loading condition for sizing the fuselage skin thickness occurs during cruise, where the lift force generates a upward bending moment of the wing, which produces the largest structural stresses in the wing-fuselage connection. The fuselage skin must be capable of transferring the forces and moments generated by the wing into the fuselage structure.

To facilitate this load transfer, a wing-supporting box (wingbox) is integrated into the fuselage. This box spans between the front and rear spars, which run through the fuselage and support the wing. It is assumed that the fuselage skin primarily carries the shear force transmitted by the wing and the wing bending moment is carried by the horizontal panels (top and bottom) of the wingbox, which act as tension and compression flanges [77].

The required skin thickness is determined using the shear stress equation (see Equation 11.5). Since the deployment bay door is assumed to carry no load, its opening reduces the structural rigidity of the fuselage. Therefore, the second moment of inertia of the fuselage cross-section is adjusted accordingly, using Equation 11.9.

$$I_{fuselage,open} = \frac{(D^4 - d^4)\pi}{64} - \frac{(D^4 - d^4)}{64}(\theta + 1/2sin2\theta) \tag{11.9}$$

Where, D is the outer diameter of the fuselage, d is the inner diameter and θ is the half of the angle of the circular cut-out.

For simplicity and manufacturability, all sides of the wingbox are assumed to have the same thickness. The bending moment from the wing is translated into an equivalent force couple, with the top panel experiencing compression and the bottom panel tension, as illustrated in Figure 11.17. The top and bottom panels are assumed to be buckling critical, where the buckling force is calculated with Equation 11.11. The moment of inertia is equal to $I = \frac{1}{12}bt^3$, where t is the thickness of the panels and b is the width of the panel, which is equal to the length between the spars.

For the fuselage skin thickness, the minimum manufacturability of $0.78[mm]$ was deemed sufficient. The wingbox needs a thickness of $4.68[mm]$ to carry the loads.

To ensure the fuselage is structurally safe under static ground loads, such as when the UAV is on the ground fully loaded at maximum takeoff weight (MTOW), additional stress calculations were performed. A statically determined beam model was used, where a fixed support is placed at the wing. The weight of the fuselage is distributed over its length; the hardware components and tail, including cruise propeller, are modelled as a point force at the nose cone of the fuselage. The winch system and half of the aerogel roll are modelled as distributed loads at their location. Using the bending stress and shear stress equations, Equation 11.4 and Equation 11.5 respectively, it was verified that a fuselage skin thickness of $0.78[mm]$ is sufficient to withstand these loads.

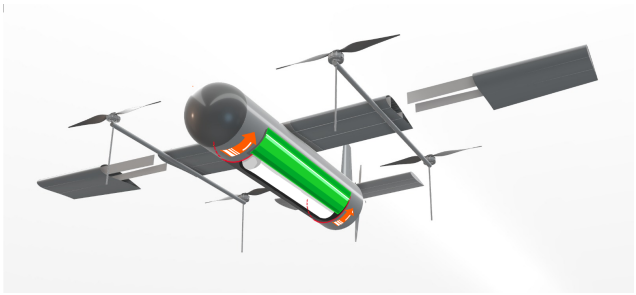

Figure 11.16: Deployment Bay Door

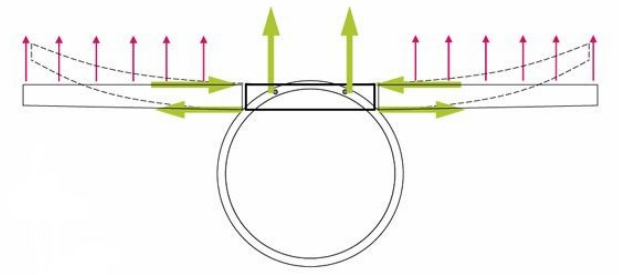

Figure 11.17: Wing-Fuselage connection and load transfer

11.5. Landing Gear

The landing gear must provide stability for the UAV on the ground, including and excluding the aerogel payload. The landing gear is designed as four rods located on the propeller booms underneath the propeller motors. Considering a ground clearance of at least $10[cm]$ between the tip of the cruise propeller blade and the ground, the landing gears rods are designed to have a length of $48[cm]$. The diameter of the landing gear rods is sized based on the compressive stresses the rods should be able to handle calculated with Equation 11.10 and considering the buckling load calculated with Equation 11.11.

$$\sigma = \frac{F}{A} \tag{11.10}$$

$$P = \frac{\pi^2 EI}{L^2} \tag{11.11}$$

Where, σ is the compressive stress, F is the compressive force, A is the cross-sectional area of the rod. The cross-sectional area of the rod is calculated with $A = \frac{\pi r^2}{2}$, where r is the radius of the rod. P is the buckling load, E is the Young's Modulus, I is the moment of inertia and L is the length of the rod. The moment of inertia of a solid rod is calculated with $I = \frac{\pi r^4}{8}$.

The compressive force per rod is calculated, with the fact that the four rods should take up the weight of the UAV at the MTOW, where the weight is considered to be located at the centre of gravity of the UAV and using a safety factor of 2. Furthermore, it is assumed that the UAV lands on its four rods equally such that no torsion is created in the propeller booms. A minimum diameter of $9[mm]$ was required for the landing gear such that the applied load was below the buckling load and that the compressive stress does not exceed the yield strength.

11.6. Compliance Matrix

In Table 11.3 the compliance matrix of the subsystems requirements considering the structure of the UAV is presented. It is indicated of the requirements are satisfied and if this is the case what the method of verification is. Elaboration is given on the requirements that are not met.

Identification	Description	Compliance	Method of Verification
REQ-SYS-STR-01	The structure's subsystem shall provide a secure connection to all other subsystems.	✓	Visual inspection
REQ-SYS-STR-02	The structure's subsystem shall use materials that maintain 95% of their stiffness in the operational temperature range.	✓	Analysis: see section 11.1
REQ-SYS-STR-03	The structure shall not degrade past its operational limit over a minimum of 50000 full-range load cycles.	×	Requires additional analysis of the model
REQ-SYS-STR-04	The critical structural elements shall be inspectable through non-destructive methods.	✓	Visual inspection
REQ-SYS-STR-05	The structure shall not yield under a UAV weight of 25 kg at a load factor of 3.5.	✓	Analysis: see section 11.2, section 11.4 and section 11.3. However additional verification might be needed.
REQ-SYS-STR-06	The structure shall not yield, while supporting the payload at a load factor of 3.5	✓	Analysis: see section 11.2, section 11.4 and section 11.3. However additional verification might be needed.
REQ-SYS-STR-07	The structure shall not yield to dynamic loads during flight with a safety factor of 2.	×	FEM analysis required
REQ-SYS-STR-08	The natural frequencies of the UAV structure shall be outside of the frequency range created through all operational loads.	×	Requires additional analysis of the model
REQ-SYS-STR-09	The exposed UAV surfaces shall not be flammable.	✓	Analysis: see section 11.1

Table 11.3: Compliance Matrix Structure Requirements

As shown in the table, several requirements have not yet been fully satisfied. At this stage of the design, REQ-SYS-STR-03 remains unmet and requires verification through a fatigue analysis. Additionally, REQ-SYS-STR-05, REQ-SYS-STR-06, and REQ-SYS-STR-07 have been verified using hand calculations; however, only the wing structure has been validated with a FEM analysis. To ensure full compliance with these requirements, a FEM analysis of the combined wing and fuselage assembly must be performed.

11.7. Sensitivity Analysis

For the structural design, the load factor during cruise is one of the most critical elements, as it directly influences the limiting load case. Therefore, it is crucial that the design remains functional even if this load factor is not entirely accurate. El Adawy et al. [78] mentions that typical load factors for fixed wing UAVs are between 2.5 and 3.8, which means that by considering 3.5 the design is already on the high end. In this sensitivity study, the load factor will be varied between 3.5 and 4.

Wing Internal Structure

For the internal wing structure, the wing box and FEM analysis are performed with varying load factors. Figure 11.18 illustrates the loading diagrams for different load factor ranges, considering the cruise condition along the semi-span of the wing.

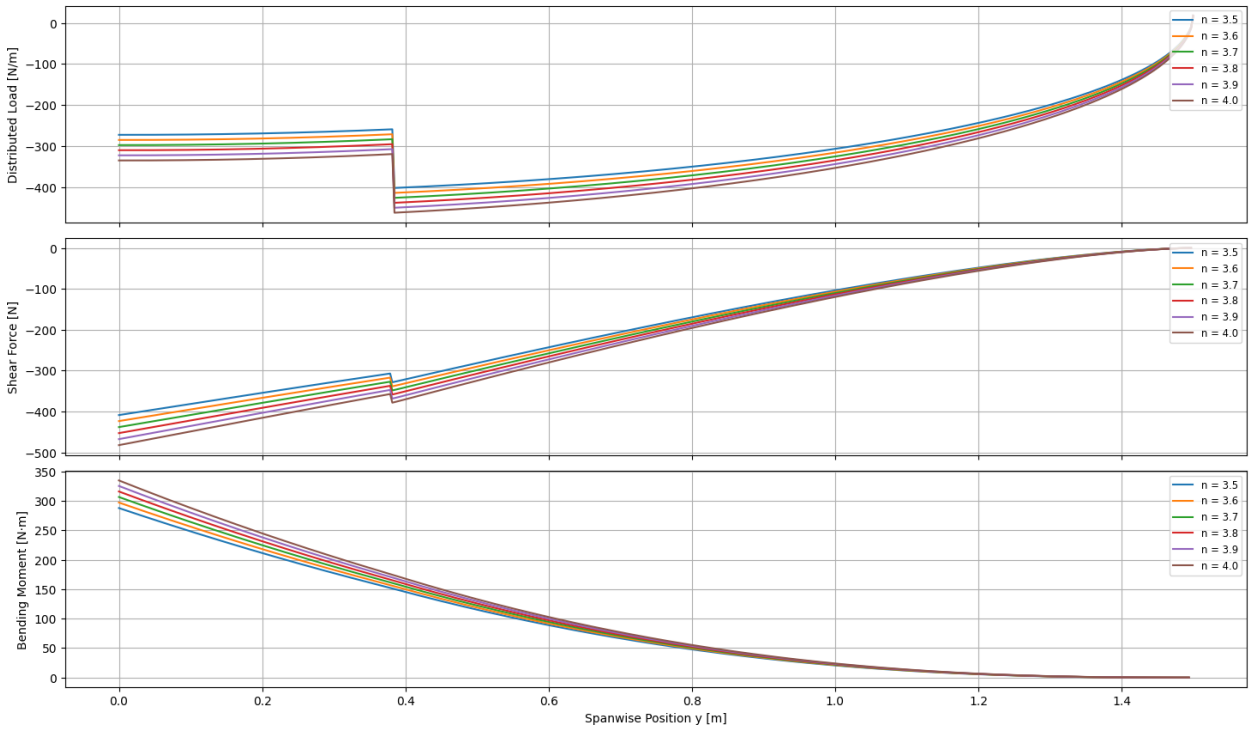

Figure 11.18: Influence loading factor on the loading diagrams.

As can be seen in the figure, there is a slight increase in both the maximum shear force and bending moment at the root chord. When considering a load factor of 4, the thickness increased by 15% compared to the thickness at a load factor of 3. However, it still remained below the minimum manufacturable thickness of $0.78[mm]$.

Furthermore, in Figure 11.19, the varying of the Von Mises, normal and shear stresses are shown, as well as the deformation. These plots are based on the FEM analysis, and therefore use the same simplified load case as described in section 11.2. The thickness of 0.78 mm is used.

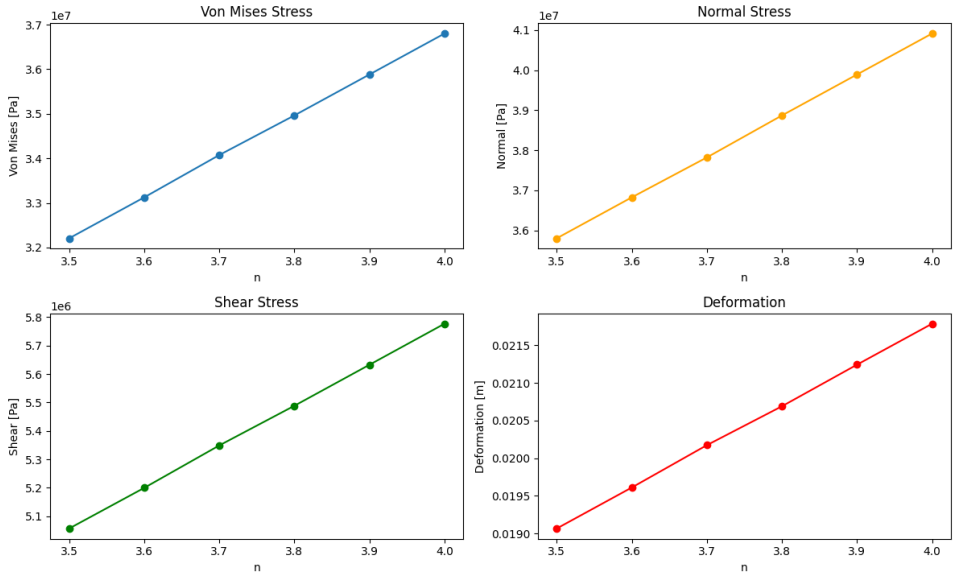

Figure 11.19: Difference in stresses and deformation in the wing due to varying load factor (n)

In these plots, it appears that all relations are linear. However, due to the fact that the load factor is only varied between 3.5 and 4. It is apparent that even taking into account the transverse direction yield strength, the stresses remain below the normal yield strength by a factor of approximately six. The same applies to the shear stresses, where the factor is fourteen. Regarding deformation, there is approximately a 14% increase when comparing a load factor of 3.5 to 4. Since this deformation is about 1.5% of the semi-span, its effect is negligible.

Fuselage Structure

Following the procedures outlined in section 11.4, the skin thickness of the fuselage is determined by maximum shear stress, while the thickness of the wingbox is based on the buckling load. Figure 11.20 and Figure 11.21 illustrate the shear stress experienced by the fuselage skin and the forces acting on the top and bottom panels of the wingbox, respectively, as they vary with different load factors. The thicknesses were set to the previously calculated values: $0.78[mm]$ for the skin and $4.68[mm]$ for the wingbox.

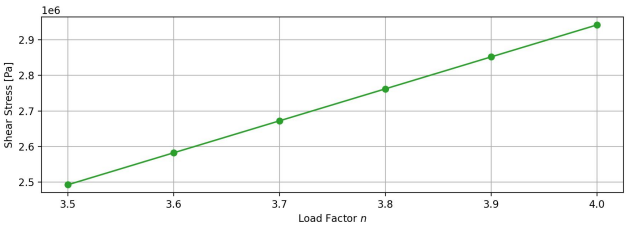

Figure 11.20: Shear stress on fuselage with varying load factor.

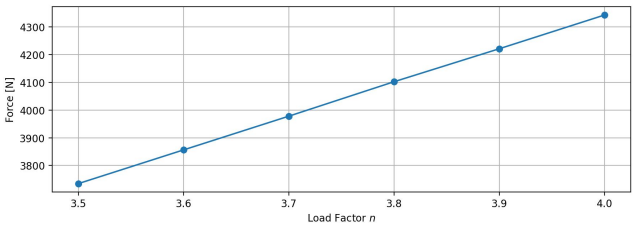

Figure 11.21: Force on top and bottom panel of wingbox with varying load factor.

It can be seen that both shear stress and force increase with a higher load factor. Nonetheless, both values remain below the maximum shear stress and maximum buckling stress, including a safety factor of two.

12

Thermal Regulation

This chapter describes the thermal regulation system and the design process that led to this system. First, the thermal design context is explained in section 12.1, outlining some operations considerations and the mission scenarios driving this design. Then in section 12.2, both the internal and external regulation system and their design approach are described. Lastly, in section 12.3, the thermal requirements are reflected upon using a compliance matrix.

12.1. Thermal Design Context

AeroShield will operate in harsh and varying thermal environments, with ambient temperatures ranging from $-20°C$ to $140°C$ (REQ-SYS-16 from section 3.3). To ensure proper operation of all UAV components, thermal regulation is necessary to ensure that the internal temperature stays within operational limits. For most hardware components, this is between $-20°C$ and $80°C$. In both wildfire and oil spill scenarios, batteries are the most sensitive, requiring an internal temperature between $-10°C$ and $45°C$ to ensure good battery health and long service life [1]. Although they tolerate short exposure to higher temperatures, the internal temperature of the UAV must remain between $-10°C$ and $45°C$ during approach and return (REQ-SYS-THM-07 from section 3.4). An exception is made during the deployment phase, where high internal heat generation and high external temperatures prohibit effective heat dissipation. To reduce the system mass, internal temperatures up to $48°C$ are allowed during deployment. High-temperature wildfire scenarios are driving thermal design, while ensuring compliance with oil spill scenarios.

In addition to regulating temperature for internal components, the thermal management system is responsible for limiting ice accretion on the UAV (REQ-SYS-THM-01 from section 3.4) and shielding external components such as the motors (REQ-SYS-THM-02 from high ambient temperatures section 3.4). These objectives are foundational for the thermal system as described in section 12.2.

12.2. System Overview

The thermal system is responsible for managing heat transfer through conduction, convection, and radiation, and consists of two sections: the internal system, responsible for regulating the temperature in the wing and fuselage areas, and the external system, responsible for preventing ice accretion on both the UAV and propellers, limiting heat transfer through radiation, and insulating the externally located VTOL motors.

Assumptions

Several assumptions about environmental conditions, components, and thermal transport were made to allow efficient thermal system design. While some introduce some simplifications, others introduce more conservative estimations to ensure reliability.

- The en-route ambient temperature during the mission is set to $35°C$, based on average temperatures during wildfire season in European countries with high chances of wildfires [2] (e.g., Greece, Balkan region).
- The on-site temperature is set to the maximum required operating temperature of $140°C$ (U-PER-01 from section 3.1).
- Transition of en-route ambient temperature to on-site ambient temperature is assumed to be instantaneous (no thermal gradient).
- The airflow over the heat sink is estimated to be the minimum relative airspeed in cruise: $100\,\mathrm{km/h}\,(\mathrm{cruisespeed}) - 20\,\mathrm{km/h}\,(\mathrm{windspeed}) = 8p0\,\mathrm{km/h}$.
- Heat dissipation is calculated using average power per phase, neglecting changes in ΔT.

[1] https://genstattu.com/bw/ [accessed: 13/06/2025]

[2] https://climate.copernicus.eu/esotc/2024/wildfires [accessed: 12/06/2025]

- The processor is assumed to operate continuously at maximum power.
- No residual heat from the previous cycle is dissipated during the approach phase.
- The method and therefore assumptions from Heat Sink Calculator are adopted, most notably: the heat sink is modelled with a uniform surface temperature [3].
- Ideal heat conduction is assumed between the components and the PCM and heat sink.
- The thermal resistance of the battery is assumed to be 0.015Ω [4].

Internal System Regulation

The internal regulation system is made up of three main elements: insulation along the walls to prevent heat transfer, phase-changing material (PCM) to store heat, and heat sinks to allow easy dissipation. The sizing of these elements was done by optimising for minimum overall mass while complying with the requirements as outlined in section 3.4. First, the resulting components are discussed. Then, the used modelling approach is elaborated upon.

- **Insulation**
  To limit heat transfer to the UAV during deployment, critical compartments should be protected. Both the fuselage compartment containing critical hardware (shown with a double line in Figure 13.3) and the separately located winch are lined with $1.0[cm]$ of Aerogel Insulation Sheets from Xinjiang Zhongtai Group[5]. Furthermore, the wing compartment up to the detachment point, shown in Figure 13.4, is lined as well. Aerogels' low thermal conductivity of $k = 0.013[W/(m \cdot K)]$ ensures effective insulation with minimal thickness, improving spatial and mass efficiency, resulting in a total mass of $0.57[kg]$.
- **Phase-changing material**
  To store the external heat entering the UAV, and the internal heat generated in the UAV during the deployment phase, two identical ClimSel™ C48 pouches from Climator [79] (each $0.26[kg]$) are located in the wing on separate sides of the fuselage. Both are connected to a heat sink and internal components using thermally conductive wires. PCMs have several advantages: they absorb thermal energy at a nearly constant temperature [80], preventing excessive temperature increases in the UAV; they are reusable, minimising turnaround time; and they operate passively, thus not increasing power requirements.
- **Heat sink**
  Finally, two identical aluminium (anodized AA6063) heat sinks [6] are located in the wing on separate sides of the fuselage. During cruise, air can flow over the heat sink. The heat dissipation is calculated by first computing the Nusselt number, Nu, for airflow over a flat plate [81], using Equation 12.1, with Reynold number $Re = 114245$ (based on $V_{airflow\_in\_cruise} = 70[km/h]$, and a Prandtl number of $Pr = 0.7268$ for air at $35°C$ [82].

$$Nu = 0.0296 \cdot Re^{4/5} \cdot Pr^{1/3} \tag{12.1}$$

  Then, this result is used to compute the forced convection heat transfer coefficient, h_{forced}, using Equation 12.2.

$$h_{forced} = \frac{Nu \cdot k_{air}}{l_{sink}} \tag{12.2}$$

  This coefficient is used to optimise the heat sink length and width for minimum mass, while fin height and thickness have been set. This results in general sink dimensions ($l \times w \times h$) of $10 \times 16 \times 4[cm]$, with a $0.5[mm]$ thick fin every $3[mm]$, weighing $0.17[kg]$ each.

In order to arrive at these general sink dimensions, first the heat transfer due to the internal components and environment was modelled. The internal components that contribute the most to heat generation are the winch, the processor, and the batteries. Assuming that the processor is operating at maximum power, it dissipates $50[W]$ continuously [83]. The winch is only activated during deployment, during which it dissipates $34[W]$ [7]. Lastly, the heat dissipation for the 2 batteries is based on the power required per phase and calculated using

[3] https://www.heatsinkcalculator.com/blog/sizing-heat-sinks-with-a-few-simple-equations/ [accessed: 16/06/2025]
[4] https://oscarliang.com/when-retire-lipo-battery/ [accessed: 17/06/2025]
[5] https://www.zhongtaiint.com/Building-material/silica-aerogel-insulation-sheets-waterproof-and-fireproof-thermal-aerogel-insulation-type-2001000-120mm [accessed: 17/06/2025]
[6] https://www.gabrian.com/aluminium-extrusions/industries/electronics/heatsinks/ [accessed: 16/06/2025]
[7] https://developer.dji.com/doc/payload-sdk-tutorial/en/model-instruction/payload-develop-criterion.html [accessed: 10/06/2025]

Equation 12.3 and Equation 12.4, with current per battery I_{batt}, power required per phase P_{req}, battery potential V_{batt}, number of batteries n_{batt}, and internal resistance R_{batt}.

$$I_{batt} = \frac{P_{req}}{V_{batt} \cdot n_{batt}} \tag{12.3}$$

$$\dot{Q}_{batt,tot} = \left(I_{batt}^2 \cdot R_{batt}\right) \cdot n_{batt} \tag{12.4}$$

The range of heat dissipated by both batteries combined differs significantly per phase: in cruise, this is approximately $50[W]$, while during deployment it is approximately $200[W]$.

Then, while setting heat sink length, heat sink width, and insulation thickness as variables to be optimised, the optimisation simulation can be set up. The heat transfer due to a temperature difference is calculated based on insulation thickness in Equation 12.5, with temperature $T[K]$, effective area (of both fuselage and wing) to be insulated $A_{eff}[m^2]$ thermal convection coefficient $h[W/(m^2 \cdot K)]$, thermal conduction coefficient $k[W/(m \cdot K)]$, and thickness $t[m]$.

$$\dot{Q} = (T_{amb} - T_{int}) \cdot A_{eff} \cdot \left(\frac{1}{(\frac{1}{h})_{air} + (\frac{t}{k})_{ins} + (\frac{t}{k})_{shell}}\right) \tag{12.5}$$

This result, combined with the heat generated by the internal components during deployment, is used to calculate the PCM mass required to keep the internal temperature at $48°C$.

To ensure that the UAVs can continue running for multiple cycles, the heat sink should not merely dissipate the heat generated during return, but they should also dissipate the heat energy stored in the PCM. The turnaround time and an additional time margin of $30[s]$ are also available for additional heat dissipation. Based on this dissipation requirement, the heat sink can be sized for optimal length and width using the approach outlined by Heat Sink Calculator [8].

The optimisation is performed using Scipy minimise function (using sequential least squares programming). The function is constrained by requiring the heat sink to dissipate, at least the amount of heat required to be dissipated during return. Lastly, several physical boundaries are implemented in the model: the insulation thickness cannot exceed $1[cm]$, the combined sink width has to be below $1[m]$, and the sink length should be below $45[cm]$.

While optimised for wildfire missions, the design remains valid for oil spill scenarios. In these conditions, the $-20°C$ ambient temperature is limiting, but the possibility to close-off the heat sink enables the UAV to use the internal component heat to maintain temperatures above $-10°C$. The internal temperature is monitored by a thermometer located inside the fuselage.

External System Regulation

A significant challenge for AeroShield's oil spill configuration is the possibility of ice accretion on the UAV surface, leading to decreased aerodynamic performance, potentially leading to total mission failure. To prevent this, the UAV is coated in a super-hydrophobic (SHP) coating, capable of passively reducing adhesion [84]. Two critical factors that influence coating performance are the delay in ice accretion, and the durability of the coating. PEEK-PEEK/PTFE/k-SiO2 is used for AeroShield systems operating for oil spills, as it presents good characteristics in both criteria. Reducing ice accretion by a factor of 43.5 compared to 7075Al alloy surfaces, and remaining super-hydrophobic after over 50 abrasion cycles [85]. To prevent ice formation on the propeller blades, the internal heat of the UAV can be transferred by conducting wires to be used in the propeller-embedded Ice Protection System (IPS) [86].

For wildfire missions, ice accretion is not a relevant concern. Instead, the heat transfer by radiation is mitigated by applying an $100[nm]$ aluminium coating, shown to have a reflectance between 80-90% (wavelength-dependent) for the similar high temperature FireDrone [87]. This minimises the pressure put on the internal regulation system.

Lastly, protecting externally located VTOL motors against high temperatures is challenging but critical. The motors have an operating temperature of $91°C$, working optimally at an ambient temperature of $60°C$ [9]. The integrated thermal management of the motors uses a self-circulating cooling system [10], which requires access

[8] https://www.heatsinkcalculator.com/blog/sizing-heat-sinks-with-a-few-simple-equations/ [accessed: 16/06/2025]

[9] https://store.tmotor.com/product/u8lite-l-kv110-u-efficiency.html?srsltid=AfmBOoqHtA2yqNLBEv4BijkDX_qmnnYOuGw4SkvopplXfF_3SB4JWl37 [accessed: 18/06/2025]

[10] https://www.mabrobotics.pl/product-page/u8-v2-lite-efficiency-type-uav-motor-t-motor [accessed: 18/06/2025]

to the airflow. Therefore, to shield it from the external temperature, a $0.85[mm]$ ZircoFlex® III [11] foil is added to each motor. The aluminium-backed ceramic foil is capable of reducing the external temperature by 85%, assisting the motors to operate in the required $140°C$. However, some important additional considerations are discussed in section 12.3.

12.3. Compliance Matrix

Table 12.1 shows the compliance matrix of the thermal requirements considering the previously presented thermal regulation system design. Requirements that are not (fully) met yet are discussed in more detail below.

Identification	Description	Compliance	Method of Verification
REQ-SYS-THM-01	The thermal subsystem shall prevent ice from forming on the UAV.	×	Analysis in section 12.2, but additional analysis is required.
REQ-SYS-THM-02	The thermal subsystem shall regulate the temperature of the motors such that it remains within the temperature range from -20°C to 60°C.	×	Analysis in section 12.2, additional analysis is required.
REQ-SYS-THM-07	The thermal subsystem shall regulate the internal temperature of the wing and fuselage compartments such that they remain within the temperature range from -10°C to 45°C.	✓	Analytically verified, see section 12.2.

Table 12.1: Compliance Matrix Thermal Requirements

As shown in the Table 12.1, both REQ-SYS-THM-01 and REQ-SYS-THM-02 are not fully verified yet. While the prevention of ice accretion will likely be sufficient for most mission scenarios, continuous exposure to the most extreme (cold and wet) environments might still introduce ice formation. For these scenarios, it should be investigated if the internally generated heat can be used to heat the wing by transporting the heat through conducting wires. Secondly, while the motors are shielded from the heat by the aluminium-backed ceramic foil, the effectiveness of the integrated self-circulating cooling system is reduced due to the high ambient temperature. Further evaluation is required to assess if this critically influences motor cooling.

12.4. Sensitivity Analysis

The thermal system is designed to handle the exact required conditions with minimum mass, leaving no excess capacity. Thus, this sensitivity analysis studies the effects on the system design for variations in ambient on-site and en-route temperatures. For this, the optimisation algorithm is run for a range of on-site temperatures ranging from $100°C$ to $160°C$, and $15°C$ to $45°C$ for en-route temperatures. The results are shown in Figure 12.3.

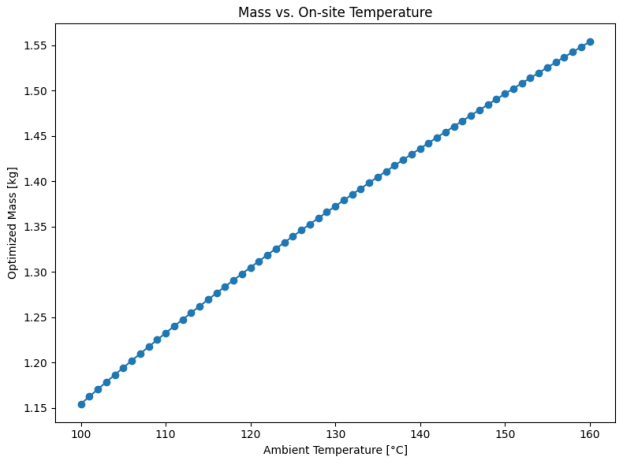

Figure 12.1: Total mass vs. on-site ambient temperature

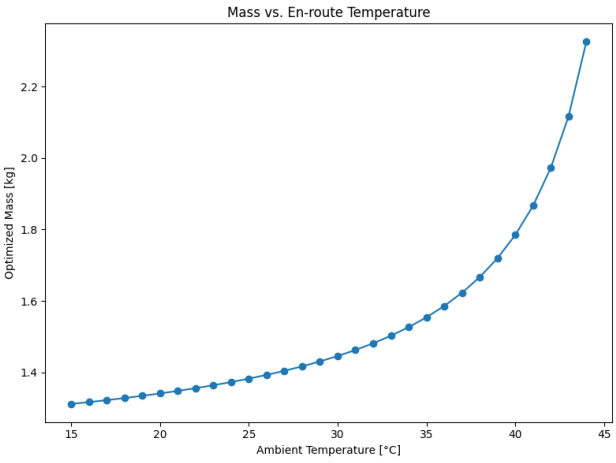

Figure 12.2: Total mass vs. en-route ambient temperature

Figure 12.3: Sensitivity of the thermal regulation system

From these figures, it becomes clear that Figure 12.1 follows an almost linear relationship, and Figure 12.2 an exponential relationship. The reason that a change in en-route temperature can have a much larger impact on overall mass is because lower external temperatures during cruise allow internally generated heat to dissipate more effectively. Not only through the heat sink, which performs better with a larger temperature difference,

[11] `https://zircotec.com/products/heat-shields/zircoflex-foil/zircoflex-iii/` [accessed: 18/06/2025]

Ambient On-Site Temperature			
	$T_{amb,onsite} = 100$	$T_{amb,onsite} = 140$	$T_{amb,onsite} = 160$
Insulation (kg)	0.43	0.57	0.63
Total PCM (kg)	0.44	0.52	0.56
Total heat sink (kg)	0.29	0.34	0.37
Total mass (kg)	$\mathbf{1.15}$	$\mathbf{1.44}$	$\mathbf{1.55}$
Ambient En-Route Temperature			
	$T_{amb,enroute} = 15$	$T_{amb,enroute} = 35$	$T_{amb,enroute} = 45$
Insulation (kg)	0.50	0.57	0.87
Total PCM (kg)	0.44	0.52	0.56
Total heat sink (kg)	0.29	0.34	0.37
Total mass (kg)	$\mathbf{1.15}$	$\mathbf{1.44}$	$\mathbf{1.55}$

Table 12.2: Effects of temperature change on the mass of components

but also through the insulated shell, since the outside temperature is lower than the internal temperature limit of $45°C$. This is particularly useful during the return phase, in which the PCM can release its stored thermal energy more efficiently, thus cooling the UAV more rapidly.

Where it might be expected that a higher on-site ambient temperature would simply require more PCM mass to store the increased heat energy, Table 12.2 shows that this coupling is not that straightforward.

Instead, it displays the behaviour of the optimization algorithm that adjusts the ratio of insulation, PCM, and heat sink mass to arrive at the optimal configuration.

An important take-away from these figures is that combining use cases forces a compromise on the thermal system mass. Currently, the constraints set by the wildfire scenario, increase the system mass for the oil spill scenario as well. However, despite the added mass, it remains advantageous to design for multiple scenarios as it leads to reductions in other areas such as development cost, flexibility, and simplified logistics.

13

System Integration

This chapter presents how all the subsytems and components are integrated together. section 13.1 presents the final design of the UAV and the associated mass budget and section 13.2 shows how the different hardware component are located within the fuselage and wing.

13.1. Final UAV Design

In this section the final UAV Design will be presented. This will contain the mass and power budget breakdown. The final UAV design in shown in Figure 13.1 and Figure 13.2

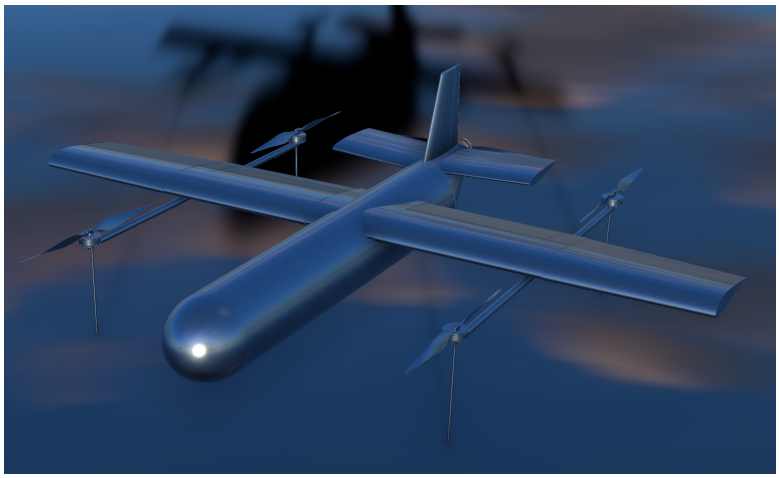

Figure 13.1: Final UAV Design (Front View)

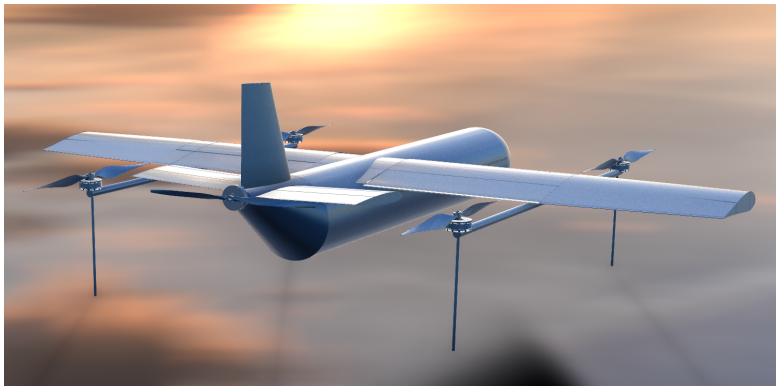

Figure 13.2: Final UAV Design (Back View)

Mass Budget

A mass budget will be presented here. The structural weight is calculated using the CAD model by inserting the density of the glass fibre. This way each structural components weight can be calculated separately and accurately. The Mass breakdown is presented in Table 13.1.

Table 13.1: Mass Breakdown

	Component	Unit mass [kg]	Amount
Structures	Fuselage Oil Spills	1.91	1
	Fuselage Wild Fires	2.34	1
	Wing	4.47	1
	Single Boom	1.68	2
	Single Landing Gear	0.05	4
	Horizontal Tail	1.17	1
	Vertical Tail	0.49	1
	Structural Weight Oil Spills	11.6	-
	Structural Weight Wild Fires	12.0	-
Hardware	Wildfire Sensor	0.92	1
	Oil Sensor	0.91	1
	SDK SkyPort	0.07	1
	Thermal Sensor	0.004	1
	Flight Controller	0.03	1
	Computer	0.7	1
	GPS	0.15	1
	Communication	0.12	1
	Motor	0.28	4
	Propeller	0.09	4
	ESC	0.17	4
	Deployment Mechanism	1.21	1
	Servo Connections	0.02	10
	Power Distribution	0.02	1
	Battery	3.62	2
	Lights	0.12	3
	Buoy	0.14	4
	Thermal System	1.4	1
	Hardware Oil Spills	15.2	-
	Hardware Wild Fires	14.6	-
UAV	Total UAV Oil Spills	26.8	-
	Total UAV Mass Wild Fires	26.6	-

As can be seen in the table, the total mass of the UAV slightly exceeds the initial traget of 25 kg. This could have a negative impact on the aerodynamic efficiency and the stability and control of the UAV. Nonenthelees, it is important to note that the mass is expected to increase further as structural reinforcements and additional refinements are incorporated into the design. Therefore, continued iterations focusing on material selection, hardware optimization, and fuselage design will be crucial in upcoming development stages to reduce the overall mass and enhance performance

13.2. Hardware Layout

An overview of how the hardware is distributed in the fuselage of the UAV and wing is provided in Figure 13.3 and Figure 13.4. Considering first the fuselage, it can be seen most of the hardware is grouped near the nose. This was done such that only a smaller section of the fuselage has to be insulated and cooled. Furthermore to balance the c.g. of the UAV it was beneficial to place these system towards the front. The hardware at the front of the UAV will be accessible through a panel at the top of the fuselage. The sensor is located within a transparent dome (section 11.1 at the nose of the fuselage to maximize the field of view. The UAV is designed to be modular, allowing users to easily exchange the wildfire detection sensor and an oil detection sensor using the Skyport gimbal connection.

The winch is located outside of the insulated area since it has to connect via a wire and pulley system to the aerogel payload. This component is separately insulated as mentioned in chapter 12. The aerogel payload is

placed based on iterations of the c.g. calculations explained in chapter 10. The current position minimises the c.g. shift after deployment of the aerogel. The cruise propeller is placed just outside of the fuselage to allow for air flow into the cooling system. The ESC is located in the wing such that it is within the insulated area. The cabling leading the the motor will be attached to the top of the fuselage.

The layout in Figure 13.3 does not show the pulley system of the deployment mechanism. The aerogel will be attached at both ends of the roll. The cables coming from the winch will be supported by pulleys that are attached near the end of each roll to allow for a controlled deployment. The wire will pass through a hollow wing box and over the PDB which is located inside of this.

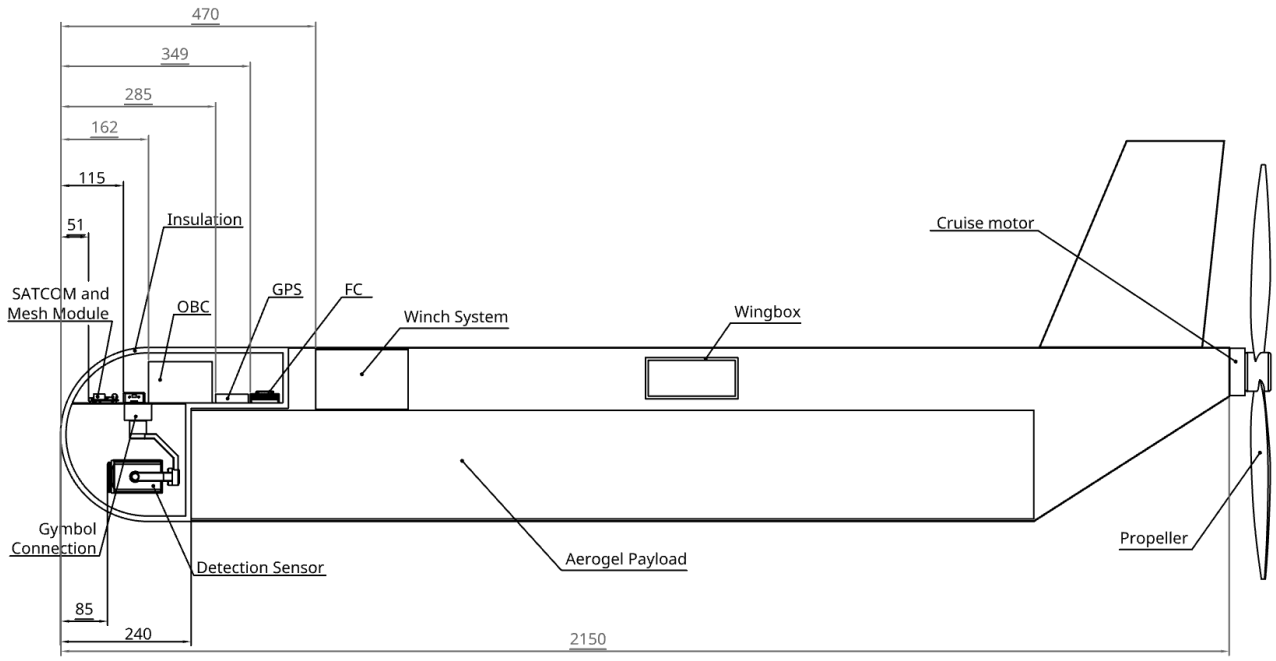

Figure 13.3: Hardware Layout in the Fuselage

For the wing the most central component is the PDB. This component is placed inside of the wing box as this has sufficient space for all the cabling that comes together at this point. The cabling to the battery can be passed through the holes in either side of the wing box. The batteries are located on either side of the wing box and can be easily accessed through the access panel described in chapter 11. Finally the heat sinks are placed slightly further along the wingspan. This location in the UAV allows for sufficient airflow over the fins to cool down the heat sink. The lights are placed all the way at the tip of wing and are attached to the front spar.

Note that the mechanisms for the actuation of the control surfaces and the ESCs for the motors are not shown in Figure 13.4. Due to time constraints these were omitted but will be included for the final report. The actuation mechanisms will be attached to the rear spar of the wing. The ESCs for the VTOL motors will be attached on the inner side of the front and aft spar near the boom. Again this choice is made due to insulation and also space availability in the booms. The ESCs for the cruise propeller is placed on the rear spar near the root of the wing.

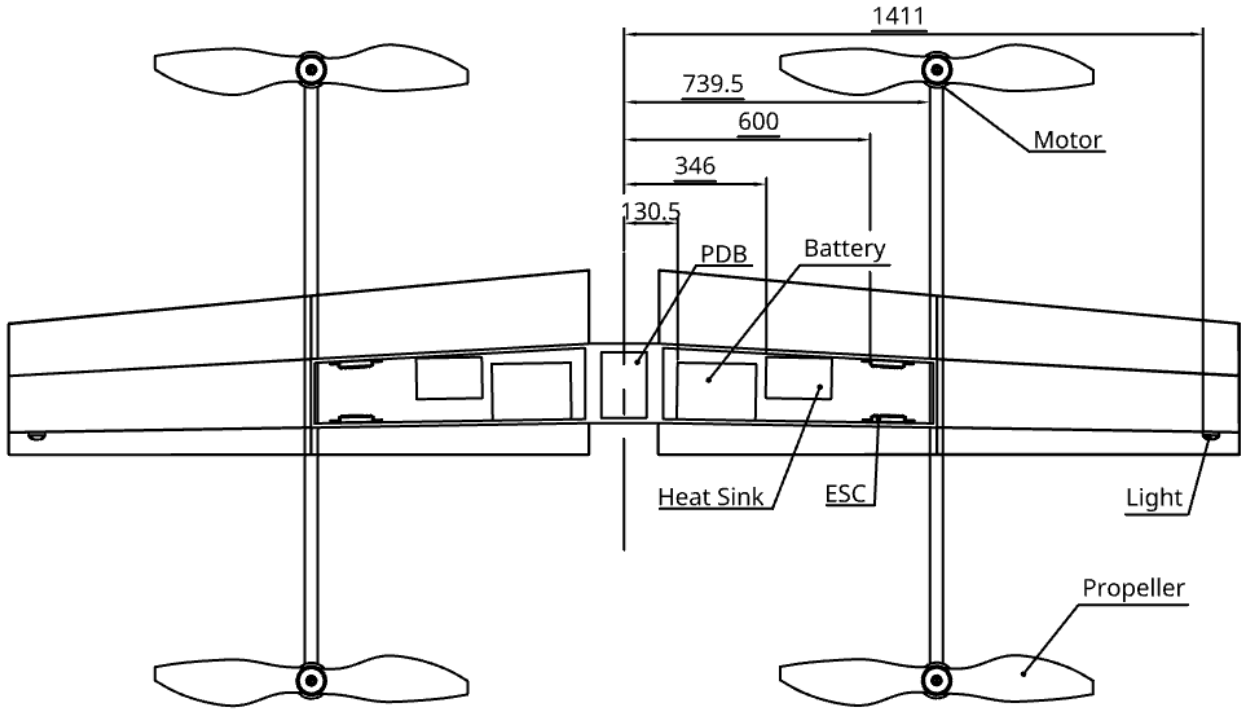

Figure 13.4: Hardware Layout in the Wing

In missions related to oil spills, the UAV will also be equipped with a buoy system. The buoys will be attached on all four of the landing gear of the UAV with a simple strap.

14

Nest Design

Now that the UAV dimensions are set, the nest can be sized. First, in section 14.2 the power and endurance are determined. Then in section 14.3 all the components are placed in the nest in a spatially-optimized and modular manner. Finally, in section 14.4 the mass budget is presented, along with the C.G. locations.

14.1. Nest Overview

The inclusion of a nest is a user requirement - namely, requirement U-GEN-03 specifies a nest to be designed for operational purposes. The nest must be able to provide sufficient power to the UAVs, allowing all 20+ UAVs to charge simultaneously within a UAV's cycle (42 minutes). Moreover, the nest must be able to provide optimal and safe housing for the UAVs when they are not in use. Lastly, the nest must provide structural rigidity and stability during deployment and allow for fast operation. The resulting configuration can be seen in Figure 14.1a and Figure 14.1b, showing the "command module" container and the "UAV storage" container, respectively.

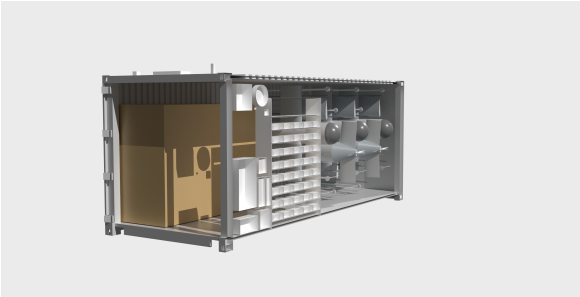

(a) Final Command Module Container Design

(b) Final UAV Storage Module Container Design

Figure 14.1: Final Rendered Nest Configurations

14.2. Power & Endurance

The nest's electrical supply is sized around a single generator that must be able to cover all the nest's peak loads and provide sufficient mission endurance. The generator must be able to be powered by bio-diesel. The total required power can be computed as the sum of each component's peak draw, assuming that all components are working simultaneously.

$$P_{\text{required}} = \sum_{i} P_{i,\text{peak}} \tag{14.1}$$

The final selected generator, GPR-J50-60T4iF Portable Generator Set, was able to provide an output of 60kW and is able to run on bio-diesel [88]. With a power factor, ϕ_{gen}, of 0.8 [88], this gives the following generator power to be used.

$$P_{\text{gen}} = P_{\text{output}} \times \phi_{\text{gen}} = 48kW \tag{14.2}$$

This power output from the GPR-J50 is well within the power requirements for the components, allowing for up to 67 UAV chargers to be charging at a time with all other nest power components functioning, as seen in Figure 14.2. This figure also shows the a power requirement of around $24[kW]$ for charging 20 UAVs, giving a sufficient margin for other power-drawing components and for potential losses in the electrical system, thereby satisfying the charging requirement. The selected generator has a runtime autonomy of 24 hours at 100% prime, allowing it to provide the $48[kW]$ for a full 24 hours before it must be refilled. Based on the UAV mission time, this results in up to 33 full-range cycles, or 55 minimum-range cycles.

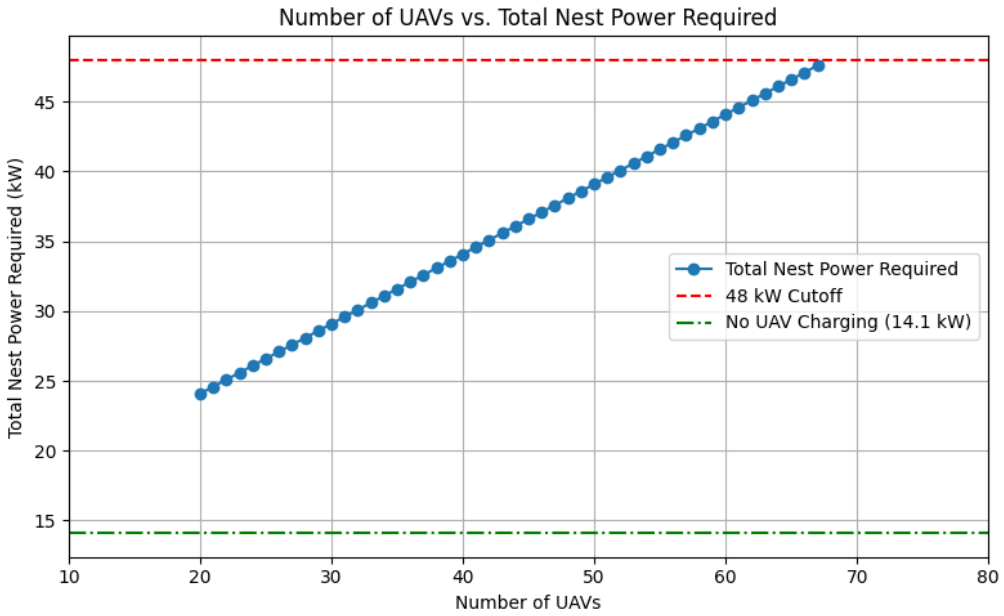

Figure 14.2: Number of UAVs vs Power Requirement

14.3. Spatial Layout & Modular Storage

The spatial layout of the nest is based on a modular design which can easily be scaled up based on the mission requirements. To accomplish this, two types of containers have been designed, a ”command” container and a ”UAV-storage” container. The command container includes the power source (generator) and all the other subcomponents that are required to successfully operate the UAV swarm. This configuration can be seen in Figure 14.3. The ”UAV-storage” container can be seen in Figure 14.4, where the spacing has been optimized to fit as many UAVs as possible in the nest. Both containers are based on a 20ft ISO-container with side-opening doors.

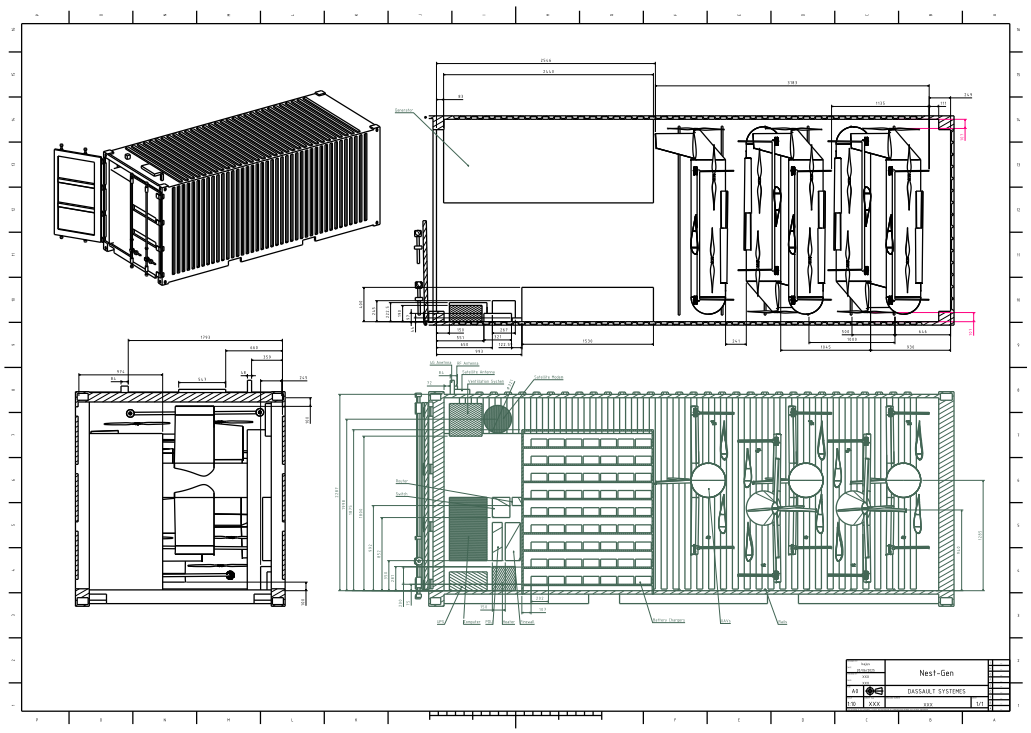

Figure 14.3: Command Container Model

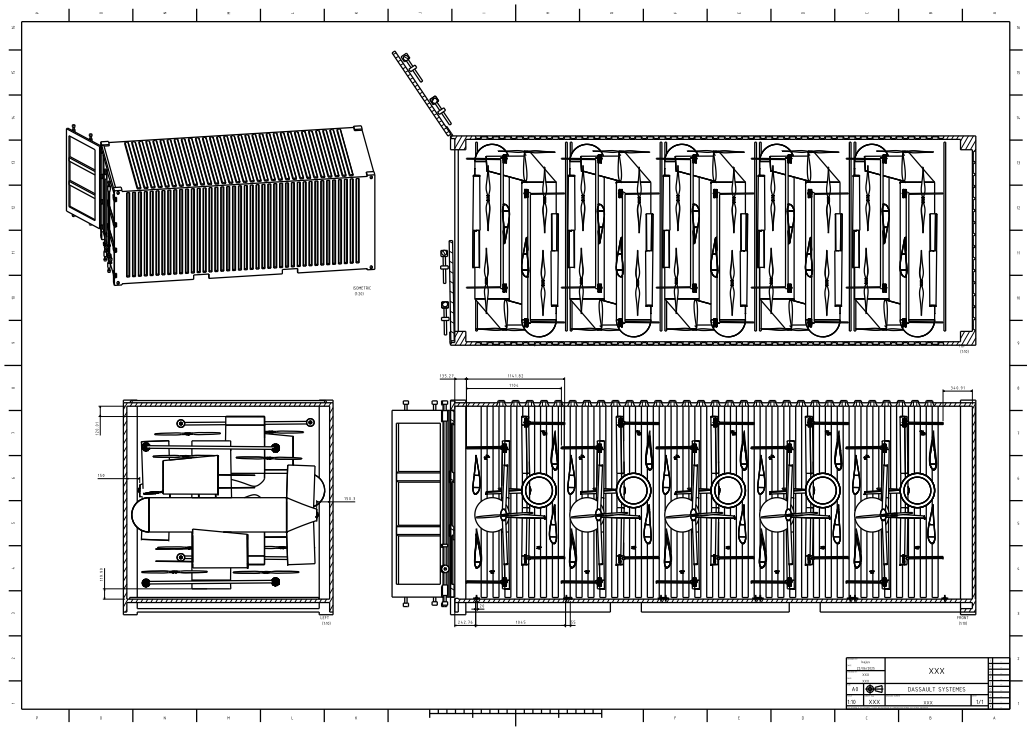

Figure 14.4: UAV-Storage Container Model

Generator & Command Component Layout

The generator is one of the most constraining components in the nest, both due to the large mass and dimensions. It must also be accessible to the operating crew in order for quick and safe generator startup and accessible refuelling allowing for minimum operational time. It was chosen to place the generator length-wise

in the container, leaving $3.46[m]$ of full-width, full-height space available.

The nest computer, ventilation system, heating system, PDU, UPS, firewall, switch, and telecommunication modules were found to fit in a $0.8[m]$ wide, $0.3[m]$ deep ”command cabinet”, allowing a $1[m]$-wide clearance in the nest for an operator to access the generator and electrical components. The battery chargers were able to be fit into a $1.4[m]$ wide, $0.3[m]$ deep shelving unit, allowing access from inside the container and outside the container. This will help optimize the amount of time it takes to bring the charged battery from its charger to the UAV outside of the nest. Together, the command cabinet and charger rack, with a margin of $20[cm]$ between components, results in a $0.3[m]$ by $2.4[m]$ system. The generator, operator space, command cabinet, and charger rack make up the ”command” module which can be fitted into any 20ft ISO-container that has a side-opening door.

UAV Layout

The UAVs are spaced out modularly at a $90°$ roll angle. with the nose pointing in the width-wise direction of the ISO-container. The detachable wings allow the UAV to be fully stored in a rectangular-prism shape with the dimensions as reported in Table 14.1. The resulting layout can be seen in Figure 14.5 .

Table 14.1: Folded UAV Dimensions for Nest Sizing

Variable	Description	Value	Unit
l_{uav}	UAV Length	2.156	$[m]$
w_{uav}	UAV Width	1.724	$[m]$
h_{uav}	UAV Height (detached)	0.491	$[m]$
h_{tail}	UAV Vertical Tail Height	0.223	$[m]$

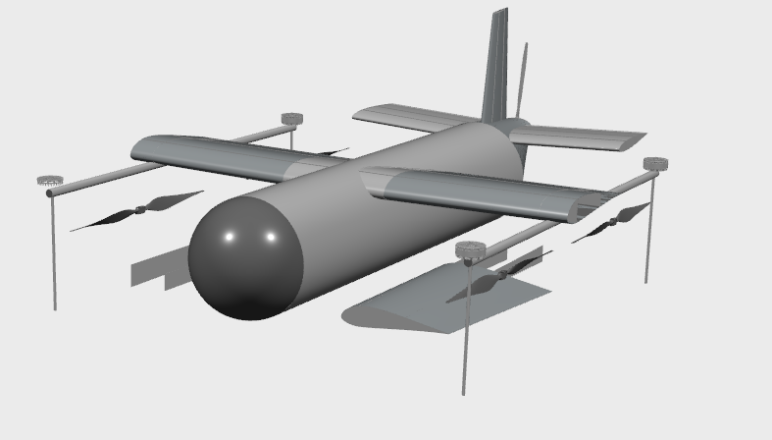

Figure 14.5: UAV in Folded Configuration

Due to the fact that the UAV width is smaller than the nest height (the dimension along which the width will lie), the UAVs can be offset in their vertical placement to avoid the tail from interfering with the fuselage. Furthermore, the UAVs can be stored by alternating the nose direction to prevent the vertical tail from interfering with the horizontal tail. With this arrangement pattern, the number of UAVs that can be fit into a container $n_{uav,container}$, can be calculated by taking the total available container length $l_{available}$

$$n_{uavs,container} = \lfloor \frac{l_{available} - h_{tail}}{h_{uav} \cdot (1 + margin)} \rfloor \tag{14.3}$$

For the ”command” container, a 20% margin resulted in a maximum of 5 UAVs ($n_{uav,c}$) that can be stored. For the UAV-storage containers, 10 UAVs ($n_{uav,s}$) can be stored in the container with a 20% margin.

$$n_{uav,c} = 5, \quad n_{uav,s} = 10 \tag{14.4}$$

To protect the UAV in transit and operation and to allow for fast and coordinated unloading of the UAVs, each UAV bay is lined with a custom-moulded cross-linked polyethylene (XLPE) foam insert. The foam will be CNC-cut to match the fuselage and wing geometry (including the vertical tail offset). This foam will conform tightly

around the fuselage and wing components to dampen vibrations during transport, and must be chemically inert to hydraulic fluids, oil and common cleaning agents. Additionally, $20[mm]$ is elastic buffer is considered under a $30[kg]$ load (assuming a 3.5 maximum lateral acceleration).

Each foam bay will be mounted on a drawer-type sliding rail such that two UAVs share one pair of rails. The number of rails required can be calculated by the ceil operator, where m is the number of ”command” containers, and k is the number of UAV-storage containers.

$$N_{\text{rails,tot}} = m \left\lceil \frac{n_{uav,c}}{2} \right\rceil + k \left\lceil \frac{n_{uav,s}}{2} \right\rceil \tag{14.5}$$

The selected rails are the SBR20-2000□series linear guides [89] based on the static load capacity of 2×30 kg, and a $3.5g$ acceleration, and a stroke of up to 2200 mm. These rails are also designed to fit the 20ft ISO-container, allowing for easy and affordable installation.

Container Layout

Based on the number of UAVs required for the mission, the number of nests will also be determined. For a UAV swarm size of 20, 3 containers must be deployed; one ”command” container, and two ”UAV-storage” containers. This allows the number of UAVs to easily increase up to 25 if the budget allows. Furthermore, based on the power and charging capabilities of the command centre, a single nest configuration with one command module may consist of up to 6 ”UAV-storage” containers, giving a total UAV count of 65. In this scenario, the customer would have to transport 7 containers in total (including the command module container).

14.4. Mass Budget & Balance

Each nest component comes with an associated mass. The total mass can be assumed to be the sum of all components, plus the UAVs stored per nest. The center of gravity of the containers has also been calculated, thereby giving an idea as to what C.G. shifts need to be taken into consideration during transportation and deployment.

Table 14.2: Final Masses of Containers

Type of Container	**Total Mass [kg]**	**Length-wise C.G location [m]**	**Width-wise C.G location [m]**	**Height-wise C.G location [m]**
Command Module (with generator)	5440 ± 500	2.22 ($\approx$ 24.7 % shift)	1.30 ($\approx$ 10% shift)	1.08 ($\approx$ 11% shift)
UAV Storage Module (no generator)	3790 ± 500	2.95 ($\approx$ 0% shift)	1.18 ($\approx$ 0% shift)	1.21 ($\approx$ 0% shift)

This is well within the maximum payload mass capacity of a container of 28.2 tons [1]. The C.G. shift for the UAV storage container module is negligible, resulting in no additional consideration to be made during transport. However, the C.G. shift of the command module nest is quite significant. For conventional shipping containers, up to 5% is generally considered acceptable, with 10% accepted under special circumstances with more advanced spreaders [2]. An 25% margin could be considered too high, potentially requiring a redesign (for example, repositioning of the generator), or adding counter-weights in the design. The design, however, is still considered to be feasible as counter-weights could easily be added due to the large available margin based on the maximum gross weight of a container. It is, however, a consideration that needs to be accounted for before transport.

[1] https://www.bws.net/toolbox/container-specifications/20-foot-dry
[2] https://wiki.unece.org/display/TransportSustainableCTUCode/3%09Principles%2Bof%2Bpacking

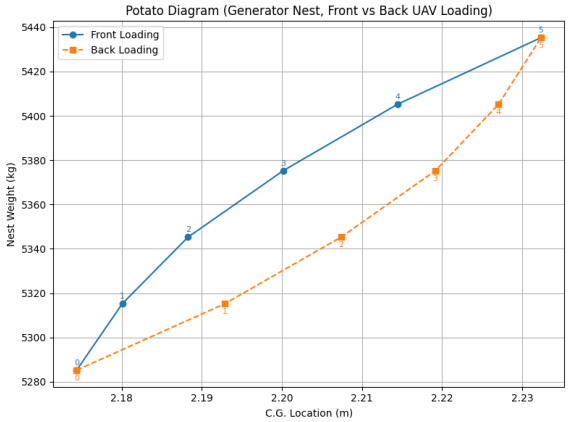

(a) Loading (potato) diagram for command module container

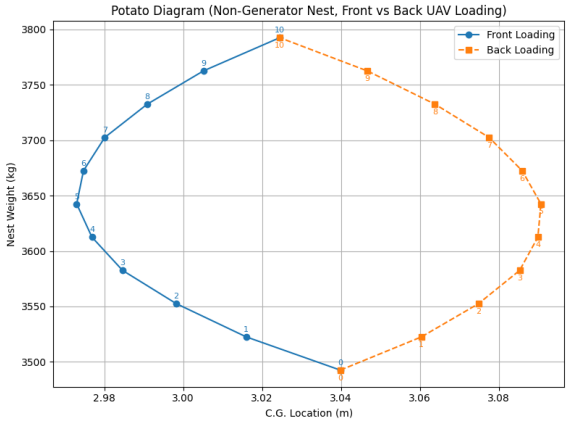

(b) Loading (potato) diagram for UAV-storage module container

Figure 14.6: Loading (potato) diagrams for nest

In addition to C.G. during transport, the C.G. shifts during loading and unloading must also be considered Figure 14.6a and Figure 14.6b show the loading diagrams for the command module (generator) and UAV-storage module (no generator) using front and back loading and unloading of the UAVs. It can be seen that for Figure 14.6b, the C.G. shift is quite high when we have 5 UAVs loaded unevenly, resulting in a maximum C.G. shift of up to 3.09 (to the rearward side). For the command module nest, Figure 14.6a shows that the minimum C.G. is achieved when there are no UAVs loaded, and as the UAVs are loaded the C.G. shifts backwards in both front and rear-loading scenarios.

14.5. Compliance Matrix

The compliance matrix of the nest requirements is visible in Table 14.3. It indicates if the requirements are met (✓) or not (×) and indicates the method of verification.

Identification	Description	Compliance	Method of Verification
REQ-SYS-NST-01	The nest shall be able to charge the UAVs in 42 minutes.	✓	Battery chargers can provide the required 60% in 36 minutes.
REQ-SYS-NST-02	The nest shall have enough capacity to charge the batteries of all UAVs at least one time.	✓	Sufficient space in the container for 20-70 UAVs
REQ-SYS-NST-03	The nest shall be able to dock all UAVs at the same time.	✓	A 3-container nest can simultaneously store 25 UAVs, and the modularity of the nest allows for easy scaling up to around 67 UAVs.
REQ-SYS-NST-04	The nest shall provide sufficient attachment points for transportation	✓	Needs to be tested with different transportation methods.
REQ-SYS-NST-05	The nest shall be able to operate within a temperature range of -20 and 35 °C.	✓	Theoretically met as all components have an operating range within. However, ventillation and cooling of the whole system must be verified.
REQ-SYS-NST-06	The nest shall be able to sustain 1.5g lateral accelerations.	✓	Still has to be verified in practice based on the manufactured parts.
REQ-SYS-NST-07	The nest shall maintain structural stability during UAV deployment.		Structural stability of the UAV-storage container is ensured, however, the command-module container will likely need to be redesigned, or counter-balanced.

Table 14.3: Compliance Matrix Nest Requirements

14.6. Sensitivity Analysis

The nest is susceptible to different input parameters which may alter the final design. One of these parameters which was assumed was the margin used to calculate how many UAVs are able to fit within a nest according to Equation 14.3. Figure 14.7 shows the effect of varying the packing margin on the number of UAVs that are able to fit into both the ”command” and ”UAV storage” containers. It can be observed that as the margin increases, the number of UAVs stored decreases quite rapidly. A margin of 0.5, for example, gives 8 UAVs in the non-generator nest, and only 4 UAVs in the generator (command) nest. This, however, is quite a large margin and is likely not required for this design, but encapsulates the possibility of the dimensions of the UAV

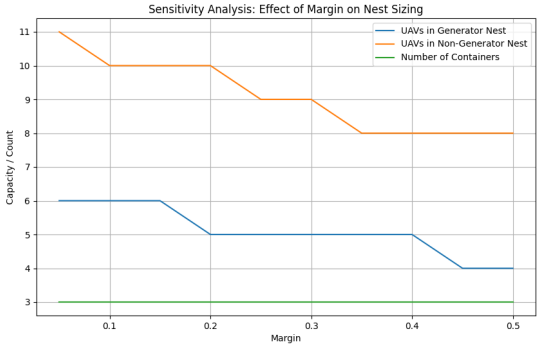

Figure 14.7: Sensitivity of different margins in UAV spacing

increasing. The effect of this would be that more nests have to be deployed, thereby resulting in a larger required ground crew or a decrease in effectively deployment time. It should also be noted that the UAV is loaded such that an increase of 24 cm in width or an increase of 19.4 cm increase in UAV length would make the packing configuration unfeasible, and other layout options would have to be explored.

Another key parameter that can be investigated is the weight & positioning. of components. It is important to keep this in mind as later in the design, more components may need to be added or removed in the containers. This is particularly important for the command-module container. Figure 14.8 show the resulting shift in C.G. when adding/removing mass in the worst-case scenarios: at the front ($x = 0$), on the right ($y = 0$) at the top of the container ($z =$ container height). Figure 14.8a shows the C.G. shifts for the command-module container. It can be observed that the container's C.G. is already quite off-centred at no added mass. It would therefore be preferable to remove mass from the side that the generator is on. On the other hand, it is preferable to add mass to the right side of the container to move the C.G. shift closer to 0. Figure 14.8b shows a similar sensitivity analysis for the UAV-storage container. This container, however, is already quite centred, so adding mass to the sides is not recommended.

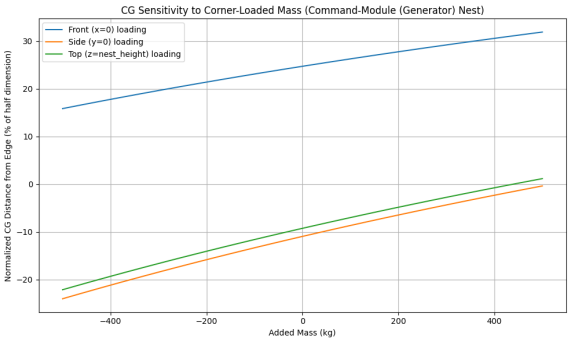

(a) Sensitivity of adding mass to command module container

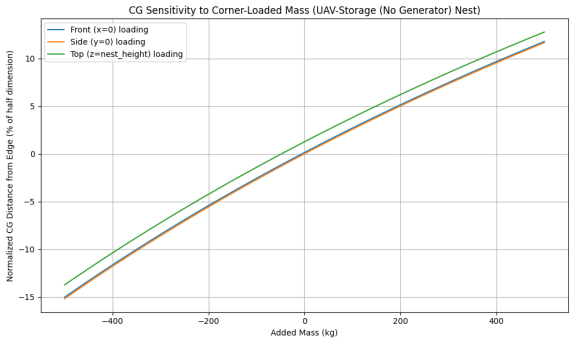

(b) Sensitivity of adding mass to UAV-storage module container

Figure 14.8: Sensitivity of adding mass to nest containers

15

Mission Logistics

With the UAVs and nest design established, the mission can be re-analysed from an end-to-end perspective. This includes the flow of people, containers, preparation and launch, continuous operation and recovery. The following chapter will elaborate on this process, starting by going over the mission as a whole in Figure 15.1, and then going into the separate mission phases: Setup & Launch, Operation and Wrap-up. The fuel and aerogel resupply logistics will then be discussed, followed by the personnel arrangement sizing.

15.1. Mission Logistics Overview

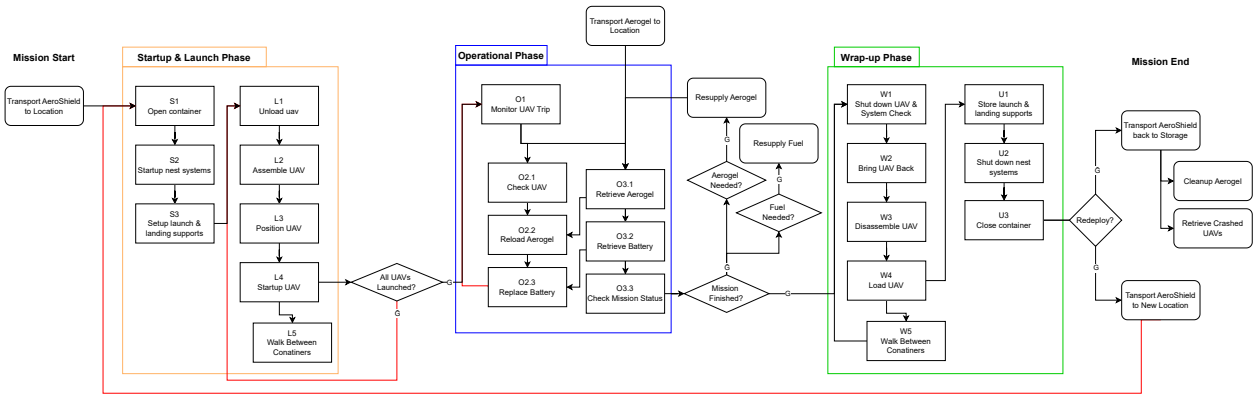

Figure 15.1: AeroShield Logistics Overview

Figure 15.1 shows the overall mission logistics overview worked out in detail. Solid arrows show normal mission flow, while dashed arrows indicate looping/resupply routes. The AeroShield mission begins once the containers are deployed at their location. For wildfires, this means that the mission begins after the containers and first round of Aerogel sheets have been deployed to the location, with the required operational crew present. This could be through, for example a fire-truck with container-carrying capabilities (Figure 15.2 [90]) or through an airdrop. For oil spills, this concerns the point when the crew arrives to the location. Once the mission is initiated. Once the mission is initialized, the setup & launch phase begins, where the nest is powered up and UAVs are launched. After this, the operation phase begins, where UAVs continuously cycle to and from the nest. Once the required perimeter or mass of aerogel has been deployed, the operation phase ends and the wrap-up phase starts. The wrap-up phase is almost the same as the setup and launch phase but largely in reverse. Overall, each of the three phases contribute to the total mission time, $t_{mission}$,

$$t_{\text{mission}} = t_{\text{setup}} + t_{\text{operation}} + t_{\text{wrapup}} \tag{15.1}$$

15.2. Setup & Launch

The setup & launch phase consists of a number of nest and UAV preparation steps that are required to get the UAVs operational. The first nest start-up phase (S1) is the opening of the container. This stage includes several steps, including releasing and lifting locks, and pulling the handles. Side-opening doors significantly reduce the time required to open the doors to under a minute [1]. This process has been estimated to take 30 seconds. The next phase regards the startup of the nest systems (S2). This includes starting up the generator, computer and connected subsystems. This is the most time-consuming aspect of the mission and has been estimated to consume 3 minutes. The next phase includes unloading the launch & landing supports, which

[1] https://swmobilestorage.com/blog/shipping-container-door/

Figure 15.2: Example of a Pre-Mission-Phase Transportation Method

consists of setting up the launch and landing platforms. Due to the back-and-forth movement between the nest and launching location, this has been estimated to take up to 60 seconds. After this, the lauch phase begins. This is a recurring sequence of steps that repeats until all UAVs are launched, meaning the total launch time is highly dependent on the number of personnel that are available and the number of UAVs required to launch. The launch phase consists of unloading the UAV from their storage configuration (e.g. sliding open the modular drawers), assembling the UAVs (e.g. attaching the wings), positioning the UAV on the launch platform (carrying it to a safe launch location) and starting it up, and letting the antennas establish a connection. These phases, together, account for up to 2 minutes, with an additional 30 seconds for if the operator has to walk between the containers.

Table 15.1: Setup & Launch Phase Steps

Step ID	Step Description	Time [s]
S1	Open container	30
S2	Startup nest systems	180
S3	Setup launch & landing supports	60
L1	Unload UAV	30
L2	Asseble UAV	30
L3	Position UAV	30
L4	Startup UAV	30
L5	Walk between containers	30

15.3. Operation

The operational phase is defined to start when the last UAV starts take-off. It is separated into two main parts, the UAV trip itself (O1), which is described in chapter 4, and the time spend back at the nest getting ready for another trip. In this time, two people split up to perform the actions. One retrieves the aerogel and battery from storage (O3.1 and O3.2). The other stays at the UAV and performs a visual inspection for damage or other issues (O2.1), then reloads the aerogel (O2.2), and replaces the battery (O2.3). Once the aerogel is delivered, the first person can already get the battery, optimizing for minimum time. Finally the mission status is checked (O3.3). If based on the mission status it is determined that the mission continues, the UAV starts another trip. Optionally, aerogel and fuel are resupplied in storage.

$$t_{turnaround} = t_{O2.1} + t_{O2.2} + t_{O2.3} \tag{15.2}$$

The total turnaround time is calculated using Equation 15.2, assuming that the operations can be performed in parallel. This will require precise timing between the two operators, possibly requiring extensive training.

Step ID	Step Description	Time [s]
O1	Monitor UAV Trip	2562
O2.1	Check UAV	15
O2.2	Reload Aerogel	30
O2.3	Replace Battery	30
O3.1	Retrieve Aerogel	30
O3.2	Retrieve Battery	30
O3.3	Check Mission Status	30

Table 15.2: Operational Phase Steps

Table 15.3: Setup & Launch Phase Steps

Step ID	Step Description	Time [s]
S1	Open container	30
S2	Startup nest systems	180
S3	Setup launch & landing supports	60
L1	Unload UAV	30
L2	Assemble UAV	30
L3	Position UAV	30
L4	Startup UAV	30
L5	Walk between containers	30

15.4. Wrap-up

Once the mission is completed, the wrap-up phase is initiated. Each UAV that lands at the nest is powered down and receives a final check for any issues (W1). It is then placed at a point where it can be safely disassembled (W2 and W3). The separate parts are then loaded back into the nest (W4), and the workers repeat this action until all UAVs are safely stored. Then, all other equipment that is still outside the nest is placed in the correct place for storage (U1). The nest systems can then be shut down (U2) and the nest can be fully closed off (U3).

In case of wildfires, it might be possible to move the nest to another location to continue mitigation. In that case, the mission is repeated from the startup & launch phase. Otherwise, the nest is returned to its storage location. After the mitigation zone is neutralized and does not pose any danger to people any more, the deployed aerogel can be retrieved. If any UAVs crashed during the mission, they can be retrieved as well.

15.5. Fuel & Aerogel Resupply

Two of the external operations that must be conducted by the operational crew is the resupply of fuel and the resupply of aerogel. Based on chapter 14, fuel resupply is necessary every 24 hours. It is critical that fuel resupply occurs with a sufficient margin to avoid the interruption of the generator. Aerogel will also need to be resupplied. A convenient method for resupplying these aerogel would be to transport them in containers. A rough calculation can be made by taking the inner dimensions of a 20ft ISO-container ($5.90m \times 2.35m \times 2.39m$):

$$N_L = \left\lfloor \frac{L}{\ell} \right\rfloor = \left\lfloor \frac{5.90}{1.50} \right\rfloor = 3 \tag{15.3}$$

$$N_W = \left\lfloor \frac{W}{d} \right\rfloor = \left\lfloor \frac{2.35}{0.25} \right\rfloor = 9 \tag{15.4}$$

$$N_H = \left\lfloor \frac{H}{d} \right\rfloor = \left\lfloor \frac{2.39}{0.25} \right\rfloor = 9 \tag{15.5}$$

$$N_{\text{cubic}} = N_L \times N_W \times N_H = 3 \times 9 \times 9 = 243 \tag{15.6}$$

By considering hexagonal (staggered) packing, this number could be increased slightly, giving a range of 240-270 aerogel cylinders.=, meaning an aerogel refill rate R_{refill} can be expected to have to occur every 8 or 9 hours based on Equation 15.7.

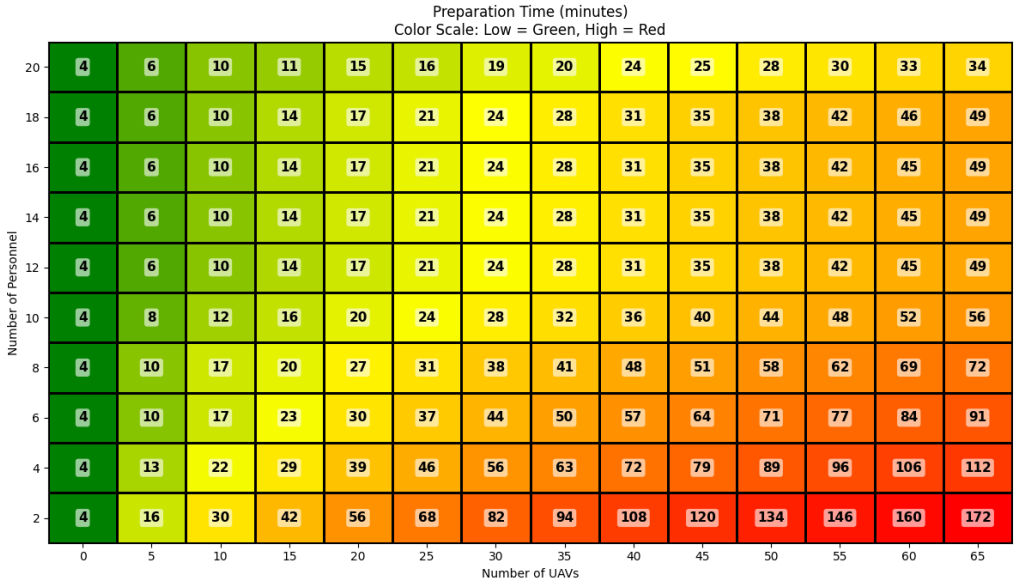

Figure 15.3: Deployment time with varying personnel vs UAV combinations

$$R_{refill} = \frac{n_{aerogel}}{n_{uav}} \cdot t_{uav}/60 \tag{15.7}$$

15.6. Personnel Arrangement

Based on the nest layout and mission logistics, an estimation can be made for the number of people required to successfully and efficiently operate the nest. As is apparent from the mission phases, at least two crew members are required for successful mission operation. This number, however, can also be increased, as the number of on-site crew decreases both preparation (setup & launch) and turnaround (O2.1 - O3.3) times. The minimum setup and launch time will be minimized when the number of crew members is equal to the number of UAVs. However, this is not a direct relationship, and the time-reduction diminishes as the number of workers increases. For a 20-UAV mission, a crew size of 6 members is recommended.

16

Mission Performance

This chapter describes the mission performance. The performance metrics are described in section 16.1, which include the general response time and the deployment rates. section 16.2 presents the compliance matrix related to the performance requirements.

16.1. Performance Metric

For the performance analysis, first it must be determined what decides the success of the design. Seeing as the primary goal of the system is disaster mitigation, time is an essential factor. This can be split into two categories: the general response time, and the deployment rate. The general response time concerns the total time it takes the swarm to cover a certain perimeter in case of wildfire or the amount of spilled oil. For oil spills, the amount of oil soaked up per kilo of aerogel is set to $14kg$, estimated based on Karatum et al. [91]. The deployment rate is more abstract, and is expressed as either the mass of oil cleaned per hour, or the perimeter laid per hour.

For the performance analysis, a standard case has been established, which will serve as the foundation for further evaluation. This standard scenario assumes the deployment of 20 UAVs, supported by six workers. The UAV swarm is required to cover a range of 20 km. For the wildfire mission, a perimeter of $500[m]$ must be established for each mission, while for the oil spill mission, the goal is to absorb $7,000[kg]$ of oil per mission. Although all design parameters are defined, there is still flexibility for varying parameters within the logistics and mission descriptions.

16.1.1. General Response Time

The breakdown of all the time estimates in the mission is given in chapter 4. For the standard case, the total response time is defined from the arrival on site (in the case of wildfires) to the time the final UAV lands back at the nest. This results in a total response time of 20 hours for wildfires. The total response time for oil spills is seven hours.

The wildfire estimation is based on a firebreak width of $3[m]$, based on the analysis by Bennet [92]. This width will be considered in the rest of the performance analysis as well. However, to compare this value to ground crew operations, it would be useful to set a firebreak width of $1[m]$ as this is more conventional [93]. For this case, the total response time changes to 7,5 hours.

These total mission times depend mainly on the distance each UAV needs to travel, as well as on the total amount of aerogel that needs to be deployed. As these are both factors that are set by the customer and not by the design of the UAV, they can be varied to show the variation in general response time for different missions. These variances are shown in Figure 16.1 and Figure 16.2.

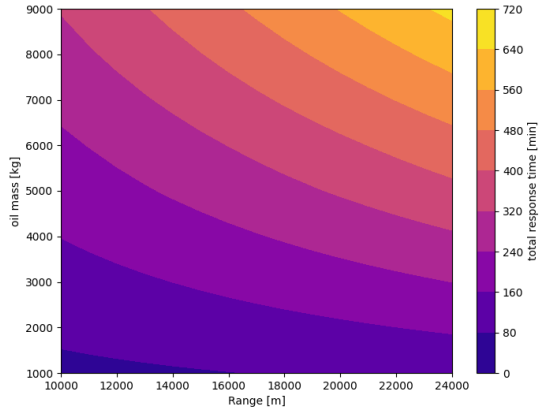

Figure 16.1: Contour plot showing the general response time as a function of range and oil spill mass

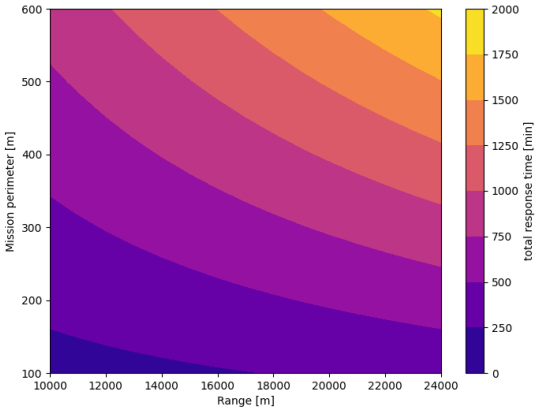

Figure 16.2: Contour plot showing the general response time as a function of range and total required perimeter

These figures illustrate the expected behaviour: deployment time increases with greater range and with a higher required quantity of aerogel. From the spacing of the contours, it can be concluded that the influence of the latter is slightly higher.

16.1.2. Deployment Rates

In the standard mission (as defined above), the deployment rate of oil spills is $946[kg/h]$ and the deployment rate of wildfires is $24[m/h]$. Note that for oil spills, it indicates kilos of oil, not of aerogel. Once the mission is set, the deployment rates will be influenced by the number of UAVs available, as well as the number of workers available to help with the assembly and setup of the nest. This relationship is shown in Figure 16.3 for oil spills, and in Figure 16.4 for wildfires.

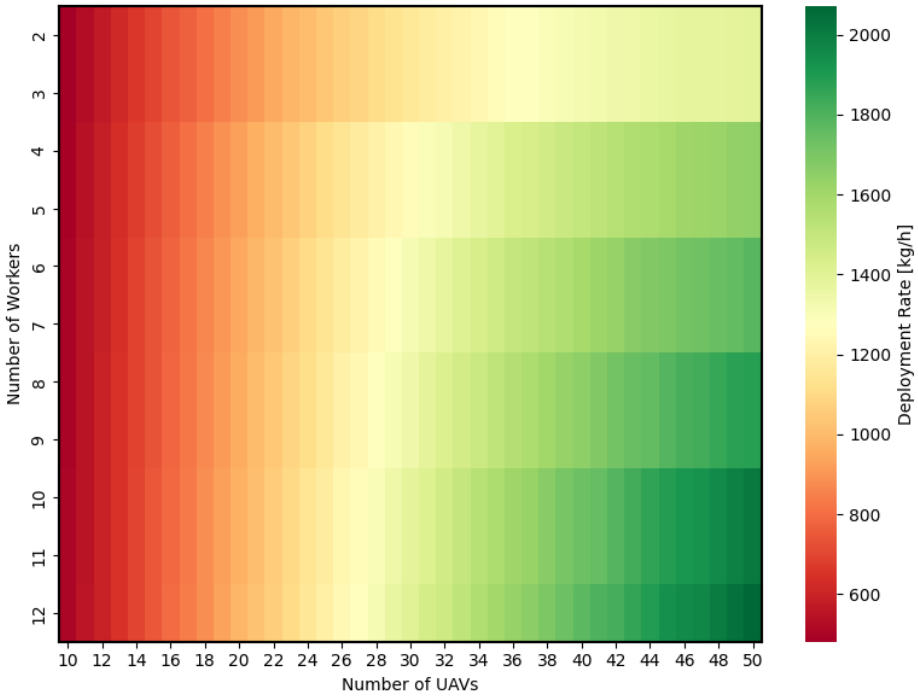

Figure 16.3: Deployment rate for oil spills as a function of the available amount of UAVs and workers

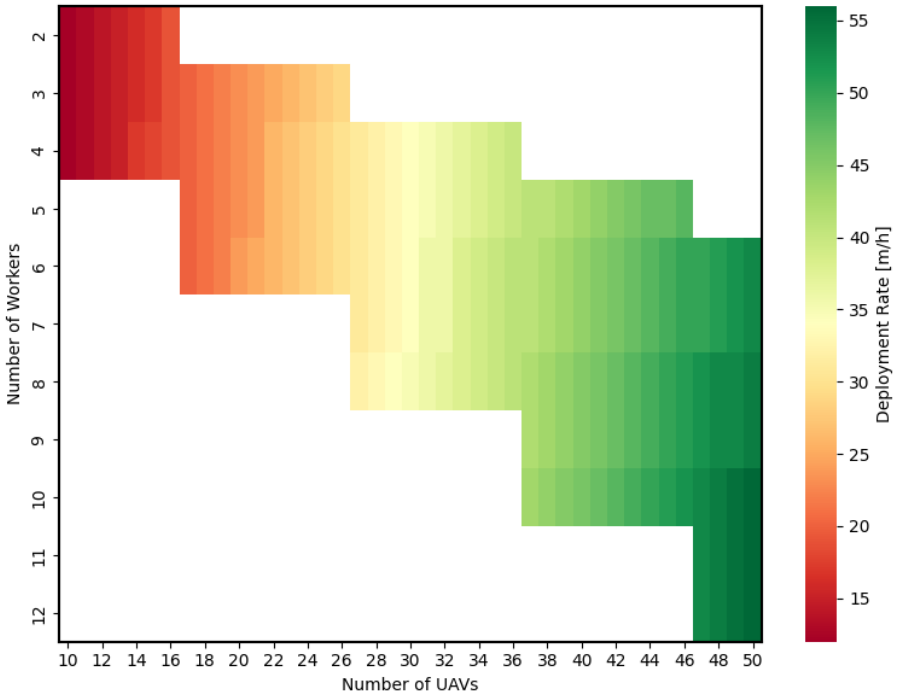

Figure 16.4: Deployment rate for wildfires as a function of the available amount of UAVs and workers

There are two main behaviours visible in these plots. The first is that, as expected, the deployment rate increases approximately linearly when the number of UAVs increases. The second is that since many of the tasks in the setup of the UAVs need to be performed in pairs (for example, lifting the UAV itself), it is more efficient to have an even number of workers. This effect increases in magnitude as the number of UAVs increases, as most of these tasks happen per UAV.

Note that for the wildfire case, the number of workers is limited to a minimum of one per nest and a maximum of two per nest. This is because the nests will be mounted on trucks and driven to the location, and it is assumed that each truck will need at least one driver and only has space for one other person in the passenger seat. Increasing the number of UAVs also should not hinder the swarm dynamics, as the UAVs are largely sequential and the algorithms can be adjusted for the increase.

16.2. Compliance Matrix

In table Table 16.1, the compliance matrix for performance is presented. Note that some of these requirements concern aspects of the design that are not touched upon in this chapter, but instead are considered in previous chapters. They are presented here to give a full overview of the performance. REQ-SYS-PER-21 and REQ-SYS-PER-22 have been adjusted for the final report, as the previous versions did not mention any time constraint, which would mean that the requirement is always met. REQ-SYS-PER-14 was removed, as it was made redundant by the previous adjustment.

Identification	Description	Compliance	Method of Verification
REQ-SYS-08	The UAV shall be able to take-off within 3 x 3 m.	✓	Automatically compliant due to VTOL capabilities
REQ-SYS-09	The UAV shall be able to take-off within a maximum of 60 s.	✓	Analysis: see section 8.2
REQ-SYS-10:	The UAV shall have a minimum Lift of 130% of MTOW [N].	✓	Analysis: see chapter 9
REQ-SYS-11	The UAV shall be able to operate in conditions with wind speeds of up to 30 km/h.	✓	Analysis: see chapter 10
REQ-SYS-12:	The UAV shall have a range of at least 20 km.	✓	Analysis: see chapter 8
REQ-SYS-13	The UAV shall be able to operate at altitudes up to 3000 m.	✓	Analysis: see chapter 8 and chapter 10
REQ-SYS-15	The UAV shall be able to deploy the aerogel with an accuracy of 0.5 m².	×	Due to complicated non-linear dynamics of the sheet hanging from the wire, this cannot be verified without a physical model
REQ-SYS-16	The UAV shall be able operate in a temperature range from -20°C to 140°C.	✓	Analysis: see chapter 12
REQ-SYS-17	The UAV swarm shall be able to deploy 100 kg aerogel in 180 min.	✓	Analysis: see subsection 16.1.2 behaviour
REQ-SYS-18	The UAV shall be able to land within 3 x 3 m².	✓	Automatically compliant due to VTOL capabilities
REQ-SYS-19	The UAV shall be able to operate in conditions with a humidity of up to 100%.		Needs further analysis, not considered in the design as of this point
REQ-SYS-20	The UAV shall be able to reach 150 m in vertical distance from the ground.	✓	Analysis: see chapter 8
REQ-SYS-21	The UAV swarm shall be able to create a wildfire containment perimeter of 500 m within one day.	✓	Analysis: see subsection 16.1.1
REQ-SYS-22	REQ-SYS-PER-15: The UAV swarm shall be able to absorb 7000 kg of oil within one day	✓	Analysis: see subsection 16.1.1

Table 16.1: Compliance Matrix Performance Requirements

17

RAMS

This chapter presents the Reliability, Availability, Maintainability, and Safety (RAMS) analyses of the AeroShield system. The reliability of AeroShield is assessed in section 17.1, providing an estimate based on system performance and failure rates. In section 17.2, design choices aimed at minimizing downtime and ensuring high system availability during maintenance are discussed. Both scheduled and unscheduled maintenance activities are outlined in section 17.3. Finally, section 17.4 presents an operational hazard analysis, identifying key safety risks and the corresponding mitigation strategies incorporated into the system's design.

17.1. Reliability

Reliability refers to the probability that the UAV swarm will perform its intended mission under specified conditions for a given time interval. In order to determine the reliability of the mission, a Fault Tree Analysis (FTA) is made to identify and analyse the potential causes of system failures that lead to the failure of the UAV. A mission is seen to be failed in case the UAVs fail, swarm communication fails or the nest fails. The FTA is seen in Figure 17.1. The FTA goes from system to subsystem to component failure level. The OR gates indicate that any events below the top event can trigger the top event to occur, while the red AND gates indicate that all events underneath the top event need to occur for the top event to occur.

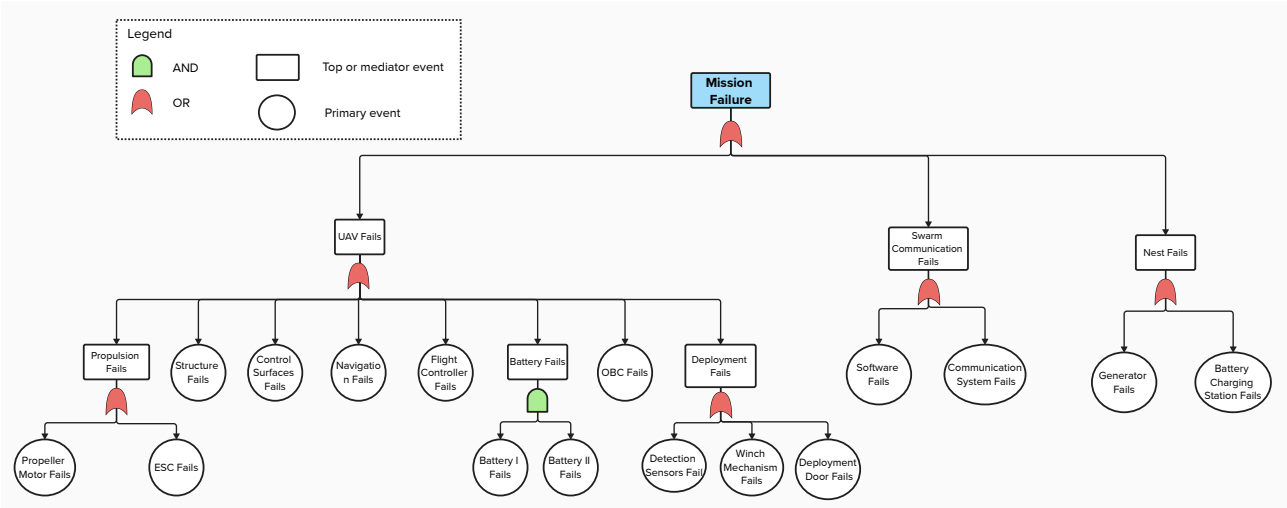

Figure 17.1: Fault Tree Analysis (FTA) of the mission failure of AeroShield.

Assuming that components fail independently, a Poisson-distribution is used to quantify the reliability. The reliability is calculated with Equation 17.1.

$$R = e^{-\lambda t} \tag{17.1}$$

Where λ is the failure rate of each component and t is the time.

For the reliability of the mission, the primary components visible in the FTA are used. The failure rate of each of these components are summarized in Table 17.1.

Component	**Failure Rate** [1/h]
Battery	$10^{-}6$
Flight Controller	$5 \cdot 10^{-5}$
Onboard Computer	$25 \cdot 20^{-6}$
Communication	$16.7 \cdot 10^{-6}$
Propeller	10^{-8}
Electronic speed controller	10^{-5}
Navigation System	$9.41 \cdot 10^{-6}$
Structure	$2.77 \cdot 10^{-6}$
Actuator	$0.19 \cdot 10^{-6}$
Payload	$1.1 \cdot 10^{-6}$
Generator	10^{-9}
Battery Charging Station	10^{-6}

Table 17.1: Failure Rate of Mission Components [94] [95][96]

The failure rate estimate of the payload include the detection of the sensors and the winch and door mechanism. The actuator failure rate indicates the failure of the control surfaces. The failure rate of the battery charging station is estimated to be the same as the failure rate of the battery and the failure rate of a bio-fuel generator is assumed to be similar to that of a diesel generator. Since there is no available data on the failure rate of swarm software, this is not taken into account. This means that the reliability of the system will slightly be overestimated.

AeroShield is expected to mitigate the disaster in approximately seven hours in case of oil spills and twenty hours in case of wildfires (chapter 16). Considering a twenty hour mission time, a reliability of 98.14% is achieved. This reliability analysis assumes that if one UAV fails, the whole mission fails. Dependent on the area of the wildfire or oil spill, there is a possibility that the mission can still be complemented with a reduced number of UAVs, which increases the reliability of the system. To achieve a reliability of 85% throughout the lifetime of AeroShield. AeroShield can be operable for approximately eight missions.

17.2. Availability

The availability analysis focuses on the maintainability and reliability of the system. A high level of reliability correlates with increased system availability. If a system is easily accessible and can be repaired quickly, the downtime for maintenance is reduced, resulting in higher availability. In the context of AeroShield, ensuring high availability is critical for the continuous containment of oil spills and the suppression of wildfires. Each UAV must be ready for redeployment with minimal downtime.

To keep AeroShield operational and ready for immediate response, several critical design and operational strategies have been implemented to enhance system availability. These strategies aim to minimise downtime, facilitate rapid recovery from failures, and maintain mission continuity even under degraded conditions. The UAVs are designed to be modular, allowing for the easy replacement of critical components. This means that if one UAV is down for repair, the other UAVs can continue the mission. Additionally, the nest includes a cleaning and repair station that allows for quick maintenance, ensuring that more extensive maintenance can be deferred to a later time.

17.3. Maintainability

Maintainability focuses on how easy it is to repair and access certain parts of the UAV and nest and to return it back to it's original state. The system is designed for high maintainability through a modular architecture, which allows for easy replacement of key components such as the detection sensors and batteries and accessible design because the propulsion systems are externally mounted and the payload is easily accessible through the fuselage panels. and the nest allows for fast recharge capabilities, due to the generator and the battery charging station and the spare batteries.

Since the UAV operates in harsh conditions, it is important that regular checks and maintenance is planned. The following maintenance activities will be performed after a full mission is completed:

- The control surfaces (propellers, wings) will be checked and if necessary, cleaned from dust, fire residue or contaminants.

- The sensors and cameras will be cleaned and calibrated.
- The current batteries will be charged and the UAV will be reloaded with fully loaded batteries.
- The structure of the UAV will be checked for damage.
- The winch wire will be checked for damage and a new roll of aerogel will be loaded into the UAV.
- The wing lock mechanism will be checked for proper functioning.

Furthermore, from the reliability analysis, it can be seen that after approximately eight missions, the reliability of the mission drops below 85% reliability. Thus after eight missions, a scheduled maintenance check will occur to check all critical components of the UAV and nest and also the connections of internal and external structure of the UAV.

In addition to routine maintenance, non-scheduled maintenance activities may be required in the event of unexpected failures or anomalies. These include:

- Replacing damaged or malfunctioning components such as motors, sensors, batteries, or electronics.
- Performing corrective repairs to restore functionality after unforeseen incidents.
- Performing software updates to resolve control or communication issues.

17.4. Safety

Safety involves minimizing the risk of harm to the environment, equipment, and personnel during mission execution. A comprehensive safety analysis for UAVs involves identifying potential hazards, assessing their risk assesment and designing mitigative systems to address these concerns [1]. Potential operational hazards are determined based on mission specific environmental conditions mission and swarm related hazards and generic UAV hazards identified in UAV safety literature and databases [97] [98].

Each hazard is evaluated based on its probability of occurrence (P) and its consequence (C). Both factors are scored on a scale of 1 to 5, where 1 indicates a highly unlikely occurrence and 5 indicates frequent occurrence for probability. For consequences, 1 signifies negligible impact, while 5 represents catastrophic consequences. The corresponding severity categories are defined in Table 18.3. The operational hazard analysis is presented in Table 17.2, and Table 17.3 illustrates the safety risk map before mitigation strategies are applied. In the operational hazard analysis, different types of hazards are identified and categorized as environmental (E), mission/swarm (M), and generic UAV hazards (G).

Table 17.2: Operational Hazard Analysis

ID	Potential Hazard	Cause	P	C	Mitigation Strategy
E1	Thermal/smoke damage	Fire proximity, obscured vision	5	5	Fire-resistant materials, infrared sensors
E2	Saltwater/corrosion damage	Low-altitude flight over ocean	4	3	Sealed electronics, anti-corrosion coating
E3	Collision with environment	Birds, trees, boats, power lines	2	4	Altitude regulation, obstacle avoidance algorithms
M1	Swarm Collision	Communication failure, desynchronisation	3	5	Redundant communication systems, update software
M2	Loss of communication	Signal jamming, terrain obstruction	3	4	Mesh network, back-up system
M3	Deployment failure	Winch system failure	3	3	Health monitoring
G1	Loss of control	Flight controller failure, sensor degradation, interference	3	4	Sensor redundancy, health monitoring
G2	Severe weather conditions	Wind gusts, rain	2	4	Strengthening airframe, water resistant coating
G3	Unexpected crash	Battery failure, critical component failure	2	5	Retrievable systems

[1] `https://mydroneguide.com/drone-risk-assessment/` [Accessed: 11-6-2025]

Table 17.3: Safety Risk Map Before Mitigation

5		G3	M1		E1
4		E3, G2	M2, G1		
3			M3	E2	
2					
1					
C / P	**1**	**2**	**3**	**4**	**5**

Table 17.4: Risk Map Legend

Severity	Risk Level
Very high	20–25
High	15–19
Moderate	10–14
Low	5–9
Very low	1–4

The risk mitigation strategies are incorporated in the design of AeroShield by the following design choices:

- The structure of the UAV consists of materials that are corrosion, water, and heat resistant in order to withstand environmental extremes.
- Critical systems like IMUs, communication modules are redundant. For example, the IMU consists of several barometers and two different communication systems are used, a mesh network and communication system based on satellite network.
- A Health Monitoring system is incorporated in the Onboard computer which continuously monitor system health of the battery, sensors and winch system.
- Obstacle avoidance and swarm logistic algorithms are used to avoid collisions.
- Pre- and post-flight inspections include checks of winch systems, sensors, and structural integrity to ensure all hazards remain controlled throughout the mission lifecycle.
- The UAV include a buoy system, in order to retrieve the UAV in case of a crash in the ocean. In case of a crash in the wildfire mission, the UAV can be retrieved based on location. Furthermore, the UAV contains a flight recorder such that the cause of failure can be investigated.

In summary, with the incorporation of these design choice, all safety risks are actively addressed by the AeroShield design and the design can be considered as safe.

18

Technical Risk Assessment

Risks are present in every design and have the potential to severely impact even the most promising projects. However, early identification and proper risk management can minimise the impact of risks. This chapter discusses this technical risk management. Firstly, technical risks and their consequence are identified in section 18.1. Then, mitigation strategies are presented in section 18.2.

18.1. Technical Risks

Technical Risk Management begins with identifying possible risks. Firstly, the project is divided into core categories where risks may arise. Then, specific risks within each category are identified and evaluated on their potential impact. Each risk is assigned a score based on its probability of occurrence (P) and the severity of its consequence (C). These are both rated on a scale from 1-5, where 1 is the lowest probability of occurrence/-consequence and 5 the highest. The results are summarised in Table 18.1.

Table 18.1: Technical Risk Analysis

Category	Risk ID	Risk	P	Consequence	C
Design	RK-DES-01	No regulatory clearance to fly over fire zones	1	AeroShield cannot be implemented	5
	RK-DES-02	UAV control compromised due to hacking or GPS failure	3	Mission failure or crash	5
	RK-DES-04	Errors or omissions in the design of a system of the UAV.	4	Increased development costs due to time lost if product fails in testing.	2
Production	RK-PRO-01	Production exceeds the scheduled time	3	Delays in delivery and deployment of AeroShield	4
	RK-PRO-02	Aerogel structures are not available	1	Production of AeroShield not possible	5
	RK-PRO-03	UAV components are not available	2	Production of AeroShield not possible	5
	RK-PRO-04	Shortage of raw materials	2	Delays in production of AeroShield	3
	RK-PRO-05	Lack of production personnel	2	Production of AeroShield not possible	3
	RK-PRO-06	Production produces a lot of greenhouse gas emissions	2	Increased environmental risk and reduced sustainability	3
Sales	RK-SAL-01	No market interest in AeroShield	1	AeroShield will not be sold	5
	RK-SAL-02	Competitor designs a similar product and has quick market reach times	2	AeroShield will have a reduced market share	4
	RK-SAL-03	Aerogel structures become too expensive	2	AeroShield implementation costs become to high	3
	RK-SAL-04	Production costs become too high	3	AeroShield development costs become too high	3
	RK-SAL-05	AeroShield system maintenance costs become too high for user	4	Less users of AeroShield, and thus lower mitigation influence	3

Category	Risk ID	Risk	P	Consequence	C
Operations	RK-OPE-01	Maintenance duration becomes too long in between missions	3	Reduced availability of AeroShield	4
	RK-OPE-02	Destructive interference with traditional mitigation methods	4	Reduced disaster mitigation, hence AeroShield will be avoided	5
	RK-OPE-03	Weather conditions are too extreme to deploy system	3	AeroShield cannot be implemented	5
	RK-OPE-04	Operating conditions exceed design limits while the system is deployed	3	Damage to AeroShield or total crash	5
	RK-OPE-05	Aerogel does not deploy correctly	3	Reduced aerogel deployment rate	3
	RK-OPE-06	UAV sensor(s) become obstructed	3	Damage to AeroShield or total crash	5
	RK-OPE-07	No suitable nest deployment site available	2	Delayed or aborted mission	3
	RK-OPE-08	Mission UAV charging time is too long	3	Reduced availability of AeroShield	4
	RK-OPE-09	UAV fails during the mission	2	Reduced number of UAVs to mitigate the disaster	2
	RK-OPE-10	UAV's swarm communication system fails	2	UAV can't communicate with other UAVs anymore	3
End-of-Life	RK-EOL-01	AeroShield components are not recyclable	3	Negative stakeholder perception	2
	RK-EOL-02	UAV lifetime shorter than expected	3	Increased maintenance costs or complete replacement of the UAV	4
	RK-EOL-03	Crashed UAVs/products left in disaster zones	3	Loss of valuable or sensitive equipment and data	2

To identify the most critical risks, the risks from Table 18.1 are visualised in a risk map in Table 18.2. Each risk level is calculated by computing the product of probability (P) and consequence (C), which determines its severity. The corresponding severity categories are defined in Table 18.3.

Table 18.2: Risk Map Before Mitigation

5	D1, P2, S1	P3	D2, O3, O4, O6	O2	
4			P1, E2 O1, O8	S2	
3		P4, P5, S3, O7	S4, O5	S5	
2			E1, E3	D4	
1					
C / P	**1**	**2**	**3**	**4**	**5**

Table 18.3: Risk Map Legend

Severity	Risk Level
Very high	20–25
High	15–19
Moderate	10–14
Low	5–9
Very low	1–4

18.2. Risk Mitigation

Table 18.4 lists the mitigation strategies that still need to be addressed at the current stage of the design and their expected effect for each risk, along with the updated probability (P_{new}) and consequence (C_{new}) scores. The risks that are already addressed in the design are removed.

Table 18.4: Mitigation Strategies

Risk ID	Mitigation Strategy	Effect	P_{new}	C_{new}
RK-DES-01	Engage early with aviation authorities to apply for waivers or regulatory exceptions for operation in emergency scenarios.	Reduces the likelihood of operational prohibition by ensuring legal compliance in wildfire zones.	1	3
RK-PRO-01	Develop a detailed production schedule with buffer periods and establish penalties/incentives for suppliers.	Reduces risk of production delays and ensures timely delivery.	2	4
RK-PRO-02	Secure agreements with aerogel suppliers early in the project and consider alternative insulation materials as a fallback.	Ensures material availability and maintains production flow even if supply issues occur.	1	3
RK-PRO-03	Use standardised modular UAV parts and possibly have multiple supplier options to reduce dependency.	Reduces risk of bottlenecks caused by single-source suppliers.	2	3
RK-PRO-05	Ensure personnel are trained in multiple roles to increase workforce flexibility and reduce dependence on specific individuals.	Maintains workforce productivity despite absences or shortages.	2	2
RK-SAL-01	Conduct market studies and outreach early on, including demonstrations for stakeholders and potential users.	Increases stakeholder engagement and reduces the likelihood of low market interest.	1	2
RK-SAL-02	File design patents and establish NDAs for collaborators to reduce intellectual property theft.	Reduces risk of competitor replication and protects market share.	1	4
RK-SAL-03	Investigate bulk production and structure geometry to reduce aerogel cost and maximise its effectiveness.	Improves cost-efficiency and economic feasibility of large-scale deployment.	1	3
RK-SAL-04	Optimise production processes and supply chains to reduce cost per unit; consider outsourcing components to reduce costs.	Reduces financial pressure and enables competitive pricing.	2	2
RK-SAL-05	Design for maintainability with modular parts and offer user training to reduce operational maintenance costs.	Increases product appeal and reduces user burden, aiding adoption.	3	2
RK-OPE-02	Design for compatibility with existing firefighting mitigation frameworks in mind and conduct joint simulation trials.	Ensures operational integration and reduces chances of mission rejection.	2	3
RK-OPE-03	Define clear weather envelopes for UAV operation.	Prevents mission failures due to unsuitable environmental conditions.	3	4
RK-OPE-04	Design system with aerospace design standard safety factors and conduct real-time monitoring of stress and environmental load limits.	Reduces chance of UAV damage during operation beyond design limits.	2	2

Risk ID	Mitigation Strategy	Effect	P_{new}	C_{new}
RK-OPE-05	Incorporate payload monitoring systems for aerogel deployments to allow for correctional manoeuvrers before fully releasing, and perform ground checks prior to every mission.	Increases probability of successful deployment.	2	3
RK-OPE-07	Collaborate directly with disaster services to locate a suitable nest deployment site, possibly at an existing emergency services site.	Reduces likelihood of deployment failure due to unavailability of suitable ground infrastructure.	1	3
RK-EOL-02	Perform lifecycle testing during development and design for component interchangeability.	Increases component lifespan and lowers total system cost.	2	2

Using the updated P- and C-scores, a new risk map is created to include the mitigation effects. This is shown in Table 18.5.

Table 18.5: Risk Map After Mitigation

5					
4	S2	P1	O3		
3	D1, P2, S3, O7	P3, O2, O5			
2	S1	P5, S4, O4, E2	S5		
1					
C / P	**1**	**2**	**3**	**4**	**5**

19

Verification & Validation

Verification and validation are the processes of checking that the team's design tools and final design perform as intended and correspond to real-world physics and acceptable mission performance. This chapter outlines the verification and validation procedures designed by the team at different design levels. In section 19.1, the design tools on which verification and validation need to be performed are described. section 19.2 includes an overview of the structuring of system and subsystem requirements verification, and section 19.3 details verification and validation procedures for entire mission scenarios.

19.1. Design Tool Verification and Validation

To aid with the final design, the team developed/will develop several computational tools with different functions. These are: (1) a sizing tool for the UAVs, (2) a sizing tool for the nest, and (3) a simulation tool for analysing operational performance.

The UAV sizing tool is by far the largest. As a result, the architecture of this sizing tool had to be made modular in nature, where each subsystem has its own file and methods for sizing the components in it and evaluating its performance. As a result, this allows for the different modules to be verified individually. This is done with unit tests for each function within a module, mostly formulae following from their respective papers and design methodologies, whose outputs have results that can be checked against hand calculations. At a higher level, the functionality of the sizing tool is verified through system tests that check the correct integration of all modules, as well as the correct flow of inputs and outputs across them.

The nest sizing tool is smaller in scale when compared to the one used for the UAVs, consisting only of a single module. The tool is based on simple volumetric considerations from the dimensions of each UAV, which can also be easily verified against hand calculations with simple inputs. The tool output is validated by cross-checking it against a parametric CAD model using the same considerations for drone size, amount per nest, amount per shelf, etc. as required by the tool.

The simulation tool for operational performance follows from the analysed effectiveness of AeroShield for containing wildfires and absorbing oil spills. In other words, it relates to the aerogel deployment rate, which directly influences the amount of fire barrier created and oil absorbed per unit time. Depending on the amount of UAVs and workers available, and the distance from nest deployment to the disaster site, this performance is evaluated for a wide range of combinations. Nonetheless, for any given configuration, hand calculations are straightforward and are used to verify the tool.

For future stages of design, this tool should be expanded to several modules that handle propagation physics for wildfires and oil spills, and more detailed operations of the AeroShield system and swarm dynamics. These would incorporate changing wildfire/oil spill disaster characteristics and AeroShield's adaptation to create the most optimal aerogel barriers. Even then, all should be individually verifiable through unit tests, by comparison with different relevant analytical models. Additionally, the expansion of this tool will require a larger amount of system tests that verify the functioning of each whole module, as well as their interactions.

19.2. System and Subsystem Requirements Verification

Verification of system and subsystem requirements, along with their verification method, is detailed in each respective chapter of the report. In the case these requirements have not yet been verified, the necessary procedures are outlined to do so in future design stages. In comparison to the requirements initially drafted in the Baseline Report, some were removed as the design developed and they proved not applicable, as explained in each chapter. Nonetheless, the original IDs for each requirement are kept.

19.3. Mission Verification and Validation

Mission verification is based on simulation testing to ensure the end-to-end intended operation of the AeroShield system. In future design stages, the team will simulate full-mission scenarios to confirm correct sequencing, timing, and command execution under nominal conditions. To verify robustness, the team will also simulate swarm response and mission performance with one or more non-operational UAVs.

Mission validation demonstrates that the built AeroShield system effectively contains wildfires and oil spills in real-world settings. Validation begins at a reduced scale, testing performance in small controlled burns and oil-spill trials within a dedicated test environment. Once data supports the required performance at this scale, validation proceeds to larger-scale exercises involving real oil-spill and wildfire scenarios. In early field trials, performance will be assessed in non-critical applications: for wildfires, aerogel barriers will be deployed alongside traditional containment methods (such as fire breaks or water bombing) so that system performance can be measured without jeopardising overall containment. Similarly for oil spills, aerogel deployment will run concurrently with standard booms. After confirming performance against requirements, final validation will occur in critical operations within real scenarios, demonstrating the capability of the system under mission-level demands.

20 Production Plan

This chapter presents the manufacturing, assembly and integration plan (MAI) for AeroShield. An overview of the phases of the plan are shown in more detail in Figure 20.1. The blocks placed underneath each other indicate that these activities can be done simultaneously. Each of the phases will be discussed in more detail in the sections of this chapter. The plan will focus mostly on the production of the UAV as this is the most complex part of the product.

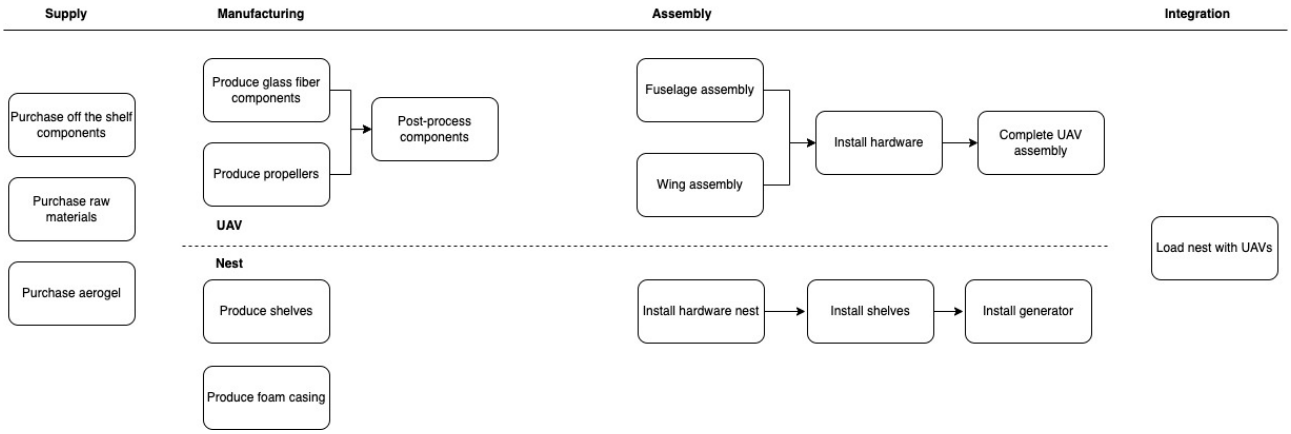

Figure 20.1: MAI plan

20.1. Manufacturing

In this section, the manufacturing method of the separate components of the UAV and nest is discussed. Before production is actually started there are some steps to be completed to set-up the manufacturing process and workspace. The UAVs will be produced nearly completely out of glass fibre composites as mentioned in section 11.1. To work with this kind of material, specific tools are needed, and the workspace should meet certain requirements (section 20.1). Next the manufacturing method for the glass fibre will be explained in section 20.1. Next to the structure of the UAV some components have to be produced for the nest. This will be explained in section 20.1.

Manufacturing Tools

To start, the correct personal protective equipment is necessary. The material will be used in a prepreg form and thus only nitrile gloves are necessary when handling the material. During post processing FFP2 dust masks should be used, as well as safety glasses.

As mentioned the material will come in a prepreg standardized form from the factory. Therefore it needs to be cut into the correct shape before it can be put into a mold. For a high production scale a machine would be more favourable over normal cutting equipment. Therefore, a static table system will be used. One example of such a system is the S135 Static Table cutting System, which can cut fibreglass-polyester blends [1]. It has a high-precision configuration, which features multi-axis motion for more defined and accurate cuts. For the laying of the prepreg, squeegees and a heat gun are beneficial. For post-processing various trimming tools such as an angle grinder or dremel are necessary. The consumables used during the production process will be described in the next section.

[1] `https://www.eastmancuts.com/products/static-table-cutting-system/`, accessed[22/06/2025]

The manufacturing area should have separate areas for cutting materials and laying. Furthermore, a clean area is needed for creating the vacuum bags such that leaks are prevented. The prepreg material is stored at -18 degrees so sufficient freezer space should be available to store the material. Additionally, an autoclave is needed. The autoclave should be capable of curing the parts under vacuum up to 160 degrees. For post-processing, a separate room should be used which is well ventilated and connected to a dust collection unit. This avoids the contamination of the air with composite dust which can pose health risks. Finally, the moulds that will be used to create the parts need to be produced. For the initial prototypes these moulds can be made out of medium density fiberboard (MDF) . One thing to note is that they need to be coated with a sealing and releasing agent. For larger scale production a more durable and dimensionally stable material should be used for the moulds. Again the requirement for the mould is that it has to retain shape up to 160 degrees and 50 psi. With PFC502 prepregs a small amount of water is released during cure (polycondensation reaction) [76]. Therefore it is recommended to use well sealed moulds made out of epoxy composite or stainless steal, as other materials like aluminium could corrode. One problem with moulds is that voids can be created while making the component. One way to monitor these voids is by using Computed Tomography (CT) scans. It looks right through the part and gives a visual depiction and statistics of voids and inclusions in the structure [99].

Composite Manufacturing Method

Depending on the mould that is used, very different parts can be produced. The general method for creating this composite parts is the same and will be detailed in this section. Before any prepreg material is applied, the mould surface has to be carefully prepared to ensure clean release, dimensional accuracy, and surface finish of the final part.

To start inspect the mould for any damage, contamination, or surface irregularities. Wipe the mould surface with lint-free cloths and a compatible solvent (e.g., isopropanol) to remove any dust, grease, or residue. Apply 3–5 coats of a release agent suitable for high-temperature composite curing (e.g., PTFE-based). Let each layer dry before applying the next.

The prepregs are stored frozen and must be properly thawed and cut prior to use. Remove prepreg rolls from the freezer and allow them to warm to room temperature inside their sealed bags prevent condensation. Open the bags only after the material is fully thawed. Always reseal unused material to prevent moisture ingress.

Cut plies to the rough dimensions needed for the part using composite scissors on a cutting table. To avoid mistakes and speed up the laying process label each ply with orientation and location. Begin placing prepreg plies directly onto the mould. Place each layer with the correct fibre orientation (e.g., 0°, ±45°, 90°). In this case it will be 0°, 45° and 90°. following the lay-up schedule. Use the squeegees or gloved hands to press prepreg into corners of the mould. Roll each ply with a hand roller to remove air and improve interlaminar bonding.

Once the layup is complete the next step is to prepare the vacuum bag. On top of your layup, stack perforated release film and heavyweight breather cloth. Make sure to wrap the breather around any corners of the mould to prevent cuts in the vacuum bag. Then place the entire package into the vacuum bag and seal it using tacky tape. Install vacuum lines and test the vacuum of the bag.

The package can then be placed in the autoclave for curing. Set the autoclave to ramp up 1–3 degrees/min to 80 degrees, then hold 30 minutes and then continue to 140 degrees, hold for 1 hour and then ramp down at the same same rate. Other curing cycles can also be found in the specification sheet of the material if needed [76]. Once the part has cooled to near ambient temperature, it can be removed from the mould. Carefully de-mould the part, starting from one edge. Avoid using sharp tools that could damage the surface. Clean and reapply release agent to the mould if it will be reused. Once all components are finished they will undergo visual inspection for voids, delamination or other inconsistencies. For the production of the propeller a different type of prepreg will be used. This means that the curing cycle will also be different than for the fibreglass. The curing cycle can be found on the data sheet [2].

To complete the parts any excess material that was left needs to be carefully removed without damaging the rest of the part. This can be done using the different tools such as a multitool (dremel), angle grinder or sanding machine. Then a quality control can be performed on the part with the same CT scan as mentioned before.

Nest components

For the nest most of the work is integrating and assembling all the hardware. Nevertheless there are two specific components that will have to be produced. As explained in section 14.3. The UAVs will be stored in polyethylene (XLPE) foam drawers. These foam blocks will contain the negative of the fuselage and all other components that they can be safely stored in the nest. Based on the CAD model the foam block can be

[2] https://www.e-aircraftsupply.com[accessed 18/06/2025]

designed in CATIA. Then using a CNC milling machine the negative of the UAV can be milled into the foam block on either side. Care should be taken when aligning the block correctly once it is flipped on to the other side. Misalignment could create holes in the negative on the other side.

The foam will act as drawers which can be pulled out of the container to grab the UAV. The frame around these drawers will also have to be produced. The shelves will be made out of 5083 series aluminium. This material is great for marine applications due to the superior corrosion resistance properties that it displays. It can be purchased in different shapes such as pipes with a square cross-section. These parts can then be cut to length using a metal saw and attached together using corner pieces. After cutting any sharp edges should be de-burred and sanded down.

20.2. Assembly and Integration

The assembly of the drone will be split up into 5 parts: Adhesives, the wing assembly, the tail assembly, the landing gear and propeller assembly, and the fuselage assembly. An overview of the assembly process is given in Figure 20.2. Tasks connected by arrows are sequential tasks, otherwise they can be conducted in parallel.

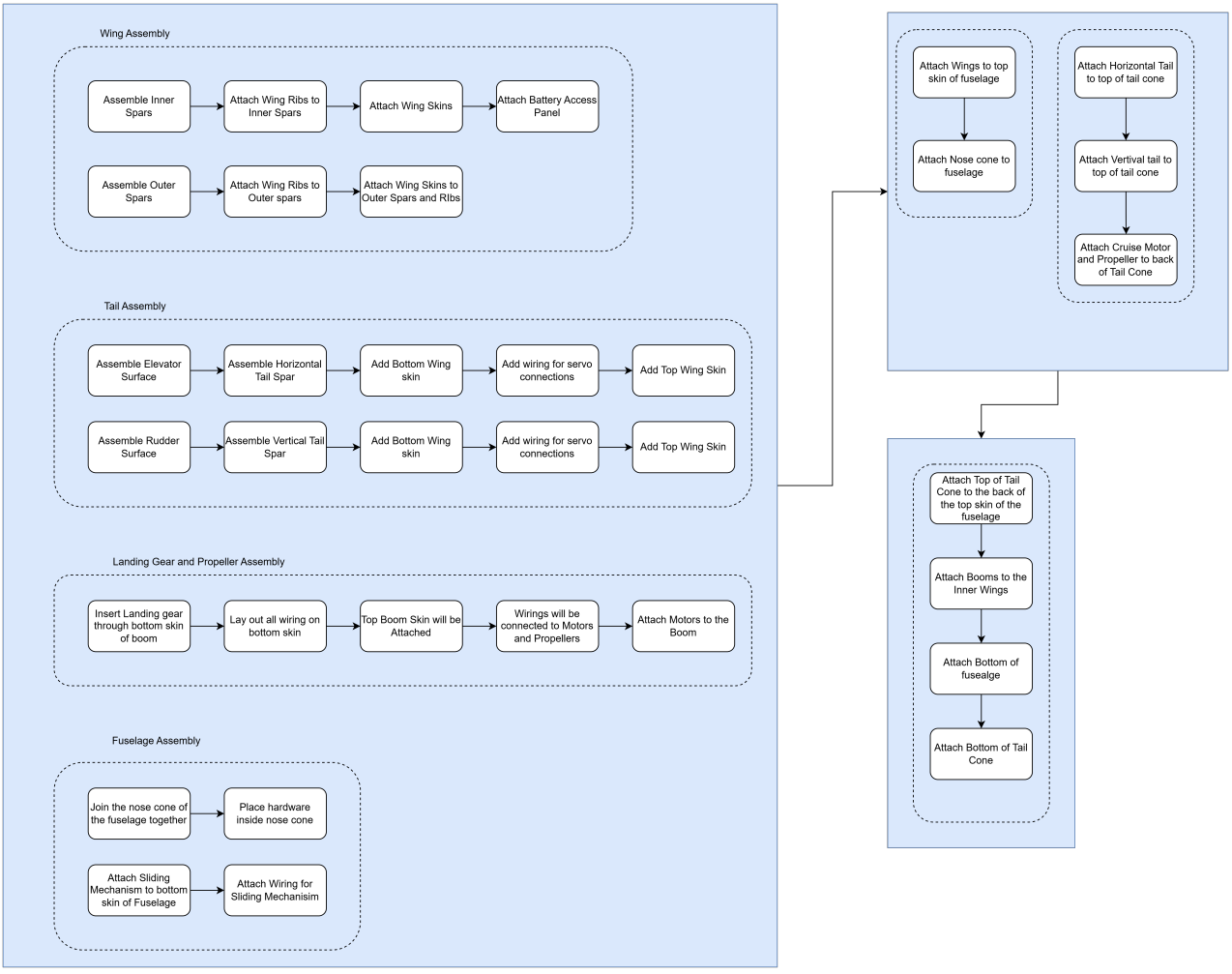

Figure 20.2: Assembly Time Flow Diagram

Adhesives

Welding or using mechanical fasteners within glass fibres introduces unwanted stresses and vibrations. An alternative is to use adhesives. Adhesives provide a strong bond line which absorbs the load much better and improves the structural integrity of the finished part [3] . They also act as sealants and deliver a much smoother finish. The main adhesives used for glass fibres are epoxies, methacrylates, and urethanes. In this case epoxies will be used as they are quite common and versatile. They are a 2 part system, consisting of a resin and harder. They combine in different ratios to produce different ranges of viscosities, cure times, clarity and flexibility.

[3] https://forzabuilt.com/blog/structural-adhesives-for-fiberglass[accessed: 17/06/2025]

The process of adhesion goes as follows: first the surface must be degreased with a solution such as isopropanol, then the surface is lightly abraded by using wet and dry grit paper, and finally it is degreased again to remove any loose particles [4]. After this, the adhesive can be applied and the two surfaces attached.

However, using adhesives can introduce an issue into being able to recycle the structure. There are some methods that can be used to resolve this issue. One potential solution is to ground the adhesives into small flakes or powder so that the composite can be reused. Another solution is to thermally decompose the adhesive joint, however it is difficult to localise and might affect the matrix of the carbon fibre itself as well. One other method is to chemically attack the bonds. For example hydrochloric acid can be used to degrade epoxy adhesives. However, it has been shown that less harsher conditions can be used, this process is called solvolysis. It used typical reaction conditions such as pressure, temperature, catalysts and solvent types which should ideally break down the polymer into lower molecular weight species [100].

Wing Assembly

The first part that needs to be manufactured is the wing. As mentioned in Figure 11.2, there are two parts of the wing, an inner and outer section. They will be manufactured separately, although in a similar manner.

For the inner wing, the first step is to manufacture the spars, the spar cross section for the inner wing is slightly different than that of the outer wing, it looks like the Roman numeral II: it has two webs with a spacing in between, which are connected via a flange at the top and bottom. Since these will be made out of glass fibres as well, the manufacturing process is a bit more complicated. There will be two U shaped beams and two flanges. The two U shaped beams will be placed on the bottom flange with a spacing in between, once that is attached, the top flange will placed. This attachment procedure is done by adhesives. A diagram of this process is shown in Figure 20.3

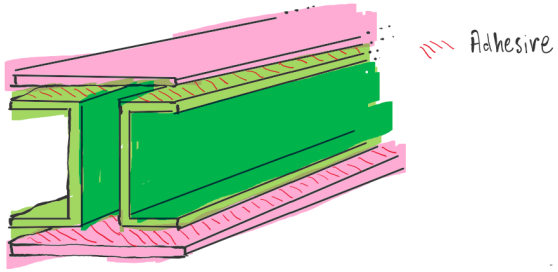

Figure 20.3: Inner Wing Spars

Once the spars are manufactured, a hole must be created in the spar close to the end so that the wiring can pass into the fuselage through the wing. Next, the battery compartment locking mechanism must be attached to the spar. Since it is quite bigger than the thickness, an extra flange must be added for greater contact area. This is shown in Figure 20.4.

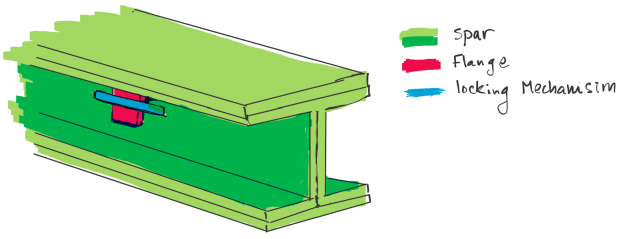

Figure 20.4: Attachment for Push Mechanism

The next step in wing production is to attach the ribs to the spars. Since there are two spars in the wings three rib sections will be needed; one for the leading edge, the middle section and the trailing edge. These ribs will be connected at the root, the middle and the tip of the wing, using an adhesive. For the inner wing only the root and middle rib will be needed. Since the thickness of the entire structure is very small (0.78 mm), including the ribs, forming adhesive connections is difficult. To solve this problem additional flanges will be added to

[4] https://permabond.com/materials_bonded/how-to-bond-fiberglass[accessed: 17/06/2025]

the ribs to form a greater contact area, as done with the pushing mechanism in the spars. An image of this is shown in Figure 20.5. This is done for both the web connection and also the wing skin connection, which will be discussed below.

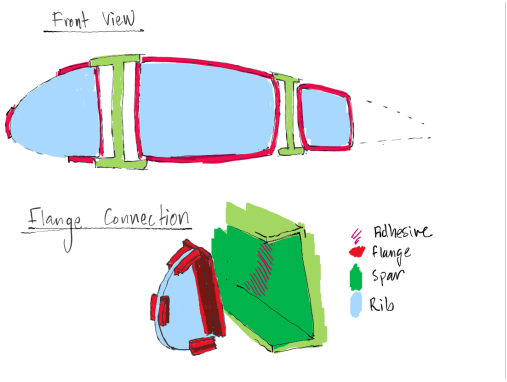

Figure 20.5: Rib Connection

Next, the wing skin can be attached; this will be done by attaching the upper and lower skins separately to the spars and ribs. But before this can be done the locking mechanism for the outer wing must be attached to the wing inner part of both wing skins. It will be connected with adhesives. The skin will also include part of the wing box which will be connected to the spars protruding out of the root. This is shown in Figure 20.6. Once again, extra flanges will have to be added to the ends of the wing skin for greater contact during adhesion. This is also demonstrated in Figure 20.6.

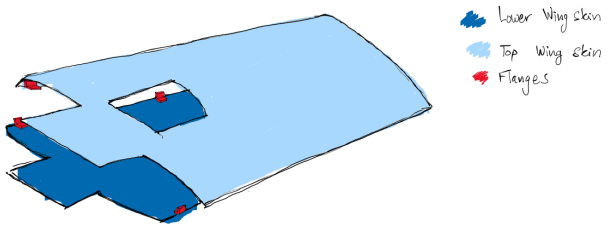

Figure 20.6: Wing Flanges

Now that the wing skin profile is defined the first step in assembling the skin is attaching the bottom skin to the spars. Once the bottom skin is attached all the wiring and electrical connections must be added. Next, the top wing skin can be attached. The top wing skin has a hole for the battery access panel, and therefore, a lid must be attached to form a closing structure. The access panel will be connected via a hinge, which will be connected with an adhesive on the inside of the wing skin. Once this is done a back panel will be added to the wing box to close off the box. A figure of the final inner wing configuration is shown in Figure 20.7

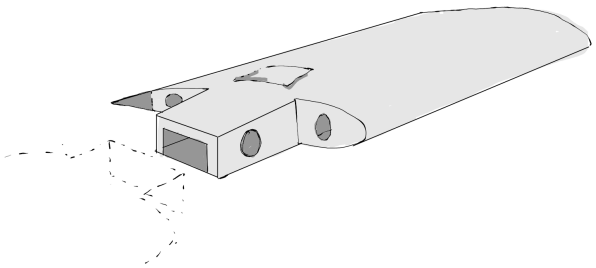

Figure 20.7: Configuration of inner wing

Now that the inner wing assembly is done, the outer wing assembly procedure can be outlined. The spars have a normal I-beam cross-section. They will simply be made by attaching two U-beams together using adhesives. This is shown in Figure 20.8.

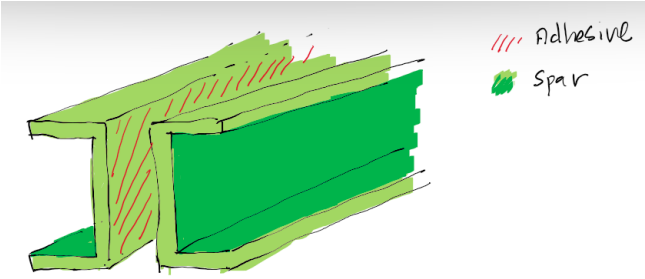

Figure 20.8: Outer Wing Spar

Once the spars have been manufactured the rest of the procedure is quite similar to the inner wing. Extra flanges will be added to the tip rib and the wing skins for extra contact with the adhesive, as mentioned before. The ribs will be first connected and then the wing skins. For the wing skins there will be a small hole at the tip of the wing where the wing tip light will slide through from the inside. This concludes the wing manufacturing procedure. The inner wing will still need to be attached to the fuselage, which will be explained in Figure 20.2. The manufacturing procedure for the outer wing is finished.

Tail Assembly

The tail manufacturing procedure will be split into two parts: the horizontal tail and the vertical tail. Before the tails, the control surfaces will have to be assembled. The control surfaces do not have any ribs or spars so only the skin will need to be attached with adhesives. Once more, extra flanges will need to be added to the skin to secure the connection. Once the wing skins are attached, a back plate will be attached with holes for the servo levers. The same procedure is followed for the elevator and rudder. A diagram of this procedure is shown in Figure 20.9

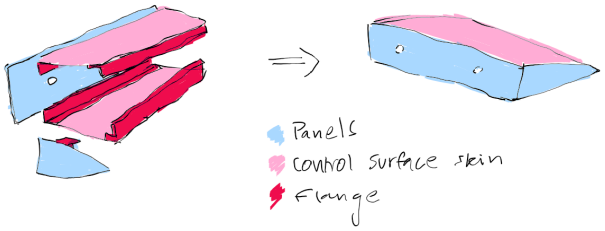

Figure 20.9: Control Surface Assembly

Now the tail surfaces can be explained. For the horizontal tail the spar will be manufactured by connecting two U beams together as in the outer wing. The spar will then be connected to the bottom wing skin. Next the wiring will be laid out inside the tail. Once the wiring for the servos is laid, the elevators can be connected at the opening of the tail to the servo levers. Once the elevator is connected the top skin of the horizontal tail can be attached. Flanges will be added to the root chord of the tail so that it can be easily connected to the fuselage later on. The same procedure is followed for the vertical tail.

Landing Gear and Propellers Assembly

The boom will be split into two sections, top and bottom, like the wing skin with attached flanges. The first step is to insert the landing gear through the hole in the bottom of the boom and attach it with adhesive and flanges. Next the wiring will be placed on the bottom part of the boom, and then the top part will be attached. Next, the wirings will be connected to the propeller motors. The motors will then be secured to the boom with adhesive. A diagram of this is shown in Figure 20.10

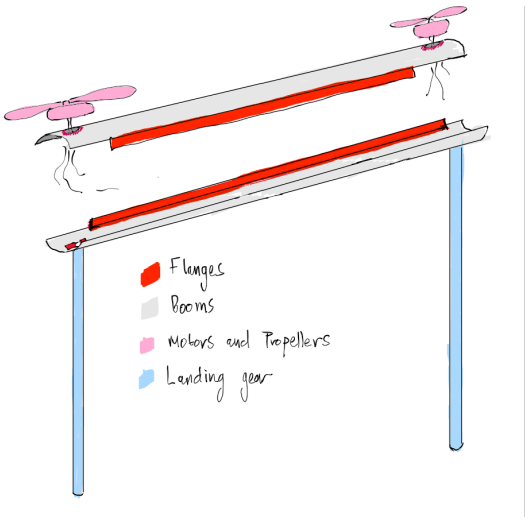

Figure 20.10: Landing Gear and Boom Assembly

Fuselage and Final Assembly

The fuselage structure will be split into 8 parts as shown in Figure 20.11 with added flanges. This is done for ease of manufacturability, and so that the hardware can be easily integrated. The first step is to join parts 1,2 and 3 which will form the nose cone of the fuselage. This will be done using adhesives and flanges once again. Once the nose cone is assembled the hardware can be placed inside. The second step is to attach the sliding mechanism to part 5 of the fuselage. First a rail mechanism will be attached with an adhesive, and the door will be slotted in. Next, the motors and wiring will be attached. This completes the main attachment procedures of the fuselage.

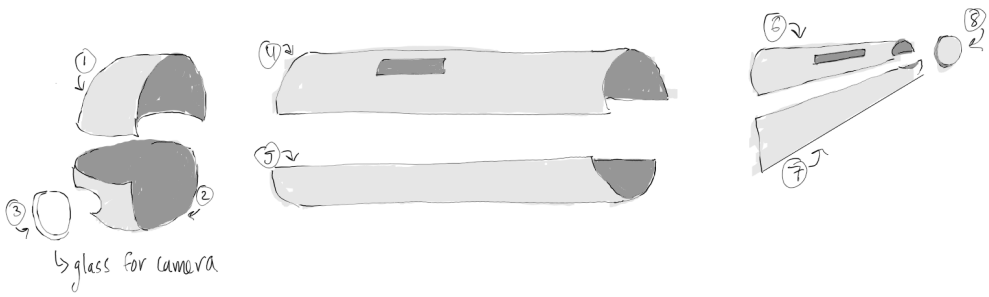

Figure 20.11: Fuselage Parts

Now that all the main components of the assembly procedure are there, the final UAV can be assembled. The first part in this procedure is attaching the inner wings to the fuselage. This will be done by inserting the wing box from both sides into part 4 of the fuselage through the hole. The back panels of the wing box will then be attached together with adhesive. Once the wing is connected the nose cone of the fuselage can be connected with adhesive to the part 4 of the fuselage. After this the horizontal and vertical tail will be connected with adhesives to part 6 of the fuselage, along with part 8, and the cruise motor and propeller. Then this combination of the tail and part 6 can be attached to part 4 of the fuselage with adhesives. Next the booms will be mounted underneath the wing with U brackets.

Since all the hardware is now in, the electrical connections between each part can be established. Once this is done part 5 and 7 of the fuselage can be connected via adhesives to the rest of the body. This completes the assembly procedure of the UAV. A diagram of these final steps is shown in Figure 20.12. One thing to note is that the extra flange attachments do exist for the final assembly as well, they are not shown for the sake of clarity in the diagrams.

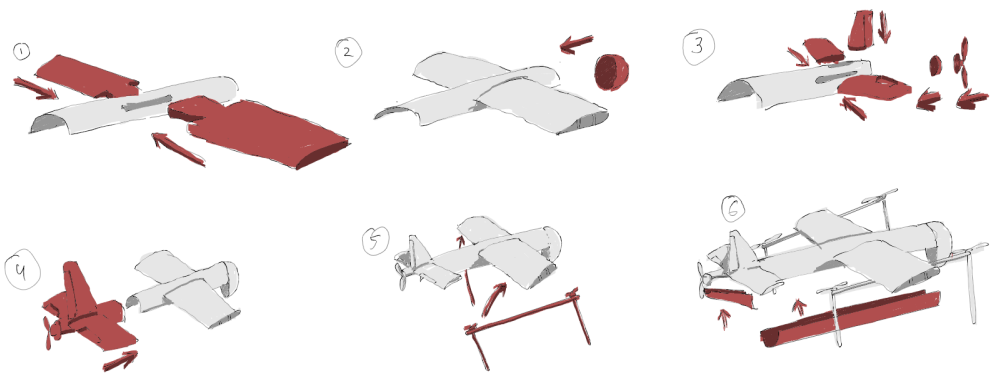

Figure 20.12: Final Assembly Steps

One problem in having so many joints is that the structure can be subject to junction fatigue. One way to minimize this process in manufacturing might be to optimize the design. This can be done by using greater overlap areas which are done by the overlapping flanges. Furthermore more scarf joints can be created rather than lap joints as they have a smoother load distribution. Adhesives which have a good fatigue resistance can be used. Not much research and analysis has been done into this topic at the current stage

21

Business Case Evaluation

AeroShield's financial feasibility is dependent on the further Research and Development (R&D) required to finalise the product, the profitability of the revenue streams AeroShield is able to incorporate, in addition to the competitive advantage it offers in the market. To give an overall idea of the business strategy, AeroShield's revenue will depend on three sources. The financial plan is discussed in section 21.1, followed by a cost analysis in section 21.2, a pricing analysis in section 21.3 and finally a financial projection in section 21.4.

21.1. Financial Plan

The first is the sale of the UAVs and the nest. This includes the 20 UAVs with the 3 containers needed for operation of the mission. The second revenue stream is annual training for operating the drone swarm. This hands-on training will not only teach employees of the client how to handle, launch and use the swarm, but also teach emergency-response drills, field-level hardware repair, and practical implications for software updates for that year. There is also a dedicated module on liability and incident-reporting protocols. The third revenue source is the sale aerogel itself. The aerogel deployment system in the UAVs requires custom aerogel blankets fitted with magnets. Instead of having clients forced to produce or procure it themselves, AeroShield can provide these specialised blankets at discounted bulk rates (beneficial for our clients) while still being able to make it profitable, allowing AeroShield to also add another way of increasing revenue. The latter two revenue streams allow for a more predictable, constant, and stable income for the company.

Another source of funds AeroShield will consider and pursue is EU grants. However, this is not included in the base projections and will not be relied upon in the financial plan, as the grants are not guaranteed. Operations are built around a warehouse centre for production and assembly (including the custom aerogel). Because of the simple access to the AeroShield technology, this warehouse space is home to the training academy.

21.2. Cost Analysis

Research & Development Cost

The first cost AeroShield will encounter is the R&D cost to finalise the product (UAVs and nest). Estimates show that the cost of the product tends to be around 15% (or around one sixth) of the total cost of R&D for the product [101][102]. Considering the UAV cost budget requirement is €50,000, one can assume the R&D budget for the UAV to be €350,000 (rounded up to the nearest €50,000). Due to the simple nature of the nest (it does not fly and just needs to be refined and assembled), it can be assumed that the nest would require around its component budget as R&D budget, which is around €150,000. Thus, the total R&D budget to finalise the products is €500,000.

UAV Cost

The costs per UAV comprise the sum of the hardware components, displayed in chapter 6, the raw materials and the production cost. The cost of the wildfire UAV hardware totals to €$23,500.12$ and the oil spill hardware sums to €$26,441.12$. There is a slight difference in price between the wildfire and oil spill configuration, caused by the need for a buoy system and a more expensive detection sensor for the oil spill mission. The structural area of the UAV that is comprised of glass fibre reinforced polymer (GFRP) is $10.737[m^2]$, meaning we will need more than $200[m^2]$ of GFRP for one swarm of UAVs. This puts the cost of GFRP for one UAV at €39.51[1]. The totals for the physical components of the UAV are detailed in Table 21.1

A cost that is important to know is the manufacturing cost of each UAV. While this is taken into account later through the inclusion of employee salaries, it is important to know how much the cost per UAV is in order to be able to price the UAVs with a profit margin in mind that takes the manufacturing cost into account. The production timeline equivalent to 1 worker manufacturing 1 UAV is assumed to be 2 weeks. In reality there are

[1] https://www.fibermax.eu/glass-fabrics/glass-fabrics-show-all/fiberglass-fabric-g025p.html[accessed:13/06/2025]

workers at different steps in manufacturing, but through using total throughput time spent on manufacturing, the conversion to time per worker per UAV can be estimated. Therefore, the equivalent labour cost is €1722.30. This cost however is not visible separately in Table 21.1 as it falls under the employee cost and will only be needed when pricing AeroShield.

Nest Cost

The nest costs comprise 3 ISO containers, where one container contains the generator, computer, and communication and charging devices, with the other containers only storing UAVs. The cost of the physical components can be found by summing the hardware costs in Table 6.1 and adding an additional €1000 for the shelving for each nest. The generator container totals €$153,653.15$, while the non-generator containers cost €$6,625.00$. Similar to the UAV, it is necessary to know the production timeline for the nests for accurate pricing. It is assumed that 1 worker would take 1 week to finish 1 nest, hence the production cost of €861.15 associated with it.

Aerogel Cost

To be able to source aerogel at the lowest cost, it will be bought in bulk from a supplier[2]. Sheets of an area of $1[m^2]$ and $3[mm]$ thickness can be obtained for a price between $0.45 and $6.00 with a minimum order quantity of $1[m^2]$. Taking into account the large bulk order required for AeroShield missions, a conservative price of $\$1.50[1/m^2]$ of aerogel is assumed. This implies a cost of aerogel for one deployment blanket to be $\$1.50 \times (1.5[m] \times 3.33[m]) = \$7.50 \approx$€$6.60$. The aerogel is then modified to include magnets (which cost €0.90 per piece, €3.60 in total), raising the total cost to €10.20 per blanket. The blankets can then be sold on to the clients for a profit.

Fixed Cost

The fixed costs for AeroShield include employees for operating the company, the headquarter facility for manufacturing and running the company, the utilities associated with it, and the machinery and tools for production. These costs will be assumed to not depend on sales and thus not change over the short term.

AeroShield will employ 10 engineers on starting engineer salaries (around €$41,335$ per year in The Netherlands [3]) for the running of the company, totalling to €$413,350$ per year. Employing engineers with different interests and skill sets will be crucial to creating a workspace highly capable of developing a refined product while also being able to handle all non-engineering aspects of a business such as sales.

A warehouse large enough to act as a headquarters and production centre will set AeroShield back an approximate €$20,000$ per month[4]. Next to that, utilities are assumed to be €$2,000$ per month due to the large size of the warehouse and energy intensive machinery required for production. Machinery and tools required to produce AeroShield, include an autoclave for the Evopreg PFC502 with glass fibre, vacuum pumps, UAV moulds, and an angle grinder to name a few. Overall, the cost of all this equipment will be estimated to total to €$250,000$.

Below is a table summarising the costs of AeroShield. The costs listed in the table will be used for the financial projections in section 21.4

[2] https://098991255698c169.en.made-in-china.com/product/paxUCubrJjhg/China-High-Quality-Chemical-Film-Aerogel-Fireproof-Waterproof-Thermal-Insulation-Felt-Silica-Aerogel-Insulation-Blanket-Roll-Price-for-Roofs-Wall-Insulation-Materials.html[accessed:9/06/2025]

[3] https://www.payscale.com/research/NL/Job=Aerospace_Engineer/Salary[accessed:16/06/2025]

[4] https://www.companyspace.com/netherlands/rent/warehouses/pageindex2?srt_field=price&srt_dir=asc[accessed:16/06/2025]

Table 21.1: Fixed and Product Costs

Type	Category	Details	Estimated Costs
Fixed Costs	R&D	One-time development of UAVs and nest system	€$500,000$
	Employees	10 engineers (avg. €$41,335$/year each)	€$413,350$/year
	Facility Rent	Workshop/production space	€$20,000$/month
	Utilities	Power/water for machinery and operations	€$2,000$/month
	Machinery & Tools	For in-house production using machines, moulds, composite tools, and assembly aids	€$250,000$
Product Costs	UAV (Wildfire)	Wildfire components, UAV material	€$23,539.63$ per UAV
	UAV (Oil spill)	Oil spill components, UAV material	€$26,480.63$ per UAV
	Nest (with generator)	20ft ISO container housing the generator, computer, communication equipment, UAV charging stations, and some UAVs	€$153,653.15$
	Nest (without generator)	20ft ISO container storing UAVs	€$6,625.00$
	Aerogel	Per deployment blanket (material + magnets)	€10.20

21.3. Pricing Analysis

Typical pricing of UAVs takes into account approximately a 25% profit margin. Consequently, as AeroShield's cost (including labour) was calculated to be €$733,545.20$ for oil spill and €$674,725.20$ for wildfires (20 UAVs with 3 nests, 1 generator container and 2 non-generator containers), AeroShield should have a minimum price of €$916,931.50$ for oil spill €$843,406.50$ for wildfires. The prices are rounded up slightly as an extra safety margin to €$920,000.00$ for oil spills and €$850,000.00$ for wildfires. The aerogel that is made to be compatible with the deployment mechanism is sold with a 20% profit margin (€12.24 per blanket). To confirm the feasibility of this pricing, it is necessary to view the price from the client's perspective as the cost for mitigation. This cost, when compared to other mitigation methods establishes whether the pricing for AeroShield is competitive.

Wildfire Mitigation Operational Price

Firefighting aircraft carry large capital and operating costs. The Canadair water-scooping aircraft start at around €30 million each[5], with hourly operating expenses near €8,000[103]. Firefighting helicopters are a bit cheaper ranging in price between $4.2 million[6] to $26 million[7] with hourly costs between €700 and €3 600. These aircraft are effective at direct suppression but alongside the high costs also face operational constraints. They require nearby water sources, and aircraft are grounded in heavy smoke or at night.

Ground crews can create firelines (or firebreak), lines of soil that has been cleared of all vegetation, to act as a barrier that prevents the spread of fire. Typical firelines are between 1 and 3 feet wide (between $0.30[m]$ and $0.91[m]$)[93]. A trained 20-person team is capable of creating an indirect fireline at a rate of $90.7[m]$ per hour[104]. Indirect refers to a fireline that is created at a distance away from the fire (similar to how AeroShield will create a firebreak), contrary to a direct fireline that is done at the fire itself. At an average wage of €10 per hour for a firefighter in Europe[8], a 20-person crew would cost €$200[1/h]$. This would mean it would cost roughly €$2,206$ per kilometre of fireline, and it would take just over 11 hours. While ground crews are versatile, flexible and cheap, they are exposed to heat, smoke and shifting fire behaviour, all of which pose great danger. Firefighters can also not work in the dark, so their operational time is limited to the day. Moreover, many EU regions are currently facing a decrease in firefighter numbers[8], meaning this method might not be as reliable when needing a large firebreak. A fireline construction using bulldozers or masticators could be a seen as better solution to due to the low personnel requirements and the ability to create $220[m]$ per hour of fireline for around $400 per hour. However, it is not able to operate in difficult terrain and a study found that only 5% of all firelines

[5] https://www.euronews.com/my-europe/2023/09/17/will-the-eus-720-million-gamble-on-firefighting-planes-pay-off[accessed: 13/06/2025]

[6] https://signalscv.com/2019/07/county-to-buy-two-additional-firefighting-firehawk-helicopters/[accessed:13/06/2025]

[7] https://www.ocregister.com/2024/08/19/new-firehawk-helicopters-boost-firefighting-capability-for-orange-county-fire-authority/[accessed:13/06/2025]

[8] https://www.reuters.com/sustainability/cop/europes-firefighters-call-reinforcements-wildfires-worsen-2023-10-30/[accessed:13/06/2025]

it produced met all requirements. Due to this poor performance and use case, bulldozers or masticators as a mitigation method will not be considered.

Controlled burns are another method of wildfire mitigation, but are rarely used in fire management in Europe. Many legal frameworks make it difficult to conduct controlled burns if not illegal[105]. There is very little information about controlled burns in Europe, suggesting it is a very scarcely used method and not relied on, and thus is not compared in cost.

AeroShield will make use of Aerogel (a blanket of size $1.5[m] \times 3.33[m]$) to act as the firebreak, which costs €12.24 for the client. Typical firelines used in the earlier cost analysis are between $0.30[m] - 0.91[m]$ in width, which is covered by the width of 1 aerogel blanket. This means that the equivalent fireline of $1[km]$ using Aerogel (including the $0.5[m]$ deployment accuracy margin) would use 354 blankets, costing a total of €$4332.96[/km]$ of aerogel for the client. This would take around 15 hours to deploy. This would result in $212.5[l]$ of biodiesel being consumed (62.5% of generator fuel capacity, well within capacity), costing around €300[9]. In total, AeroShield costs approximately€$4633[/km]$ of fireline deployment. This is around double the price of the ground crew, but has the benefit of not exposing people to the fire, reducing the number of people needed for a mitigation operation and also allowing for non-stop operation (as what is required for it's operation such as fuel and aerogel blankets can be easily resupplied, as long as there is enough stock present). It is also significant to note that this deployment cost can decrease if aerogel is recovered. Aerogel can be reused if the fire did not reach certain parts of the firebreak or was not as intense and did not damage the aerogel.

Oil Spill Mitigation Operational Price

Existing oil-spill response techniques vary in cost structure and environmental impact. Mechanical skimming removes oil with booms and pumps at an estimated $\$16.675$ per litre of oil recovered (≈ €$14.34[1/L]$). However, this method has the consequence of also taking in large volumes of water along with the oil, reducing net recovery efficiency[31].

In-situ burning collects the oil in one spot using booms so that there is enough for a sustained burn and ignites it. This method comes out much cheaper than skimming, as it costs $\$5.42[1/L]$(≈ €$4.77[1/L]$), yet generates toxic emissions and is restricted to open-water scenarios away from sensitive coastlines[31].

As another mitigation method, chemical dispersants are sprayed from aircraft or vessels to break the oil down into fine droplets, allowing them to mix more easily into the water. Microbes in the water can then break the oil down. It is usually done so that less oil stays at the surface of the water where it could affect birds, fish or drift into vulnerable coastal areas. While this method is cheap, around $\$3.7828[1/L]$ (≈ €$3.33[1/L]$), it shifts the ecological burden to the wildlife in the water and seabed, so it is not a completely sustainable solution[31].

Bioremediation harnesses microorganisms to break down oil into innocuous end-products (CO_2, water, biomass). One commercially available bioremediation product, SpillRemed, is priced at $\$78$ per gallon of oil (€18.13 per litre)[106]. Although bioremediation is often promoted as a sustainable alternative to physical or chemical clean-up methods, its real-world deployment in Europe remains scarce due to the lack of a standardised procedure for its use. It requires extensive risk assessments, environmental impact studies, and approval, which is why in Europe mechanical recovery of oil is the primary mitigation pathway.

Much like aerogel in AeroShield, traditional sorbents operate on the same oil absorption principle. This method costs approximately $\$4,000$ (€3520) per ton of oil removed.

By contrast, AeroShield's aerogel absorption comes at a previously established cost of €12.24 per blanket for the client. Each deployment blanket contains $3[kg]$ of Aerogel. The absorption ratio of the aerogel blanket is $14[g]$ of oil per gram of aerogel, one deployment blanket is able to absorb $42[kg]$ of oil [91]. This means that per $1000[kg]$ of oil needed to be absorbed, the associated aerogel cost is €291.43 for the client. This would take just over an hour, meaning around €21.16 of biodiesel is used[10], bringing the total cost per 1 ton of oil removed to €312.59. Taking a conservative estimate of the density of crude oil (density $0.95[kg/L]$ [11]), per litre, €0.30 of aerogel blanket is needed, which is cheaper than all other methods. A further benefit of aerogel is that the material retains more than 85% of its absorption performance after 6 cycles of use, meaning mitigation cost can greatly decrease if the client wishes to reuse the aerogel as the slight cost of maximum absorption capacity [107].

[9] https://www.statista.com/statistics/1196513/average-monthly-biodiesel-price-in-spain/[accessed:17/06/2025]
[10] https://www.statista.com/statistics/1196513/average-monthly-biodiesel-price-in-spain/[accessed:17/06/2025]
[11] https://www.tribonet.org/wiki/density-of-lubricating-oil/[accessed:16/06/2025]

Table 21.2: Cost Comparison

Method	Details	Estimated Cost per km or per litre	Notes
		Wildfires	
AeroShield	Aerogel blanket deployment	€$4633[1/km]$	Deploys reusable aerogel blankets; 24 hours operation capability
Ground Crews	20-person crew, 11 hours to complete 1 km	€$2,206.04[1/km]$	Limited manpower, slower, only operational during the day
Aircraft	Canadair, helicopters, etc.	€$700 - 8,000[1/h]$	Non-operational in heavy smoke/night, needs refill water bodies
Controlled Burns	Rare or banned in most EU regions	Not applicable	Legal and safety constraints in Europe
		Oil Spills	
AeroShield	Absorbs oil at 2:1 mass ratio	€$312.59[1/ton]$ or €$0.30[1/l]$	Reusable up to 6x with >85% capacity retention
Skimming	Mechanical removal of oil	€$14.34[1/l]$	High equipment and operational costs
In-Situ Burning	Burn oil on-site	€$4.77[1/l]$	Environmentally risky and detrimental, limited by weather conditions
Chemical Dispersants	Break oil down into small droplets with chemicals	€$3.33[1/l]$	Potential toxic impact on marine ecosystems
Bioremediation	Microbial breakdown (slow process)	€$18.13[1/l]$	Long time frame, limited use in Europe
Sorbents	Traditional absorbents	€$3520[1/ton]$	Less efficient than aerogel

Training Price

Alongside operational cost, training is also required to be able to operate AeroShield. It will be priced at €$10,000$ for the first year which includes 3 people, which are required to hold a specific drone license before training (as AeroShield requires at least 3 operators) and would take place over 5 days, which is in line with typical Specific category drone license trainings[12]. Every following year, the trainings are €$5,000$ for 3 people, in order to confirm the operator's abilities, as well as to keep them informed with any updates AeroShield may have had. An AeroShield Operator Certificate is awarded after the training, which is a contractual prerequisite for maintaining the warranty on AeroShield. Incidents caused by certified operators remain covered under our technical-support and spares-replacement programme, while mishandling by uncertified staff voids that cover. The training also authorises certificate holders to perform all first-line repairs (for example propeller swaps and sensor replacements). If the client wishes to train more operators, which is recommended for improved AeroShield deployment rate, every additional person would cost €$3,000$ in the first year and €1500 every year after that to be trained.

Final Price Evaluation

AeroShield's upfront investment of €$850,000$ for wildfires allows for mitigation without much safety compromise compared to other methods. While AeroShield costs around double the ground crew per kilometre of firebreak, the 24-hour operational period AeroShield can operate in means firefighting is no longer limited to daylight hours. Comparing the upfront cost of €$850,000$ to the €$30\ million$ price tag of the Canadair aircraft recently ordered by the EU shows the availability of firefighting funds to invest in such larger technology and operations. Therefore, AeroShield is shown to be priced well according to the added benefits it offers to the market.

For oil spills, the €$920,000$ package cleans oil the lowest cost per litre. When comparing to the closest competitor, the sorbents, AeroShield boasts a more than a 90% reduction in mitigation cost over the sorbents. If one were to buy AeroShield to use instead of sorbents, the cost saving from the lower oil absorption cost will return back the €$920,000$ AeroShield cost after absorbing 286.8 tons of oil. The reusability of the aerogel also allows for further reduction in unit cost. This ideal pricing of AeroShield allows higher market capitalisation and offers a route for clients to see a return for investing in the AeroShield technology.

[12] https://www.droneflightacademy.eu/nl/opleidingen/dronepilot-advanced?_gl=1*10d3iiz*_up*MQ..*_gs*MQ..&gclid=EAIaIQobChMI9-_Y7pP4jQMVmLKDBx30tSLvEAMYAiAAEgIuCfD_BwE[accessed:16/06/2025]

21.4. Financial Projection

Financial projection is critical to determine the return on investment of AeroShield. The financial projection will consist of 2 business scenarios over the span of the first 5 years: a worst case scenario and an optimal scenario. As such, the range of financial performance of AeroShield can be determined. Both scenarios will make use of the required €$500,000$ R&D cost to finalise the design (which crucially does not include any other business costs such as employee costs).

The worst case scenario (depicted in Figure 21.1) consists of AeroShield requiring 18 months of R&D to finalise the design. The first year after completing the R&D, AeroShield will make 3 sales. The second year will also consist of 3 sales, after which the third year 5 sales are made, with the fourth and fifth year after R&D completion consisting of 10 sales.

The optimal scenario (shown in Figure 21.2) has AeroShield completing the R&D for design in 12 months, and the first year after design completion obtaining 5 sales. The second year consists of 7 sales, the third 10 and the fourth 15 sales.

For all scenarios, due to the fact that AeroShield has 2 products (one for wildfires and one for oil spills) it is assumed that each sale is of an average value of these two products (€$880,169.00$) consisting of 20 UAVs. Moreover, it is assumed that each year around €$10,000$ worth of aerogel is bought from each client, and that the only the required amount of 3 operators per client are given the trainings.

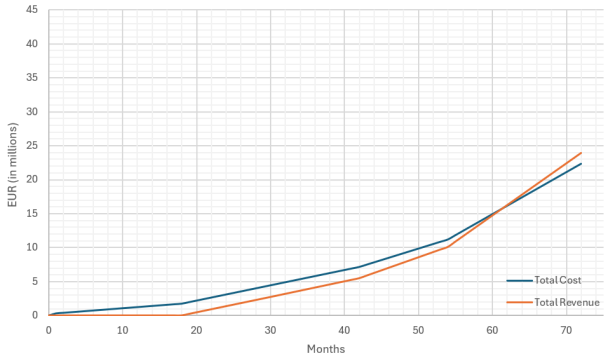

Figure 21.1: Worst case financial projection

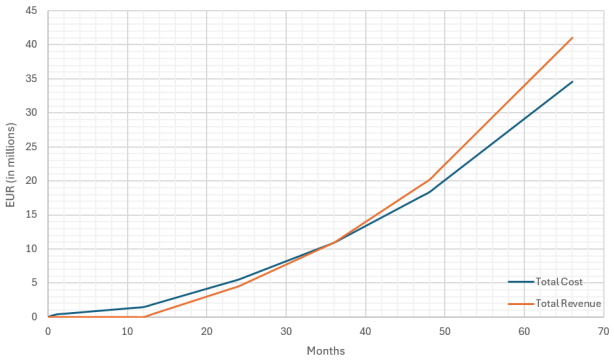

Figure 21.2: Optimal case financial projection

Figure 21.1 shows that in the worst case scenario, the break-even point is reached in the 6th year, or 62nd month (including the initial R&D period), whereas break-even is reached at the end of the 3rd year, or 36th month in Figure 21.2 for the optimal case. The highest cumulative loss can be found in the worst case projection, reaching a deficit of around €1.77 million in the 18th month. This should be taken into account when considering the investment necessary for AeroShield to succeed. Adding a margin, one can assume an investment of €2 million to be sufficient to give AeroShield the best chance of succeeding. Considering such an investment, the optimal case will generate a 100% return on investment within 49 months (beginning of the 5th year) from the start of R&D. The worst case will give a 100% return on investment in the beginning of the 7th year, assuming growth remains constant.

In terms of yearly returns on investment, in the 5th year, the worst case financial projection predicts a yearly profit of just over €1.78 million, which equates to a 89.2% yearly return on investment. For the optimal case, the projection in the 5th year predicts a yearly profit of just over €3.10 million, signifying a 155% yearly return on investment. However, there is a chance of a decreased demand for aerogel blankets due to other mitigation methods being preferred or no major disasters occurring in the region (for example, an oil spill might simply not happen). Considering the possibility of clients not buying any aerogel, the break-even point delayed in the worst case by only 3 months and only 1 month for the optimal scenario. While the returns are very high due to the high profit margin nature of this business, it is important to note that these profits are only available after a long period of no revenue, which brings a lot of risk for investors. Even so, it is likely that the high returns will attract investors, hence demonstrating the financial feasibility of AeroShield.

During this period, AeroShield will also apply for EU grants in order to be potentially able to invest more into scaling the business of AeroShield. This will naturally boost AeroShield's capacity for business and accelerate its growth, however due to the unpredictable nature of these grants, it has not been included in any projections. Revenue from selling maintenance services or spare parts are similarly difficult to predict, and therefore are not included in estimates for the business case. It is nonetheless something to consider in a future, more detailed financial analysis.

Due to the low cost of AeroShield compared to the allowed budget, there is budget left over for licensing of wildfire/oil spill software (unless open-source software is found and used). This specifically refers to software focused on fire and oil spread prediction and detection. The cost of such software is, nevertheless, not known, which would need to be accounted for in future, more in-depth financial analyses.

22

Sustainability Analysis

In this chapter, the sustainability analysis of AeroShield is performed. Sustainability is an important design parameter as it helps reduce resource consumption, reduce greenhouse gas emissions, and improve recyclability, ultimately supporting long-term ecological balance, regulatory compliance, and social responsibility. In section 22.1, sustainability requirements will be discussed, section 22.2 will see a life cycle assessment containing a carbon cost analysis, and finally section 22.3 will focus on end-of-life strategies of AeroShield.

22.1. Sustainability Requirements

Several system requirements were set to ensure the sustainability in the design process of AeroShield. *REQ-SYS-05* states that the nest should source 100% of its electricity from renewable energy. This requirement is met by integrating a bio-diesel generator that uses HVO100, a bio-diesel made out of 100% renewable resources such as used cooking oil and frying fat [108]. *REQ-SYS-06* states that AeroShield will comprise at least 50% recyclable components by mass, and *REQ-SYS-07* states that the system needs to be modular. In the upcoming sections, this will be discussed in detail.

22.2. Life Cycle Assessment

Functional Unit

A life cycle assessment (LCA) measures the environmental impact of a product through every phase of its life [109]. The method used for AeroShield is the ”cradle-to-grave” assessment, which analyses the process from its raw materials, through the production phase, until the final disposal of the product. Modular subsystems are assumed to be replaceable and may be evaluated separately for potential reuse or refurbishment.

Carbon costs

Understanding the embodied carbon of AeroShield is essential for evaluating its overall environmental impact. Embodied carbon refers to the total greenhouse gas emissions associated with the extraction, production, and assembly of materials and components before the UAV is even deployed. Quantifying these emissions provides valuable insights into the product’s carbon footprint across its lifecycle. Additionally, it highlights opportunities for impact reduction through design optimization or more sustainable manufacturing practices. The glass fibre material has an embodied carbon of $2.63[\frac{kgCO_2}{kg_{material}}]$ [110]. The entire structure therefore accounts for $21.60[kgCO_2]$. Compared to a drone like the DJI Flycart drone (with a frame made out of EPP), which has an embodied carbon of $30[kgCO_2]$ in its frame [111], this is a reasonable amount. The primary contributor to AeroShield’s energy consumption are the batteries, which are (individually) charged in the nest by a bio-diesel generator, as mentioned in section 22.1. The Li-Po battery itself (described in section 6.2) has an embodied carbon of $50[\frac{kgCO_2}{kg_{material}}]$, based on the Watt-hours of the battery ([112]), which thus accounts for $361.9kgCO_2$. The aerogel used during the mission has an embodied carbon of $4.3[\frac{kgCO_2}{kg_{material}}]$ ([113]). For the nest, there are a couple of components that contribute to the carbon emissions. The 3 ISO containers have an embodied carbon of about $0.422[\frac{kgCO_2}{kg_{material}}]$ each([114]), which comes down to total value of $134196[kgCO_2]$. The generator used in the nest has an embodied carbon of $3.16[\frac{kgCO_2}{kg_{material}}]$ [115], and the bio-diesel, which was already mentioned in the previous section, has $0.04[\frac{kgCO_2}{kg_{material}}]$ [116]. All of these calculations are summarized in Table 22.1.

Table 22.1: Carbon Costs in AeroShield

Material/Component	Weight [kg]	Carbon emissions [$\frac{kgCO_2}{kg_{material}}$]	Carbon costs
UAV			
GFRP	8.214	2.63	21.60
Battery	7.238	50	361.9
Aerogel	5	4.3	21.5
Total UAV	20.452	-	405
Nest			
ISO container	$3 \cdot 2200$	0.422	2785.2
Generator	950	3.16	3000
Biodiesel	176.8	0.04	7.072
Total Nest	7726.8	-	5792.3

The table gives a clear overview of the total carbon costs. While the overall number may seem high, it's important to remember that a significant part of this is a one-time investment (namely, the ISO container and the generator). The carbon footprint of the UAVs themselves is more important, as they carry out the missions and contribute to ongoing environmental impact throughout their use. The total carbon cost of the UAV is $405[kgCO_2]$, which is quite small. Generally, the carbon footprint of a single drone production ranges between 432 and $545[kgCO_2]$ [117].

Aerogel Material

It is crucial for the sustainability analysis to consider the behaviour of aerogel when it is deployed. Aerogels are highly porous with extensive surface areas. Therefore, they have remarkable thermal and chemical properties to be used in wildfires and oil spills mitigation missions, which is exactly what AeroShield is designed for. Nonetheless, the aerogel will not degrade or fall apart when it is dropped in the water [118]. It was also proved that the structure of aerogel nanoparticles was maintained during thermal modification, so it can be assumed that aerogel has enough thermal stability to not pollute in the application in wildfires [119]. Additionally, the aerogel should be recovered after the disaster mitigation is completed, althoug this step is outside the scope of this project.

Product development

The development of AeroShield plays an important role in the LCA. Some parts will be produced specifically for AeroShield, while other parts and components will be bought. It is important to be aware of the existing infrastructure and technologies to evaluate the sustainability of the development method. Sustainable product development requires not only selecting low-impact materials, but also leveraging existing industrial capabilities to minimize unnecessary emissions, as well as selecting materials for longevity. The existing infrastructure for producing glass fibre structures is technologically advanced in Europe [120]. By utilizing mature production capabilities already in place, the product avoids the environmental and economic costs associated with building new facilities. This enhances the overall efficiency and scalability of the manufacturing phase.

22.3. End-of-Life

At the conclusion of its operational lifespan, AeroShield requires a carefully planned end-of-life (EOL) strategy to ensure environmental responsibility. EOL planning is an integral part of the product's sustainability assessment, as it directly influences recyclability, safe disposal, and the potential for component repurposing. The actual EOL trajectory depends on factors such as quality of maintenance, user handling, and design. These factors will be taken into account when deciding to move forward with the end of life stage of the product. Due to the modularity of the design of AeroShield, a handful of subsystems can be taken out of the AeroShield configuration and be recycled separately. Key components are designed for easy removal, supporting both ongoing maintenance and eventual EOL processing. They ensure easier maintenance and repair, without affecting the integrity of the product. The design also supports the reusing of serviceable modules in future UAV platforms or as spare parts, extending the lifecycle of individual components and reducing material waste. The batteries, which are embedded in the wings, can be removed without changing the structure of the wing, by a push panel on top of the structure.

The GFRP can be recycled in a couple of different ways, too. It can be mechanically recycled by shredding

the material into small particles and then using it in concrete, asphalt, or other lower-grade composites. The GFRP can also be thermally recycled, by using pyrolysis. Heating the GFRP in an oxygen-free environment will decompose the resin and leave the glass fibres behind. This is a energy-intensive process though, and not yet widely commercialized. An alternative for the GFRP parts of AeroShield could be the integration of GFRP scrap into non-structural applications, like barriers or park furniture.
In reference to *REQ-SYS-06*, approximately 50% of the mass of GFRP can be considered recyclable [121]. Similarly, the lithium-polymer battery is also estimated to be 50% recyclable [122]. On a subsystem level, recyclability varies: for example, the motors are close to 100% recyclable, while the propellers are estimated at around 30%, when they are taken out of the UAV assembly and are recycled separately [123]. Taking these variations into account, the overall recyclability of AeroShield can reasonably be estimated at around 50% recovery to raw materials. Therefore, the system is considered to meet the recyclability requirement.

22.4. Compliance Matrix

In Table 22.2 the compliance matrix is presented for the system requirements related to sustainability. For each requirement it is indicated of the requirements are met (✓) or not ($\times$) and the method of verification.

Table 22.2: Compliance Matrix Deployment Requirements

Identification	Description	Compliance	Method of Verification
REQ-SYS-01	Aerogel shall release no more than 0.01% by weight of particles between 100 nm and 10 nm.	✓	Analysis, as discussed in Table 22.2
REQ-SYS-02	Aerogel shall demonstrate no increase in marine toxicity (LC_{50})	✓	Analysis, as discussed in Table 22.2
REQ-SYS-05	The nest shall source 100% of its electricity from renewable energy.	✓	Analysis, as discussed in section 22.1
REQ-SYS-06	The system shall comprise at least 50% recyclable components by mass.	✓	Analysis, as discussed in section 22.3
REQ-SYS-07	The system shall be modular.	✓	Analysis, as discussed in section 22.3

23

Post Design Process

In this chapter, the activities that need to be taken after the design project will be explained. In section 23.1 the Project Design and Development Logistics block diagram is presented. The activities presented in the block diagram are further divided and planned on a timeline presented in a Gantt-chart in section 23.2.

23.1. Project Design and Development Logic

The design and development logistics include the activities to be executed after the DSE phase. This process is displayed in Figure 23.1. The green blocks represent time-ordered steps in this process, while the grey blocks represent sub-steps of the accompanied green block, indicated by the dashed arrows. First, contacting potential customers is crucial for the development of AeroShield, as without customers, there is no reason to start production. Based on customer feedback, further development can also be done, so that the system precisely matches the needs of that specific customer. Based on this feedback and the financial position of the customer, the budget can be updated and refined. A prototype will be manufactured and validated, and this could also inspire further development. To manufacture this prototype, an initial supply chain must be established, so that it is clear where all materials and parts are sourced from. Once this iteration is completed to customer and engineer satisfaction, the UAVs can be certified. As the design will not be altered after this stage, the system can now receive a final price and be sold. This means that production will start, and that personnel will need to be trained. Finally, the system is distributed to the clients, and continuous maintenance support is offered to them.

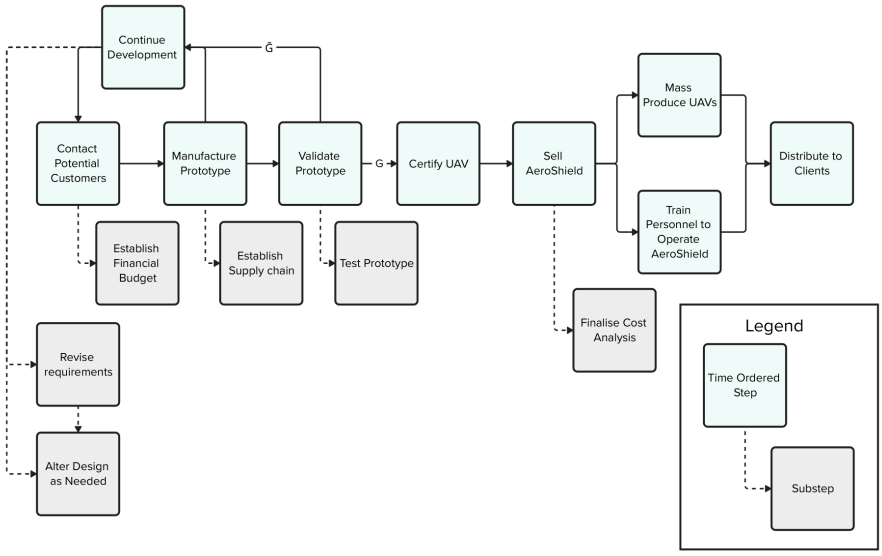

Figure 23.1: Block Diagram Project Design and Development Logistics

23.2. Project Gantt Chart

In this section, the project Gantt Chart will be displayed. It provides an overview of the tasks that need to take place after the DSE and when they need to take place. It is a further development of the project design and development logic diagram presented in Figure 23.1. The Gantt Chart is displayed in Figure 23.2.

ID	Task Description	Duration [Days	Start Date	End Date	2025				2026				2027				2028			
					Q1	Q2	Q3	Q4	Q1	Q2	Q3	Q4	Q1	Q2	Q3	Q4	Q1	Q2	Q3	Q4
1	**DSE**	**75**	**22/04/2025**	**27/06/2025**																
2	**Contact Potential Customers**	**30**	**01/07/2025**	**31/07/2025**																
2.1	Schedule meetings with potential customers	10	01/07/2025	21/07/2025																
2.2	Update design Requirements according to feedback recieved	10	21/07/2025	31/07/2025																
2.3	Establish Revised Budget	10	21/07/2025	31/07/2025																
3	**Further Detailed Design**	**130**	**01/08/2025**	**09/12/2025**																
3.1	Detailed Design of Subsystems	45	01/08/2025	15/09/2025																
3.2	Establish Connections Between all Subsystems	15	15/09/2025	30/09/2025																
3.3	Make Detailed Electrical Diagrams with all Electrical Components Used	15	30/09/2025	15/10/2025																
3.4	Make a Detailed CAD Model Including all Subsystems and Connections	30	15/10/2025	14/11/2025																
3.5	Perform a Complete Mission Simulation	15	14/11/2025	29/11/2025																
3.6	Design a Complete Manufacturing Plan	10	29/11/2025	09/12/2025																
4	**Manufacture Prototype**	**255**	**09/12/2025**	**21/08/2026**																
4.1	Manufacture a Small Scale UAV Prototype	20	09/12/2025	29/12/2025																
4.2	Test Small Scale UAV Prototype	10	29/12/2025	08/01/2026																
4.3	Validate Small Scale UAV Prototype	10	08/01/2026	18/01/2026																
4.4	Manufacture Real Scale UAV Prototype	60	18/01/2026	19/03/2026																
4.5	Test Real Scale UAV Prototype	15	19/03/2026	03/04/2026																
4.6	Validate UAV Prototype	15	03/04/2026	18/04/2026																
4.7	Manufacture Whole Swarm of UAVs	80	18/04/2026	07/07/2026																
4.8	Test the Swarm in a Real Life Scenarios	30	07/07/2026	06/08/2026																
4.9	Validate whole Swarm behaviour	15	06/08/2026	21/08/2026																
5	**Certify Aeroshield**	**260**	**21/08/2026**	**08/05/2027**																
5.1	Manufacture UAV Swarm and Nest for Certifying	80	21/08/2026	09/11/2026																
5.2	Certify Aeroshield	180	09/11/2026	08/05/2027																
6	**Sell Aeroshield**	**70**	**08/05/2027**	**17/07/2027**																
6.1	Advertise Aeroshield	30	08/05/2027	07/06/2027																
6.2	Contact Previous Customers	10	07/06/2027	17/06/2027																
6.3	Establish Contracts between customers	30	17/06/2027	17/07/2027																
7	**Production**	**500**	**17/07/2027**	**28/11/2028**																
7.1	Production Planning	90	17/07/2027	15/10/2027																
7.2	Mass Produce Aeroshield	365	15/10/2027	14/10/2028																
7.3	Distribute to Clients	30	14/10/2028	13/11/2028																
7.4	Train Personel to operate Aeroshield	15	13/11/2028	28/11/2028																
8	**Maintanence**																			
8.1	Perform Maintanence on Sold Components																			

Legend

Task Duration		Major Deadline	
Sub Task Duration			
No Value			

Figure 23.2: Project Gantt Chart

24

Conclusion

In this report, the complete design of AeroShield was outlined. AeroShield comprises of a swarm of 20 UAVs that are autonomously capable of deploying aerogel blankets to mitigate wildfires and oil spills. A market analysis settled on the fact that AeroShield will address existing market gaps in areas like mitigation effectiveness, response time, and accessibility. After a mission strategy was presented, and swarm logistics were addressed, the design of the UAV was explained. The UAVs feature a 3-meter span hybrid wing VTOL quadcopter configuration. They are stored in a nest containing three ISO containers and a bio-diesel generator to charge the batteries of the UAVs. The swarm consists of 20 UAVs, that are manually deployed from the nest, and can operate missions autonomously. The aerogel will be deployed in a blanket configuration from the container in the fuselage via a winch system with magnets. The UAV design for AeroShield is displayed in Figure 24.1.

The final performance of the AeroShield design was optimized for the total response time and the deployment rate. For wildfire missions, the response time is 7.5 hours, and the deployment rate is $24[m/h]$. For oil spill missions, the response time is 7 hours, and the deployment rate is $946[kg/h]$ (kilos of oil recovered per hour). These metrics rely on the number of workers at the nest and the number of UAVs available.

Due to time constraints, the design of AeroShield has not yet been fully finalized. The following recommendations are proposed to complete a detailed design: First, mass calculations should be performed after the UAV system has been manufactured and assembled. This process can add and subtract weight in some sections due to assembling procedures. Second, prototype testing of both the UAV and the nest is essential to evaluate subsystem performance and integration. This testing phase should follow immediately after prototype manufacturing. Finally, the thermal management system could be further improved through external regulation of the motor, such as embedding it more deeply at the ends of the booms. Also, it needs to be considered that there are going to be holes in the wing for the air flow in the thermal management system, so that needs to be further analysed in terms of loads.

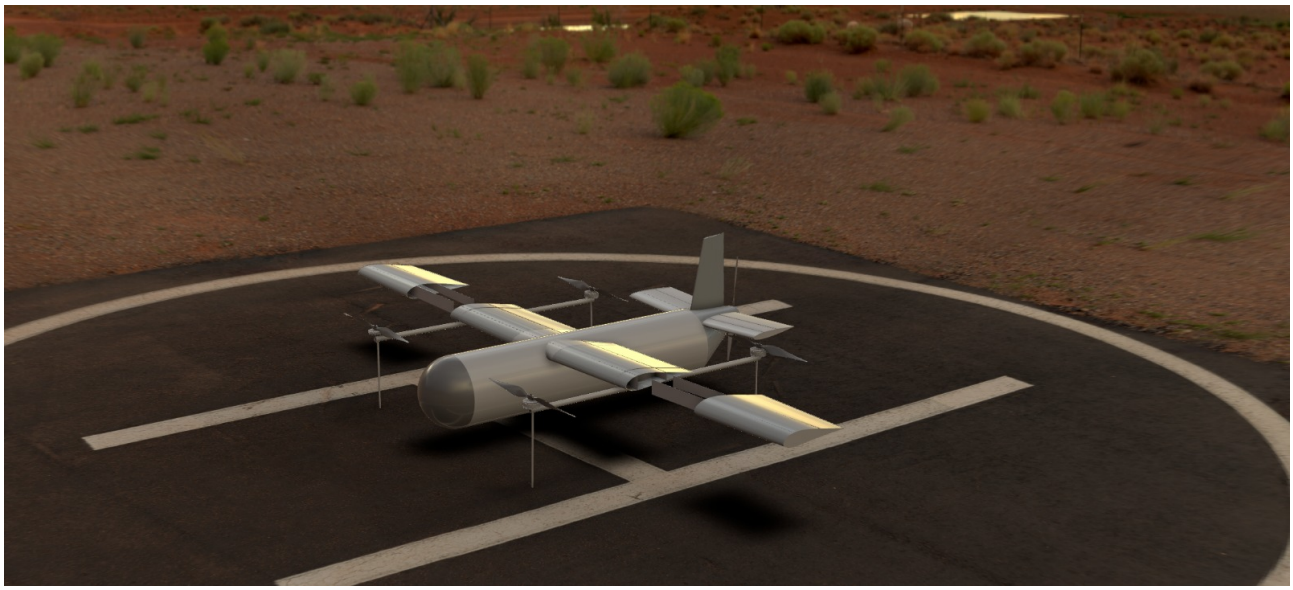

Figure 24.1: AeroShield UAV Design

References

[1] Grand View Research. “Aerogel Market Size, Share Trends Analysis Report By Product (Silica, Polymers, Carbon), By Form (Blanket, Particle), By End-use, By Technology (Supercritical Drying), By Region, And Segment Forecasts, 2025 - 2030”. In: *Grand View Research* (2024).

[2] Our World in Data. *Wildfires*. URL: https://ourworldindata.org/wildfires.

[3] San-Miguel-Ayanz J et al. “Forest Fires in Europe, Middle East and North Africa 2022”. In: (2025). ISSN: 1831-9424. DOI: 10.2760/348120.

[4] San-Miguel-Ayanz J et al. “Forest Fires in Europe, Middle East and North Africa 2023”. In: (2024). ISSN: 1831-9424. DOI: 10.2760/8027062.

[5] ITOPF. *Oil Tanker Spill Statistics 2024*. 2025. URL: https://www.itopf.org/knowledge-resources/data-statistics/oil-tanker-spill-statistics-2024.com (visited on 04/28/2025).

[6] Office of Response and Restoration. *How Oil Harms Animals and Plants in Marine Environments*. URL: https://response.restoration.noaa.gov/oil-and-chemical-spills/oil-spills/how-oil-harms-animals-and-plants-marine-environments.html.

[7] Mordor Intelligence. *Aerogel Market Size Share Analysis - Growth Trends Forecasts (2025 - 2030)*. URL: https://www.mordorintelligence.com/industry-reports/aerogel-market.

[8] Made-in-China. *Silica Aerogel Price*. URL: https://www.made-in-china.com/products-search/hot-china-products/Silica_Aerogel_Price.html?pv_id=1iq88dqvle0d&faw_id=null&bv_id=1iq8cv4upb60.

[9] Joint Research Centre. *2023 among the five worst years for wildfires in Europe, but 2024 provides some relief*. 2024. URL: https://joint-research-centre.ec.europa.eu/jrc-news-and-updates/2023-among-five-worst-years-wildfires-europe-2024-provides-some-relief-2024-11-19_en.

[10] San-Miguel-Ayanz J et al. “Advance report on Forest Fires in Europe, Middle East and North Africa 2024”. In: (2025). ISSN: 1831-9424. DOI: 10.2760/1264626.

[11] Western Fire Chiefs Association. *How Fast Do Wildfires Spread?* URL: https://wfca.com/wildfire-articles/how-fast-do-wildfires-spread/.

[12] Forest Service US Department of Agriculture. *Drones help make fighting fires safer, cheaper, better throughout Rocky Mountain Region*. 2024. URL: https://www.fs.usda.gov/inside-fs/delivering-mission/deliver/drones-help-make-fighting-fires-safer-cheaper-better (visited on 04/28/2025).

[13] BBC. *The Portuguese drone that douses wildfires from above*. 2023. URL: https://www.bbc.com/future/article/20230609-can-we-use-firefighting-drones-put-out-wildfires (visited on 04/28/2025).

[14] B. Aydin et al. “Use of Fire-Extinguishing Balls for a Conceptual System of Drone-Assisted Wildfire Fighting”. In: *MDPI* (2019).

[15] P. Burgherr. “In-depth analysis of accidental oil spills from tankers in the context of global spill trends from all sources”. In: *Journal of Hazardous Materials* (2006).

[16] C. Nunez C. Dell’Amore. *3 Surprising Sources of Oil Pollution in the Ocean*. URL: https://www.nationalgeographic.com/science/article/140325-texas-pollution-oil-spills-animals-science.

[17] TROY BEAVER. *Ensure Rapid Response Time for Effective Spill Control*. URL: https://www.halenhardy.com/rapid-response/.

[18] A. Maure, M. Cerrolaza, and R. Berríos. “Modelling the behavior of crude oil spills in shallow bodies of water”. In: *Environmental Software* 10.4 (1995), pp. 241–249. ISSN: 0266-9838. DOI: https://doi.org/10.1016/0266-9838(95)00016-X. URL: https://www.sciencedirect.com/science/article/pii/026698389500016X.

[19] C. Allred. *Drones are Revolutionizing Oil Spill Response: Here’s How*. 2023. URL: https://thedronelifenj.com/drones-oil-spill-response/ (visited on 04/28/2025).

[20] Parrot Drones SAS. *ANAFI USA*. URL: https://www.parrot.com/en/drones/anafi-usa.

[21] DJI. *Support for Matrice 300 RTK*. URL: https://www.dji.com/nl/support/product/matrice-300.

[22] AgEagle Aerial Systems Inc. *eBee X Series*. URL: https://ageagle.com/drones/ebee-x/.

[23] L3Harris. *Autonomous Systems*. URL: https://www.l3harris.com/all-capabilities/autonomous-systems (visited on 05/01/2025).

[24] workboat365. *L3HARRIS TECHNOLOGIES DELIVERS FIRST UNMANNED VEHICLE FOR OIL SPILL RESPONSE*. URL: https://workboat365.com/l3harris-technologies-delivers-first-unmanned-vehicle-for-oil-spill-response/.

[25] Office of Response and Restoration. *How Do Oil Spills out at Sea Typically Get Cleaned Up?* URL: https://response.restoration.noaa.gov/about/media/how-do-oil-spills-out-sea-typically-get-cleaned.html.

[26] Jingjing Sun et al. “Facing the Wildfire Spread Risk Challenge: Where Are We Now and Where Are We Going?” In: *Fire* 6 (June 2023), p. 228. DOI: 10.3390/fire6060228.

[27] Emily Grant and Jennifer D. Runkle. “Long-term health effects of wildfire exposure: A scoping review”. In: *The Journal of Climate Change and Health* 6 (2022), p. 100110. ISSN: 2667-2782. DOI: https://doi.org/10.1016/j.joclim.2021.100110. URL: https://www.sciencedirect.com/science/article/pii/S2667278221001073.

[28] John Reynolds, Paul R Coronado, and Lawrence W. Hrubesh. “Hydrophobic aerogels for oil-spill clean up - Synthesis and characterization”. In: *Journal of Non-Crystalline Solids* 292 (2001). DOI: 10.1016/S0022-3093(01)00882-1.

[29] D. Helton. *Attempting to Answer One Question Over and Over Again: Where Will the Oil Go?* 2025. URL: https://response.restoration.noaa.gov/about/media/attempting-answer-one-question-over-and-over-again-where-will-oil-go.html.

[30] C. Henry. *Recalling the Early Hours—and Challenges—of the Deepwater Horizon Oil Spill*. 2022. URL: https://response.restoration.noaa.gov/about/media/recalling-early-hours-and-challenges-deepwater-horizon-oil-spill.html.

[31] Dagmar Schmidt Etkin. “Worldwide Analysis of Marine Oil Spill Cleanup Cost Factors”. In: *Proceedings of the Arctic and Marine Oilspill Program (AMOP) Technical Seminar*. Presented June 2000. Environment Canada. Calgary, Alberta, Canada, June 2000.

[32] National Institute of Environmental Health Sciences. *Safety and Health Awareness for Oil Spill Cleanup Workers*. Worker Education and Training Program, 2010.

[33] European Commission. *EU Civil Protection Mechanism*. Accessed: 2025-06-17. 2023. URL: https://civil-protection-humanitarian-aid.ec.europa.eu/what/civil-protection/eu-civil-protection-mechanism_en.

[34] Witt O’Brien’s. *Comprehensive Environmental Solutions*. 2025. URL: https://www.wittobriens.com/solutions/environmental-services#environmentalResponse (visited on 04/28/2025).

[35] NRC. *Emergency Response*. 2025. URL: https://nrcc.com/services/emergency-response/ (visited on 04/28/2025).

[36] B. Kumru. “Project Description”. In: *AE3200 Design Synthesis* (2025).

[37] Erwin Mooij. *Tips Tops - Baseline Report PMSE Deliverables*. Accessed: 2025-04-30. 2025.

[38] Office of Reponse and Restoration. *Who Takes Care of the Problem of Oil Spills?* URL: https://response.restoration.noaa.gov/training-and-education/education-students-and-teachers/who-takes-care-problem.html (visited on 04/25/2025).

[39] Saadia Afridi et al. “Unveiling the Impact of Drone Noise on Wildlife: A Crucial Research Imperative”. In: *2024 International Conference on Unmanned Aircraft Systems (ICUAS)*. 2024, pp. 1409–1416. DOI: 10.1109/ICUAS60882.2024.10557094.

[40] Office of Reponse and Restoration. *Who Pays for Oil Spills?* URL: https://response.restoration.noaa.gov/about/media/who-pays-oil-spills.html (visited on 04/25/2025).

[41] Business.gov.nl. *Rules for flying drones*. URL: https://business.gov.nl/regulation/drones/ (visited on 04/25/2025).

[42] European Union Aviation Safety Agency. *Specific Category — Civil Drones*. Accessed: 2025-04-30. 2025. URL: https://www.easa.europa.eu/en/domains/drones-air-mobility/operating-drone/specific-category-civil-drones.

[43] NASA Earth Observatory. *Climate Change Pushes Fires to Higher Ground*. URL: https://earthobservatory.nasa.gov/images/148789/climate-change-pushes-fires-to-higher-ground (visited on 04/30/2025).

[44] P. Kaniewski P. Pasek. “A review of consensus algorithms used in Distributed State Estimation for UAV swarms”. In: *IEEE Xplore* (2022). DOI: 10.1109/TCSET55632.2022.9766903.

[45] G.Vachtsevanos S.Al-Hasan. “Intelligent route planning for fast autonomous vehicles operating in a large natural terrain”. In: *Robotics and Autonomous Systems* (2002). DOI: 10.1016/S0921-8890(02)00208-7.

[46] Niki Patrinopoulou et al. “A Distributed Framework for Persistent Wildfire Monitoring with Fixed Wing UAVs”. In: *Drones and Autonomous Vehicles* 1.3 (2024). DOI: 10.35534/dav.2024.10009.

[47] Rafael Bailon-Ruiz, Arthur Bit-Monnot, and Simon Lacroix. “Real-time wildfire monitoring with a fleet of UAVs”. In: *Robotics and Autonomous Systems* 152 (2022), p. 104071. DOI: https://doi.org/10.1016/j.robot.2022.104071. URL: https://www.sciencedirect.com/science/article/pii/S0921889022000355.

[48] A. Sempf. “Swarm Communication”. In: *Medium* (2015).

[49] AirSight. *Drone Communication - Data Link*. 2025. URL: https://www.airsight.com/learn/airspace-security/drone-fundamentals/drone-communication-data-link (visited on 06/17/2025).

[50] O. Bimber R. Nathan I. Kurmi. “Drone swarm strategy for the detection and tracking of occluded targets in complex environments”. In: *Nature* (2023). DOI: 10.1038/s44172-023-00104-0.

[51] Velodyne. *Velodyne LiDaR Puck*. URL: https://www.amtechs.co.jp/product/VLP-16-Puck.pdf (visited on 05/19/2025).

[52] Glen Martin. “HUMBOLDT COUNTY / World’s tallest tree, a redwood, confirmed”. In: *SFGate* (Sept. 2006). URL: https://www.sfgate.com/bayarea/article/HUMBOLDT-COUNTY-World-s-tallest-tree-a-2550557.php.

[53] Airmobi Limited. *Airmobi V32 Full Electric Long Endurance VTOL Drone*. 2025. URL: https://www.airmobi.com/product/airmobi-v32-full-electric-long-endurance-vtol-drone/ (visited on 05/16/2025).

[54] Lee Spring. *Part Number LE 037E 13 S*. URL: https://www.leespring.com/extension-springs?search=LE037E13S# (visited on 06/03/2025).

[55] NEW WING ADVANCED TECHNOLOGY CO., LTD. *PAYLOAD WINCH FOR DRONE*. Specification Sheet. Version 1.0. 2025.

[56] TE Connectivity. *NEMA WC 27500-*SD (AS22759/34 Basic Wire Spec.)* 2025. URL: https://www.farnell.com/datasheets/2342860.pdf (visited on 06/18/2025).

[57] CMI. *Spec Sheet for CMI RP113*. URL: https://cdn.shopify.com/s/files/1/0393/0605/files/RP113specs.pdf?v=1611078352 (visited on 06/03/2025).

[58] Hyab Magneter. *Electromagnet / Electropermanent*. 2025. URL: https://hyab.com/uploads/pdfenfile/71-2515-en.pdf?id=1481 (visited on 06/18/2025).

[59] Maxim Tyan et al. “Comprehensive preliminary sizing/resizing method for a fixed wing – VTOL electric UAV”. In: *Aerospace Science and Technology* 71 (2017), pp. 30–41. DOI: 10.1016/j.ast.2017.09.008. URL: https://www.sciencedirect.com/science/article/pii/S1270963817300871.

[60] A.R Serrano A.M Kamal. “Design methodology for hybrid (VTOL + Fixed Wing) unmanned aerial vehicles”. In: *Aeronautics and Aerospace Open Access Journal* 2 (2018).

[61] H.N.J. Dekker et al. “Aerodynamic Interactions of Side-by-Side Rotorsin Ground Proximity”. In: *AIAA Journal* 60 (2022). DOI: 10.2514/1.J061105.

[62] B. Xu et al. “Modeling of Lithium-Ion Battery Degradation for Cell Life Assessment”. In: *IEEE* (2016).

[63] A. Carnovale and X. Li. “A modeling and experimental study of capacity fade for lithium-ion batteries”. In: *Energy and AI* 2 (2020), p. 100032. ISSN: 2666-5468. DOI: https://doi.org/10.1016/j.egyai.2020.100032. URL: https://www.sciencedirect.com/science/article/pii/S266654682030032X.

[64] DSE Group 26. “AeroShield: Fire Suppression and Oil Spill Mitigation by Drone Swarms Midterm Final”. In: *AE3200 Design Synthesis* (2025).

[65] A. Cervone and F. Oliviero. *AE2111-II Aerospace System Design*. Lecture Slides, Aerospace Engineering, TU Delft. 2025.

[66] M. aldheeb et al. “Aerodynamics of porous airfoils and wings”. In: *Acta Mechanica* 229 (2018).

[67] Mohammad H. Sadraey. *Aircraft Design: A Systems Engineering Approach*. 1st. The Atrium, Southern Gate, Chichester, West Sussex, PO19 8SQ, United Kingdom: John Wiley & Sons, Ltd., 2013.

[68] NASA Glenn Research Center. *Shape Effects on Drag*. https://www1.grc.nasa.gov/beginners-guide-to-aeronautics/shape-effects-on-drag/. Accessed: 17 June 2025.

[69] The Contact Patch. *Propeller Thrust*. https://www.thecontactpatch.com/fluids/f1518-propeller-thrust. [Online; accessed 16 June 2025]. Apr. 2021.

[70] Or D. Dantsker et al. “Performance Testing of APC Electric Fixed-Blade UAV Propellers”. In: *AIAA Aviation and Aeronautics Forum and Exposition*. AIAA Paper 2022-4020. Chicago, IL, June 2022. DOI: 10.2514/6.2022-4020. URL: https://arc.aiaa.org/doi/full/10.2514/6.2022-4020.

[71] T-MOTOR. *U8 Lite L Efficiency Multirotor UAV Motor KV95*. https://store.tmotor.com/product/u8lite-l-kv95-u-efficiency.html. Accessed: 17 June 2025.

[72] DSE Group 26. “AeroShield: Fire Suppression and Oil Spill Mitigation by Drone Swarms Baseline Final”. In: *AE3200 Design Synthesis* (2025).

[73] MatWeb / ASM. *Ti–6Al–4V (Grade 5) Material Data Sheet*. https://www.matweb.com/search/datasheet.aspx?MatGUID=b350a789eda946c6b86a3e4d3c577b39. Accessed: 2025-06-16.

[74] MatWeb / ASM. *Aluminum 5052-H32 Material Data Sheet*. https://www.matweb.com/search/DataSheet.aspx?MatGUID=96d768abc51e4157a1b8f95856c49028. Accessed: 2025-06-16.

[75] Summers P.T., Chen Y., and Rippe. “Overview of aluminum alloy mechanical properties during and after fires”. In: *Fire Science Reviews* 4.3 (2015).

[76] Composites Evolution Ltd. *Evopreg PFC502*. 2021. URL: https://compositesevolution.com/wp-content/uploads/2022/03/Evopreg%C2%AE-PFC502_Technical-Data-Sheet.pdf (visited on 06/15/2025).

[77] Roelof Vos and Maurice Hoogreef. “Semi-Analytical Weight Estimation Method for Fuselages with Oval Cross-Section”. In: *Collection of Technical Papers - AIAA/ASME/ASCE/AHS/ASC Structures, Structural Dynamics and Materials Conference* (2013). DOI: 10.2514/6.2013-1719.

[78] M. El Adawy et al. “Design and fabrication of a fixed-wing Unmanned Aerial Vehicle (UAV)”. In: *Ain Shams Engineering Journal* (2023).

[79] Climator. *Climsel C48*. 2025. URL: https://climator.com/wp-content/uploads/2024/06/Prodblad-ClimSel-C48-230815.pdf (visited on 06/18/2025).

[80] Jiyuan Liang, Xuelai Zhang, and Jun Ji. “Hygroscopic phase change composite material”. In: *Journal of Energy Storage* 36.1 (2021), pp. 2–11. DOI: 110.1016/j.est.2021.102395. URL: https://doi.org/10.1016/j.est.2021.102395.

[81] Mohammad Khademia and Abbas Mozafarib. “INTEGRAL ENERGY EQUATION MODEL FOR HEAT CONVECTION TO TURBULENT BOUNDARY LAYER ON A FLAT PLATE”. In: *Frontiers in Heat and Mass Transfer* 7.33 (2016), pp. 1–8. DOI: 10.5098/hmt.7.33. URL: https://www.researchgate.net/publication/310899735.

[82] Penn State Mechnical Engineering. *PROPERTY TABLES AND CHARTS*. Data Sheet. Version 1.0. 2012.

[83] NVIDIA. *Jetson AGX Orin Series*. Specification Sheet. Version 1.0. 2022.

[84] L. Zhou, X. Yi, and Q. Liu. “A Review of Icing Research and Development of Icing Mitigation Techniques for Fixed-Wing UAVs”. In: *Drones* 7.12 (2023), p. 709. DOI: 10.3390/drones7120709. URL: https://doi.org/10.3390/drones7120709.

[85] H. Luo et al. “Efficient Fabrication of Wear-Resistant PEEK Matrix Composite Coating with Superhydrophobicity for Self-Cleaning and Anti-Icing Applications”. In: *Polymer-Plastics Technology and Materials* 60.10 (2021), pp. 1106–1121. DOI: 10.1080/25740881.2021.1882490.

[86] A. Ramachandran and G. Pamula. “Thermal Management for Unmanned Aerial Vehicle Payloads: Mechanisms, Systems, and Applications”. In: *Drones* 9.5 (2025), p. 350. DOI: 10.3390/drones9050350.

[87] Wiley Advanced. *Supplementary Material for ”FireDrone: Multi-environment thermally-agnostic aerial robot*. Supplementary Sheet. Version 1.0. 2023.

[88] W Power Products. *GPR□J50□60T4IF Portable Generator Set*. https://www.wpowerproducts.com/product/gpr-j50-60t4if-portable-generator-set-p-9954/. Accessed: 18 June 2025.

[89] VEVOR. *Lineaire geleiderail set SBR20 – 2200 mm (2 stuks) met 4 schuifblokken*. https://www.vevor.nl/lineaire-geleiderail-c_10531/vevor-lineaire-geleider-lineaire-rail-2-stuks-sbr20-2200mm-koolstofstaal-aluminium-geleiderail-met-4-stuks-sbr20uu-schuifblokken-lineair-lager-lagerblok-cnc-onderdelen-voor-3d-printer-freesdraaibank-p_010322688456. Accessed: 18 June 2025.

[90] *Brandweer West Vlaanderen – container met slede*. https://cboxcontainers.nl/uploads/images/projects/original/brandweer-west-vlaanderen-1-web.jpg. Accessed: 18 June 2025.

[91] Osman Karatum et al. “Flexible, Mechanically Durable Aerogel Composites for Oil Capture and Recovery”. In: *ACS Applied Materials & Interfaces* 8.1 (2016). PMID: 26701744, pp. 215–224. DOI: 10.1021/acsami.5b08439. eprint: https://doi.org/10.1021/acsami.5b08439. URL: https://doi.org/10.1021/acsami.5b08439.

[92] M. Bennett. “Reducing Fire Risk on Your Forest Property”. In: *Pacific Northwest Extension Publication* 618 (2010), pp. 1–40.

[93] Elizabeth Dodson. *Cost, Production, and Effectiveness of Masticated Fireline*. Technical Report Pub. 798. University of Montana, College of Forestry and Conservation, 2016.

[94] Peng Han et al. “Quantitative Ground Risk Assessment for Urban Logistical Unmanned Aerial Vehicle (UAV) Based on Bayesian Network”. In: *Sustainability* 14 (May 2022), p. 5733. DOI: 10.3390/su14095733.

[95] Mohammad Pourgol, Ahmad Khayyati, and Saeed Shiri. “Development of an Efficient Approach for Reliability Analysis Using the Comparative Study of Several Static and Dynamic Methods; Case Study of an Unmanned Aerial Vehicle”. In: *International Journal of Reliability* 3 (July 2020), pp. 45–53. DOI: 10.30699/IJRRS.3.1.5.

[96] Enrico Petritoli, Fabio Leccese, and Lorenzo Ciani. “Reliability and Maintenance Analysis of Unmanned Aerial Vehicles”. In: *Sensors* 18 (Sept. 2018), p. 3171. DOI: 10.3390/s18093171.

[97] Christine Belcastro et al. “Hazards Identification and Analysis for Unmanned Aircraft System Operations”. In: *Aerospace Research Central* (June 2017). DOI: 10.2514/6.2017-3269.

[98] Jake Ferrigan. “Safety Risk Assessment for UAV Operation”. In: *AeroTract Geospatial* (2022).

[99] T.Schuett. “CT scanning: A Differentiating Facto”. In: *Mold Making Technology* (2012).

[100] J.Goodenough et al. “Reversible adhesives and debondable joints for fibre-reinforced plastics: Characteristics, capabilities, and opportunities”. In: *Science Direct* 299 (2023).

[101] NASA. *Space Systems Engineering: Cost Estimating Module*. Technical Report. Version 1.0.

[102] L.A. Curtis et al. “Affordable In-Space Transportation”. In: *NAsA Technical Memorandum* (1996). URL: https://ntrs.nasa.gov/api/citations/19960054362/downloads/19960054362.pdf.

[103] Statista. *Estimated operating costs for wildfire suppression in the Mediterranean in 2021, by type*. 2023. URL: https://www.statista.com/statistics/1296801/operating-costs-to-suppress-wildfires-in-the-mediterranean/ (visited on 06/17/2025).

[104] National Wildfire Coordinating Group (NWCG). *Fire Line Production Rate Tables*. Technical Report. Published by request of NWCG’s Fuels Management Committee. NWCG Fuels Management Committee, 2021.

[105] Orsolya Valkó et al. “Review: Prospects and limitations of prescribed burning as a management tool in European grasslands”. In: *Basic and Applied Ecology* 15.1 (2014), pp. 26–33. ISSN: 1439-1791. DOI: https://doi.org/10.1016/j.baae.2013.11.002. URL: https://www.sciencedirect.com/science/article/pii/S1439179113001497.

[106] Pietro Tedesco et al. “Bioremediation for the recovery of oil polluted marine environment, opportunities and challenges approaching the Blue Growth”. In: *Marine Pollution Bulletin* 200 (2024), p. 116157. ISSN: 0025-326X. DOI: https://doi.org/10.1016/j.marpolbul.2024.116157. URL: https://www.sciencedirect.com/science/article/pii/S0025326X24001346.

[107] Yirong Zhang and Yixiang Wang. “Construction of three-dimensional aerogels from electrospun cellulose fibers as highly efficient and reusable oil absorbents”. In: *Separation and Purification Technology* 353 (2025), p. 128604. ISSN: 1383-5866. DOI: https://doi.org/10.1016/j.seppur.2024.128604. URL: https://www.sciencedirect.com/science/article/pii/S1383586624023438.

[108] Neste My Renewable Diesel. *Lagere broeikasgasemissies met Neste My Renewable Diesel*. 2025. URL: https://www.neste.com/products-and-innovation/neste-my-renewable-diesel (visited on 06/05/2025).

[109] Ecochain. *Life Cycle Assessment Guide*. 2025. URL: https://ecochain.com/blog/life-cycle-assessment-lca-guide/#:~:text=An%20LCA%20measures%20the%20environmental,where%20do%20they%20come%20from%3F (visited on 06/11/2025).

[110] Y Li et al. “The Carbon Footprint Calculation of the GFRP Pedestrian Bridge at Tai-Jiang national park”. In: *IRSPSD International* 1.4 (2013), pp. 13–28.

[111] DJI Enterprise. *DJI Flycart 30 Specs*. 2025. URL: https://www.dji.com/nl/flycart-30/specs (visited on 06/13/2025).

[112] IVL Svenska Miljoinstitut. *Climate impact of electric car batteries*. 2020. URL: https://www.ivl.se/english/ivl/press/press-releases/2019-12-04-new-report-on-climate-impact-of-electric-car-batteries.html (visited on 06/13/2025).

[113] Yang Liu et al. “Evaluation the life cycle carbon emissions of the aerogel glazing under different weather conditions”. In: *Journal of Cleaner Production* 437 (2023). DOI: 10.1016/2024.140651.

[114] ITCO. *Tank Containers: A Sustainable Solution for Bulk Liquid Transport*. 2011. URL: https://international-tank-container.org/storage/uploads/ITCOSustainabilityFinal.pdf (visited on 06/13/2025).

[115] Feace. *The carbon footprint of diesel generators*. 2024. URL: https://www.feace.com/single-post/the-carbon-footprint-of-diesel-generators (visited on 06/13/2025).

[116] Stella Bezergianni and Loukia Chrysikou. “Life cycle assessment of renewable biodiesel produced via waste cooking oil hydrotreatment”. In: *Conventional and Future Energy for Automobiles* 1.1 (2015).

[117] WADI. *LCA Report*. Tech. rep. WADI, 2020.

[118] Shashank Garg, Simranjeet Singh, and Nabila Shehata. “Aerogels in wastewater treatment: A review”. In: *Journal of the Taiwan Institute of Chemical Engineers* 166.1 (2025), p. 105299. DOI: https://doi.org/10.1016/j.jtice.2023.105299.

[119] Hong Nguyen, Phuong Hoang, and Ngo Dinh. “Synthesis of Modified Silica Aerogel Nanoparticles for Remediation of Vietnamese Crude Oil Spilled on Water”. In: *J. Brazil. Chem. Soc* 29.8 (2018), pp. 1714–1720.

[120] Glass Fibre Europe. *Strategy on Advanced Materials*. 2025. URL: https://glassfibreeurope.eu/strategy-on-advanced-materials/ (visited on 06/12/2025).

[121] Guido Grause et al. “Recovery of glass fibers from glass fiber reinforced plastics by pyrolysis”. In: *Journal of Material Cycles and Waste Management* 15.1 (2013), pp. 122–128.

[122] Omar Velazquez, Johanna Valio, and Markus Reuter. “A Critical Review of Lithium-Ion Battery Recycling Processes from a Circular Economy Perspective”. In: *Batteries* 5.4 (2019). DOI: 10.3390/5040068.

[123] Design Life Cycle. *Drones*. 2025. URL: https://www.designlife-cycle.com/drones (visited on 06/20/2025).